FROM GENES TO COMMUNITIES

AN INTEGRATIVE APPROACH TO THE EVOLUTION OF VARANIDAE

CARLOS JOAQUÍN PAVÓN VÁZQUEZ

SUPERVISOR: J. SCOTT KEOGH

A thesis submitted for the degree of Doctor of Philosophy of

The Australian National University

August 2021

DECLARATION

This thesis comprises four chapters that have been submitted or are going to be submitted to peer-reviewed journals as original articles. Chapters I and II are under review in *Evolution*. Chapter III is in press in *Systematic Biology*. Finally, Chapter IV has been prepared for submission to *Molecular Ecology*, but may be split into two manuscripts (one on the population genetics and one on the phylogeny and taxonomy). Chapter IV contains some taxonomic recommendations, but should not be used as the reference for those taxonomic recommendations. The version published in a widely circulated journal should be used as the taxonomic reference. I am lead and corresponding author in each chapter. My supervisor, J. Scott Keogh, also contributed significantly to all chapters. Other co-authors are Ian G. Brennan (Chapters I and III), Paul Doughty (Chapter IV), Damien Esquerré (Chapters II and IV), Stephen C. Donnellan (Chapter IV), and Alexander Skeels (Chapter I). This thesis contains 70,798 words. No part of this thesis has been submitted previously for any other degree.

Carlos Joaquín Pavón Vázquez

August 2021

FROM GENES TO COMMUNITIES: AN INTEGRATIVE APPROACH TO THE EVOLUTION OF VARANIDAE

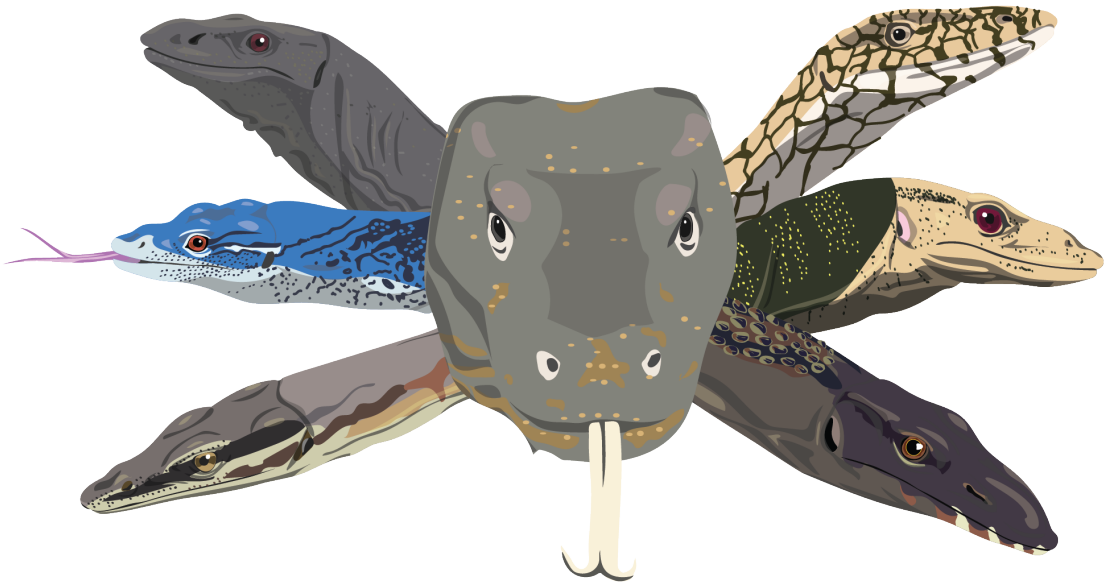

Carlos Joaquín Pavón Vázquez

ACKNOWLEDGMENTS

I would like to thank Scott for his unconditional academic and personal support. From my first day in Canberra I knew I made the right choice. You were an exceptional supervisor, but above all you were fun to be around and a good friend. I appreciate all the hard work that goes into making sure that your students have everything they need to boost their careers and be happy people. I will always be grateful for having been part of the lab.

I thank the members of my panel, Craig and Rob, for the fruitful and insightful meetings. Just being around you and the people in your lab has been a great opportunity to learn and become a better scientist. E&E would be a really different place without the hard work of Audra, Wes, and Jack. I would also like to thank all the people from admin, IT, maintenance, and cleaning for keeping things running from behind the scenes. My ANU experience wouldn't have been as satisfying and smooth without the sacrifice of the people taking the bureaucratic burden, so big thanks to Scott, Adrienne, Mike, Rob, and Celeste.

I want to thank all the students and postdocs in E&E for their academic help, but above all for the fun and sometimes hilariously absurd experiences we have shared. I want to particularly thank the people in the Keogh, Moritz, and Cardillo labs: Damien, Connie (honorary member), Octavio, Putter, Bank, Mitzy, Ian, Zoe, Leo, Jessica, Mel, and Alex. I wish I had spent more time with Regina and Eduardo, thank you for the good times and yummy food. Many other students and postdocs in E&E have been good friends that I will miss dearly. I have a terrible memory and I don't want to exclude anyone, so I will play it safe and just extend my gratitude to everyone.

I thank my co-authors (Alex, Damien, Ian, Paul, Scott, and Steve) for their hard work. For their kind help during specimen examination, I want to thank the staff of the following institutions: AMS, ANWC, BPBM, MNHN, NHM, NTM, QM, SAMA, USNM, WAM, and ZFMK. I also want to thank the people of Australia and each of the cities I visited during my PhD for making me feel welcome. We should never forget that most of the research we do is paid by the people. All the specimens that I examined were once living, breathing beings. I cannot make it up to them, but I sincerely hope that my research positively impacts the public perception of these animals and their conservation.

I wouldn't be here if it wasn't for you Profe Adrián. I am forever in your debt, you are a great mentor and friend. I will never forget that a lot of who I am as a scientist and person comes from you. I would also like to specially thank Uri. You have been a good

and trusted friend, I've learned a lot from you. I thank Levi, Adam, Britt, and Peter for their help and all the fun times in the field. I thank Steve, Luis, Jonathan, and Alexis for their academic support. Many other people have helped me throughout my career and I'm really grateful that they're a part of my life, namely Oscar, Mundo, Marysol, Rubi, Leslie, Eric, Rosario, Manuel, and Luis.

Finalmente, quiero agradecer a mi familia. Este logro es más suyo que mío, y es el fruto de muchos sacrificios que ustedes hicieron a lo largo de sus vidas para que la mía pudiera ser mejor. Ustedes son las personas que más feliz me hacen y no hay ningún día en que no piense en ustedes y los extrañe. Tía More y Marcos, los quiero muchísimo, cada día sin ustedes me pesa. Agradezco a mis tíos y primos por el apoyo y los buenos momentos. A mi abue Yolanda por siempre estar dispuesta a ayudarnos y recordarme que estamos en sus pensamientos. A mi papá por ser un ejemplo de honestidad y trabajo. A mi mamá por su amor incondicional y por los apapachos. A mi hermano por el apoyo y las tonterías, eres mi mejor amigo. A mi esposa por apoyarme en las rarezas que acompañan a mi profesión y por su amor, que me ha dado una razón para vivir. A todos ustedes los amo mucho y estoy eternamente agradecido de que sean mi familia.

Dedico esta tesis a mi abuelita. Soy la persona más afortunada por haber crecido a tu lado. Te amo infinitamente, nada puede llenar el gran vacío que dejas en mi vida. Te llevas mi corazón por siempre.

ABSTRACT

Why do organisms look the way they do? Why do they live where they do? Why are some groups more diverse than others? These basic questions are often addressed at different scales using a particular set of methods. For example, the first question could be addressed by either looking at phenotypes across a phylogeny in a comparative framework or by looking at fine scale variation across the landscape within a species. However, it has been challenging to build a conceptual and methodological bridge linking ecological processes and population dynamics with evolutionary and biogeographic patterns above the species level. In this thesis, I present research spanning a broad range in the continuum between micro- and macroevolution. Appropriately, my study system is monitor lizards (Squamata: Varanidae), the terrestrial vertebrate genus showing the largest disparity in body size. These charismatic reptiles display notable variation in species richness, morphology, and ecology across the three continents and numerous oceanic islands they call home. I gathered large molecular, morphological, and environmental datasets and analysed them using process-based methods linking ecological and population-level processes with speciation and macroevolutionary patterns. I used this integrative approach to identify the drivers of genetic, phenotypic, and lineage diversification in Varanidae at different evolutionary scales. In Chapter I, I show that the diversification dynamics of three endemic varanid radiations in Indo-Australasia have been dictated by a combination of geography and interspecific interactions. In Chapter II, I demonstrate that ontogenetic lability is behind morphological diversification in varanids and their kin, and that ontogenetic ecological shifts in ecology explain some of the ontogenetic variation in the group. In Chapter III, I used a comprehensive approach to uncover signs of ancient hybridization between the iconic Komodo dragon and a group of Australian varanids, corroborating the Australian origin of the former. In Chapter IV, I evaluate species limits in spiny-tailed monitors and present genomic and phenotypic evidence for local adaptation despite extensive gene flow. Together, these chapters show how the integration of multiple sources of evidence can offer insight into the long-term evolutionary consequences of developmental, ecological, and population-level processes.

TABLE OF CONTENTS

Introduction……1

Chapter I……4

Competition and geography underlie speciation and morphological evolution in Indo-Australasian monitor lizards

Chapter II……42

Ontogenetic drivers of morphological evolution in monitor lizards and allies (Squamata: Paleoanguimorpha), a clade with extreme body size disparity

Chapter III……72

A comprehensive approach to detect hybridization sheds light on the evolution of Earth's largest lizards

Chapter IV……103

Geographic sorting of genetic and phenotypic variation through gene flow and selection in a monitor lizard species complex

Synthesis……146

References……149

Supplementary Material……153

Chapter I……154

Chapter II……168

Chapter III……192

Chapter IV……222

INTRODUCTION

The presence of life separates our planet from the countless astronomical objects in the universe (as far as we know). Thus, it is no surprise that there is great interest in how the approximately 8.7 million species that currently inhabit Earth (Mora et al. 2011) originated. A range of possibilities have been explored since antiquity (Ruse 2009), but our understanding of the origins of biodiversity reached a turning point with the publication of Darwin's *On the Origin of Species*. Darwin (1859) formalized the concepts of evolution by natural selection and, perhaps more importantly, common ancestry; i.e., that species descend from common ancestors in a way that can be depicted as a branching tree. A more recent revolution in evolutionary biology was prompted by the ever-increasing availability of large molecular datasets, surges in computational power, and the development of new tools to characterize and analyse phenotypes. This progress has answered many long-standing questions on the origins of biodiversity, but has also uncovered additional issues requiring attention and novel ways in which we can address old questions.

Despite decades of ongoing research, it remains unclear what are the long-term evolutionary consequences of ecological, developmental, and population-level processes (Simons 2002; Klingenberg 2010; Hembry and Weber 2020). Particular attention has been paid to the macroevolutionary significance of interspecific interactions. These are at the core of many macroevolutionary theories, such as ecological opportunity and adaptive radiation, the Red Queen theory, clade replacement theories, and coevolutionary arms races (Harmon et al. 2019). Recently, novel conceptual and methodological approaches have been developed to evaluate the effects on interspecific interactions over deep time scales. These have revealed that interspecific interactions have had a profound impact on lineage diversity, geographic distributions, and phenotypic evolution (Pedersen et al. 2014; Condamine et al. 2019; Brennan et al. 2021)

The field of evolutionary developmental biology (evo-devo) has largely focused on the genetic, epigenetic, and morphological aspects of embryologic development, and how they relate to broad-scale patterns of morphological variation (Müller 2007). In contrast, the evolution and long-term effects of postnatal development remain relatively understudied. Ontogenetic allometry, changes in the phenotype as a consequence of growth, is traditionally considered to be an evolutionary constraint because size imposes restrictions on morphological variation (Simpson 1944; Gould and Lewontin 1979;

Klingenberg 2016). However, recent empirical studies have shown that postnatal ontogeny is evolutionary labile and may be molded by selection (Klingenberg 2010; Esquerré et al. 2017; Gray et al. 2019). In this way, the study of postnatal ontogenetic allometry has shed light on the mechanisms underpinning morphological evolution.

Infraspecific patterns of genetic and morphological variation are shaped by a variety of processes, such as gene flow, selection, genetic drift, mutation, and founder effects (Hedrick 2011). Evolutionary research in the early twentieth century largely focused on the study of these evolutionary forces as generators and shapers of biological variation (Huxley 1942). However, whether all of these forces play a major role in macroevolution is still being discussed actively (Erwin 2000; Simons 2002). The generation of large molecular datasets and creation of new analytical approaches has provided new tools for evaluating the relevance of processes occurring within and between populations over geological timescales. Gene flow was particularly challenging to detect and quantify before genomic scale data became available. Traditionally considered a homogenising agent (Mayr 1942; Slatkin 1985), there has been a recent reappraisal of the creative potential of gene flow. Gene flow can increase the variation upon which selection can act (Barrett and Schluter 2008; Grant and Grant 2019), being a major factor behind some classical examples of adaptive radiation (Lamichhaney et al. 2015; Meier et al. 2017), and promote speciation when interspecific hybrids are self-compatible (or parthenogenetic) and incompatible with parental lineages (Mallet 2007).

Empirically testing the issues presented above requires the selection of a suitable taxon to serve as model. Monitor lizards (Squamata: Varanidae) are a group of around 80 described extant species with a collective distribution that includes most of Africa, southern Asia, the Indo-Australian Archipelago, Micronesia, Melanesia, and Australia (Pianka and King 2004; Brennan 2021). Varanids reach their highest diversity in Australia, which is home to 30 described species (Wilson and Swan 2017). In areas of northern Australia, as many as 10 species live sympatrically (Cogger and Heatwole 1981). Other relatively small regions have a high diversity, such as Melanesia (18 species) and the Philippine archipelago (10 species). In contrast, there are only five species in the huge African continent (Koch et al. 2013; Uetz et al. 2020).

Varanids show a conserved body plan: all species have relatively long snouts, four pentadactyl limbs, and long tails. This is reflected by the classification of all living varanids under a single genus (*Varanus*). However, varanids differ substantially in a trait that crucially affects the ecology, life history, and morphology of animals: body size (Thompson 1917; Kingsolver and Pfennig 2004). In fact, *Varanus* is the terrestrial vertebrate genus showing the largest variation in body size (Pianka 1995). The largest monitor, the Komodo dragon (*Varanus komodoensis*), is also the largest living lizard. It

is a powerful carnivore exceeding 3 m in total length that can take down large prey such as deer, buffalo, and humans (Auffenberg 1981). The even larger megalania (*V*. *priscus*) is a recently extinct species that surpassed 5 m in total length, making it the largest terrestrial lizard to have ever lived (Molnar 2004). In contrast, the smallest species, the closely related *V*. *brevicauda* and *V*. *sparnus*, reach only around 25 cm in total length (Doughty et al. 2014). While morphological variation in monitor lizards is largely explained by allometric effects associated with body size disparity (Thompson and Whiters 1997; Christian and Garland 1996; Clemente et al. 2011). However, some of the morphological variation reflects the ecology of each species. The evolution of body size itself seems to have been influenced by habitat use (Collar et al. 2011), which coupled with foraging mode, diet, and bipedal scouting behaviour also seem to have driven size-independent phenotypic evolution in the family (Thompson and Whiters 1997; Thompson et al. 2008; Schuett et al. 2009; Openshaw and Keogh 2014; Openshaw et al. 2016).

The variety of environmental conditions that varanids face worldwide, the cooccurrence of varanid species across much of their range, and the ecomorphological variation in the group, make monitor lizards an appropriate model to analyse the complex interactions between environment, ecological interactions, genotype, and phenotype across space and time. Here, I gathered and compiled molecular, morphological, and environmental data for all varanid species. I used these data to evaluate the effects of past events and current conditions on genetic and morphological variation, using a combination of recently developed and novel approaches. My findings shed light on how the environment shapes biodiversity, on the long-term consequences of ecological scale processes, and on the evolutionary history of the iconic monitor lizards.

CHAPTER I

Competition and geography underlie speciation and morphological evolution in Indo-Australasian monitor lizards

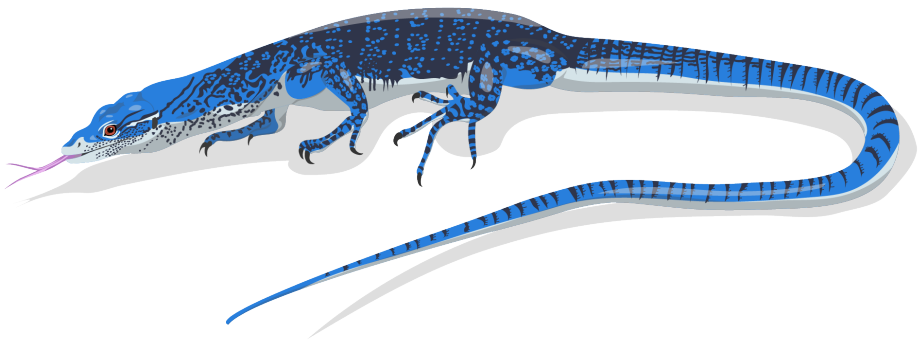

COMPETITION AND GEOGRAPHY UNDERLIE SPECIATION AND MORPHOLOGICAL EVOLUTION IN INDO-AUSTRALASIAN MONITOR LIZARDS

Carlos J. Pavón-Vázquez[1,2], Ian G. Brennan[1], Alexander Skeels[3,4], J. Scott Keogh[1]

[1]Division of Ecology and Evolution, Research School of Biology, Australian National University, Canberra, ACT 2601, Australia

[2]E-mail: cjpvunam@gmail.com

[3]Landscape Ecology, Department of Environmental Systems Science, Institute of Terrestrial Ecosystems, ETH Zürich, 8092 Zürich, Switzerland

[4]Swiss Federal Research Institute for Forest, Snow and Landscape Research (WSL), 8903 Birmensdorf, Switzerland

Abstract

How biotic and abiotic factors act together to shape biological diversity is a major question in evolutionary biology. The recent availability of large datasets and development of new methodological approaches provide new tools to evaluate the predicted effects of ecological interactions and geography on lineage diversification and phenotypic evolution. Here, we use a near complete phylogenomic-scale phylogeny and a comprehensive morphological dataset comprising more than a thousand specimens to assess the role of biotic and abiotic processes in the diversification of monitor lizards (Varanidae). This charismatic group of lizards shows striking variation in species richness among its clades and multiple instances of endemic radiation in Indo-Australasia (i.e., the Indo-Australian Archipelago and Australia), one of Earth's most biogeographically complex regions. We found heterogeneity in diversification dynamics across the family. Idiosyncratic biotic and geographic conditions appear to have driven diversification and morphological evolution in three endemic Indo-Australasian radiations. Furthermore, incumbency effects partially explain patterns in the biotic exchange between Australia and New Guinea. Our results offer insight into the dynamic history of Indo-Australasia, the evolutionary significance of competition, and the long-term consequences of incumbency effects.

Keywords: Biogeography, ecological interactions, incumbency, morphology, Varanidae, *Varanus*

Abiotic and biotic factors act together to shape biodiversity. The evolutionary significance of abiotic factors such as climate change, tectonics, and mountain uplift in lineage and phenotypic diversification is well established (Badgley et al. 2017; Hoorn et al. 2018; Esquerré et al. 2019; Covreur et al. 2021). Ecological interactions, and particularly interspecific competition, are also thought to drive many key evolutionary processes, such as adaptive radiation and clade replacement (Stanley 1973; Stroud and Losos 2016; Harmon et al. 2019; Hembry and Weber 2020). However, evaluating the evolutionary significance of competition at deep time scales has been particularly challenging (Schenk et al. 2013; Harmon et al. 2019). Recently developed theoretical and methodological frameworks explicitly incorporate proxies for competition into models of lineage and phenotypic diversification (e.g., Etienne et al. 2012; Drury et al. 2016; Brennan et al. 2021). Lineage diversity, biogeography, and morphology are commonly employed, assuming that competition requires sympatry and increases with lineage density and morphological similarity. These approaches have been used to gain insight into the relevance of ecological interactions for lineage diversification and phenotypic evolution in insular and continental radiations (e.g., Valente et al. 2015; Drury et al. 2016, 2018; Skeels and Cardillo 2019a; Brennan et al. 2021).

Another approach to investigate the relevance of competition in diversification dynamics is the study of incumbency effects. Incumbency effects are the advantages a lineage gains by being present in an area earlier than ecologically similar taxa (Alroy 1996; Rowsey et al. 2019). Several predictions can be made about the ecological and evolutionary outcomes of incumbency, including lower diversification rates in secondary colonizers (hereafter “immigrants”) due to reduced ecological opportunity and morphological disparity between incumbents and immigrants due to biotic filtering (Gillespie 2004). Incumbency effects have been thoroughly documented in the ecological timescale (Shulman et al. 1983; Drake 1991; Fukami et al. 2007; Fukami 2015), but there is mixed support for the relevance of these effects over evolutionary timescales (Schenk et al. 2013; Rowsey et al. 2018, 2019).

Indo-Australasia is one of the most geologically complex and biodiverse regions of Earth (Myers et al. 2000; Lohman et al. 2011), making it a suitable location to study the interplay between geography and competition in evolutionary dynamics. This region includes Australia and the more than 20,000 islands that separate it from mainland Asia (Lohman et al. 2011). Beginning in the Eocene, the history of Indo-Australasia has been marked by extensive island formation as a result of the northern subduction of the Australian plate as it approached Asia (Hall 2002). This paved the ground for the biotic interchange between mainland Asia and Australia, and also provided opportunity for in-

situ radiation in the Indo-Australian Archipelago (Lohman et al. 2011; Moyle et al. 2016; Andersen et al. 2018). In the Quaternary, sea level fluctuations, environmental change, and mountain uplift shaped biogeographic patterns at a finer scale (Lohman et al. 2011; Brown et al. 2013; Byrne et al. 2008, 2011). Within the conditions laid by this geographic context, competition also seems to have influenced speciation, morphological evolution, and community assemblage (Rowsey et al. 2018, 2019; Skeels and Cardillo 2019a; Brennan et al. 2021; Skeels et al. 2021).

In this study, we use phylogenetic, biogeographic, and morphological data to characterize the diversification history and morphological evolution of monitor lizards, highlighting the influence of competition and geography in the evolution of Indo-Australasian lineages. Monitor lizards constitute the family Varanidae, a group of around 80 species—all in the genus *Varanus*—distributed in Africa, southern Asia, numerous Pacific islands, and Australia (Pianka and King 2004; Brennan et al. 2021). Species richness is phylogenetically and geographically heterogeneous in Varanidae. For example, Africa has only five monitor species, the comparatively tiny Philippine archipelago 10 species, and Australia over 30 species. Major biogeographic regions are occupied primarily by endemic radiations of closely related taxa, with few instances of secondary colonization by species from other clades (Fig. 1). These endemic radiations vary in their age, species richness, biogeographic context (insular or continental), and phenotypic diversity, providing a unique opportunity to comparatively study diversification dynamics in closely related species with a similar biology. Three Indo-Australasian clades are specially diverse, concentrating more than 80% of varanid diversity. These radiations are mainly distributed in Australia, Malesia, and New Guinea, respectively.

Despite the fact that Australia and New Guinea have been intermittently connected throughout the Pleistocene (Voris 2000), there has been limited interchange of taxa between the varanid radiations occurring on each of these landmasses. Presently, only three species of a mainly New Guinean clade inhabit Australia (*V. chlorostigma*, *V. doreanus*, and *V. keithhornei*), and the same number of species from a primarily Australian clade are present in New Guinea (*V. panoptes*, *V. salvadorii*, and *V. scalaris*). All six species represent recent independent colonization events. This suggests that the earlier presence of varanids in each of the two regions could be preventing the establishment and diversification of secondary colonizers.

Here, we analyze the most complete comparative dataset of monitor lizards assembled to date using recently developed methods to characterize their lineage and phenotypic diversification dynamics. Our data consist of a phylogeny based primarily on a large multi-locus alignment (Brennan et al. 2021), linear morphometric data for body

size and body shape, and two-dimensional geometric morphometric data for head shape. Specifically, we ask: 1) Is the higher diversity of the Indo-Australasian radiations associated with higher rates of speciation and morphological evolution? 2) Has species diversity and morphological disparity accumulated in each of these clades in a way that is consistent with their biotic and/or geographic context? 3) Does the biotic exchange between Australia and New Guinea show signs of incumbency effects? Our results offer insight into the biogeography of the Indo-Australasian region, the long-term consequences of ecological interactions, and the importance of incumbency effects in the shaping of diversity and the geographic sorting of morphological variation.

Materials and Methods

Taxonomic background

There are approximately 80 extant varanid species classified in one genus (*Varanus*) and 11 subgenera (Bucklitsch et al. 2016; Brennan et al. 2021) (Fig. 1). Uncertainty exists around the taxonomy of several nominal species of the mainly New Guinean *Euprepiosaurus* and *Hapturosaurus* subgenera and mainly Australian *Odatria*. This required us to make decisions on what we are treating as species for the purposes of this study, in order to fit the assumptions of the comparative methods we used. These decisions are reflected in our assessment of a Varanidae that comprises 81 extant species. Additional details are found in the Supporting Information.

Phylogenetics

We used the time-calibrated phylogeny of Brennan et al. (2021) which is based on exons obtained through anchored hybrid enrichment (Lemmon et al. 2012) as our backbone phylogeny. This tree includes over 70% of varanid diversity, but importantly excludes the sister group of varanids (Lanthanotidae) and numerous Indo-Australasian taxa for which molecular data are available. Thus, we added tips based on previous studies and our own analyses of publicly available molecular data (Table S1). Our final tree included 76 tips: 72 currently recognized varanid species, two lineages that likely represent unacknowledged species-level diversity (*V*. *a*. *insulanicus* and *V*. sp. Solomon Islands), and two outgroups (*Shinisaurus crocodilurus* and *L*. *borneensis*) (Figs. 1, S1). Additional details about how the phylogeny was estimated are found in the Supporting Information.

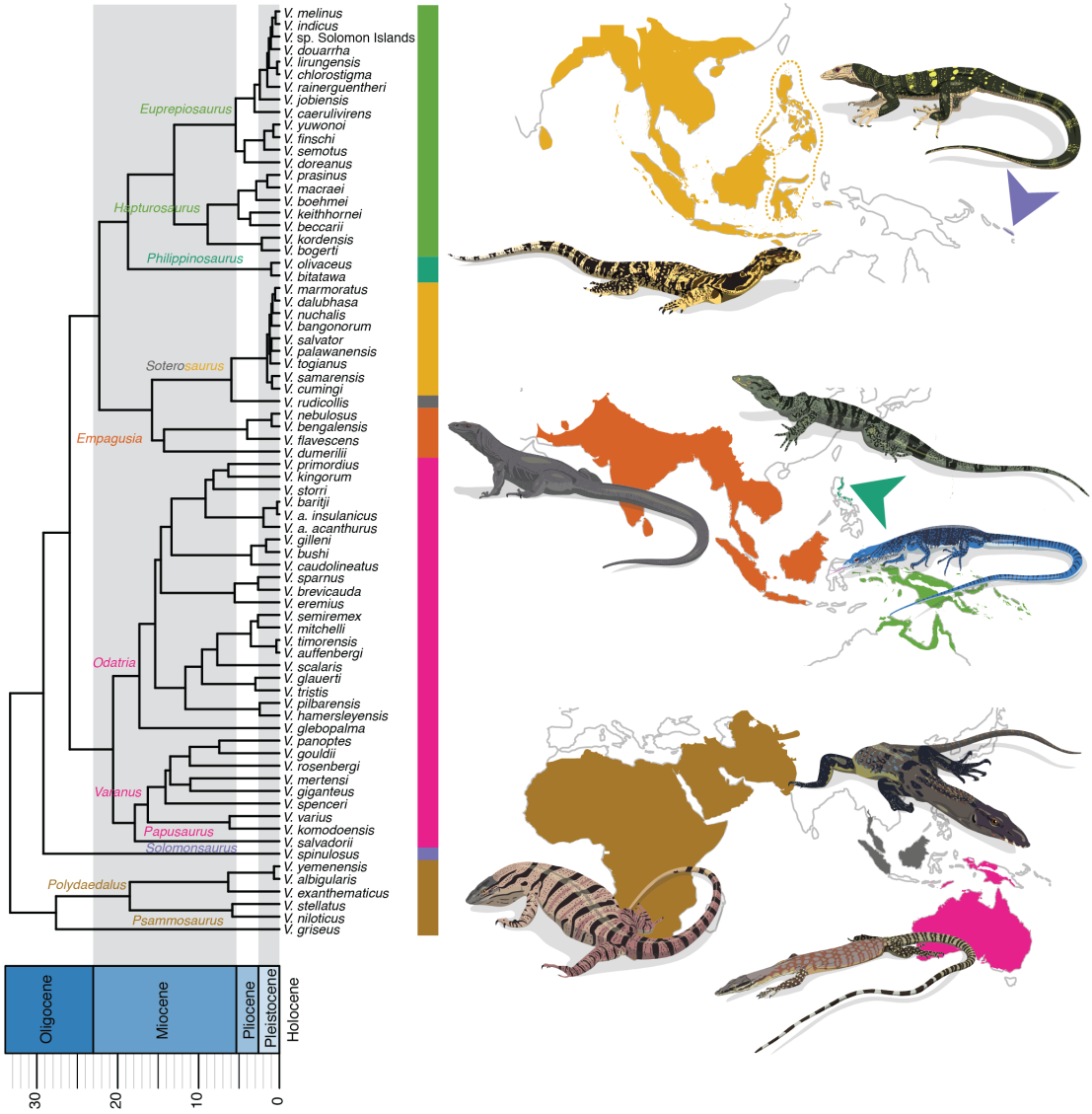

Figure 1. Phylogeny and biogeography of Varanidae. The tree is a time-calibrated phylogeny, where subgenera are indicated at nodes and main geographic clades are indicated by the colored bars on the right. Maps depict the distribution of main geographic clades. The dotted line delineates the distribution of the Malesian clade excluding *Varanus salvator*. Representatives of each clade are illustrated.

Morphological data

Body size is one of the most ecologically and evolutionarily important phenotypic characters, significantly impacting a variety of other biological traits (Thompson 1917; Kingsolver and Pfennig 2004). In varanids, body shape and head shape show strong phylogenetic signal, but ecology also seems to be an important driver of their evolution (Thompson and Whiters 1997; Pepin 2001; Thompson et al. 2009; Collar et al. 2011; Openshaw and Keogh 2014; Openshaw et al. 2014). Thus, one of us (first author) recorded body size (as snout-vent length), 13 external measurements describing body shape variation, and obtained photographs of the head in dorsal and lateral view for geometric morphometrics (Tables S2–S5). Our sampling included all the species

recognized in this study (see Supporting Information), except for *V. bitatawa*, *V. mabitang*, and *V. semotus*. However, we were able to obtain linear morphometric data and head photographs for these species from the literature (Gaulke and Curio 2001; Gaulke 2010; Welton et al. 2010; Weijola et al. 2016), except for dorsal photographs of *V. mabitang*, which was excluded from the analyses of head shape in dorsal view.

We analyzed body size separately from other characters using maximum snout-vent length (SVL) as a proxy (Stamps and Andrews 1992), which was obtained either from the literature or our own specimen examination when it resulted in new maximum SVL records (Table S2). For the remaining linear traits, we corrected for body-size using log-shape ratios, calculating size as the geometric mean of all the measurements, dividing each trait by size, and log-transforming the resulting ratios (Mosimann, 1970). We characterized dorsal and lateral head shape using landmark-based, two-dimensional geometric morphometrics (Fig. S2). We performed a generalized Procrustes analysis (GPA) to remove the effects of size, location, and orientation (Gower 1975), taking bilateral symmetry into account for the dorsal view and using the symmetric component of shape in subsequent analyses. More details on the processing of morphological data are found in the Supporting Information.

In summary, we obtained four morphological datasets: SVL, corresponding to log transformed maximum SVL (based on examined specimens and the literature); body, corresponding to the log-shape ratios of 13 linear morphometric characters, excluding SVL (total specimens (n) = 1,041; mean sample size per species ($\bar{X}$) = 12.85); dorsal-head, corresponding to the aligned Procrustes coordinates of the head in dorsal view (n = 1,022; $\bar{X}$ = 12.78); and lateral-head, corresponding to the aligned Procrustes coordinates of the head in lateral view (n = 1,090; $\bar{X}$ = 13.46). Except for maximum SVL, we used the species means of each trait in all downstream analyses.

Biogeography

Based on our phylogeny, we divided Varanidae into eight major geography-concordant clades (included subgenera/species in parentheses): Afro-Arabian (*Polydaedalus* and *Psammosaurus*), Australian (*Odatria*, *Papusaurus*, and *Varanus*), Malesian (*Soterosaurus*, except for *V. rudicollis*), Malay (*V. rudicollis*), Melanesian (*Solomonsaurus*), Oriental (*Empagusia*), Papuan (*Euprepiosaurus* and *Hapturosaurus*), and Philippine (*Philippinosaurus*) (Fig. 1). We reconstructed the biogeographic history of monitor lizards for downstream analyses using maximum likelihood in the 'BioGeoBEARS 1.1.2' (Matzke 2013) R package. We classified the range of monitor lizards into discrete areas primarily based on the zoogeographic realms of Holt et al.

(2013) (Fig. S3). Additional details and the results of this analysis are presented in the Supporting Information.

Diversification of Indo-Australasian radiations

To gain insight into how different ecological and biogeographic settings drive diversification we compared the three most speciose varanid radiations, all of which occur in Indo-Australasia: the Australian, Malesian, and Papuan clades. These radiations vary in their richness (31, 11, and 24 species, respectively), crown age (~21 Ma, ~2 Ma, and ~13 Ma), and biogeographic context (mainly continental, mainly insular, and a large central island with smaller satellite islands).

First, we tested whether the high diversity of the Australian, Malesian, and Papuan clades is associated with accelerated speciation rates. We estimated branch-specific rates in ClaDS (Maliet et al. 2019), a Bayesian approach that relies on a model where shifts in diversification rates occur at each cladogenetic event (Maliet et al. 2019). Using 'RPANDA 1.7' (Morlon et al. 2016), we fitted the ClaDS2 model, which assumes varying extinction rates and constant turnover. We accounted for incomplete taxon sampling and ran three chains for 200,000 generations with a thinning of 1,000. To detect clade-specific shifts in speciation rates without having to specify hypotheses a priori we used the "search.shift" function of 'RRphylo 2.4.7' (Castiglione et al. 2018). This function takes branch-specific rates and computes the difference between the mean rates of all clades of a given size (four in our case) and the rest of the tree. Clade-specific differences are then compared to a null distribution of rate differences obtained through the randomization of branch rates. Probability values (p) > 0.975 indicate significantly higher rates at the 0.05 significance level, while p < 0.025 indicates rates are significantly lower. The clade with the largest difference with the rest of the tree is selected from each set of nested clades with significant differences. Additionally, we used the same function to compare background rates to those of Indo-Australasian clades. When clades are specified, "search.shift" compares the mean rates of each individual clade with background rates, excluding the other clades for which shifts are being evaluated. It also tests for differences between background rates and all the clades taken together, considering that they evolve under a single rate (Castiglione et al. 2018).

We characterized the tempo and mode of diversification of each endemic radiation to evaluate whether they are consistent with their ecological and geographic setting. To initially detect signs of temporal variation in speciation rates, we obtained lineage-through-time (LTT) plots with 'phytools 0.7.62' (Revell 2012) and compared them to a null distribution of 1,000 LTTs simulated under a pure-birth process. We also calculated the γ statistic. Negative values of γ indicate that the internal nodes of a phylogeny are

closer to the root than expected (i.e., early burst or rate decrease), while positive values indicate that internal nodes are closer to the tips (i.e. acceleration or constant rates with extinction) (Pybus and Harvey 2000; Fordyce 2010). We performed a two-tailed test of γ that accounts for incomplete sampling in our phylogeny as implemented in 'phytools', obtaining a null distribution of the statistic for 10,000 phylogenies simulated under a pure-birth process from which some taxa are pruned to reflect the empirical sampling proportion (Monte Carlo constant-rates test [MCCR]; Pybus and Harvey 2000). Additionally, we employed 'RPANDA 1.7' (Morlon et al. 2011, 2016) and 'DDD 4.4' (Etienne and Haegeman 2020) to fit a total of 13 pure-birth, birth-death, and diversity dependent models through maximum likelihood. We fitted these models to the best tree of each clade and a sample of 100 trees generated using the "swapONE" function of 'RRphylo'. These trees had 25% of tip positions and node lengths modified from the best tree, forcing nodes with PP > 0.95 to be monophyletic. We compared models based on their sample-size-corrected AIC (AICc) and AICc weights (AICcw).

Finally, we inferred the geographic mode of speciation for each endemic radiation. Besides informing about the abiotic factors responsible for speciation, inferring the geographic mode of speciation can shed light on the ecological and evolutionary processes that have been responsible for diversification and community assemblage (Fitzpatrick et al. 2009; Stroud and Losos 2016; Skeels and Cardillo 2019b). Inference based solely on present day species' distributions without accounting for historical processes can be misleading (Warren et al. 2014). Thus, we implemented the dynamic range evolution and diversification model (DREaD), a process-based simulation approach that has been shown to accurately recover the geographic mode of speciation (Skeels and Cardillo 2019b). DREaD models speciation in a continuous geographic space instead of discrete areas. Thus, estimation of some of the metrics requires polygons depicting the species' ranges. We obtained these from Roll et al. (2017) and updated them to reflect current knowledge on the distribution and taxonomy of varanids (Supporting Information). Skeels and Cardillo (2019b) generated 30 phylogenetic and biogeographic summary metrics from 35,731 simulations of the DREaD model under different scenarios of environmental change, niche evolution, dispersal rate, clade size, and geographic speciation modes. Following Skeels and Cardillo (2019b), we obtained the empirical values for 14 of these metrics for each clade and used linear discriminant analysis (LDA) and two approximate Bayesian computation (ABC) methods (i.e., multinomial logistic regression (mnL) and neural net (NN)) to compare them against the simulated values and select among vicariant, parapatric, sympatric, founder-event, and mixed modes of speciation.

Morphological evolution of Indo-Australasian radiations

To visualize differences in morphological diversity across the varanid phylogeny we plotted clade-specific boxplots of maximum SVL and performed principal component analysis (PCA) on the body and head shape datasets. We overlaid the phylogeny on the PCA plots to frame morphological variation in a phylogenetic context (Sidlauskas 2008). We also estimated the degree of ecological diversity in varanids, using morphology as a proxy. In order to do this, we detected shifts towards different adaptive optima in 'l1ou 1.42' (Khabbazian et al. 2016). The method is based on the lasso (Tibshirani and Taylor 2011) and an OU model of trait evolution. The approach does not require a priori assumptions on the location of shifts and can handle multivariate data. We performed the analyses on the SVL dataset and first PCs of each multivariate dataset accounting for 95% of variation. Model selection was based on the phylogenetic-aware information criterion (pBIC), which is more conservative than other information criterions (Khabbazian et al. 2016).

To assess variation in the rates of morphological evolution we estimated branch-specific rates for each morphological dataset in 'RRphylo' (Castiglione et al. 2018). For all analyses of SVL, we considered the same character as covariate so that larger rates are not misleadingly inferred for lineages with larger body sizes (Castiglione et al. 2018). We first used the "RRphylo" function, which estimates branch specific rates of evolution and ancestral states for multivariate data based on phylogenetic ridge regression (Castiglione et al. 2018). Then we employed the hypothesis-free implementation of the "search.shift" function to detect shifts in the rates of morphological evolution. We also used the "search.shift" function to compare the background rates of morphological evolution with those of each Indo-Australasian clade and all of them together. We used the "overfitRR" function to evaluate the sensitivity of both implementations of "search.shift" to sampling and phylogenetic uncertainty. This function tests the robustness of results by iteratively removing tips and rearranging them. We specified 100 tree-modification iterations, forcing nodes with PP > 0.95 to remain monophyletic, removing 25% of tips, and modifying the position and age of 25% of tips and nodes, respectively.

To explore temporal trends of morphological disparity in the Australian, Malesian, and Papuan clades we obtained a disparity-through-time (DTT) plot for each clade using 'geiger 2.0.6.4' (Pennell et al. 2014). For each clade and morphological dataset, we specified Euclidean distance as disparity measure. We tested whether DTT deviates from expectations under BM using the rank envelope test (Murrell 2018), which compares the empirical DTT with 2,500 simulations under Brownian motion (BM). Additionally, for each clade we calculated the morphological disparity index (MDI), which

indicates whether disparity is mainly driven by differences between (MDI < 0) or within (MDI > 0) subclades, and assessed its significance by comparing it to values of MDI obtained from 1,000 simulations under BM (Harmon et al. 2003). Finally, we used a model fitting approach to characterize the dynamics of morphological evolution in each of the three Indo-Australasian clades. We first fitted multivariate models of trait evolution that account for measurement error/intraspecific variation to each of our multivariate datasets in 'RPANDA'. We used the function "fit_t_pl", which uses penalized likelihood to overcome complications arising when the number of traits approaches or exceeds the number of species (Clavel et al. 2019). We compared BM, Ornstein-Uhlenbeck (OU), and early burst (EB) models, ranking them based on the generalized information criterion (GIC). We fitted the multivariate models to the best tree and the sample of 100 trees obtained with "swapONE" (see above). The implementation of models that explicitly incorporate interspecific competition such as linearly and exponentially diversity dependent models (DDl, DDe) and the matching competition model (MC) (Drury et al. 2016) with the "fit_t_comp" function of 'RPANDA' is limited to univariate data. Thus, we fitted these models to the SVL dataset and the first PC of each multivariate dataset. We limited competition to species occurring in the same region based on 50 stochastic character maps obtained from the results of the preferred 'BioGeoBEARS' model. We compared the models incorporating competition against each other and against BM, OU, and EB models fitted in 'geiger 2.0.6.4' (Pennell et al. 2014) based on their AICc and AICcw.

Incumbency effects

The large size of the Australian and Papuan clades compared to other varanid clades and the recurrent connection between these two landmasses provide a suitable system to evaluate incumbency effects. We investigated the potential impact of incumbent lineages on the diversification rates of immigrants by fitting a series of island-assembly models using the R package 'DAISIE 1.4' (Valente et al. 2015). This framework uses the temporal accumulation of species from phylogenetic and island-age information to estimate diversification parameters (speciation, extinction, immigration). For the Australian and New Guinea monitor faunas, we started by identifying taxa as endemic (incumbent) or non-endemic (immigrant), with the maximum possible immigration-time of immigrant taxa set as the taxon's age. We designed and fit 35 models which estimated shared or split diversification rates for incumbent and immigrant lineages, fixed some parameters to zero (extinction and immigrant speciation), and estimated speciation and immigration rates as a function of diversity dependence (linear or exponential). The specifics of all 35 models and our procedure are described in the Supporting Information.

We fit each model in parallel 10 times using a custom function ("search.surface.DAISIE"; Supporting Information) with random starting values for the necessary parameters to avoid accepting suboptimal likelihoods. Parameter values for the best model fit were then used as starting values to ensure that the optimization had converged on an appropriate result. We compared models using AIC plus the Bayesian Information Criterion (BIC), as it has proved to be more conservative and exhibit lower error rates in the comparison of 'DAISIE' models (Valente et al. 2020).

We also tested whether there is evidence for incumbency effects on the phenotype. We started by visually comparing each immigrant species to the incumbent taxa with which it co-occurs in its secondary range, as well as to close relatives of those incumbent taxa (Rowsey et al. 2019). We employed boxplots for SVL and PCA plots for the multivariate datasets. Additionally, we compared the empirical values of the disparity between the immigrant and incumbent species to a null distribution of disparity values. For each morphological dataset, we calculated Euclidean distances between each immigrant taxon and the species of the incumbent clade with which it co-occurs in the immigrant taxa's secondary range. We used the mean of these distances (*d*) as test statistic. To obtain a null distribution of *d*, we performed 1000 iterations where we calculated *d* for a sample of taxa containing one species taken at random from the clade to which the immigrant taxon belongs and a random sample of species from the incumbent clade, the number of species being equal to that with which the immigrant taxon co-occurs. To obtain *p*, we calculated the proportion of simulated values greater than or equal to the empirical value. Low *p* values would indicate that the immigrant and incumbent taxa are more different to each other than expected by chance given the morphological variation present in their respective clades, suggesting that biotic filtering is precluding ecologically similar immigrants from becoming established (Gillespie 2004; Rowsey et al. 2019).

Results

Diversification of Indo-Australian radiations

Results of the diversification analyses are summarized in Table 1. ClaDS revealed substantial variation in speciation rates across the varanid phylogeny (Fig. 2a, b). Th hypothesis-free implementation of "search.shift" suggests that rates are particularly high in a clade nested within the Papuan radiation—*indicus* group (p = 1)—and low in the Afro-Arabian (p = 0.001) and Australian clades (p = 0.001). The guided implementation

of “search.shift” indicates that the rates of Indo-Australasian radiations are higher than background rates, both when compared individually and together (Table S6).

The LTT plots show that, in general, lineages accumulated earlier than expected under a pure-birth process in the Australian clade and later than expected in the Papuan clade (Fig. S4). The deviation is clearer in the Australian radiation. In the Malesian clade there are more lineages than expected roughly halfway through its evolutionary history. Similarly, the γ statistic indicates that internal nodes are clustered towards the past in the Australian (γ = –1.7, p = 0.09) and Malesian clades (γ = –2.74, p = 0.006), and towards the present in the Papuan clade (γ = 0.79, p = 0.32), but the test was only significant for the Malesian clade. Models with diversity-dependent speciation rates were favored for the Australian and Malesian clades, while a pure-birth model where speciation rates first decrease and then increase towards the present best fit the Papuan clade (Fig. 3a; Tables S7–S9).

The DREaD analyses (Fig. 3b; Table S10) suggest that founder-event speciation has driven the diversification of the Australian clade (PP: LDA = 0.51, mnL = 0.49, and NN = 0.59). However, a mixed mode of speciation is also well supported (PP: LDA = 0.31, mnL = 0.47, and NN = 0.16), and a plot of the first two linear discriminant functions (LDs) (accounting for over 95% of variation) shows that the clade falls where clusters of simulations performed under all different modes meet. Vicariance is well supported as the main speciation mode in the Malesian clade (PP: LDA = 0.99, mnL = 0.98, and NN = 0.88). In the case of the Papuan clade, the importance of founder events is evident (PP: LDA = 0.99, mnL = 0.33, and NN = 0.48), but a mixed mode is well supported too (PP: LDA = 0.004, mnL = 0.59, and NN = 0.29), and the first two LDs are intermediate between the clusters simulated under the founder-event and vicariant modes.

Table 1. Proportion of simulated values of d greater than or equal to the empirical value. Large values indicate that immigrants and incumbents are more similar to each other than random members of their respective clades. Significant p values are shown in bold (considering a one-tailed test with a significance level of 0.05).

Method	Australian	Malesian	Papuan
Speciation rate shifts (unguided)	1 (negative)	0	1 (positive)
Speciation rates (guided)	High	High	High
γ	Negative (n.s.)	Negative	Positive (n.s.)
Diversification models (best tree)	Bdl_Dc	Bdl	Bl
Diversification models (tree sample)	Bdl	Bdl	Bl
Geographic speciation mode	Founder	Vicariance	Founder/Mixed

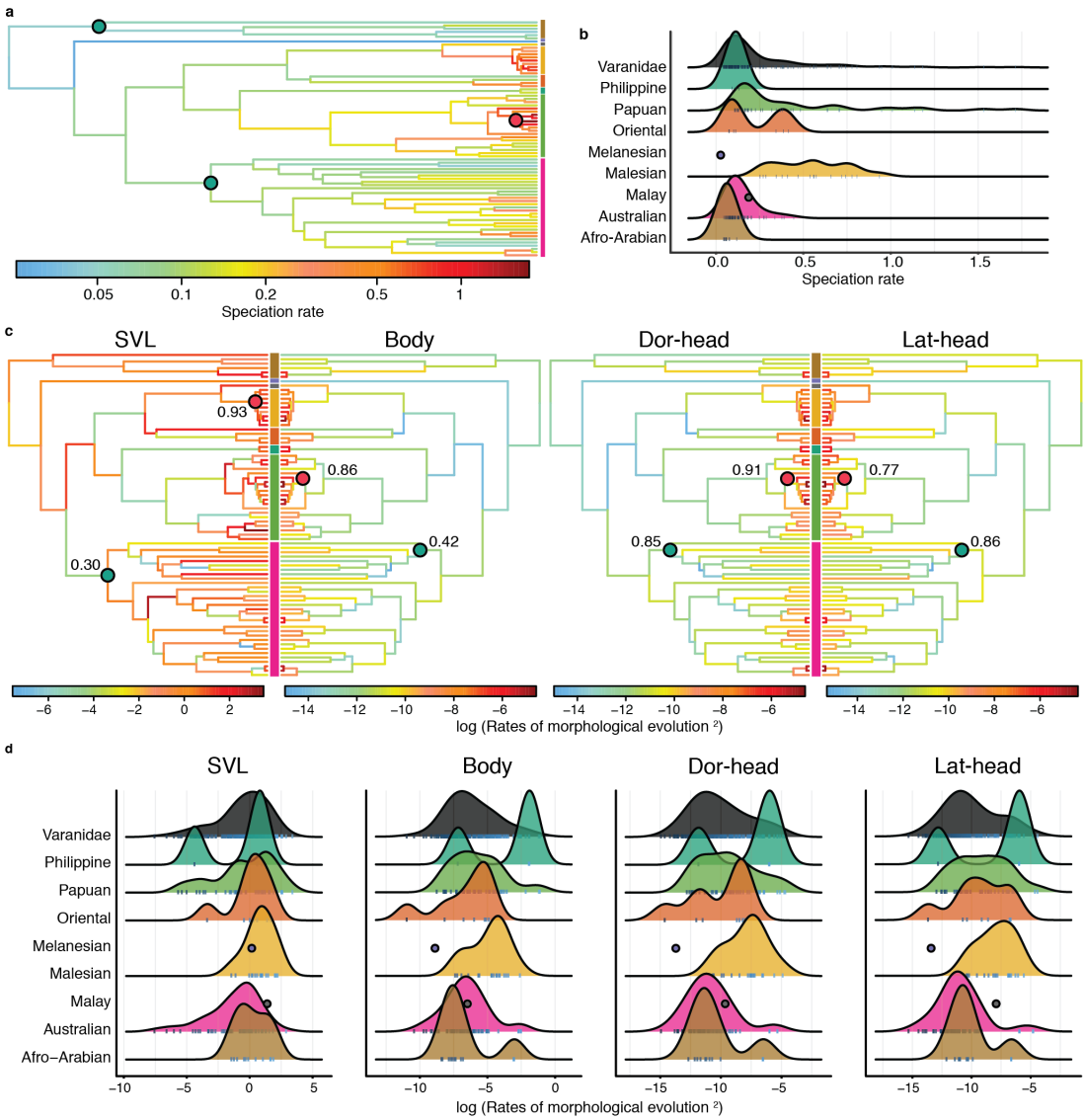

Figure 2. Diversification rate heterogeneity in Varanidae. a) Branch-specific speciation rates under the ClaDS2 model. Shifts identified through an unguided approach are represented by circles (red = positive; green = negative). b) Ridgeline plots of branch-specific speciation rates. c) Branch-specific rates of morphological evolution. Shifts identified through an unguided approach are represented by circles (red = positive; green = negative). Numbers next to circles indicate the proportion of trees with modified relationships, branch lengths, and taxon sampling in which these shifts were recovered. d) Ridgeline plots of branch-specific rates of morphological evolution.

Morphological evolution of Indo-Australian radiations

Results of the morphological analyses are summarized in Table 2. The boxplots and PCA plots show that, in general, the most morphologically diverse clade is the Australian clade (Fig. 4a). All 'l1ou' analyses detected adaptive shifts in the phenotype (Fig. 4b). For all datasets except dorsal-head, the Australian radiation showed a higher number of shifts than other clades.

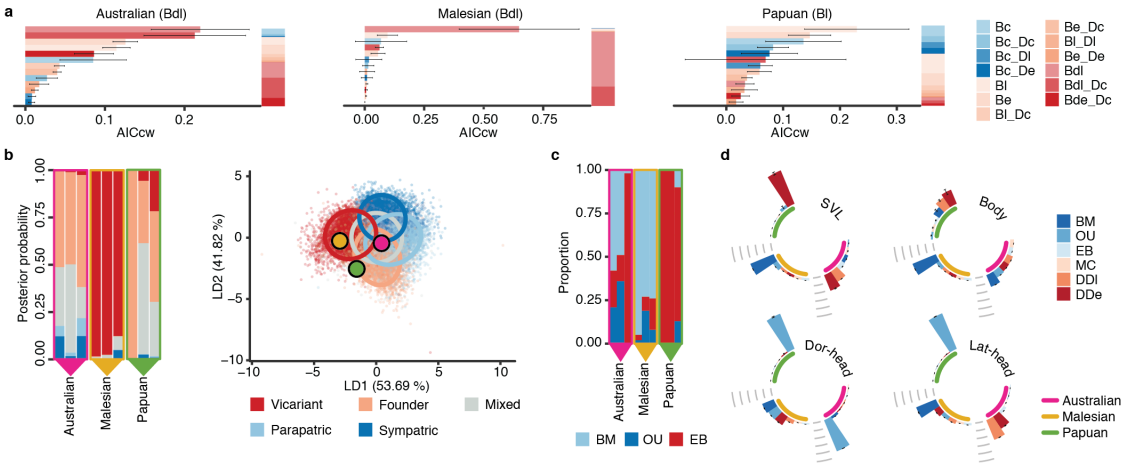

Figure 3. Tempo and mode of diversification in Indo-Australasian varanids. a) Mean and standard deviation of the AICcw of 13 diversification models evaluated for a sample of 100 trees (horizontal bars) and the best tree (stacked vertical bars) (B = speciation, D = extinction, c = constant, l = linear time dependence, e = exponential time dependence, dl = linear diversity dependence, de = exponential diversity dependence). The model with the largest AICcw is indicated in parentheses. b) Geographic mode of speciation. Boxes delineate the results for each clade shown in the legend. Support for each mode was obtained through linear discriminant analysis (left), multinomial logistic regression (middle), and neural net (right). The plot on the right shows the first two discriminant functions obtained from the LDA of empirical summary statistics and those obtained from simulations under different modes of speciation. The 95% confidence ellipses are shown for each mode. c) Proportion of trees (among a sample of 100) supporting each of three models fitted using "fit_t_pl". For each clade, results are presented for body shape (left), dorsal head shape (middle), and lateral head shape (right). d) Mean and standard deviation of the AICcw of 6 evolutionary models evaluated for a sample of 50 biogeographic stochastic maps. For each multivariate dataset, analyses were based on PC1. Inner bars indicate the geographic clades. Grey lines indicate 0.2 increases in the AICcw from 0 to 1.

Rates of morphological evolution inferred by 'RRphylo' are heterogeneous (Fig. 2c, d). The unguided approach detected a positive shift in SVL for the Malesian clade (p = 0.995); positive shifts within the Papuan clade, specifically in the clade containing *V. jobiensis* and its sister group, in all datasets except for SVL (p = 1 in all datasets); and negative shifts in the Australian clade, specifically in the ancestral node of the whole clade for SVL (p = 0.001) and among a clade containing large-bodied species for the other datasets (p = 0.002 in body dataset, p = 0.001 in other datasets). The approach testing for differences between background rates and those of the Indo-Australian clades revealed several instances in which rates of morphological evolution were significantly higher in the Malesian and Papuan clades, while rates were significantly lower for SVL in the Australian clade (Table S6). The location of the shifts identified through the free and directed approaches was moderately robust to sampling and phylogenetic uncertainty (Fig. 2c).

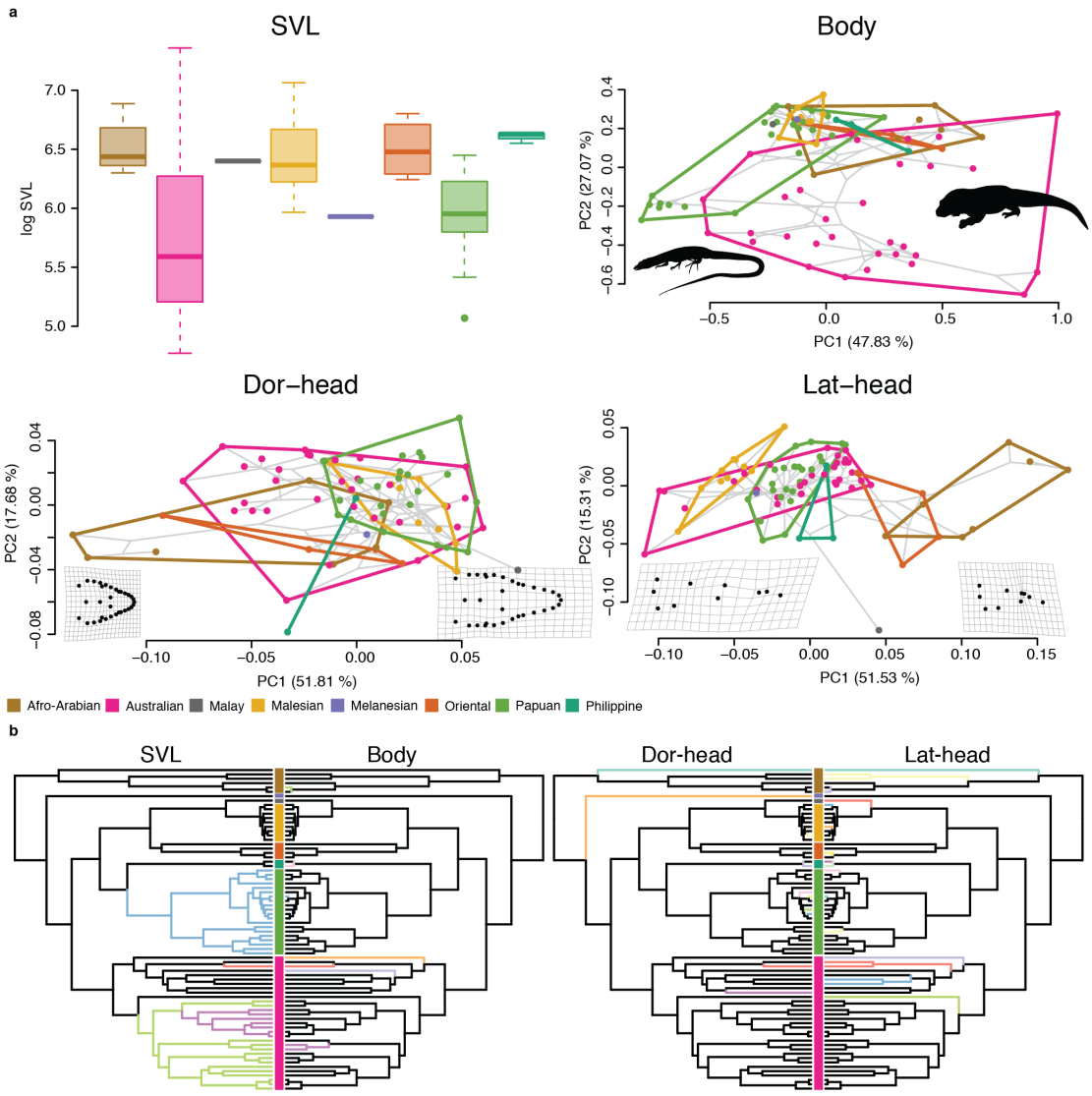

Figure 4. Morphological variation in Varanidae. a) Variation by clade. In the PCA plots, the phylogeny is represented by the grey lines, convex hulls are shown for each geographic clade (outlines), and phenotypic extremes for PC1 are illustrated by silhouettes and deformation grids. b) Adaptive shifts identified by 'l1ou'. Each selective regime is represented by a different color.

The rank envelope test detected significant deviation from BM in the head shape datasets for the Australian clade and in all datasets for the Papuan clade (Fig. S5; Table S11). The MDI of the SVL dataset was significant in the Australian clade (negative MDI), the dorsal-head dataset in all clades (positive MDI), and the lateral head dataset in the Papuan clade (positive MDI) (Table S12). The multivariate analyses favor an EB model for all datasets in the Papuan clade and the lateral-head dataset in the Australian clade (Fig. 3c; Tables S13–S14). The univariate analyses (Tables S15–S16) support a positive exponential relationship between rates and diversity for SVL in the Papuan clade. A negative exponential relationship was supported for SVL in the Australian clade and body shape in the Papuan clade. A negative linear relationship was supported for lateral

head shape in the Australian clade (Fig. 3d). BM was favored across all multivariate and univariate analyses for the Malesian clade. Some of these results were sensitive to uncertainty in phylogenetic and biogeographic reconstruction (Fig. 3c, d).

Table 2. Summary of morphological diversification analyses. Results that were not significant are indicated by "n.s.". "BM" indicates Brownian motion, "EB" early burst, "OU" Ornstein-Uhlenbeck, "DDl" linear diversity dependence, and "DDe" exponential diversity dependence.

	Australian				Malesian				Papuan			
Method	SVL	Body	Dorsal-head	Lateral-head	SVL	Body	Dorsal-head	Lateral-head	SVL	Body	Dorsal-head	Lateral-head
Morphological rate shifts (unguided)	1 (negative)	1 (negative)	1 (negative)	1 (negative)	1 (positive)	0	0	0	0	1 (positive)	1 (positive)	1 (positive)
Morphological rates (guided)	Low	n.s.	n.s.	n.s.	High	High	High	High	n.s.	n.s.	High	High
l1ou' shifts	3	4	2	4	0	0	1	2	1	1	4	3
Rank envelope test	n.s.	n.s.	Significant	Significant	n.s.	n.s.	n.s.	n.s.	Significant	Significant	Significant	Significant
MDI	Negative	Positive (n.s.)	Positive	Positive (n.s.)	Positive (n.s.)	Positive (n.s.)	Positive	Positive (n.s.)	Positive (n.s.)	Negative (n.s.)	Positive	Positive
Multivariate evolution models (best tree)	–	EB	BM	EB	–	BM	BM	BM	–	EB	EB	EB
Multivariate evolution models (tree sample)	–	BM	BM	EB	–	BM	BM	BM	–	EB	EB	EB
Univariate evolution models	DDe	BM	OU	DDl	BM	BM	BM	BM	DDe	DDe	OU	OU

Incumbency effects

The best fitting 'DAISIE' model when the Australian clade is the incumbent lineage and Papuan taxa are immigrant lineages was a model where immigrant speciation rates equal zero and there is linear diversity dependence of speciation rates in the incumbent clade and immigration rates (Fig. 5a; Supporting Information). In general, the best ranked models incorporate diversity dependence in incumbent speciation rates and null speciation in immigrants. The carrying capacity estimated by the best model is 36.32, close to the 31 species in the Australian clade. The best model when the Papuan clade is incumbent is one where the speciation rates of Australian immigrants equal zero and there is no diversity dependence in the rates of incumbent speciation and immigration. All the top ranked models show null immigrant speciation rates. The carrying capacity estimated by the best model with diversity dependence is 41.62, far from the 24 species in the Papuan clade.

The boxplots and PCA plots show that immigrant taxa usually have phenotypes outside or at the margins of the range of variation present in the incumbent taxa with which the immigrants are sympatric (Fig. 5b). However, neither of the tests evaluating whether observed morphological distances between immigrants and incumbents are higher than between randomly chosen members of each clade is significant (Table 3). In other words, immigrants are usually morphologically different from sympatric incumbents, but the degree of differentiation is not exceptional compared with the baseline disparity between the Australian and Papuan clades. Instead, our tests suggest that some immigrants and incumbents are more similar to each other than random members of their respective clades (Table 3).

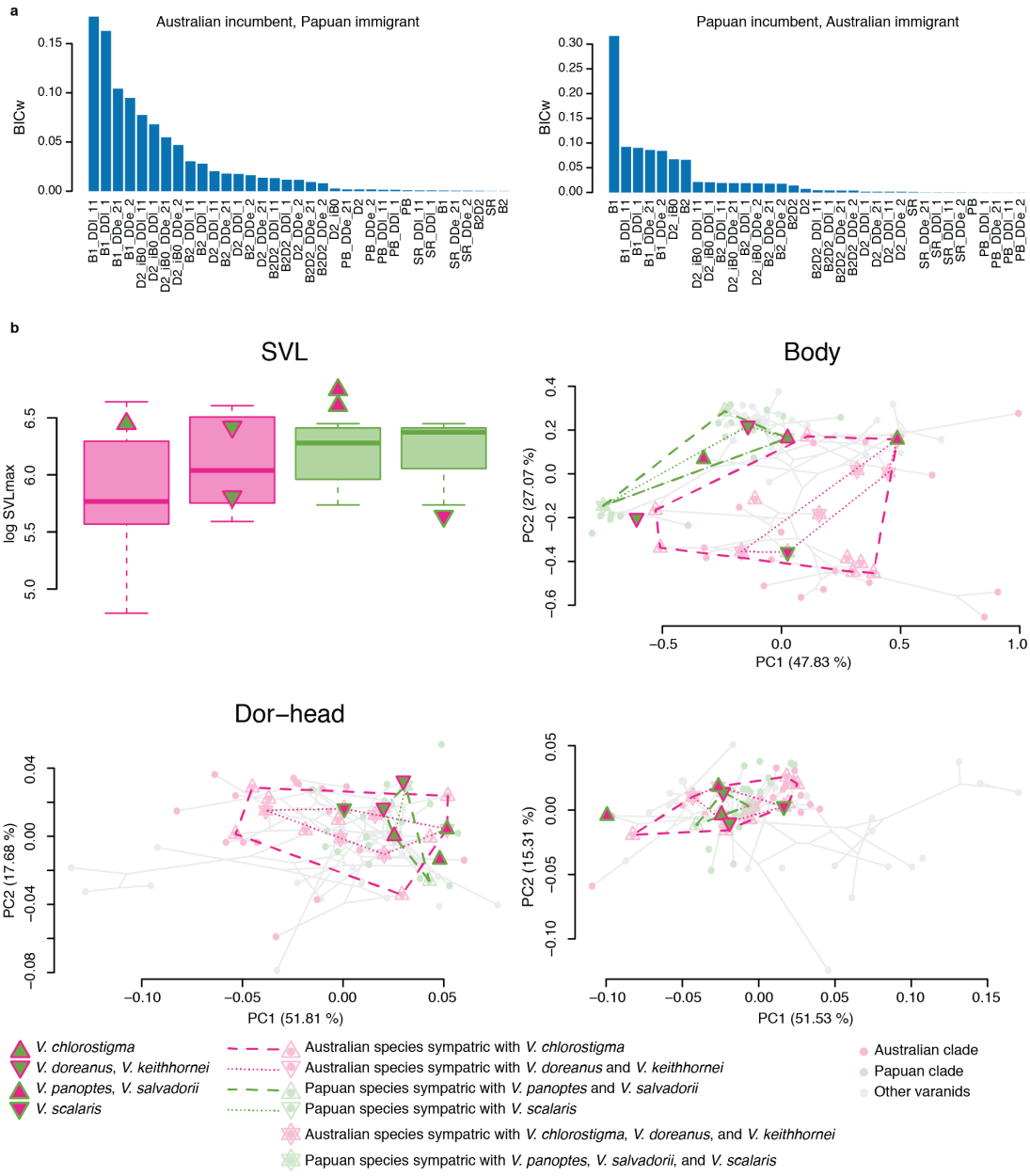

Figure 5. Incumbency effects in the exchange of varanid species between Australia and New Guinea. a) BIC weights (BICw) for different models evaluated in 'DAISIE' (B1 = Birth-death model with speciation in incumbent clade and no speciation in immigrants; B2 = Birth-death model with separate speciation rates for incumbents and immigrants; B2D2 = Birth-death model with separate speciation and extinction rates for incumbents and immigrants; D2 = Birth-death model with separate extinction rates for incumbents and immigrants; PB = Pure-birth model with equal speciation rates in incumbents and immigrants; SR = Birth-death model with equal speciation and extinction rates in incumbents and immigrants; DDe = exponential diversity dependence; DDl linear diversity dependence; iB0 = no speciation in immigrants; 1= linear diversity dependence in speciation rate; 2= exponential diversity dependence in speciation rate; 11 = linear diversity dependence in speciation and immigration rates; 21 = exponential diversity dependence in speciation and immigration rates). b) Comparison of the phenotype of secondary colonizers and the species in the incumbent clade with which they are sympatric. Boxplots (SVL) and convex hulls (other datasets) are shown for each incumbent community.

Table 3. Proportion of simulated values of *d* greater than or equal to the empirical value. Large values indicate that immigrants and incumbents are more similar to each other than random members of their respective clades. Significant *p* values are shown in bold (considering a one-tailed test with a significance level of 0.05).

Immigrant	*p* SVL	*p* body	*p* dor-head	*p* lat-head
V. chlorostigma	0.542	**0.996**	**1**	**0.987**
V. doreanus	0.948	0.858	**0.991**	**0.972**
V. keithhornei	**0.954**	0.271	0.8	0.732
V. panoptes	0.71	0.246	0.691	0.879
V. salvadorii	0.532	0.716	0.861	0.127
V. scalaris	0.481	0.636	**0.995**	0.937

Discussion

Here we compared the diversification dynamics of three speciose radiations in the Indo-Australasian region and tested for incumbency effects in the biotic exchange between two major landmasses in the region, Australia and New Guinea. Our results highlight how geographic setting and interspecific interactions act together to shape and sort biodiversity.

Diversity patterns in Varanidae

The three most speciose clades have their origin and highest diversity in Australia (Australian clade), the Philippines (Malesian clade), and New Guinea (Papuan clade) (Fig. 1). The Afro-Arabian clade and its sister group which is mainly distributed in Indo-Australasia have roughly the same age and yet diversity is much higher in the latter (Fig. 1). Groups such as elapid snakes (Keogh 1998) and pythons (Esquerré et al. 2020) also show greater richness and ecomorphological diversity in Indo-Australasia (particularly Australasia) than elsewhere, presumably due to ecological opportunity associated with the colonization of the region. Rates of speciation are particularly high in the Malesian and Papuan clades (Fig. 2a, b), congruent with previous work showing increased speciation rates in insular varanids (Zhu et al. 2020). The unguided approach used to search for rate shifts detected a positive shift in the *indicus* group, which has colonized numerous islands in the Pacific (Weijola et al. 2019). The importance of island colonization for varanid diversification is also reflected by the prominence of founder-event speciation in our biogeographic (Supporting Information) and DREaD analyses (Fig. 3b). Varanids are more morphologically diverse and have apparently explored more adaptive regimes in the Indo-Australasian region, particularly in Australia (Fig. 4). However, rates of morphological evolution in the Australian clade are closer to

background rates and a negative shift was even detected for SVL, while rate acceleration was detected in the Malesian and Papuan clades (Fig. 2c, d). This suggests that diversification in Indo-Australasia has been heterogeneous.

Heterogeneity in rates of diversification and morphological evolution is likely pervasive in taxa that are widespread and show significant variation in morphology, ecology, and/or life history (e.g., Jetz et al. 2012; Siqueira et al. 2020). Thus, models that allow diversification rates to vary substantially along phylogenies, such as the ones implemented here with ClaDS and 'RRphylo', may more accurately portrait evolutionary histories than models assuming constant rates or a few shifts (Maliet et al. 2019). To summarize, varanid diversity is higher in Indo-Australasia, but our results suggest that idiosyncratic processes have shaped diversity in the clades that occur there. This is inconsistent with a scenario where increased ecological opportunity in the region is the main driver of diversification. Instead, we propose that the evolutionary history of each clade has been mainly driven by the interplay between geographic context, interspecific competition, and clade age.

Diversification of Indo-Australasian radiations

The Australian clade is the oldest and most species rich among the three compared clades, and also shows remarkable ecomorphological diversity. The smallest (*V. sparnus*) and largest (*V. komodoensis*) varanids are part of this clade. Furthermore, species in the Australian clade use their habitat in all the ways shown by other clades (arboreal, semiaquatic, and terrestrial) plus some novel ones, such as dwarf and short-limbed monitors that shelter in the base of *Triodia* grass clumps, spiky-tailed species that inhabit rock crevices, and lizards with long tails and limbs that vertically navigate rocky escarpments (Pianka and King 2004). This and some of our analyses suggest that the Australian clade could represent a continental adaptive radiation that reached equilibrium following ecological opportunity. The favored 'DDD' and 'DAISIE' models support a density dependent diversification process, and the diversity of the Australian clade (31) is close to the estimated carrying capacity (30.66 and 36.32, respectively). This is accompanied by a negative MDI in SVL, support for an EB model when analyzing body and lateral head shape through the multivariate approach using the best tree, and support for diversity dependent models in some of the univariate analyses. Furthermore, we detected more adaptive shifts in this clade than in any other. Ecological opportunity may have arisen after release from competition, following the colonization of a region with few large diurnal predators compared to Africa and the Asian mainland. This may have also allowed *Odatria* to become miniaturized and diversify due to the reduced predation pressure (Sweet and Pianka 2007; Brennan et al. 2021).

Our DREaD analyses suggest that several speciation modes acted throughout the history of the Australian clade, but founder event had a predominant role. Australia is the flattest continent and has remained relatively tectonically stable (Blewett 2012). This means that classic processes that promote vicariance such as mountain uplift and island formation have not been as prevalent as in other regions. Instead, it seems like increased Miocene aridification has played a major role in the diversification of the Australian biota (Byrne et al. 2008, 2011; Brennan and Keogh 2018), and most speciation events in Australian varanids occurred in this period (Fig. 1). Habitat expansions and contractions coupled with founder event aided by the relatively high vagility of monitor lizards probably explain biogeographic patterns of Australian monitors. Founder event is apparently an important mode of speciation in adaptive radiations such as lemurs, diprotodont marsupials, and *Liolaemus* lizards (Skeels and Cardillo 2019b). High dispersal abilities could predispose taxa to adaptive radiation by colonization, allowing them to reach new regions, expand their range there becoming locally adapted, and coming back into secondary contact promoting character displacement and/or adaptive hybridization (Lamichhaney et al. 2015; Meier et al. 2017; Taylor and Larson 2019). However, founder-event speciation could be widespread in vertebrates, regardless of their status as adaptive radiations (Skeels and Cardillo 2019b). Furthermore, high vagility can prevent speciation by facilitating population homogenization through gene flow. More research is needed to understand how speciation occurs during adaptive radiation (Stroud and Losos 2016; Martin et al. 2015).

While there is evidence for the recognition of the Australian clade as an adaptive radiation, conflict and uncertainty in our results should be acknowledged. Rapid speciation following ecological opportunity is commonly considered a trademark of adaptive radiation (Schluter 2000), but rates of the Australian radiation are not exceptionally high. In the unguided approach, where the Papuan and Malesian clade are included in rate comparisons, the rates of the Australian clade were found to be significantly low. Additionally, negative shifts in morphological rates were detected, a positive MDI was calculated for the dorsal-head dataset, and support for early burst or models that incorporate competition is not unanimous across morphological datasets and is sensitive to uncertainty and analytical approach (Table 2). The slower rates of the Australian radiation compared to the Malesian and Papuan clades could reflect its continental setting, which is expected to be more stable than insular systems. Geographic context and comparisons with closely related taxa must be considered for the identification of adaptive radiations (Bromham and Woolfit 2004; Poe et al. 2018). It has been repeatedly shown that classical examples of adaptive radiation such as the Galapagos finches and Caribbean anoles do not show clear acceleration in speciation rates (Burns et al. 2014; Givnish 2015; Poe et al. 2018). This reveals the need to

reevaluate the processes behind the exceptional diversity of putative adaptive radiations or reconsider whether rate acceleration should be considered as one of their defining traits (Givnish 2015; Poe et al. 2018).

The Malesian and Papuan radiations show particularly high rates of speciation and morphological evolution. However, they are morphologically and ecologically less diverse than the Australian clade (Fig. 4). This could reflect the older age of the Australian radiation compared to the Papuan clade and specially the Malesian clade, more stringent ecological limits in the regions where the latter clades occur than in Australia, or be a consequence of the inverse time-scaling of rates of speciation and morphological evolution (Rabosky 2009; Harmon et al. 2010).

The Malesian clade appears to have diversified rapidly in the Pleistocene, mainly through vicariance (Fig. 3b), with limited ecomorphological differentiation. All members of the Malesian clade are large semiaquatic lizards, only differing slightly in habitat preferences. This is likely reflected by the preference for BM models of morphological evolution. There is strong support for a diversity dependent model of lineage diversification, which could reflect the limited capacity of the Philippine archipelago to host large and ecologically similar predatory lizards. Most species occur in the Philippine archipelago (Fig. 1), where sea level fluctuations resulted in the formation and dissolution of what have been called Pleistocene Aggregate Island Complexes (PAICs) (Brown and Diesmos 2002). Welton et al. (2014) proposed that divergence times indicate a possible role for sea level fluctuations in the dispersal and diversification of the Malesian clade. However, the biogeographic relevance of PAICs has been recently questioned, as environmental barriers within PAICs and current island geography seem to be more important drivers of divergence in several taxa (Esselstyn and Brown 2009; Siler et al. 2010; Brown et al. 2013; Hosner et al. 2014). A well-resolved phylogeny of the Malesian clade seems necessary to shed light on its biogeographic history.

An early divergence in the Papuan clade separates the highly arboreal *Hapturosaurus* from the more generalist *Euprepiosaurus*. Ecological differences within these subgenera are less pronounced (Pianka and King 2004). This could explain why the EB model, which is traditionally considered to indicate radiation following ecological opportunity, is favored in the multivariate morphological analyses. However, colonization of the Papuan region by this clade predates significant diversification (Figs. 1, S3) and most of our results suggest that rates of speciation and morphological evolution have increased towards the present. Part of it could be explained geographically. For a long time, large portions of northern New Guinea existed as island arcs, only forming a significant landmass between 12 and 5 Ma (Hill and Hall 2003; van Ufford and Cloos 2005). Thus, increased diversification rates towards the present in the Papuan clade could indicate

that, while conditions for colonization and persistence existed in proto-Papua, significant diversification was only possible closer to the present as land area increased. The insular nature of proto-Papua and its present-day surrounding islands is probably also reflected by the support for founder-event as a major driver of speciation. The large support for a mixed mode could reflect the speciation events that occurred following the accretion of New Guinea. As noted by Weijola et al. (2019), other New Guinean and Melanesian groups are deeply divergent from their sister taxa but their crown age is young, such as *Tribolonotus* skinks (Rittmeyer and Austin 2015). These observations are also consistent with a scenario of high extinction in ancient Melanesian island arcs, and supported by the presence of old but monospecific lineages such as the Solomons frogmouth *Rigidipenna inexpectata* (Oliver et al. 2020), Solomon Islands skink *Corucia zebrata* (Skinner et al. 2011; Weijola et al. 2019), and *V. spinulosus*. Increased rates towards the present in the Papuan clade could also be a result of the rapid speciation in the *indicus* group (Fig. 2), which has been accompanied by moderate morphological (Fig. 4) and ecological differentiation. There are several instances of sympatry in the Papuan clade, and the sympatric species usually differ in ecology and microhabitat preferences (Weijola 2010; Weijola et al. 2019). Overall, our results suggest that the Papuan clade could represent a radiation that has not reached equilibrium and that has been shaped by a combination of ecological opportunity following the colonization of the Papuan region, tectonics, and competition. This is further indicated by our 'DAISIE' analyses, which indicate a much higher carrying capacity for the Papuan clade than currently observed. Thus, the clade could represent a good model to study the non-equilibrium early stages of radiation.

Incumbency effects in Varanidae

Our results show mixed support for incumbency effects in the biotic exchange between Australia and New Guinea. Speciation of immigrants is practically null. It may be argued that this is simply because of their recent immigration, but then it is unclear why there are no old immigrants except for *V. salvadorii* (available infraspecific sampling suggests that the secondary colonization by taxa present in both regions has been recent; Weijola et al. 2019; Brennan et al. 2021). This could indicate that extinction in the immigrant clades has been high, possibly because they fail to diversify in their secondary range as a consequence of niche saturation by the incumbent taxa. Incumbency effects are stronger in Australia, where there is diversity dependence on the speciation of the incumbent clade and immigration. 'DAISIE' further suggests that the carrying capacity has almost been reached, and that could explain the failure of the immigrants to speciate, the diversity dependence on immigration rates, and the occupation of fringe habitats by

the immigrants. *V. chlorostigma* mostly inhabits the coastal margin of northern Australia, while *V. doreanus* and *V. keithhornei* inhabit narrow coastal strips of rainforest in north-eastern Australia. Carrying capacity has apparently not been reached in New Guinea, but recent immigration coupled with the geography of New Guinea could explain the failure to diversify of the immigrants coming from Australia. The Central Range of New Guinea is an important barrier for lowland taxa (Tallowin et al. 2018) and only the oldest immigrant (*V. salvadorii*) is present north of it. It may be that southern New Guinea has already reached its current carrying capacity, especially considering that competition may be increased by the sympatry of all Australian immigrants in that region.

Visualization of morphological variation hinted that biotic filtering could be playing a role in the geographic sorting of morphological variation. However, our randomization test indicated that immigrants are not more different from incumbents than random members of both clades. Instead, in some cases they are more similar than expected, i.e. sympatric immigrants and incumbents share similar adaptations. This suggests that abiotic filtering governed by environmental conditions could have played a major role in dictating which species colonize which regions. Different vegetation types dominate northern Australia and southern New Guinea: tropical savannas are widespread in northern Australia, while tropical rainforest is mostly confined to a narrow strip in the eastern portion of the continent (Bowman 2000; Bowman et al. 2010); in New Guinea, savannas are mostly confined to the south-central Trans-Fly region, while most of southern New Guinea is covered by rainforest (Paijmans 1976; Joseph et al. 2019). These differences in habitat may be limiting colonization. On one hand, each varanid immigrant occupies similar habitats in Australia and New Guinea. On the other hand, some New Guinean varanids that are closely associated with rainforest are absent in mainland Australia, such as *V. jobiensis* and *V. prasinus* (but see Koch and Eidenmüller 2019), and several Australian savanna species do not occur in New Guinea, such as *V. mertensi* and *V. primordius*.

Our results are consistent with a scenario in which abiotic filtering determines which taxa become established, assuming a baseline phenotypic difference between incumbent and immigrant taxa. Subsequently, immigrants fail to diversify and expand their range because of their morphological similarity with incumbents and niche occupation by the latter. This would make immigrants vulnerable to extinction and cause the overrepresentation of recent immigrations with respect to ancient ones. Our study aligns with what appears to be an emerging consensus: incumbency can have evolutionary consequences, but its effects on speciation and morphology are decoupled and its impact can be eclipsed by that of other evolutionary processes (Schenk et al. 2013; Rowsey et al. 2019, 2020; Reijenga et al. 2021).

Incumbency effects may have shaped other varanid communities, e.g. the Malesian-Philippine and Malay-Oriental communities. The crown age of the Philippine clade is younger than that of the Malesian clade and crown ages are usually better indicators of colonization times than stem ages (García-Verdugo et al. 2019). Thus, the members of the Philippine clade are likely secondary colonizers. Interestingly, the Philippine clade has only three species despite its old stem age, and they are exceptional among varanids for their mainly frugivorous diet accompanied by unique adaptations such as blunt teeth and a large caecum (Gaulke 2010). The Philippine clade could have been pushed into this unique niche by competition with the Malesian clade. Conversely, the Malay lineage (*V. rudicollis*) is also relatively old and has failed to diversify, perhaps by competition with the Oriental clade and/or the diverse mammalian carnivores of mainland southeast Asia. Same as the Philippine lineage, *V. rudicollis* shows a unique morphology. It has slit nares and a bulbous and long snout (Figs. 1, 4a) that apparently help it forage among decaying plant matter (Bennet 2004). The Philippine and Malay lineages occupy different regions of morphospace with respect to the Malesian and Oriental clades (Fig. 4a), respectively, but the low number of species in most of these lineages prevented us from conducting any formal tests.

Caveats

Conflicting signal between our analyses could potentially reflect methodological shortcomings. Some of our results were sensitive to sampling and uncertainty in the phylogenetic and biogeographic reconstruction. The size of the analyzed clades may also bias analyses based on model fitting, particularly those concerning the Malesian radiation. Additionally, rate slowdowns inferred from extant-only phylogenies should not be directly interpreted as evidence for adaptive radiation following ecological opportunity. There are alternative explanations for the rate slowdowns characteristic of early burst models (Rabosky and Lovette 2008; Aristide and Morlon 2019), such as protracted speciation (Etienne and Rosindell, 2012), decreasing chances for vicariance as ranges become smaller with each speciation event (Pigot et al. 2010), correlation of speciation with a temporally variable abiotic factor (Condamine et al. 2019), and increased extinction (Moen and Morlon 2014). Additionally, ecological, developmental, or genetic constraints can lead to the time-scaling of the rates of speciation and morphological evolution (Foote 1994; Rabosky 2009; Harmon et al. 2010; Rabosky et al. 2013). Several approaches that we employed attempt to overcome some of these shortcomings by integrating proxies for competition into parameter estimation.

Finally, there is a more general deficiency related to how informative the phylogenies of extant species are about diversification dynamics (Liow et al. 2010; Rabosky and

Hurblert 2015; Marshall 2017). This is a consequence of identifiability issues (Louca and Pennell 2020)—meaning that any given tree is consistent with numerous diversification scenarios (Louca and Pennell 2020)—and problems arising from the exclusion of fossil taxa (Quental and Marshall 2010; Marshall 2017). Some of the approaches employed here, such as accounting for phylogenetic uncertainty and the employment of the ClaDS2 model (which bounds parameter estimation based on a set of biologically realistic priors), only partially overcome these issues (Morlon et al. 2020). Ultimately, the data itself (i.e., the geographic and phylogenetic sorting of richness and morphological diversity) and analyses with few assumptions (such as our test of incumbency effects on morphology) are indicative of the relevance of biotic and abiotic factors in the evolution of varanids.

Conclusions

Rates of diversification and morphological evolution are not homogeneous in Varanidae. Three clades have reached remarkable diversity in Indo-Australasia, but in a way that is not consistent with a single main driver (such as ecological opportunity) acting across the region. Instead, heterogeneity in geography and community composition throughout Indo-Australasia has given rise to radiations that differ in age, richness, and ecomorphological diversity, providing unique insight into the processes responsible for the generation and sorting of biodiversity. Our results show that interspecific interactions can have evolutionary consequences, highlighting the need for the development of methods and conceptual frameworks linking evolutionary processes with the insight obtained from direct observations in ecological timescales (Harmon et al. 2019).

Author Contributions

CJPV conceived the project, collected novel data, and led writing; CJPV, IGB, and AS designed the study and analysed the data; all authors participated in writing and in the interpretation of the results.

Acknowledgments

We thank A. Allison, A.P. Amey, W. Böhme, U. Bott, R.D. Bray, P.D. Campbell, P.J.

Couper, M. Cugnet, G.M. Dally, K. de Queiroz, P. Doughty, A. Drew, M. Flecks, M.E. Hagemann, M.R. Hutchinson, L. Joseph, C. Kovach, S. Mahony, D. Rödder, J.J.L. Rowley, J.W. Streicher, N. Vidal, and A.H. Wynn for the support during specimen examination in their respective institutions; M. Arvizu Meza for help with specimen examination; A. Koch for donating a mitochondrial sequence of *V. bogerti*; D.L. Rabosky and two anonymous reviewers for their pertinent suggestions; and members of the Keogh and Moritz labs in ANU for insightful discussion on this project. Illustrations in Fig. 1 were inspired by photographs under a Creative Commons Attribution-Share Alike 4.0 International license (Afro-Arabian, Papuan, and Oriental); photographs in the public domain (Malesian and Philippine); photographs by Matthijs Kuijpers purchased for artistic reference (Malay); or photographs by O. Jiménez Robles (Australian) and Rockabirdie Reptiles (Melanesian). This study was funded by an Australian Research Council grant to JSK. The graduate education of CJPV was financed by the Australian Government Research Training Program.

Data Accessibility Statement

Molecular data is publicly available from the Dryad Digital Repository at https://dx.doi.org/10.5061/dryad.tx95x69t8 and https://doi.org/10.5061/dryad.m0n61, and from the National Center for Biotechnology Information (see details in Supplementary Material). Morphological data is included in the Supplementary Material.

Literature Cited

Alroy, J. 1996. Constant extinction, constrained diversification, and uncoordinated stasis in North American mammals. Palaeogeo. Palaeoclim. Palaeoecol. 127:285–311.

Andersen, M. J., J. M. McCullough, W. M. Mauck, B. T. Smith, and R. G. Moyle. 2018. A phylogeny of kingfishers reveals an Indomalayan origin and elevated rates of diversification on oceanic islands. J. Biogeogr. 45:269–281.

Aristide, L. and H. Morlon. 2019. Understanding the effect of competition during evolutionary radiations: an integrated model of phenotypic and species diversification. Ecol. Lett. 22:2006–2017.

Badgley, C., T. M. Smiley, R. Terry, E. B. Davis, L. R. G. DeSantis, D. L. Fox, S. S. B. Hopkins, T. Jezkova, M. D.Matocq, N. Matzke, J. L. McGuire, A. Mulch, B. R. Riddle, V. L. Roth, J. X. Samuels, C. A. E. Strömberg, and B. J. Yanites. 2017.

Biodiversity and topographic complexity: modern and geohistorical perspectives. Trends Ecol. Evol. 32:211–226.

Bennett, D. 2004. *Varanus rudicollis*. *In* Pianka, E. R., and D. R. King (eds.). Varanoid Lizards of the World. Indiana University Press, Bloomington, IN.

Blewett, R (ed.). 2012. Shaping a nation: a geology of Australia. ANU Press, Canberra, ACT.

Bowman, D. M. 2000. Australian rainforests. Islands of green in a land of fire. Cambridge University Press, Cambridge, CBE.

Bowman, D. M. J. S., G. K. Brown, M. F. Braby, J. R. Brown, L. G. Cook, M. D. Crisp, F. Ford, S. Haberle, J. Hughes, Y. Isagi, L. Joseph, J. McBride, G. Nelson, and P. Y. Ladiges. 2010. Biogeography of the Australian monsoon tropics. J. Biogeogr. 37:201–216.

Brennan, I. G., A. R Lemmon, E. M. Lemmon, D. M. Portik, V. Weijola, L. Welton, S. C. Donnellan, and J. S. Keogh. 2021. Phylogenomics of monitor lizards and the role of competition in dictating body size disparity. Syst. Biol. 70:120–132.

Brennan, I. G., and J. S. Keogh. 2018. Miocene biome turnover drove conservative body size evolution across Australian vertebrates. Proc. R. Soc. B 285:20181474.

Bromham, L., and M. Woolfit. 2004. Explosive radiations and the reliability of molecular clocks: island endemic radiations as a test case. Syst. Biol. 53:758–766.

Brown, R. M., and A. C. Diesmos. 2002. Application of lineage-based species concepts to oceanic island frog populations: the effects of differing taxonomic philosophies on the estimation of Philippine biodiversity. Silliman J. 42:133–162.

Brown, R. M., C. D. Siler, C. H. Oliveros, J. A. Esselstyn, A. C. Diesmos, P. A. Hosner, C. W. Linkem, A. J. Barley, J. R. Oaks, M. B. Sanguila, L. J. Welton, D. C. Blackburn, R. G. Moyle, A. Townsend Peterson, and A. C. Alcala. 2013. Evolutionary processes of diversification in a model island archipelago. Annu. Rev. Ecol. Evol. Syst. 44:411–435.

Bucklitsch, Y., W. Boehme, and A. Koch. 2016. Scale morphology and micro-structure of monitor lizards (Squamata: Varanidae: *Varanus* spp.) and their allies: implications for systematics, ecology, and conservation. Zootaxa 4153:1–192.

Burns J., A. J. Shultz, P. O. Title, N. A. Mason, F. K. Barker, J. Klicka, S. M. Lanyon, and I. J. Lovette. 2014. Phylogenetics and diversification of tanagers (Passeriformes: Thraupidae), the largest radiation of Neotropical songbirds. Mol. Phylogenet. Evol. 75:41–77.

Byrne, M., D. A. Steane, L. Joseph, D. K. Yeates, G. J. Jordan, D. Crayn, K. Aplin, D. J. Cantrill, L. G. Cook, M. D. Crisp, J. S. Keogh, J. Melville, C. Moritz, N. Porch, J. M. K. Sniderman, P. Sunnucks, and P. H. Weston. 2011. Decline of a biome: evolution, contraction, fragmentation, extinction and invasion of the Australian mesic zone biota. J. Biogeogr. 38:1635–1656.

Byrne, M., D. K. Yeates, L. Joseph, M. Kearney, J. Bowler, M. A. J. Williams, S. Cooper, S. C. Donnellan, J. S. Keogh, R. Leys, J. Melville, D. J. Murphy, N. Porch, and K-H. Wyrwoll. 2008. Birth of a biome: insights into the assembly and maintenance of the Australian arid zone biota. Mol. Ecol. 17:4398–4417.

Castiglione, S., G. Tesone, M. Piccolo, M. Melchionna, A. Mondanaro, C. Serio, M. Di Febbraro, and P. Raia. 2018. A new method for testing evolutionary rate variation and shifts in phenotypic evolution. Methods Ecol. Evol. 9:974–983.

Clavel, J., L. Aristide, and H. Morlon. 2019. A penalized likelihood framework for high-dimensional phylogenetic comparative methods and an application to new-world monkeys brain evolution. Syst. Biol. 68:93–116.

Collar, D. C., J. A. Schulte II, J. B. Losos. 2011. Evolution of extreme body size disparity in monitor lizards (*Varanus*). Evolution 65:2664–2680.

Condamine, F. L., J. Rolland, and H. Morlon. 2019. Assessing the causes of diversification slowdowns: temperature-dependent and diversity-dependent models receive equivalent support. Ecol. Lett. 22:1900–1912.

T. L. P. Couvreur, G. Dauby, A. Blach-Overgaard, V. Deblauwe, S. Dessein, V. Droissart, O. J. Hardy, D. J. Harris, S. B. Janssens, A. C. Ley, B. A. Mackinder, B. Sonké, M. S. M. Sosef, T. Stévart, J-C. Svenning, J. J. Wieringa, A. Faye, A. D. Missoup, K. A. Tolley, V. Nicolas, S. Ntie, F. Fluteau, C. Robin, F. Guillocheau, D. Barboni, and P. Sepulchre. 2021. Tectonics, climate and the diversification of the tropical African terrestrial flora and fauna. Biol. Rev. 96:16–51.

Drake, J. A. 1991. Community-assembly mechanics and the structure of an experimental species ensemble. Am. Nat. 137:1–26.

Drury, J. P., J. A. Tobias, K. J. Burns, N. A. Mason, A. J. Shultz, and H. Morlon. 2018. Contrasting impacts of competition on ecological and social trait evolution in songbirds. PLoS Biol. 16:e2003563.

Drury, J., J. Clavel, M. Manceau, and H. Morlon. 2016. Estimating the effect of competition on trait evolution using maximum likelihood inference. Syst. Biol. 65:700–710.

Esquerré, D., I. G. Brennan, R. A. Catullo, F. Torres-Pérez, and J. S. Keogh. 2019. How mountains shape biodiversity: The role of the Andes in biogeography, diversification, and reproductive biology in South America's most species-rich lizard radiation (Squamata: Liolaemidae). Evolution 73:214–230.

Esquerré, D., S. Donnellan, I. G. Brennan, A. R. Lemmon, E. Moriarty Lemmon, H. Zaher, F. G. Grazziotin, and J. S. Keogh. 2020. Phylogenomics, biogeography, and morphometrics reveal rapid phenotypic evolution in pythons after crossing Wallace's line. Syst. Biol. 69:1039–1051.

Esselstyn, J. A., and R. M. Brown. 2009. The role of repeated sea-level fluctuations in the generation of shrew (Soricidae: *Crocidura*) diversity in the Philippine Archipelago. Mol. Phylogenet. Evol. 53:171–181.

Etienne, R. S., and B. Haegeman. 2020. DDD: Diversity-Dependent Diversification. R package version 4.4. Available at https://CRAN.R-project.org/package=DDD. Accessed December 1, 2020.

Etienne, R. S., and J. Rosindell. 2012. Prolonging the past counteracts the pull of the present: protracted speciation can explain observed slowdowns in diversification. Syst. Biol. 61:204–213.

Etienne, R. S., B. Haegeman, T. Stadler, T. Aze, P. N. Pearson, A. Purvis, and A. B. Phillimore. 2012. Diversity-dependence brings molecular phylogenies closer to agreement with the fossil record. Proc. R. Soc. B Biol. Sci. 279:1300–1309.

Fitzpatrick, B. M., J. A. Fordyce, and S. Gavrilets. 2009. Pattern, process and geographic modes of speciation. J. Evol. Biol. 22:2342–2347.

Foote, M. 1994. Morphological disparity in Ordovician-Devonian crinoids and the early saturation of morphological space. Paleobiology 20:320–344.

Fordyce, J. A. 2010. Host shifts and evolutionary radiations of butterflies. Proc. R. Soc. B Biol. Sci. 277:3735–3743.

Fukami, T. 2015. Historical contingency in community assembly: integrating niches, species pools, and priority effects. Annu. Rev. Ecol. Evol. Syst. 46:1–23.

Fukami, T., H. J. E. Beaumont, X-X. Zhang, and P. B. Rainey. 2007. Immigration history controls diversification in experimental adaptive radiation. Nature 446:436–439.

García-Verdugo, C., J. Caujapé-Castells, and I. Sanmartín. 2019. Colonization time on island settings: lessons from the Hawaiian and Canary Island floras. Bot. J. Linn. Soc. 191:155–163.

Gaulke M., and E. Curio. 2001. A new monitor lizard from Panay Island, Philippines. Spixiana 24:275–286.

Gaulke, M. 2010. Overview on the present knowledge on *Varanus mabitang* Gaulke and Curio, 2001, including new morphological and meristic data. Biawak:50–58.

Gillespie, R. G. 2004. Community assembly through adaptive radiation in Hawaiian spiders. Science 303:356–359.

Givnish, T. J. 2015. Adaptive radiation versus 'radiation' and 'explosive diversification': why conceptual distinctions are fundamental to understanding evolution. New Phytol. 207:297–303.

Gower, J. C. 1975. Generalized procrustes analysis. Psychometrika 40:33–51.

Hall, R. 2002. Cenozoic geological and plate tectonic evolution of SE Asia and the SW Pacific: computer-based reconstructions, model and animations. J. Asian Earth Sci. 20:353–434

Harmon, L. J., C. S. Andreazzi, F. Débarre, J. Drury, E. E. Goldberg, A. B. Martins, C. J. Melián, A. Narwani, S. L. Nuismer, M. W. Pennell, S. M. Rudman, O. Seehausen, D. Silvestro, M. Weber, and B. Matthews. 2019. Detecting the macroevolutionary signal of species interactions. J. Evol. Biol. 32:769–782.

Harmon, L. J., J. B. Losos, T. J. Davies, R. G. Gillespie, G. L. Gittleman, W. B. Jennings, K. H. Kozak, M. A. McPeek, F. Moreno-Roark, T. J. Near, A. Purvis, R. E. Ricklefs, D. Schluter, J. A. Schulte II, O. Seehausen, B. L. Sidlauskas, O. Torres-Carvajal, J. T. Weir, A. Ø. Mooers. 2010. Early bursts of body size and shape evolution are rare in comparative data. Evolution 64:2385–2396.

Harmon, L. J., J. A. Schulte II, A. Larson, and J. B. Losos. 2003. Tempo and mode of evolutionary radiation in iguanian lizards. Science 301:961–964.

Hembry, D. H., and M. G. Weber. 2020. Ecological interactions and macroevolution: a new field with old roots. Annu. Rev. Ecol. Evol. Syst. 51:215–243.

Hill, K. C., and R. Hall. 2003. Mesozoic-Cenozoic evolution of Australia's New Guinea margin in a west Pacific context. *In* Hillis, R. R., and R. D. Muller (eds.). Evolution and dynamics of the Australian Plate. The Geological Society of America, Boulder, CO.

Holt, B. G., J. P. Lessard, M. K. Borregaard, S. A. Fritz, M. B. Araújo, D. Dimitrov, P-H. Fabre, C. H. Graham, G. R. Graves, K. A. Jønsson, D. Nogués-Bravo, Z. Wang, R. J. Whittaker, J. Fjeldså, and C. Rahbek. 2013. An update of Wallace's zoogeographic regions of the world. Science 339:74–78.

Hoorn, C., A. Perrigo, and A. Antonelli (eds.). 2018. Mountains, climate and biodiversity. Wiley Blackwell, Oxford, OX.

Hosner, P. A., L. A. Sánchez-González, A. T. Peterson, and R. G. Moyle. 2014. Climate-driven diversification and Pleistocene refugia in Philippine birds: evidence from phylogeographic structure and paleoenvironmental niche modeling. Evolution 68:2658–2674.

Jetz, W., G. H. Thomas, J. B. Joy, K. Hartmann, and A. O. Mooers. 2012. The global diversity of birds in space and time. Nature 491:444–448.

Joseph, L., K. D. Bishop, C. A. Wilson, S. V. Edwards, B. Iova, C. D. Campbell, I. Mason, and A. Drew. 2019. A review of evolutionary research on birds of the New Guinean savannas and closely associated habitats of riparian rainforests, mangroves and grasslands. Emu 119:317–330.

Keogh, J. S. 1998. Molecular phylogeny of elapid snakes and a consideration of their biogeographic history. Biol. J. Linn. Soc. 63:177–203.

Khabbazian, M., R. Kriebel, K. Rohe, and C. Ané. 2016. Fast and accurate detection of evolutionary shifts in Ornstein–Uhlenbeck models. Methods Ecol. Evol. 7:811–824.

Kingsolver, J. G., and D. W. Pfennig. 2004. Individual-level selection as a cause of Cope's rule of phyletic size increase. Evolution 58:1608–1612.

Koch, A., and B. Eidenmüller. 2019. Is the New Guinea emerald tree monitor lizard (*Varanus prasinus*) native to mainland Australia? Biawak 13:32–42.

Lamichhaney, S., J. Berglund, M. S. Almén, K. Maqbool, M. Grabherr, A. Martinez-Barrio, M. Promerová, C-J. Rubin, C. Wang, N. Zamani, B. R. Grant, P. R. Grant, M. T. Webster, and L. Andersson. 2015. Evolution of Darwin’s finches and their beaks revealed by genome sequencing. Nature 518:371–375.

Lemmon, A. R., S. A. Emme, and E. Moriarty Lemmon. 2012. Anchored hybrid enrichment for massively high-throughput phylogenomics. Syst. Biol. 61:727–744.

Liow, L. H., T. B. Quental, and C. R. Marshall. 2010. When can decreasing diversification rates be detected with molecular phylogenies and the fossil record? Syst. Biol. 59:646–659.

Lohman, D. J., M. de Bruyn, T. Page, K. von Rintelen, R. Hall, P. K. L. Ng, H.-T. Shih, G. R. Carvalho, and T. von Rintelen. 2011. Biogeography of the Indo-Australian archipelago. Annu. Rev. Ecol. Evol. Syst. 42:205–226.

Louca, S., and M. W. Pennell. 2020. Extant timetrees are consistent with a myriad of diversification histories. Nature 580:502–505.

Maliet, O., F. Hartig, and H. Morlon. 2019. A model with many small shifts for estimating species-specific diversification rates. Nat. Ecol. Evol. 3:1086–1092.

Marshall, C. R. 2017. Five palaeobiological laws needed to understand the evolution of the living biota. Nat. Ecol. Evol. 1:0165.

Martin, C. H., J. S. Cutler, J. P. Friel, C. Dening Touokong, G. Coop, and P. C. Wainwright. 2015. Complex histories of repeated gene flow in Cameroon crater lake cichlids cast doubt on one of the clearest examples of sympatric speciation. Evolution 69:1406–1422.

Matzke, N. J. 2013. Probabilistic historical biogeography: new models for founder-event speciation, imperfect detection, and fossils allow improved accuracy and model-testing. Front. Biogeogr. 5:242–248.

Meier, J. I., D. A. Marques, S. Mwaiko, C. E. Wagner, L. Excoffier, and O. Seehausen. 2017. Ancient hybridization fuels rapid cichlid fish adaptive radiations. Nat. Comm. 8:1–11.

Moen, D., and H. Morlon. 2014. Why does diversification slow down?. Trends Ecol. Evol. 29:190–197.

Morlon, H., F. Hartig, and S. Robin. 2020. Prior hypotheses or regularization allow inference of diversification histories from extant timetrees. bioRxiv 2020.07.03.185074.

Morlon, H., E. Lewitus, F. L. Condamine, M. Manceau, J. Clavel, and J. Drury. 2016. RPANDA: an R package for macroevolutionary analyses on phylogenetic trees. Methods Ecol. Evol. 7:589–597.

Morlon, H., T. L. Parsons, J. B. Plotkin. 2011. Reconciling molecular phylogenies with the fossil record. Proc. Natl. Acad. Sci. USA 108:16327–16332.

Mosimann, J. E. 1970. Size allometry: size and shape variables with characterizations of the lognormal and generalized gamma distributions. J. Am. Stat. Assoc. 65:930–945.

Moyle, R. G., C. H. Oliveros, M. J. Andersen, P. A. Hosner, B. W. Benz, J. D. Manthey, S. L. Travers, R. M. Brown, and B. C. Faircloth. 2016. Tectonic collision and uplift of Wallacea triggered the global songbird radiation. Nat. Comm. 7:1–7.

Myers, N., R. A. Mittermeier, C. G. Mittermeier, G. A. B. da Fonseca, and J. Kent. 2000. Biodiversity hotspots for conservation priorities. Nature 403:853–858.

Oliver, P. M., H. Heiniger, A. F. Hugall, L. Joseph, and K. J. Mitchell. 2020. Oligocene divergence of frogmouth birds (Podargidae) across Wallace's Line. Biol. Lett. 16:20200040.

Openshaw, G. H., and J. S. Keogh. 2014. Head shape evolution in monitor lizards (*Varanus*): interactions between extreme size disparity, phylogeny and ecology. J. Evol. Biol. 27:363–373.

Openshaw, G. H., D. C. D'Amore, M. Vidal-García, and J. S. Keogh. 2017. Combining geometric morphometric analyses of multiple 2D observation views improves interpretation of evolutionary allometry and shape diversification in monitor lizard (*Varanus*) crania. Biol. J. Linn. Soc. 120:539–552.

Paijmans, K. (ed). 1976. New Guinea vegetation. Commonwealth Scientific and Industrial Research Organization, Australian National University Press, Canberra, ACT.

Pennell, M. W., J. M. Eastman, G. J. Slater, J. W. Brown, J. C. Uyeda, R. G. FitzJohn, M. E. Alfaro, and L. J. Harmon. 2014. geiger v2. 0: an expanded suite of methods for fitting macroevolutionary models to phylogenetic trees. Bioinformatics 30:2216–2218.

Pepin, D. J. 2001. Evolution and life history of varanid lizards. Ph.D. thesis. Washington University, St. Louis, MO.

Pianka, E., and D. King (eds.). 2004. Varanoid lizards of the world. Indiana University Press, Bloomington, IN.

Pigot, A. L., A. B. Phillimore, I. P. Owens, and C. D. L. Orme. 2010. The shape and temporal dynamics of phylogenetic trees arising from geographic speciation. Syst. Biol. 59:660–673.

Poe, S., A. Nieto-Montes de Oca, O. Torres-Carvajal, K. de Queiroz, J. A. Velasco, B. Truett, L. N. Gray, M. J. Ryan, G. Köhler, F. Ayala-Varela, and I. Latella. 2018. Comparative evolution of an archetypal adaptive radiation: innovation and opportunity in *Anolis* lizards. Am. Nat. 191:E185–E194.

Pybus, O. G., and P. H. Harvey. 2000. Testing macro–evolutionary models using incomplete molecular phylogenies. Proc. R. Soc. Lond. B Biol. Sci. 267:2267–2272.

Quental, T. B., and C. R. Marshall. 2010. Diversity dynamics: molecular phylogenies need the fossil record. Trends Ecol. Evol. 25:434–441.

Rabosky, D. L. 2009. Ecological limits and diversification rate: alternative paradigms to explain the variation in species richness among clades and regions. Ecol. Lett. 12:735–743.

Rabosky, D. L., and A. H. Hurlbert. 2015. Species richness at continental scales is dominated by ecological limits. Am. Nat. 185:572–583.

Rabosky, D. L., and I. J. Lovette. 2008. Density-dependent diversification in North American wood warblers. Proc. R. Soc. B. 275:2363–2371.

Rabosky, D. L., F. Santini, J. Eastman, S. A. Smith, B. Sidlauskas, J. Chang, and M. E. Alfaro. 2013. Rates of speciation and morphological evolution are correlated across the largest vertebrate radiation. Nat. Comm. 4:1–8.

Reijenga, B. R., D. J. Murrell, D. J. and A. L. Pigot. 2021. Priority effects and the macroevolutionary dynamics of biodiversity. Ecol. Lett. (in press).

Revell, L. J. 2012. phytools: an R package for phylogenetic comparative biology (and other things). Methods Ecol. Evol. 3:217–223.

Rittmeyer, E. N., and C. C. Austin. 2015. Combined next-generation sequencing and morphology reveal fine-scale speciation in Crocodile Skinks (Squamata: Scincidae: *Tribolonotus*). Mol. Ecol. 24:466–483.

Roll, U., A. Feldman, M. Novosolov, A. Allison, A. M. Bauer, R. Bernard, M. Böhm, F. Castro-Herrera, L. Chirio, B. Collen, G. R. Colli, L. Dabool, I. Das, T. M. Doan, L. L. Grismer, M. Hoogmoed, Y. Itescu, F. Kraus, M. LeBreton, A. Lewin, M. Martins, E. Maza, D. Meirte, Z. T. Nagy, C. C. Nogueira, O. S. G. Pauwels, D. Pincheira-Donoso, G. D. Powney, R. Sindaco, O. J. S. Tallowin, O. Torres-Carvajal, J-F. Trape, E. Vidan, P. Uetz, P. Wagner, Y. Wang, C. D. L. Orme, R. Grenyer, and S. Meiri. 2017. The global distribution of tetrapods reveals a need for targeted reptile conservation. Nat. Ecol. Evol. 1:1677–1682.

Rowsey, D. M., L. R. Heaney, and S. A. Jansa. 2018. Diversification rates of the “Old Endemic” murine rodents of Luzon Island, Philippines are inconsistent with incumbency effects and ecological opportunity. Evolution 72:1420–1435.

Rowsey, D. M., L. R. Heaney, and S. A. Jansa. 2019. Tempo and mode of mandibular shape and size evolution reveal mixed support for incumbency effects in two clades of island-endemic rodents (Muridae: Murinae). Evolution 73:1411–1427.

Rowsey, D. M., R. M. Keenan, and S. A. Jansa. 2020. Dietary morphology of two island-endemic murid rodent clades is consistent with persistent, incumbent-imposed competitive interactions. Proc. R. Soc. B 287:20192746.

Schenk, J. J., K. C. Rowe, and S. J. Steppan. 2013. Ecological opportunity and incumbency in the diversification of repeated continental colonizations by muroid rodents. Syst. Biol. 62:837–864.

Schluter, D. 2000. The ecology of adaptive radiation. Oxford University Press, Oxford, OX.

Shulman, M. J., J. C. Ogden, J. P. Ebersole, W. N. McFarland, S. L. Miller, and N. G. Wolf. 1983. Priority effects in the recruitment of juvenile coral reef fishes. Ecology 64:1508–1513.

Sidlauskas, B. 2008. Continuous and arrested morphological diversification in sister clades of characiform fishes: a phylomorphospace approach. Evolution 62:3135–3156.

Siler, C. D., J. R. Oaks, J. A. Esselstyn, A. C. Diesmos, and R. M. Brown. 2010. Phylogeny and biogeography of Philippine bent-toed geckos (Gekkonidae: *Cyrtodactylus*) contradict a prevailing model of Pleistocene diversification. Mol. Phylogenet. Evol. 55:699–710.

Siqueira, A. C., R. A. Morais, D. R. Bellwood, and P. F. Cowman. 2020. Trophic innovations fuel reef fish diversification. Nat. Comm. 11:1–11.

Skeels, A., and M. Cardillo. 2019a. Equilibrium and non-equilibrium phases in the radiation of *Hakea* and the drivers of diversity in Mediterranean-type ecosystems. Evolution 73:1392–1410.

Skeels, A., and M. Cardillo. 2019b. Reconstructing the geography of speciation from contemporary biodiversity data. Am. Nat. 193:240–255.

Skeels, A., R. Dinnage, I. Medina, and M. Cardillo. 2021. Ecological interactions shape the evolution of flower color in communities across a temperate biodiversity hotspot. Evol. Lett. 5:277–289.

Skinner, A., A. F. Hugall, and M. N. Hutchinson. 2011. Lygosomine phylogeny and the origins of Australian scincid lizards. J. Biogeogr. 38:1044–1058.

Stamps, J. A., and R. M. Andrews. 1992. Estimating asymptotic size using the largest individuals per sample. Oecologia 92:503–512.

Stanley, S. 1973. Effects of competition on rates of evolution, with special reference to bivalve mollusks and mammals. Syst. Zool. 22:486-506.

Stroud, J. T., and J. B. Losos. 2016. Ecological opportunity and adaptive radiation. Annu. Rev. Ecol. Evol. Syst. 47:507–532.

Sweet, S. S., and E. R. Pianka. 2007. Monitors, mammals and Wallace's Line. Mertensiella 16:79–99.

Tallowin, O. J., K. Tamar, S. Meiri, A. Allison, F. Kraus, S. J. Richards, and P. M. Oliver. 2018. Early insularity and subsequent mountain uplift were complementary drivers of diversification in a Melanesian lizard radiation (Gekkonidae: *Cyrtodactylus*). Mol. Phylogenet. Evol. 125:29–39.

Taylor, S. A., and E. L. Larson. 2019. Insights from genomes into the evolutionary importance and prevalence of hybridization in nature. Nat. Ecol. Evol. 3:170–177.

Thompson, D. W. 1917. On growth and form. Cambridge University Press, Cambridge, CBE.

Thompson, G. G., C. J. Clemente, P. C. Withers, B. G. Fry, and J. A. Norman. 2009. Is body shape of varanid lizards linked with retreat choice? Aust. J. Zool. 56:351–362.

Thompson, G.G. and P. C. Withers. 1997. Comparative morphology of Western Australian varanid lizards (Squamata: Varanidae). J. Morphol. 233:127–152.

Tibshirani, R. J., and J. Taylor. 2011. The solution path of the generalized lasso. Annals Stat. 39:1335–1371.

Valente, L. M., A. B. Phillimore, and R. S. Etienne. 2015. Equilibrium and non-equilibrium dynamics simultaneously operate in the Galápagos islands. Ecol. Lett. 18:844–852.

Valente, L., A. B. Phillimore, M. Melo, B. H. Warren, S. M. Clegg, K. Havenstein, R. Tiedemann, J. C. Illera, C. Thébaud, T. Aschenbach, and R. S. Etienne. 2020. A simple dynamic model explains the diversity of island birds worldwide. Nature 579:92–96.

van Ufford, A. Q., and M. Cloos. 2005. Cenozoic tectonics of New Guinea. AAPG Bull. 89:119–140.

Voris, H. K. 2000. Maps of Pleistocene sea levels in Southeast Asia: shorelines, river systems and time durations. J. Biogeogr. 27:1153–1167.

Warren, D. L., M. Cardillo, D. F. Rosauer, and D. I. Bolnick. 2014. Mistaking geography for biology: inferring processes from species distributions. Trends Ecol. Evol. 29:572–580.

Weijola, V. S. Å. 2010. Geographical distribution and habitat use of monitor lizards of the north Moluccas. Biawak 4:7–23.

Weijola, V., S. C. Donnellan, and C. Lindqvist. 2016. A new blue-tailed monitor lizard (Reptilia, Squamata, *Varanus*) of the *Varanus indicus* group from Mussau Island, Papua New Guinea. ZooKeys 568:129–154.

Weijola, V., V. Vahtera, C. Lindqvist, and F. Kraus. 2019. A molecular phylogeny for the Pacific monitor lizards (*Varanus* subgenus *Euprepiosaurus*) reveals a recent and rapid radiation with high levels of cryptic diversity. Zool. J. Linn. Soc. 186:1053–1066.

Welton, L. J., C. D. Siler, D. Bennett, A. Diesmos, M. R. Duya, R. Dugay, E. L. B. Rico, M. Van Weerd, and R. M. Brown. 2010. A spectacular new Philippine monitor lizard reveals a hidden biogeographic boundary and a novel flagship species for conservation. Biol. Lett. 6:654–658.

Welton, L. J., P. L. Wood Jr, J. R. Oaks, C. D. Siler, and R. M. Brown. 2014. Fossil-calibrated phylogeny and historical biogeography of Southeast Asian water monitors (*Varanus salvator* Complex). Mol. Phylogenet. Evol. 74:29–37.

Zhu, X-M., Y. Du, Y-F. Qu, H. Li, J-F. Gao, C-X. Lin, X. Ji, and L-H Lin. 2020. The geographical diversification in varanid lizards: the role of mainland versus island in driving species evolution. Curr. Zool. 66:165–171.

CHAPTER II

Ontogenetic drivers of morphological evolution in monitor lizards and allies (Squamata: Paleoanguimorpha), a clade with extreme body size disparity

ONTOGENETIC DRIVERS OF MORPHOLOGICAL EVOLUTION IN MONITOR LIZARDS AND ALLIES (SQUAMATA: PALEOANGUIMORPHA), A CLADE WITH EXTREME BODY SIZE DISPARITY

Carlos J. Pavón-Vázquez[1,2], Damien Esquerré[1], J. Scott Keogh[1]

[1]Division of Ecology and Evolution, Research School of Biology, Australian National University, Canberra, ACT 2601, Australia

[2]E-mail: cjpvunam@gmail.com

Abstract

Heterochrony, change in the rate or timing of development, is thought to be one of the main drivers of morphological evolution, and allometry, trait scaling patterns imposed by size, is traditionally thought to represent an evolutionary constraint. However, recent studies suggest that the ontogenetic allometric trajectories describing how organisms change as they grow may be labile and adaptive. Here we investigated the role of postnatal ontogenetic development in the morphological diversification of Paleoanguimorpha, the monitor lizards and allies, a clade with extreme body size disparity. We obtained linear and geometric morphometric data for more than 1,600 specimens belonging to three families and 60 species to undertake one of the largest comparative studies of ontogenetic allometry to date. We found that heterochrony is the main driver of morphological divergence at shallow evolutionary scales, while changes in the magnitude and direction of ontogenetic change are found mainly between clades. Furthermore, some patterns of ontogenetic variation and morphological disparity appear to reflect ontogenetic transitions in habitat use. Our study teases apart how different evolutionary shifts in ontogeny contribute to the generation of morphological diversity.

Keywords: Allometry, heterochrony, *Lanthanotus*, ontogeny, *Shinisaurus*, *Varanus*

Evolutionary and ontogenetic changes in body size have an important effect in many other traits (Gould 1966; Klingenberg 2016). These size-related changes in phenotypic traits are referred to as allometry (Huxley and Teissier 1936; Klingenberg 2016). Historically, allometry has been considered an evolutionary constraint as restrictions imposed by size are expected to limit the number of possible morphologies (Simpson

1944; Gould and Lewontin 1979). There are three main approaches that have been employed to characterize allometric scaling: static allometry compares individuals belonging to the same species and developmental stage; ontogenetic allometry compares different developmental stages within a species; and evolutionary allometry compares different species within the same developmental stage (Cock 1966; Klingenberg and Zimmermann 1992). A comparatively understudied aspect of allometry is the evolution of ontogenetic allometry (i.e., the interspecific comparison of ontogenetic allometries). This approach has revealed that evolutionary shifts in ontogenetic allometries can occur at relatively shallow timescales, promoting morphological diversification. These shifts can be adaptive, reflecting the ecological characteristics of taxa (e.g. Adams and Nistri, 2010; Wilson and Sánchez-Villagra 2010; Esquerré et al. 2017; Gray et al. 2019).

Ontogenetic allometric trajectories can be conceptualized as vectors describing how shape changes with size through ontogeny (Fig. 1). The evolution of ontogenetic allometric trajectories can proceed in several ways. Traits that scale proportionally to body size are said to display isometry, while traits that scale disproportionally show allometry (Huxley and Teissier 1936; Klingenberg 2016). Evolutionary shifts in the size-trait intercept when the direction of shape change with size remains constant produce non-overlapping parallel trajectories (Frédérich and Vandewalle 2011). Overlapping trajectories can diverge through heterochrony, understood as an evolutionary change in the rate or timing of developmental processes (Klingenberg 1998) that results in either paedomorphosis or peramorphosis (Gerber and Hopkins 2011). Paedomorphic taxa exhibit a “juvenile-like” morphology compared to the ancestral phenotype, either through the early onset of maturity (progenesis) or a deacceleration of development (neoteny) (Gould 1977). Peramorphic taxa exhibit a more “adult-like” morphology, either through the late onset of maturity (hypermorphosis) or an acceleration of development (acceleration) (Gould 1977). Finally, evolution of ontogenetic allometric trajectories can involve shifts in the direction of phenotypic change. This can result in ontogenetic convergence, when adults of different taxa are more similar to each other than juveniles, or in ontogenetic divergence, when it is juveniles that are more similar to each other (Adams and Nistri 2010).

Paleoanguimorpha is a lizard clade with a distribution encompassing Africa, southern Asia, many Pacific islands, and Australia (Vidal and Hedges 2009; Pianka and King 2004). The group is comprised of the families Shinisauridae, Lanthanotidae, and Varanidae. Shinisauridae and Lanthanotidae are represented by a single living species each: the Chinese crocodile lizard *Shinisaurus crocodilurus* from southeastern China and northern Vietnam (van Schingen et al. 2016), and the Borneo earless monitor *Lanthanotus borneensis* from Borneo (Yaap et al. 2012). Both of these taxa are poorly

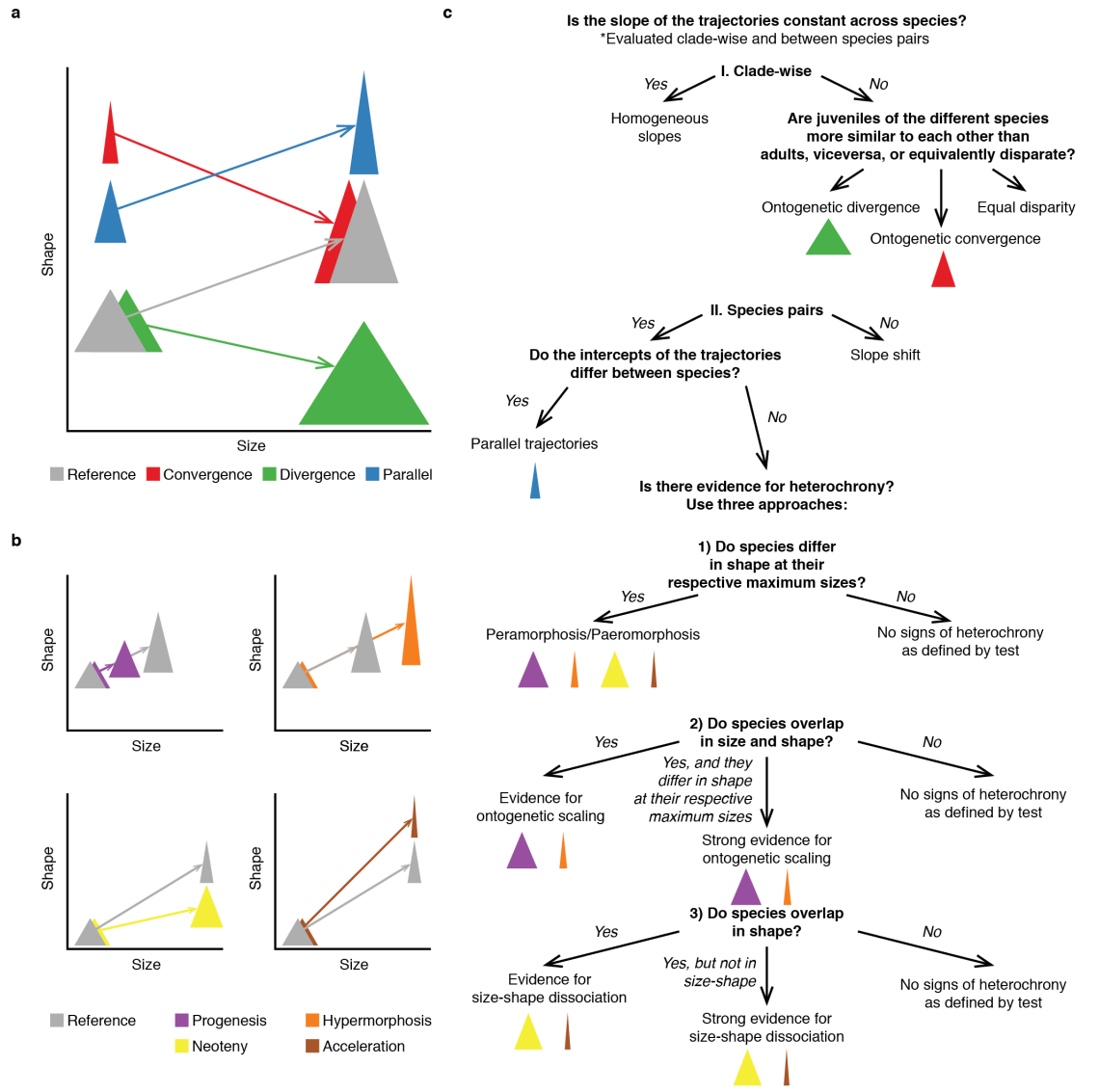

Figure 1. Evolutionary changes in ontogenetic allometric trajectories and approach used to identify them. a) Non-heterochronic changes; trajectories are represented by arrows; triangles represent juvenile and adult shape, and are connected by arrows representing the trajectories. b) Heterochronic changes. c) Approach used to identify evolutionary shifts in the trajectories. Modified from Futuyma (1986), Esquerré et al. (2017), and Navalón et al. (2021).

known inhabitants of riparian habitats. *Shinisaurus* regularly climbs overhanging vegetation (van Schingen et al. 2015), while *Lanthanotus* shelters in burrows or under leaf litter (Pianka 2004a; Yaap et al. 2012). In contrast, living monitor lizards (Varanidae) are classified into a single genus (*Varanus*), 11 subgenera, and around 80 species that show notable ecological and morphological diversity throughout their wide distribution (Pianka and King 2004; Brennan et al. 2021). There is extreme size variation in Paleoanguimorpha. *Shinisaurus* and *Lanthanotus* average around 40 cm in total length (Pianka 2004a; Ziegler et al. 2008), the smallest monitor (*V. sparnus*) is only around 20 cm long (Doughty et al. 2014), the largest living monitor (*V. komodoensis*) surpasses 3 m (Ciofi 2004), and the colossal extinct *V. priscus* probably exceeded 5 m (Molnar 2004).

This makes *Varanus* the terrestrial vertebrate genus with the largest disparity in body size (Pianka 1995). Additionally, many varanids undergo notable changes in size and ecology as they grow. For example, *V. komodoensis* hatchlings average only 42 cm in total length, are heavily arboreal, and feed on small prey. As they grow, they become strictly terrestrial and depend mainly on large ungulate prey (Ciofi 2004; Purwandana et al. 2016). Other monitors experience similar ontogenetic transitions in diet and habitat use (Losos and Greene 1998; Böhme et al. 2004; Gaulke and Horn 2004; King and King 2004; Pianka 2004b).

The presence of ecological shifts and remarkable interspecific and ontogenetic size disparity make Paleoangumorpha a suitable model to study how ontogenetic evolution drives morphological diversification. In this study, we measured over 1,600 specimens belonging to 60 living paleoanguimorph species to infer the macroevolutionary patterns of ontogenetic variation. We characterized ontogenetic changes in the shape of the body, limbs, and head through a combination of linear morphometrics and two-dimensional geometric morphometrics. Specifically, we ask whether habitat use and associated ontogenetic shifts are reflected in evolutionary and ontogenetic allometries, what evolutionary ontogenetic changes are responsible for morphological differentiation at different timescales, and what has been the tempo and mode of evolution of the ontogenetic allometric trajectories.

Materials and Methods

Taxonomic sampling

We obtained morphometric data for all three genera in Paleoanguimorpha and most of the 11 subgenera within *Varanus*, except for the monotypic *Solomonsaurus*. Taxonomic uncertainty in Varanidae required us to make decisions on what we are treating as taxonomic units in this study (Supporting Information). We aimed to characterize the ontogenetic series of each sampled species, ranging from hatchlings to large adults. We did not include species for which we could not measure small juveniles and large adults, or obtain a sample size ≥ 5. In total, we analyzed 60 species (Table S1).

Morphometrics

All analyses were performed in R 3.6.2 (R Core Team 2019). We used a 95% significance level and, unless noted, accounted for the false discovery rate (type I error) by adjusting probability values (*p*) when performing large numbers of pairwise

comparisons (Benjamini and Hochberg 1995). We obtained nine and ten linear measurements describing body and limb morphology, respectively (Fig. S1; Tables S2–S3). We corrected for body size while retaining allometric effects using log-shape ratios. For this, we calculated individual size as the geometric mean of all the measurements (both datasets combined), divided each trait by size, and log-transformed the resulting ratios (Mosimann, 1970). For each dataset, we assessed sexual dimorphism through an analysis of variance and, since our sampling is male-biased, discarded females of those species showing a significant effect of sex on morphology (Table S1). Our final sampling included 1,676 specimens for the body dataset (5–132 per species, $\bar{x}$ = 27.93) and 1,720 for the limbs dataset (5–132 per species, $\bar{x}$ = 28.67). We characterized head shape using two-dimensional geometric morphometrics. We photographed the head in dorsal view and recorded 12 landmarks and 20 semi-landmarks (Fig. S1; Table S4) that were sled based on the minimization of bending energy (Gunz and Mitteroecker 2013) in the 'geomorph 3.0.3' R package (Adams and Otarola-Castillo 2013). To remove the effects of size, location, and orientation we performed a generalized Procrustes analysis (GPA) (Gower 1975), taking bilateral symmetry into account and using the symmetric component of shape in subsequent analyses (Mardia et al. 2000; Klingenberg et al. 2002). We evaluated sexual dimorphism using the procedure described above and removed females of dimorphic species, resulting in a total sample size of 1,654 specimens (5–127 per species, $\bar{x}$ = 27.5) (Table S1). We then repeated the GPA on the retained individuals. Across datasets, only two species have a sample size of five, 88.33% of species are represented by ten specimens or more, and more than 63% of species are represented by 20 specimens or more (Table S1). Additional details on the recording and processing of morphological data are found in the Supporting Information.

Trajectory analyses

We characterized ontogenetic allometric trajectories through several approaches, performing independent analyses on each dataset. In the analyses of the body and limbs datasets, shape was described by the log-shape ratios and the log-transformed geometric mean of all measurements was used as proxy for size. The analyses of head shape were based on the Procrustes-aligned coordinates and log-transformed centroid size was used as proxy for size.

We evaluated whether each species displays isometry or allometric scaling by fitting a linear model with shape as response variable and size as predictor (Esquerré et al. 2017) in 'geomorph 4.0.0' (Adams et al. 2021). We assessed significance through residual randomization with 10,000 permutations. A significant relationship between size

and shape indicates allometric scaling, while independence between size and shape suggests isometry.

We assessed whether there is evidence for evolutionary shifts in the angle, length, and intercept of the ontogenetic allometric trajectories through a variety of approaches (Fig. 1). First, we performed a homogeneity of slopes test (HOST) to evaluate whether the ontogenetic allometric slopes differ between species (Adams and Nistri 2010; Collyer and Adams 2013). To do this, we fitted two nested linear regressions with the "procD.lm" function of geomorph, assessing significance through 10,000 residual randomization iterations. The first was a multiple regression where shape was specified as response variable, while size and species were treated as independent predictors. The second indicates a model where the species trajectories are unique by adding the interaction between size and species as predictor. We then used the "anova" function of 'RRPP 1.0.0' (Collyer and Adams 2018, 2021) to compare the models through their *F* statistics in a manner similar to a likelihood ratio test. To visualize ontogenetic allometric variation, we plotted size against the first principal component (PC) of shape as predicted by the full model with unique allometries (Adams and Nistri 2010). We also visualized the trajectories as vectors in morphospace, plotting the first two PCs of predicted shape.

Based on the regressions under the unique-allometry model, we performed interspecific pairwise comparisons of the angles and lengths of the ontogenetic allometric trajectories. Significance was assessed by comparing the empirical values with those obtained through residual randomization. Adjustment of *p* values is not necessary because the residuals are randomly placed in the same way for every test statistic, meaning that each pairwise contrast is a separate comparison derived from the same test (Collyer et al. 2015). The pairwise comparisons were performed with the "pairwise" and "summary" functions of 'RRPP', which also return estimates of the angle and length of the trajectories. We then evaluated whether the species pairs sharing a common slope display overlapping (common intercept) or parallel (differing intercept) trajectories. This was performed with the "int.test" R function (Piras et al. 2011), which performs a multivariate linear regression of shape on size and compares the Euclidean distances between intercepts to a null distribution obtained through permutation. We performed 10,000 permutations and adjusted *p* to account for type I error.

Finally, we used hierarchical partitioning to estimate the independent effects of trajectory attributes (angle, length, and intercept) on morphological disparity. Briefly, hierarchical partitioning performs multiple regression and averages the effect of each variable based on a given goodness-of-fit measure (Chevan and Sutherland 1991). For each species pair, we characterized morphological disparity as the Euclidean distance between the adult phenotypes, disparity in trajectory angles as degrees, disparity in

trajectory lengths as the absolute difference between the estimated lengths, and disparity in trajectory intercepts as the Euclidean distance between intercepts. Morphological disparity was obtained from the phenotypes predicted by the unique-allometry model for the largest individuals of each species, disparity in the angles and lengths was obtained from the regressions under the unique-allometry model, and the intercept distances were obtained from the "int.test" analysis. We performed the hierarchical partitioning analyses on the 'hier.part 1.0.6' R package (Mac Nally and Walsh 2004), based on the Gaussian family function and specifying R^2 as goodness-of-fit measure.

Heterochrony

For those species pairs sharing a common slope and intercept (61.07% of species pairs in body dataset, 67.34% in limbs, and 82.6% in head), we evaluated whether heterochronic changes have contributed to phenotypic differentiation. In the absence of information on age, it is challenging to infer the processes responsible for heterochronic shifts (e.g., progenesis vs. neoteny) (Godfrey and Sutherland 1995). Thus, studies based on wild caught individuals rely on the identification of paedomorphosis and peramorphosis for the detection of heterochrony (Piras et al. 2011; Esquerré et al. 2017). Here, we used three different approaches to detect heterochrony. First, we performed interspecific pairwise comparisons of the adult morphology, using the distance between the phenotypes at maximum size as test statistic. This was performed with the "peram.test" R function (Piras et al. 2011), and significance assessed through 10,000 permutations. Pairwise *p* values were adjusted to account for type I error. Second, we tested whether species overlap in shape and size-shape space (i.e., species look the same and have the same size in a segment of their ontogenetic trajectory), with heterochrony involving the extension or truncation of trajectories (ontogenetic scaling) (Mitteroecker et al. 2005; Gerber and Hopkins 2011). In this approach (Tfh1), the sum of the squared residuals from the multivariate regression of shape on size is used as test statistic. Finally, we tested whether species pairs overlap in shape space, with heterochrony involving the dissociation between size and shape (Mitteroecker et al. 2005; Gerber and Hopkins 2011). In this approach (Tfh2), the sum of squared distances from each specimen to its nearest point on the multivariate regression line in shape space is used as test statistic. In both Tfh tests, significance is assessed by randomizing the taxonomic identity of individuals (10,000 permutations for Tfh1 and 500 for Tfh2). To be conservative, in these tests we did not correct for type I error because heterochrony is the null hypothesis.

Morphological variation in juveniles and adults

We performed the HOST as explained above on Varanidae and each varanid subgenus containing two or more species. For each clade in which the null hypothesis of common slopes was rejected, we tested whether there is evidence for ontogenetic convergence or divergence. The procedure is based on Adams and Nistri (2010) and Esquerré et al. (2017). For each species, we obtained the predicted shapes of the largest adult and smallest juvenile from the regressions under the unique-allometry model. We then calculated the pairwise Euclidean distances among juveniles and adults and summed them to obtain a measure of disparity among juveniles (D_j) and adults (D_a). The test statistic is $D = Dj - Da$, which takes a positive value when adults belonging to the different species are more similar to each other than are juveniles (convergence), and a negative value when juveniles are more similar to each other than are adults (divergence). A null distribution of D is obtained by randomizing the morphology of individuals with respect to their size. For positive values of D, we obtained p values by calculating the proportion of permuted values that were larger than or equal to the empirical value. For negative values, we calculated the proportion of permuted values that were smaller than or equal to the empirical value.

We also evaluated the influence of phylogeny, size, and habitat use on juvenile and adult morphology. Our phylogeny is primarily based on a phylogenomic-scale time-calibrated tree (Brennan et al. 2021), trimmed to match our sampling (see Supporting Information for details) (Fig. S2; Table S5). For each species, we obtained the predicted phenotype for the largest adult and smallest juvenile from the unique-allometry regressions. We estimated phylogenetic signal as the multivariate version of Blomberg's K (Blomberg et al. 2003; Adams 2014) for each morphological dataset and growth stage employing the "physignal" function of 'geomorph'. We evaluated the significance of the phylogenetic signal through 10,000 permutations. To assess whether phylogenetic signal differs significantly between growth stages we calculated ΔK = adult K (K_a) – juvenile K (K_j). We obtained a null distribution of ΔK by randomizing the morphology of individuals with respect to their size and obtained p values by calculating the proportion of permuted values that were larger than or equal to the empirical value.

We evaluated the influence of size, habitat use, and their interaction on juvenile and adult shape through a multivariate approach based on the phylogenetic ANOVA of Garland et al. (1993), hereafter referred to as phylogenetic MANOVA. The shapes predicted for the largest and smallest specimens of each species were specified as adult and juvenile shape, respectively. In the case of adults, size was specified as log-transformed maximum snout-vent-length (SVL; commonly used as a proxy of body size in reptiles), which was obtained from the literature or our own specimen examination

(Table S1). In the case of juveniles, we employed log-transformed minimum SVL, which was obtained from our sample. Based on natural history literature (Table S1), we classified each species and growth stage independently into six habitat use categories: amphibious (semiaquatic species), canopy (arboreal species that use narrow branches high in trees), cryptic (species that spend considerable time under cover), escarpment (species that move vertically on rocky cliffs), terrestrial (species that move extensively through open habitats), and trunk (arboreal species that use the wider limbs of trees). In our procedure, we first performed principal component analysis (PCA) on the shapes of adults and juveniles and retained the first PCs that cumulatively account for 95% of variance or more. We then fitted a linear model using the "procD.lm" function of 'geomorph', with the PCs as response variables and size, habitat, and their interaction as predictors. Next, we fitted a Brownian motion model on the PCs in 'mvmorph 1.1.1' (Clavel et al. 2015) and simulated 10,000 datasets under the estimated parameters to obtain a null distribution of *F* statistics. Finally, we compared the empirical *F* statistics with the null distribution to obtain a *p* value. Additionally, to visualize the phylogenetic and ecological influence on morphology we plotted the phylomorphospace of juveniles and adults. We plotted the first two PCs, colored each species according to its subgenus or ecology, and overlaid the phylogeny on the plot using the 'phytools 0.7.62' R package (Revell 2012).

Evolution of trajectories

We estimated the phylogenetic signal and evaluated the influence of adult size and habitat use in the length and slope of the ontogenetic allometric trajectories obtained from the regressions under the unique-allometry model. We calculated Blomberg's K and assessed its significance using the "physignal" function. We then performed the phylogenetic MANOVA to assess the influence of adult size, habitat use, and their interaction on the trajectory attributes. In the case of the slopes, it was necessary to reduce dimensionality by keeping the first PCs that account for 95% of variance or more. We specified the log-transformed maximum SVL as proxy for adult size and classified the species that experience ontogenetic shifts in habitat use in a different category to either the juvenile or adult ecology; e.g., those species that are trunk dwellers as juveniles and become terrestrial as adults were grouped together and separate from those that are either trunk dwellers or terrestrial throughout their lives. Additionally, we visualized allometric diversity in the group by plotting the phyloallomspace: a two-dimensional plot of the first two PCs of the multivariate slopes of the ontogenetic allometric trajectories (Esquerré et al. 2017).

To infer the evolutionary mode of the ontogenetic allometric trajectories, we fitted evolutionary models to the trajectory lengths and first PC of the slopes. For some analyses requiring it, we obtained stochastic maps for habitat use and biogeographic history (Supporting Information) (Figs. S3–S4). We used the R packages 'geiger 2.0.6.4' (Pennell et al. 2014), 'mvmorph 1.1.1' (Clavel et al. 2015), and 'RPANDA 1.7' (Morlon et al. 2016) to fit eight models: 1) Brownian motion (BM); 2) BM with different parameters for each habitat use category (BMS) (non-censored approach of O'Meara et al. 2006); 3) Ornstein-Uhlenbeck model (OU); 4) OU with multiple optima, one for each habitat use category (OUM); 5) early burst model (EB); 6) matching-competition model (MC); 7) linear diversity dependent (DDl); and 8) exponential diversity dependent (DD2). We limited competition in the last three models to those taxa occurring in sympatry. We compared the models based on the sample-size-corrected Akaike information criterion (AICc) and respective weights (AICcw).

To examine the rates of evolution of the trajectory attributes (length and slope), we estimated branch-specific rates of evolution based on phylogenetic ridge regression in 'RRphylo 2.4.7' (Castiglione et al. 2018). We specified the trajectory lengths themselves as covariates so that rates are not artificially inflated for species experiencing large magnitudes of ontogenetic change (Castiglione et al. 2018). To visualize rate variation across the phylogeny, we log-transformed the absolute rates, because 'RRphylo' indicates the direction of phenotypic change by labeling shifts as positive or negative. We used the "search.shift" function of 'RRphylo' to detect rate shifts. This function calculates the difference between background rates and each clade containing a minimum number of species (specified by the user; six in this case). Clade-specific rates are then compared against this null distribution of rate differences to detect shifts ($p > 0.975$ indicates significantly higher rates and $p < 0.025$ indicates significantly lower rates) (Castiglione et al. 2018). We evaluated the sensitivity of our results to taxon sampling and phylogenetic uncertainty using the "overfitRR" function, which iteratively removes and rearranges tips (Castiglione et al. 2018). We specified 100 tree-modification iterations removing 25% of tips and modifying the position and age of 25% of tips and nodes, respectively. Nodes with a posterior probability above 0.95 were forced to remain monophyletic.

Results

Trajectory analyses

Most species display allometric scaling, but numerous taxa are isometric for head

shape (21 species; 8 for body shape and 6 for limb shape) (Table S6). The HOST rejected the null hypothesis of homogeneous slopes in Paleoanguimorpha across datasets (Table S7). Shape was strongly influenced by size, species, and their interaction (Table S8). The direction of ontogenetic change is somewhat conserved across species and mainly involves the relative widening of the tail, either lengthening or shortening of the tail, shortening of the fourth toe, elongation of the upper leg, and shortening and widening of the snout (Figs. 2, S5–S11). Interestingly, a high proportion of species (78.57%) that transition in ecology from arboreal to terrestrial have relatively longer tails as juveniles (Table S9), a trait that is associated with arboreality in varanids (Collar et al. 2011). The same ontogenetic morphometric shift is found in 47.83% of the species that do not show ontogenetic shifts in habitat use. Members of the highly arboreal varanid subgenus *Hapturosaurus* show some of the more distinctive trajectories, particularly in body and limb shape (Figs. 2–3).

We found numerous significant differences in the length and slope of trajectories, both between and within clades (Figs. 3, S12–S13; Tables S10–S17). Head shape trajectories are more phylogenetically conserved than the trajectories of the body and limbs. Shifts in the length and slope of trajectories are more common between clades, but are also found within clades and between sister species. The “int.test” analyses revealed that none of the species pairs sharing a common slope have parallel trajectories (Tables S18–S20). The hierarchical partitioning analyses (Tables S21–S22) suggest that angle differences between the trajectories have the largest independent effect on adult morphological disparity in the body (explaining 77.26% of variance) and limbs (71.01%). Differences in the trajectory lengths explain most of the variance in adult head shape (52.27%).

Heterochrony

The “peram.test” analyses show that most species pairs sharing a common slope and intercept differ in adult morphology (Fig. 3; Tables S23–S25). This indicates that paedomorphosis and peramorphosis are widespread in the group. Almost all comparisons with *Lanthanotus* were significant and the visualization of the trajectories shows that as varanids grow they move closer to the phenotype of *Lanthanotus*, suggesting that Varanidae is paedomorphic with respect to its sister family

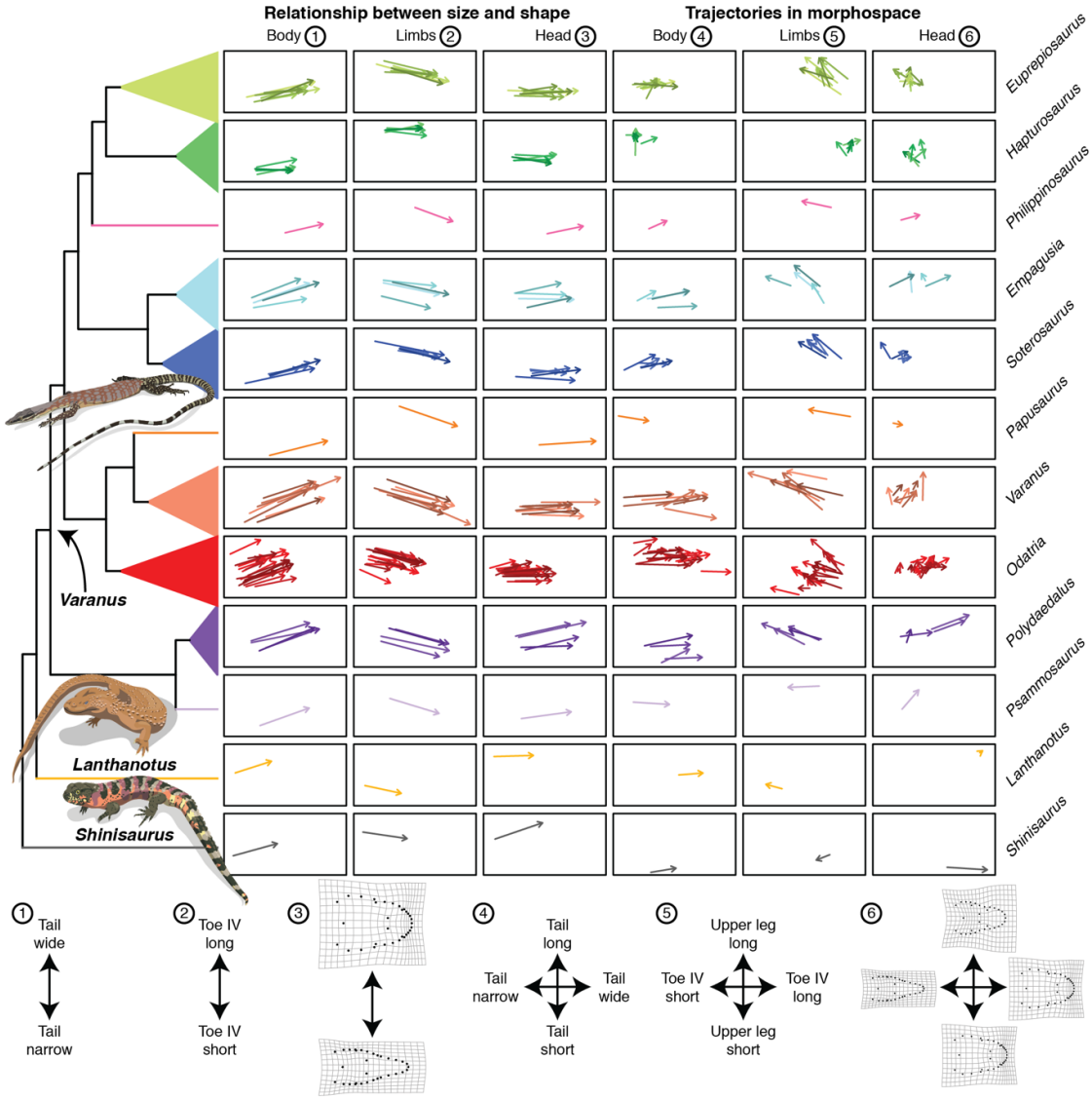

Figure 2. Ontogenetic allometric trajectories of Paleoanguimorpha. Each arrow represents the trajectory of a species as it grows. In the first three columns, the horizontal axis represents size (log-transformed geometric mean of linear measurements for body and limbs; log-transformed centroid size for head) and the vertical axes the first principal component (PC) of the predicted shape. In the last three columns, trajectories are plotted in morphospace: the horizontal and vertical axes represent the first and second PCs of the variables describing predicted shape, respectively. The tree (with arbitrary branch lengths) shows the relationships between the genera and subgenera within *Varanus*. The bottom diagrams are numbered in the same order as the columns and indicate the phenotypes at the extremes of each axis. The trait contributing the most to each PC is shown for the linear measurements and deformation grids of each extreme phenotype with respect to the average phenotype are shown for head shape.

Lanthanotidae. Heterochrony, as defined in the "peram.test", is more common than shifts in the slope of trajectories, especially within clades. In all datasets, we found evidence for ontogenetic scaling through the Tfh1 test (Fig. 3; Tables S26–S28). However, heterochrony through dissociation between size and shape as inferred from the Tfh2 test was more common (Fig. 3; Tables S29–S31). Amongst all datasets, body shape showed

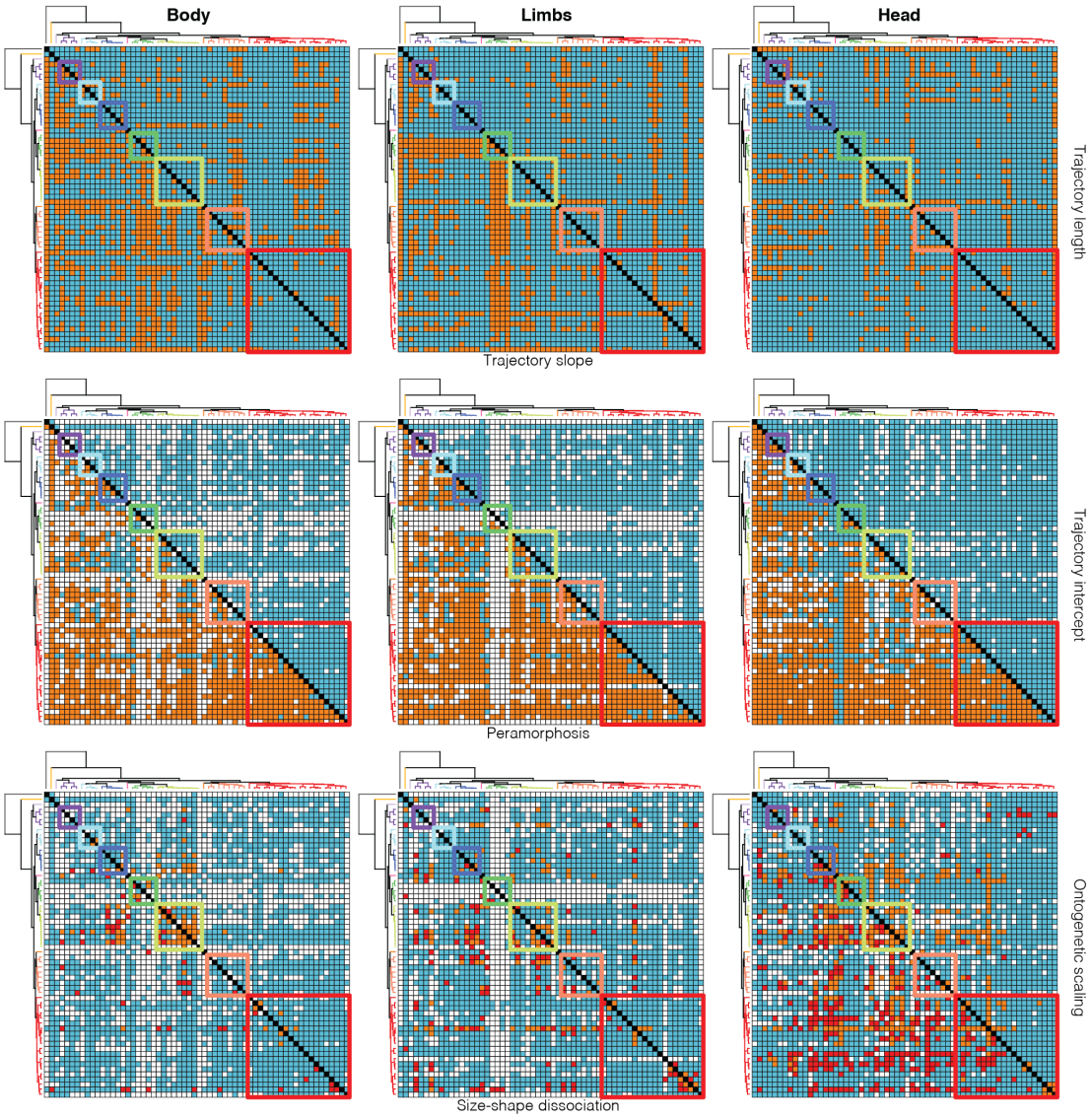

Figure 3. Phylogenetic patterns of variation in ontogenetic allometric trajectories and heterochrony in Paleoanguimorpha. Each grid is a square matrix where cells represent a pairwise comparison between species (diagonal in black). The phylogenetic tree depicting interspecific relationships is shown in the axes. Squares with colored borders indicate comparisons within clades (colors follow Fig. 2). White cells indicate comparisons that were not performed and blue cells represent negative results. Orange cells in the top row of grids indicate species pairs that differ significantly in trajectory length (upper triangle) or trajectory slope (lower triangle). Orange cells in the middle row indicate species pairs that have a common slope but differ significantly in intercept (upper triangle) or pairs that have a common slope and intercept but different adult shape, suggesting peramorphosis/paedomorphosis (lower triangle). In the upper triangle of the bottom row, orange cells indicate species pairs that overlap in size-shape space, while red cells indicate those species that overlap in size-shape space and differ significantly in adult shape (strong evidence for heterochrony by ontogenetic scaling). In the lower triangle, orange cells indicate species pairs that overlap in shape space, while red cells indicate those species that overlap in shape space but not in size-shape space (strong evidence for heterochrony by size-shape dissociation).

the least cases of heterochrony for both Tfh tests. The two kinds of heterochrony as defined by these tests are found both between and within clades, and between one pair

of sister species (*V. bushi* and *V. gilleni*). Heterochrony between *Lanthanotus* and members of Varanidae more commonly involved size-shape dissociation, in agreement with the peramorphic phenotype but smaller size of *Lanthanotus*.

Morphological variation in juveniles and adults

The HOST revealed that slopes are heterogeneous in most clades and datasets, except for limb shape in the varanid subgenera *Polydaedalus* and *Soterosaurus*, and head shape in the subgenus *Hapturosaurus* (Tables 1, S7). Across all datasets, we found evidence for ontogenetic divergence in Paleoanguimorpha and Varanidae (Table 1). Members of the subgenus *Empagusia* ontogenetically diverge in body shape, and those of *Odatria*, *Polydaedalus*, and *Soterosaurus* ontogenetically diverge in head shape. We found no significant instance of ontogenetic convergence.

Table 1. Test of ontogenetic convergence and divergence. Analyses were performed on each clade for which the hypothesis of homogeneous slopes was rejected (*p*-HOST). For positive values of *D*, *p-D* is the proportion of permuted values of *D* that were greater than or equal to the empirical value. For negative values of *D*, *p-D* is the proportion of permuted values of *D* that were less than or equal to the empirical value.

Clade	Body			Limbs			Head		
	p-HOST	*D*	*p-D*	*p*-HOST	*D*	*p-D*	*p*-HOST	*D*	*p-D*
Paleoanguimorpha	< 0.001***	–155.19	0.001***	0.002**	–173.84	< 0.001***	< 0.001***	–28.17	< 0.001***
Varanidae	< 0.001***	–140.42	0.001***	0.003**	–165.95	< 0.001***	< 0.001***	–23.13	< 0.001***
Empagusia	0.001***	–1.46	0.04*	0.01**	–0.34	0.31	< 0.001***	0.04	0.36
Euprepiosaurus	0.01**	–0.86	0.34	0.001***	–0.86	0.31	< 0.001***	–0.08	0.36
Hapturosaurus	0.03*	0.66	0.14	0.002**	0.4	0.08	0.1	—	—
Odatria	0.002**	3.57	0.32	0.01*	1.23	0.41	0.003**	–2.52	< 0.001***
Polydaedalus	0.02*	0.55	0.23	0.11	—	—	0.03*	–0.26	0.02*
Soterosaurus	0.02*	–1.04	0.19	0.38	—	—	0.02*	–0.16	0.02*
Varanus	< 0.001***	–0.62	0.44	0.009**	0.46	0.44	< 0.001***	–0.33	0.07

All morphological datasets displayed significant phylogenetic signal for both adults and juveniles ($p < 0.001$) (Table S32). Adults displayed higher phylogenetic signal than juveniles (body: $K_a = 0.29$, juvenile $K_j = 0.26$; limbs: $K_a = 0.26$, $K_j = 0.19$; head: $K_a = 0.50$, $K_j = 0.33$). However, ΔK was only significant for head shape (body: $\Delta K = 0.03$, $p = 0.34$; limbs: $\Delta K = 0.07$, $p = 0.56$; head: $\Delta K = 0.16$, $p = 0.03$). The phylogenetic MANOVA found significant deviation from Brownian motion in the relationship of body shape with habitat ($p = 0.0002$ in adults; $p = 0.0003$ in juveniles); limb shape with habitat ($p = 0.0001$ in adults and juveniles) and size ($p = 0.001$ in adults; $p = 0.04$ in juveniles); and head shape and size ($p = 0.03$ in adults; $p = 0.02$ in juveniles). Other results were not significant (Table S33). The phylomorphospace visualization mirrors these results (Fig. S14). Phylogenetic clustering is apparent in all datasets, but

clustering by habitat use more evident in body shape and limb shape than in head shape.

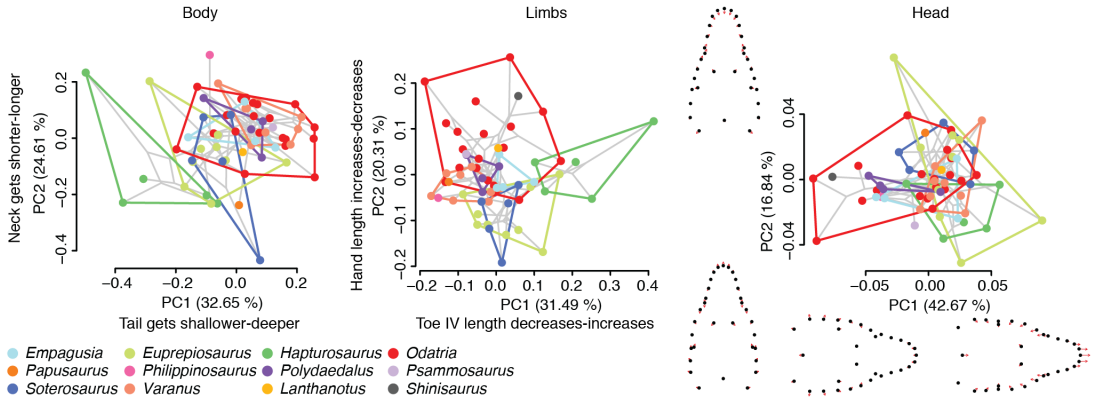

Figure 4. Phyloallomspace of Paleoanguimorpha. Axes correspond to the first two principal components (PCs) of the slopes of the ontogenetic allometric trajectories. The phylogenetic tree and inferred ancestral conditions (nodes) are shown in light gray. For the linear measurements, we show the trait whose slope contributes majorly to each PC and how it changes ontogenetically at the lower and upper extremes of each axis (separated by dash, in that order). For head shape, we show the average landmark configuration of juveniles of the species at each extreme (black points) and how landmarks move as each species grows (red arrows). Convex hulls are shown for each clade.

Evolution of trajectories

We found no significant phylogenetic signal in the length of ontogenetic allometric trajectories (Table S32). In contrast, we found significant phylogenetic signal in the slope of the trajectories (body: $K = 0.08$, $p = 0.02$; limbs: $K = 0.09$, $p = 0.009$; head: $K = 0.08$, $p = 0.03$) (Table S32). The phylogenetic MANOVA found no significant influence of ecology or adult body size in trajectory lengths, and for the slopes it only found a significant relationship between the slopes of limb shape trajectories and adult body size ($p = 0.03$) (Table S33). The strong influence of phylogeny and weaker influence of habitat use on the slopes can be visualized in the phyloallomspace (Figs. 4, S15). The OU model was supported for the length of ontogenetic allometric trajectories across all datasets (Fig. 5) (Tables S34–S35). The OUM model was preferred for the slope of the body trajectories. The OU and MC models were strongly supported for the slope of the limb and head trajectories, respectively (Fig. 5; Tables S35–S36).

The evolutionary rates of the length and slope of the ontogenetic allometric trajectories are heterogeneous in Paleoanguimorpha (Fig. 5). Shifts towards faster rates were found mostly among the varanid subgenus *Euprepiosaurus*. Shifts towards slower rates were found among the clade containing the varanid subgenera *Papusaurus* and

Varanus. The positive shifts were generally robust to phylogenetic uncertainty and sampling, in contrast with some of the negative shifts (Fig. 5).

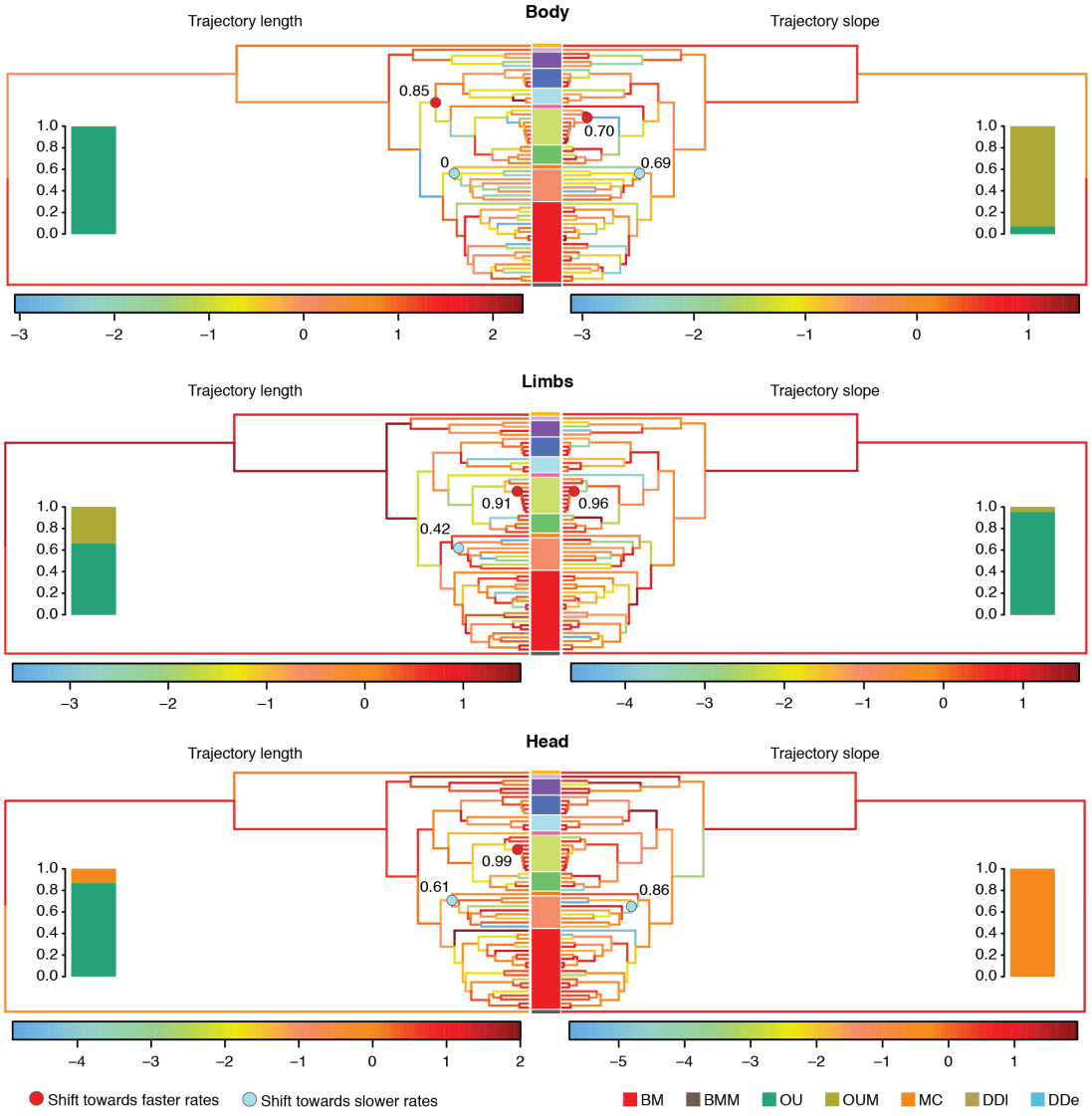

Figure 5. Evolution of ontogenetic allometric trajectories in Paleoanguimorpha. Rates of evolution of the length and slope of the trajectories are shown for each branch (natural logarithm of absolute rate). Colored bars between the mirrored trees indicate clades (colors follow Fig. 2). Circles indicate significant shifts and numbers indicate the proportion of trees with modified relationships, branch lengths, and taxon sampling in which these shifts were recovered. Bars indicate the support (AICcw) for different evolutionary models.

Discussion

As has been proposed previously (Adams and Nistri 2010; Sanger et al. 2013; Esquerré et al. 2017; Gray 2019), our results suggest that heterochrony is behind the phenotypic differentiation of closely related species, while the magnitude and direction of

ontogenetic shape change evolve more slowly but are certainly evolutionarily malleable. It is worth noting that our study is limited by sampling, and that biologically significant differences may not be statistically significant and vice versa. Thus, individual pairwise comparisons should be interpreted with caution, especially when they involve species with few sampled individuals. However, our sample sizes are relatively large for most species and the numerous pairwise comparisons increase power for the elucidation of phylogenetic patterns of ontogenetic variation.

Heterochrony

Previous research has shown that morphological diversification may proceed through changes in the slope of ontogenetic allometric trajectories (Adams and Nistri 2010), their intercept (Mitteroecker et al. 2004), heterochrony (Piras et al. 2011), or a combination of these (Esquerré et al. 2017). Heterochrony is thought to be one of the main drivers of morphological evolution (Gould 1977; McKinney 1988; Voje et al. 2013). Size-related phenotypic changes are pervasive and thus allometry acts as a strong integrating factor in body plans (Klingenberg 1996, 2010). This limits the amount of achievable morphological variation, with most evolutionary changes occurring along a path of least resistance that aligns with the slope of the allometric trajectories; i.e., the simplest way of attaining morphological modification is through a change in the timing or rate of development along a conserved allometric trajectory (McKinney 1988; Klingenberg 1996, 2010). Thus, heterochronic evolutionary shifts are expected to occur more often at shallower timescales, while the slopes of the trajectories require more time to diverge (Cock 1966; Voje et al. 2013). Our results align with this prediction: heterochronic changes are largely responsible for morphological evolution among closely related species. Significant interspecific differences in the magnitude and direction of ontogenetic change are more common between major clades, with the latter having the largest independent effect on body and limb shape variation. On the other hand, we did not detect any parallel trajectories showing a common slope but divergent intercept. The hierarchical partitioning analyses also suggest that intercept differences have a relatively small independent effect on morphological disparity. In pythons, another reptile clade showing extreme body size disparity (Esquerré et al. 2017), heterochrony also seems to be responsible for morphological divergence at shallower scales, changes in the angle and length of slopes are more common at deeper scales, and significant intercept differences are uncommon.

Heterochrony has probably played a central role in some remarkable evolutionary transitions, such as the evolution of the avian and human skulls (Bhullar et al. 2012; Gould 1977). Previous studies with limited sampling of taxa and traits have shown that

heterochrony in Varanidae explains growth patterns (Frynta et al. 2010), sexual dimorphism (Frýdlová et al. 2017), and the huge size of the extinct *V. priscus* (Erickson et al. 2003). Our results show that heterochrony also has been an important driver of differentiation, mostly within but also between clades. The type of heterochrony that appears to be more common in Paleoanguimorpha is one where morphological transformation follows changes in maximum adult size (as indicated by the peramorphosis test) (Fig. 3). Notably, heterochrony may be behind the origin of the varanid body plan. The length, slope, and intercept of the ontogenetic allometric trajectory of *Lanthanotus*, the sister of Varanidae, are similar to those of many varanid species (Fig. 3). However, adult shape differs markedly between them and, across datasets, the trajectories of most varanids move them closer to the phenotype of *Lanthanotus* as they grow. Thus, varanids seem to be paedomorphic with respect to *Lanthanotus*. However, *Lanthanotus* is smaller than most varanids. This is consistent with heterochrony by acceleration with size-shape dissociation. Accordingly, we found more instances of size-shape dissociation than of ontogenetic scaling between *Lanthanotus* and varanids. Size-shape dissociation is also more common than ontogenetic scaling in all Paleoanguimorpha. This suggests that neoteny/acceleration have been more prevalent than progenesis/hypermorphosis.

The clade containing the largest varanids (*Varanus* + *Papusaurus*) is sister to that containing the smallest (*Odatria*), providing a unique opportunity to examine the association between size, shape, and ontogeny. Many pairwise differences in body shape between the two clades are mainly the result of shifts in the slope of the ontogenetic allometric trajectories (Fig. 3). Differences in the limbs and head are mainly driven by heterochrony, particularly through size-shape dissociation in the case of the head. In general, limb proportions are paedomorphic in the miniaturized *Odatria*. In contrast, head shape appears to be peramorphic in *Odatria*, explaining the support for size-shape dissociation. The smallest species included in our sampling, *V. brevicauda*, is peramorphic across datasets with respect to its most closely related species in this study, *V. eremius*, and also with respect to some members of the *Varanus* + *Papusaurus* clade. In fact, *V. brevicauda* has the most “adult-like” body shape of all sampled paleoanguimorphs (Fig. 2). The peramorphosis of *Lanthanotus*, *V. brevicauda*, and head shape in *Odatria* may seem surprising. However, instances of peramorphosis in miniaturized taxa and paedomorphosis in giants have been noted before, such as skull hyperossification in miniaturized frogs (Trueb and Alberch 1985) and paedomorphosis in the skull of giant sauropodomorph dinosaurs (Foth et al. 2016). On the other hand, the morphology of the largest living varanid, *V. komodoensis*, appears to be the result of different processes acting on different body parts. Body shape has been differentiated between this species and its sister, *V. varius*, by a change in the slope of the ontogenetic

allometric trajectory, while the limbs and head of *V. komodoensis* are peramorphic with respect to *V. varius*. *Varanus komodoensis* has the most "adult-like" limb proportions among paleoanguimorphs. Thus, heterochrony resulting in peramorphosis is largely responsible for the shape of the smallest and largest paleoanguimorphs.

The ecology and evolution of ontogeny

Our results suggest that ontogenetic shifts in habitat use may impact morphological evolution. Disparity in the evolutionary patterns between life stages has been thoroughly documented in animal taxa that undergo metamorphosis, where life stages are expected to be subjected to very different selective pressures and vary independently (Sherratt et al. 2017; Bonett et al. 2018; Kolker et al. 2019). However, evolutionary consequences of ontogenetic ecological shifts also have been demonstrated in taxa with more gradual ontogenetic change (Adams and Nistri 2010; Esquerré et al. 2017). The results of the ontogenetic convergence/divergence test suggest that adaptive optima differ intraspecifically between juveniles and adults. We found several instances of ontogenetic divergence across all datasets, indicating that juveniles belonging to different species are more similar to each other than adults and accordingly there is lower phylogenetic signal in juveniles across datasets, significantly for head shape. This could reflect the observation that species differing in adult ecology are arboreal when they are juveniles (Pianka and King 2004). This transition occurs in species that are terrestrial or amphibious as adults, while arboreal and escarpment-dwelling species remain as such throughout their lives and share similar adaptations for vertical and acrobatic movement, such as long tails and narrow bodies (Bedford and Christian 1996; Collar et al. 2011). Thus, many species with differing adult ecologies benefit from similar adaptations for climbing as juveniles.

An ecological interpretation of the differing patterns between ontogenetic stages is further supported by the ontogenetic tail reduction experienced by many species that transition from trunk-dwelling to terrestrial or amphibious. The ecological relevance of body shape is also supported by the phylogenetic MANOVA, which suggests that shape is correlated with habitat use independently of size in both adults and juveniles. Furthermore, most species exhibit negative ontogenetic allometry in the length of the digits, another trait that is correlated with climbing performance in lizards (Colli et al. 1992). Moreover, the lengths of the upper and lower hindlimbs exhibit positive ontogenetic allometry, which may provide an adaptive advantage in terrestrial habitats (Clemente et al. 2009; Collar et al. 2011). However, more research is needed to understand whether these allometric changes result in improved performance or simply maintain function as body size increases. The phylogenetic MANOVA indeed suggests

that size has an equivalent effect on limb and head shape across the habitat use categories. Adults show more variation in body size than juveniles, and so the higher morphological disparity of adults could simply be a consequence of traits scaling allometrically to retain performance. Our results are therefore not conclusive on whether differences in phylogenetic patterns of morphological variation between juvenile and adult paleoanguimorphs are driven by habitat use.

Our analyses of the trajectory attributes under a comparative framework offer insight into the tempo and mode of evolution of ontogenetic development. The magnitude of ontogenetic shape change follows a OU model, consistent with stabilizing selection limiting allometric variation (Voje et al. 2013; Houle et al. 2019). Furthermore, trajectory lengths did not display significant phylogenetic signal or a strong correlation with maximum adult size and/or ecology deviating from BM. This perhaps indicates that the magnitude of ontogenetic shape change is so conserved across Paleoanguimorpha that it is very similar among distantly related taxa, as also suggested by the pairwise comparisons (Fig. 3). On the other hand, the direction of ontogenetic shape change displays strong phylogenetic signal, suggesting that it has evolved but not as fast as to overcome phylogenetic effects. Additionally, some variation appears to reflect ecological diversity, since an evolutionary model with multiple adaptive optima best fits the body slopes, and interspecific competition appears to have driven the evolution of the head slopes as suggested by the support for the MC model. Furthermore, the specialized arboreal varanids of the *Hapturosaurus* subgenus show trajectories that are very distinctive (Fig. 2). In some *Hapturosaurus* species, ontogenetic change goes in a different direction and the magnitude of change in the group is comparatively small. This is probably because while other species climb less often as they grow, members of *Hapturosaurus* remain highly arboreal. The specialized arboreal python *Morelia viridis* also shows a trajectory that differs markedly from other pythons (Esquerré et al. 2017). However, the phylogenetic MANOVA did not detect any significant correlation between any of the trajectory attributes and habitat use. The regressions that do not account for phylogeny detected a significant relationship of habitat with the limb trajectory lengths and the trajectory angles of all datasets. This means that habitat use covaries with these trajectory attributes, but it is challenging to untangle the effects of common descent and selection.

There is substantial variation in the evolutionary rates of the trajectory lengths and slopes (Fig. 5). Moderately and strongly supported shifts towards slower rates were detected in a clade that includes the largest varanids, such as *V. giganteus*, *V. komodoensis*, *V. salvadorii*, and *V. varius*, suggesting that large size may be imposing constraints on the evolution of ontogenetic allometric trajectories. Gould (1966) suggested that decreases in the slope of allometric trajectories are necessary to develop

large body sizes, in order to avoid non-viable or maladaptive phenotypes in adults. However, a meta-analysis of static allometries did not support this prediction (Voje et al. 2013). More research on the relationship between size, the attributes of ontogenetic allometric trajectories, and their evolutionary rates is needed to test Gould's (1966) hypothesis. Positive shifts were found mostly in the *Euprepiosaurus* varanid subgenus, a group that has rapidly diversified with moderate ecological differentiation (Weijola et al. 2019).

Conclusions

Here we show that different types of ontogenetic shifts are responsible for morphological diversification in Paleoanguimorpha, a lizard group exhibiting extreme body size disparity and ontogenetic ecological shifts. Heterochrony has allowed these lizards to morphologically diversify along a path of least-evolutionary resistance, playing a central role in phenotypic evolution. Heterochrony may also be behind the origin of the varanid body plan and has been the main driver of evolution at shallow evolutionary scales. The magnitude and direction of ontogenetic change are more evolutionarily conserved, mostly distinguishing major clades. Ecological factors may explain some of the variation in the angles of the ontogenetic allometric trajectories, as exemplified by the unique slopes of a highly specialized arboreal clade. Our results also suggest that ontogenetic shifts in habitat use may have evolutionary consequences. Selection favouring traits that enhance climbing performance may explain the phenotypic similarity of juveniles belonging to distantly related clades. In adults, selection for climbing appears to be relaxed and interspecific differences accentuate. Finally, the evolutionary rates of the ontogenetic allometric trajectories are highly variable, and we detected several rate accelerations and slowdowns. Our study further confirms that postnatal ontogenetic development should be considered as an evolutionary labile and potentially adaptive attribute of organisms.

Author Contributions

CJPV and JSK conceived the project, CJPV collected novel data and led writing; CJPV and DE performed analyses; all authors participated in writing and in the interpretation of the results.

Acknowledgments

We thank A. Allison, A.P. Amey, W. Böhme, U. Bott, R.D. Bray, P.D. Campbell, P.J. Couper, M. Cugnet, G.M. Dally, K. de Queiroz, P. Doughty, A. Drew, M. Flecks, M.E. Hagemann, M.R. Hutchinson, L. Joseph, C. Kovach, S. Mahony, D. Rödder, J.J.L. Rowley, J.W. Streicher, N. Vidal, and A.H. Wynn for granting access to herpetological collections and for their support during specimen examination; M. Arvizu Meza for help with specimen examination; T. Bonnet and E. Sherratt for statistical advice; and A. Koch and A. Schmitz for sharing molecular data of *V. bogerti*. Illustrations in Fig. 1 were inspired by photographs under a Creative Commons Attribution-Share Alike 4.0 International license (*Lanthanotus* by Chien C. Lee; *Shinisaurus* by Greg Hume) and a photograph by O. Jiménez Robles (*Varanus*). This study was funded by an Australian Research Council grant to JSK. The graduate education of CJPV was sponsored by the Australian Government Research Training Program.

Data Accessibility Statement

Morphological data is included in the Supporting Information. Molecular data is publicly available from the Dryad Digital Repository at https://dx.doi.org/10.5061/dryad.tx95x69t8 and https://doi.org/10.5061/dryad.m0n61, and from the National Center for Biotechnology Information (see details in Supplementary Material).

Literature Cited

Adams, D. C. 2014. A generalized K statistic for estimating phylogenetic signal from shape and other high-dimensional multivariate data. Syst. Biol. 63:685–697.

Adams, D. C., and A. Nistri. 2010. Ontogenetic convergence and evolution of foot morphology in European cave salamanders (family: Plethodontidae). BMC Evol. Biol. 10:1–10.

Adams, D.C., M. L. Collyer, A. Kaliontzopoulou, and E. K. Balken. 2021. Geomorph: Software for geometric morphometric analyses. R package version 4.0. Available at https://cran.r-project.org/package=geomorph.

Adams, D. C., and E. Otárola-Castillo. 2013. geomorph: an R package for the collection and analysis of geometric morphometric shape data. Methods Ecol. Evol. 4:393–399.

Bedford, G. S., and K. A. Christian. 1996. Tail morphology related to habitat of varanid lizards and some other reptiles. Amphibia-Reptilia 17:131–140.

Benjamini, Y., and Y. Hochberg. 1995. Controlling the false discovery rate: a practical and powerful approach to multiple testing. J. Roy. Stat. Soc. B Met. 57:289–300.

Blomberg, S. P., T. Garland Jr, and A. R. Ives. 2003. Testing for phylogenetic signal in comparative data: behavioral traits are more labile. Evolution 57:717–745.

Böhme, W., K. M. Philipp, and T. Ziegler. 2004. *Varanus doreanus*. *In* Pianka, E. R., and D. R. King (eds.). Varanoid Lizards of the World. Indiana University Press, Bloomington, IN.

Bonett, R. M., J. G. Phillips, N. M. Ledbetter, S. D. Martin, and L. Lehman. 2018. Rapid phenotypic evolution following shifts in life cycle complexity. Proc. R. Soc. B 285:20172304.

Brennan, I. G., A. R Lemmon, E. M. Lemmon, D. M. Portik, V. Weijola, L. Welton, S. C. Donnellan, and J. S. Keogh. 2021. Phylogenomics of monitor lizards and the role of competition in dictating body size disparity. Syst. Biol. 70:120–132.

Bhullar, B. A. S., J. Marugán-Lobón, F. Racimo, G. S. Bever, T. B. Rowe, M. A. Norell, and A. Abzhanov. 2012. Birds have paedomorphic dinosaur skulls. Nature 487:223–226.

Castiglione, S., G. Tesone, M. Piccolo, M. Melchionna, A. Mondanaro, C. Serio, M. Di Febbraro, and P. Raia. 2018. A new method for testing evolutionary rate variation and shifts in phenotypic evolution. Methods Ecol. Evol. 9:974–983.

Chevan, A., and M. Sutherland. 1991. Hierarchical partitioning. Am. Stat. 45:90–96.

Ciofi, C., and M. E. de Boer. 2004. Distribution and conservation of the Komodo monitor (*Varanus komodoensis*). Herpetol. J. 14: 99–107.

Clavel, J., G. Escarguel, and G. Merceron. 2015. mvMORPH: an R package for fitting multivariate evolutionary models to morphometric data. Methods Ecol. Evol. 6:1311–1319.

Clemente, C. J., G. G. Thomson, and P. C. Withers. 2009. Evolutionary relationships of sprint speed in Australian varanid lizards. J. Zool. 278:270–280.

Cock, A. G. 1966. Genetical aspects of metrical growth and form in animals. Q. Rev. Biol. 41:131–190.

Collar, D. C., J. A. Schulte II, J. B. Losos. 2011. Evolution of extreme body size disparity in monitor lizards (*Varanus*). Evolution 65:2664–2680.

Colli, G. R., A. F. B. Araújo, R. Silveira, and F. Roma. 1992. Niche partitioning and morphology of two syntopic *Tropidurus* (Sauria: Tropiduridae) in Mato Grosso, Brazil. J. Herpetol. 26:66–69.

Collyer, M. L., and D. C. Adams. 2013. Phenotypic trajectory analysis: comparison of shape change patterns in evolution and ecology. Hystrix 24:75–83.

Collyer, M. L., and D. C. Adams. 2018. RRPP: an R package for fitting linear models to high-dimensional data using residual randomization. Methods Ecol. Evol. 9:1772–1779.

Collyer, M. L., and D. C. Adams. 2021. RRPP: Linear Model Evaluation with Randomized Residuals in a Permutation Procedure. Available at https://cran.r-project.org/web/packages/RRPP.

Collyer, M. L., D. J. Sekora, and D. C. Adams. 2015. A method for analysis of phenotypic change for phenotypes described by high-dimensional data. Heredity 115:357–365.

Doughty, P., L. Kealley, A. Fitch, and S. C. Donnellan. 2014. A new diminutive species of *Varanus* from the Dampier Peninsula, western Kimberley region, Western Australia. Rec. West. Aust. Mus. 29:128–140.

Erickson, G. M., A. De Ricqles, V. De Buffrénil, R. E. Molnar, and M. K. Bayless. 2003. Vermiform bones and the evolution of gigantism in *Megalania*—how a reptilian fox became a lion. J. Vert. Paleontol. 23:966–970.

Esquerré, D., E. Sherratt, and J. S. Keogh. 2017. Evolution of extreme ontogenetic allometric diversity and heterochrony in pythons, a clade of giant and dwarf snakes. Evolution 71:2829–2844.

Foth, C., B. P. Hedrick, and M. D. Ezcurra. 2106. Cranial ontogenetic variation in early saurischians and the role of heterochrony in the diversification of predatory dinosaurs. PeerJ 4:e1589.

Frédérich, B., and P. Vandewalle. 2011. Bipartite life cycle of coral reef fishes promotes increasing shape disparity of the head skeleton during ontogeny: an example from damselfishes (Pomacentridae). BMC Evol. Biol. 11:82.

Frýdlová, P., V. Nutilová, J. Dudák, J. Žemlička, P. Němec, P. Velenský, T. Jirásek, and D. Frynta. 2017. Patterns of growth in monitor lizards (Varanidae) as revealed by computed tomography of femoral growth plates. Zoomorphology 136:95–106.

Frynta, D., P. Frýdlová, J. Hnízdo, O. Šimková, V. Cikánová, and P. Velenský. 2010. Ontogeny of sexual size dimorphism in monitor lizards: males grow for a longer period, but not at a faster rate. Zool. Sci. 27:917–923.

Futuyma, D. J. 1986. Evolutionary biology. Sinauer Associates Inc., Sunderland, MA.

Garland, T., Jr., A. W. Dickerman, C. M. Janis, and J. A. Jones. 1993. Phylogenetic analysis of covariance by computer simulation. Syst. Biol. 42:265–292.

Gaulke, M., and H-G. Horn. 2004. *Varanus salvator* (nominate form). *In* Pianka, E. R., and D. R. King (eds.). Varanoid Lizards of the World. Indiana University Press, Bloomington, IN.

Gerber, S., and M. J. Hopkins. 2011. Mosaic heterochrony and evolutionary modularity: the trilobite genus *Zacanthopsis* as a case study. Evolution 65:3241–3252.

Godfrey, L. R., and M. R. Sutherland. 1995. Flawed inference: why size-based tests of heterochronic processes do not work. J. Theor. Biol. 172:43–61.

Gould, S. J. 1966. Allometry and size in ontogeny and phylogeny. Biol. Rev. 41:587–638.

Gould, S. J. 1977. Ontogeny and phylogeny. Harvard University Press, Cambridge, MA.

Gould, S. J., and R. C. Lewontin. 1979. The spandrels of San Marco and the Panglossian paradigm: a critique of the adaptationist programme. Proc. R. Soc. Lond. B Biol. Sci. 205:581–598.

Gower, J. C. 1975. Generalized procrustes analysis. Psychometrika 40:33–51.

Gray, J. A., E. Sherratt, M. N. Hutchinson, and M. E. Jones. 2019. Changes in ontogenetic patterns facilitate diversification in skull shape of Australian agamid lizards. BMC Evol. Biol. 19:7.

Gunz, P., and P. Mitteroecker. 2013. Semilandmarks: a method for quantifying curves and surfaces. Hystrix 24:103–109.

Houle, D., L. T. Jones, R. Fortune, and J. L. Sztepanacz. 2019. Why does allometry evolve so slowly? Integr. Comp. Biol. 59:1429–1440.

Huxley, J. S., and G. Teissier. 1936. Terminology of relative growth. Nature 137:780–781.

King, D. R., and R. A. King. 2004. *Varanus rosenbergi*. *In* Pianka, E. R., and D. R. King (eds.). Varanoid Lizards of the World. Indiana University Press, Bloomington, IN.

Klingenberg, C. P. 1996. Multivariate allometry. *In* Marcus, L. F., M. Corti, A. Loy, G. Naylor, and D. E. Slice (eds.). Advances in morphometrics. Plenum Press, New York, NY.

Klingenberg, C. P. 1998. Heterochrony and allometry: the analysis of evolutionary change in ontogeny. Biol. Rev. 73:79–123.

Klingenberg, C. P. 2010. Evolution and development of shape: integrating quantitative approaches. Nat. Rev. Genet. 11:623–635.

Klingenberg, C. P. 2016. Size, shape, and form: concepts of allometry in geometric morphometrics. Dev. Genes Evol. 226:113–137.

Klingenberg, C. P., M. Barluenga, and A. Meyer. 2002. Shape analysis of symmetric structures: quantifying variation among individuals and asymmetry. Evolution 56:1909–1920.

Klingenberg, C. P., and M. Zimmermann. 1992. Static, ontogenetic, and evolutionary allometry: a multivariate comparison in nine species of water striders. Am. Nat. 140:601–620.

Kolker, M., S. Meiri, and R. Holzman. 2019. Prepared for the future: A strong signal of evolution toward the adult benthic niche during the pelagic stage in Labrid fishes. Evolution 73:803–816.

Losos, J. B., & Greene, H. W. 1988. Ecological and evolutionary implications of diet in monitor lizards. Biol. J. Linn. Soc. 35:379–407.

Mac Nally, R., and C. J. Walsh. 2004. Hierarchical partitioning public-domain software. Biodivers. Conserv. 13:659–660.

Mardia, K. V., F. L. Bookstein, and I. J. Moreton. 2000. Statistical assessment of bilateral symmetry of shapes. Biometrika 87:285–300.

McKinney, M. L. (ed.). 1988. Heterochrony in evolution. Springer, Boston, MA.

Mitteroecker, P., P. Gunz, M. Bernhard, K. Schaefer, and F. L. Bookstein. 2004. Comparison of cranial ontogenetic trajectories among great apes and humans. J. Hum. Evol. 46:679–698.

Mitteroecker, P., P. Gunz, and F. L. Bookstein. 2005. Heterochrony and geometric morphometrics: a comparison of cranial growth in *Pan paniscus* versus *Pan troglodytes*. Evol. Dev. 7:244–258.

Molnar, R. E. 2004. Dragons in the dust: the paleobiology of the giant monitor lizard Megalania. Indiana University Press, Bloomington, IN.

Morlon, H., E. Lewitus, F. L. Condamine, M. Manceau, J. Clavel, and J. Drury. 2016. RPANDA: an R package for macroevolutionary analyses on phylogenetic trees. Methods Ecol. Evol. 7:589–597.

Mosimann, J. E. 1970. Size allometry: size and shape variables with characterizations of the lognormal and generalized gamma distributions. J. Am. Stat. Assoc. 65:930–945.

Navalón, G., S. M. Nebreda, J. A. Bright, M. Fabbri, R. B. J. Benson, B.-A. Bhullar, J. Marugán-Lobón, and E. J. Rayfield. 2021. Craniofacial development illuminates the evolution of nightbirds (Strisores). Proc. R. Soc. B. 288:20210181.

O'Meara, B. C., C. Ané, M. J. Sanderson, and P. C. Wainwright. 2006. Testing for different rates of continuous trait evolution using likelihood. Evolution 60:922–933.

Orme, D., R. Freckleton, G. Thomas, T. Petzoldt, S. Fritz, N. Isaac, and W. Pearse. 2018. caper: Comparative Analyses of Phylogenetics and Evolution in R. R package version 1.0.1. Available at https://CRAN.R-project.org/package=caper. Accessed July 5, 2020.

Pennell, M. W., J. M. Eastman, G. J. Slater, J. W. Brown, J. C. Uyeda, R. G. FitzJohn, M. E. Alfaro, and L. J. Harmon. 2014. geiger v2. 0: an expanded suite of methods for fitting macroevolutionary models to phylogenetic trees. Bioinformatics 30:2216–2218.

Pianka, E. R. 1995. Evolution of body size: varanid lizards as a model system. Am. Nat. 146:398–414.

Pianka, E. R. 2004a. *Lanthanotus borneensis*. *In* Pianka, E. R., and D. R. King (eds.). Varanoid Lizards of the World. Indiana University Press, Bloomington, IN.

Pianka, E. R. 2004b. *Varanus bengalensis*. *In* Pianka, E. R., and D. R. King (eds.). Varanoid Lizards of the World. Indiana University Press, Bloomington, IN.

Pianka, E., and D. R. King (eds.). 2004. Varanoid lizards of the world. Indiana University Press, Bloomington, IN.

Piras, P., D. Salvi, G. Ferrara, L. Maiorino, M. Delfino, L. Pedde, and T. Kotsakis. 2011. The role of post-natal ontogeny in the evolution of phenotypic diversity in *Podarcis* lizards. J. Evol. Biol. 24:2705–2720.

Purwandana, D., A. Ariefiandy, M. J. Imansyah, A. Seno, C. Ciofi, M. Letnic, and T. S. Jessop. 2016. Ecological allometries and niche use dynamics across Komodo dragon ontogeny. Sci. Nat. 103:27.

R Core Team. 2019. R: A language and environment for statistical computing. R Foundation for Statistical Computing, Vienna, Austria. Available at https://www.R-project.org/. Accessed December 25, 2019.

Revell, L. J. 2012. phytools: an R package for phylogenetic comparative biology (and other things). Methods Ecol. Evol. 3:217–223.

Sanger, T. J., E. Sherratt, J. W. McGlothlin, E. D. Brodie III, J. B. Losos, and A. Abzhanov. 2013. Convergent evolution of sexual dimorphism in skull shape using distinct developmental strategies. Evolution 67:2180–2193.

Sherratt, E., M. Vidal-García, M. Anstis, and J. S. Keogh. 2017. Adult frogs and tadpoles have different macroevolutionary patterns across the Australian continent. Nat. Ecol. Evol. 1:1385–1391.

Simpson, G. G. 1944. Tempo and mode in evolution. Columbia University Press, New York, NY.

Trueb, L., and P. Alberch. 1985. Miniaturization and the anuran skull: a case study of heterochrony. *In* Duncker, H. R., and G. Fleischer (eds). Functional morphology of the vertebrates. Gustav Fischer Verlag, New York, NY.

van Schingen, M., C. T. Pham, H. A. Thi, T. Q. Nguyen, M. Bernardes, M. Bonkowski, and T. Ziegler. 2015. First ecological assessment of the endangered crocodile lizard, *Shinisaurus crocodilurus*, Ahl, 1930 in Vietnam: microhabitat characterization and habitat selection. Herpetol. Conserv. Biol. 10:948–958.

van Schingen, M., M. D. Le, H. T. Ngo, C. T. Pham, Q. Q., Ha, T. Q., Nguyen, and T. Ziegler. 2016. Is there more than one crocodile lizard? An integrative taxonomic approach reveals Vietnamese and Chinese *Shinisaurus crocodilurus* represent separate conservation and taxonomic units. Zool. Gart. 85:240–260.

Vidal, N. and S. B. Hedges. 2009. The molecular evolutionary tree of lizards, snakes, and amphisbaenians. C. R. Biol. 332:129–139.

Voje, K. L., T. F. Hansen, C. K. Egset, G. H. Bolstad, and C. Pélabon. 2013. Allometric constraints and the evolution of allometry. Evolution 68:866–885.

Weijola, V., V. Vahtera, C. Lindqvist, and F. Kraus. 2019. A molecular phylogeny for the Pacific monitor lizards (*Varanus* subgenus *Euprepiosaurus*) reveals a recent and rapid radiation with high levels of cryptic diversity. Zool. J. Linn. Soc. 186:1053–1066.

Wilson, L. A. and M. R. Sánchez-Villagra. 2010. Diversity trends and their ontogenetic basis: an exploration of allometric disparity in rodents. Proc. R. Soc. B: Biol. Sci. 277:1227–1234.

Yaap, B., G. D. Paoli, A. Angki, P. L. Wells, D. Wahyudi, and M. Auliya. 2012. First record of the Borneo Earless Monitor *Lanthanotus borneensis* (Steindachner, 1877) (Reptilia: Lanthanotidae) in West Kalimantan (Indonesian Borneo). J. Threat. Taxa 4:3067–3074.

Ziegler, T., L. K. Quyet, V. N. Thanh, R. Hendrix, and W. Böhme. 2008. A comparative study of crocodile lizards (*Shinisaurus crocodilurus* AHL, 1930) from Vietnam and China. Raffles B. Zool. 56:181–187.

CHAPTER III

A comprehensive approach to detect hybridization sheds light on the evolution of Earth's largest lizards*

*In press in *Systematic Biology*. Available at: https://doi.org/10.1093/sysbio/syaa102

A COMPREHENSIVE APPROACH TO DETECT HYBRIDIZATION SHEDS LIGHT ON THE EVOLUTION OF EARTH'S LARGEST LIZARDS

Carlos J. Pavón-Vázquez[1*], Ian G. Brennan[1], J. Scott Keogh[1]

[1]Division of Ecology and Evolution, Research School of Biology, The Australian National University, Canberra, Australian Capital Territory 2601, Australia.

*Corresponding author: Carlos J. Pavón-Vázquez, cjpvunam@gmail.com.

Abstract

Hybridization between species occurs more frequently in vertebrates than traditionally thought but distinguishing ancient hybridization from other phenomena that generate similar evolutionary patterns remains challenging. Here, we used a comprehensive workflow to discover evidence of ancient hybridization between the Komodo dragon (*Varanus komodoensis*) from Indonesia and a common ancestor of an Australian group of monitor lizards known colloquially as sand monitors. Our data comprises >300 nuclear loci, mitochondrial genomes, phenotypic data, fossil and contemporary records, and past/present climatic data. We show that the four sand monitor species share more nuclear alleles with *V. komodoensis* than expected given a bifurcating phylogeny, likely as a result of hybridization between the latter species and a common ancestor of sand monitors. Sand monitors display phenotypes that are intermediate between their closest relatives and *V. komodoensis*. Biogeographic analyses suggest that *V. komodoensis* and ancestral sand monitors co-occurred in northern Australia. In agreement with the fossil record, this provides further evidence that the Komodo dragon once inhabited the Australian continent. Our study shows how different sources of evidence can be used to thoroughly characterize evolutionary histories that deviate from a treelike pattern, that hybridization can have long-lasting effects on phenotypes and that detecting hybridization can improve our understanding of evolutionary and biogeographic patterns.

Keywords: Biogeography, introgression, Komodo dragon, phylogenetic networks, phylogenomics, reticulation, *Varanus*

Natural hybridization, the successful crossing of individuals from distinct populations or groups of populations (Harrison and Larson 2014), has long been of interest to

evolutionary biologists (Mallet 2008). Interspecific hybridization has long been recognized as playing an important role in the evolutionary process (Stebbins 1959), and Charles Darwin even devoted an entire chapter to it in the Origin of Species (Darwin 1859). Recently, technical and methodological advances have revealed numerous instances of ancient hybridization (Li et al. 2016; Meier et al. 2017; Taylor and Larson 2019), often by detecting introgression (i.e., the transfer of alleles between species through hybridization and backcrossing). This has shown that hybridization is more widespread in nature than traditionally considered and that it can have important evolutionary consequences (Taylor and Larson 2019), affecting key features such as genetic variability, fitness, diversification rates, and reproductive mode (e.g., Mallet 2005; Lampert and Schartl 2008; Meier et al. 2017; Patton et al. 2020). However, detecting ancient hybridization remains practically challenging. It often requires the generation of large molecular datasets, and methods used to infer ancient hybridization based on molecular data need to account for other evolutionary phenomena that generate similar patterns, particularly incomplete lineage sorting (ILS; i.e., the retention of ancestral genetic polymorphism across species). Explicit phylogenetic networks depict phylogenetic relationships as a reticulate network instead of a bifurcating tree whenever ILS is insufficient to explain the distribution of genetic variation. In those cases, hybridization or other processes that cause deviation from a treelike pattern such as horizontal gene transfer and admixture may better explain the data (Cao et al. 2019). Another commonly used approach is the calculation of the *D* statistic in a test known as ABBA-BABA, which indicates whether the patterns of allele sharing between four taxa are more congruent with ILS or introgression (Green et al. 2010; see Materials and Methods).

Hybridization poses practical challenges to evolutionary biology and conservation. There is a broad body of literature devoted on how to alleviate the negative effects it can have on phylogenetic inference (Page and Charleston 1997; Meyer et al. 2017). Concern exists over introgression involving endangered and/or evolutionarily unique taxa, which can result in decreased fitness (Mallet 2005). However, evaluation of the phenotypic and genotypic signatures of hybridization can also shed light on the historic processes responsible for observable biological patterns. The study of natural hybrid zones has been crucial for understanding the nature of species boundaries, the speciation process, and the heritability of organismal traits (Stebbins 1959; Barton and Hewitt 1989; Taylor and Larson 2019). Furthermore, hybridization can play a fundamental role in the creation of novel genetic combinations on which natural selection can act upon, as has been documented in textbook examples of adaptive radiation (Lamichhaney et al. 2015; Meier et al. 2017; Taylor and Larson 2019). Hybridization can therefore play a central role in the sorting of phenotypic variation, often resulting in increased fitness (The *Heliconius*

Genome Consortium 2012; Arnold and Kunte 2017; Karimi et al. 2020). Finally, the detection of hybridization can impose temporal and spatial bounds that can yield insight into the timing and geographic location of evolutionary events, as hybridization requires sympatry. This has been the case with hominin evolution (Green et al. 2010; Villanea and Schraiber 2019; Chen et al. 2020).

Some of the best documented examples of hybridization are found in lizards, where it is often associated with parthenogenesis and polyploidy (Fujita and Moritz 2009). Despite reports of parthenogenesis and polyploidy in monitor lizards (Lenk et al. 2005; Iannucci et al. 2019), hybridization in the group remains largely untested. Monitor lizards (Squamata: Varanidae) are a family of around 80 living species that are remarkable among non-avian reptiles for their intelligence, aerobic capacity, and ecomorphological diversity, particularly in body size (Pianka and King 2004; Uetz 2019). The largest living lizard is the Komodo dragon (*Varanus komodoensis*), a powerful ~3 m carnivore capable of killing large prey such as pig, deer, buffalo, and occasionally humans (Auffenberg 1981), arguably with the help of a venomous bite (Fry et al. 2009). The Komodo dragon belongs to an Australasian clade (hereafter called the large Australasian monitors clade [LAMc]) that includes eight other extant species (Brennan et al. 2021), among them other giant monitors exceeding 2 m in total length, such as the crocodile monitor from the lowlands of New Guinea (*V. salvadorii*), the perentie from the Australian arid zone (*V. giganteus*), and also the extinct megalania (*V. priscus*) from eastern Australia, which was probably 5–7 m long (Molnar 2004). The Komodo dragon is presently restricted to western Flores and four other smaller nearby islands in the Indonesian Lesser Sundas (Ciofi et al. 1999). The remaining extant members of the LAMc are *V. mertensi* from the Australian monsoonal tropics, *V. varius* from eastern Australia, and a group of four species informally referred to as sand monitors: *V. gouldii*, *V. panoptes*, *V. rosenbergi*, and *V. spenceri*. Sand monitors are restricted to Australia, except for *V. panoptes* from northern Australia and southern New Guinea (Pianka and King 2004) (Fig. 1).

Several studies have looked at the evolutionary relationships within the LAMc, mostly as part of broader phylogenetic studies (Ast 2001; Fitch et al. 2006; Conrad et al. 2011; Vidal et al. 2012; Pyron et al. 2013; Lin and Wiens 2017; Brennan et al. 2021). The recovered topologies vary depending on the employed phylogenetic methods and data sources. The topology recovered by Brennan et al. (2021) using hundreds of nuclear loci differs from previous studies that employ mitochondrial data exclusively (Ast 2001; Fitch et al. 2006) or fewer nuclear loci (Vidal et al. 2012). Furthermore, the number of gene trees supporting most branches within the LAMc is relatively low compared with other varanid clades (Brennan et al. 2021), evidencing phylogenetic incongruence among loci. These studies have shed light on the evolution of the LAMc, but the causes of phylogenetic incongruence remain under explored. Here, we implemented a

comprehensive approach incorporating a phylogenomic dataset which included both hundreds of nuclear loci and mitochondrial genomes, phenotypic data, locality records, and fossil data to test whether phylogenetic incongruence is partially caused by ancient hybridization. We found molecular and phenotypic evidence for ancient hybridization between the Komodo dragon and sand monitors.

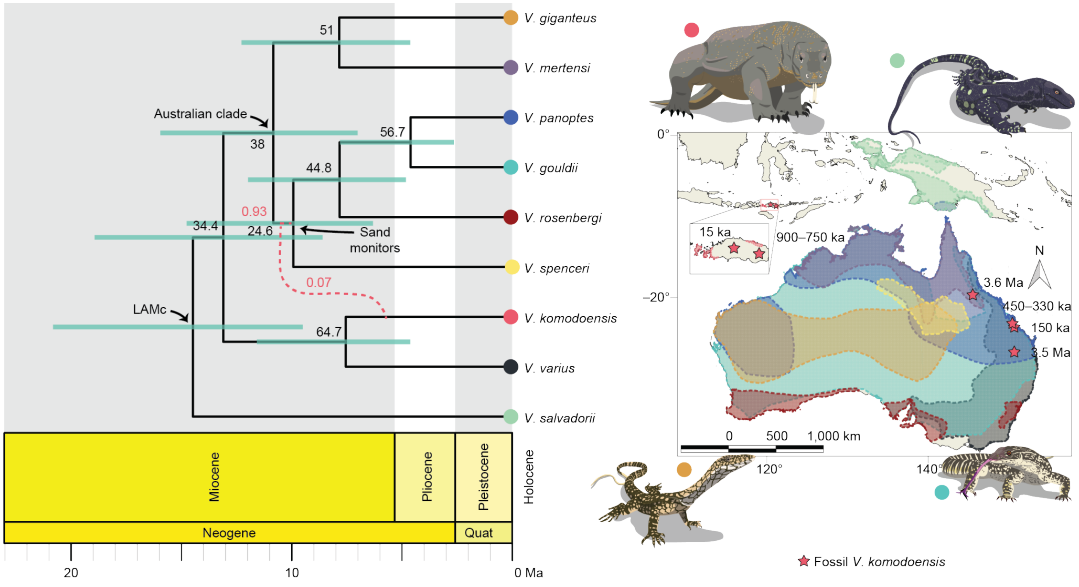

Figure 1. Phylogeny and distribution of large Australasian monitors. The phylogeny is a species tree based on nuclear data, obtained in ASTRAL, and time-calibrated with MCMCTree. Blue bars represent the 95% credibility interval for divergence dates. Numbers in nodes indicate gene concordance factors. Bootstrap values were 100 for all nodes. The red dotted line indicates the most likely reticulation event as suggested by our results, with the proportion of alleles inherited from each of the involved taxa specified by the red number (results from SNaQ; see Fig. 2b). Representatives of each clade are illustrated (scaled roughly proportionally to each other). The map depicts the current distribution of living taxa and fossil records (stars; approximate age shown next to each) of *V. komodoensis* (based on Ciofi et al. (1999) and IUCN (2019)). Colors in the map and illustrations follow the circles at the tips of the phylogeny.

Materials and Methods

Here we outline the employed materials and methods and the reasoning behind their use. Additional details are found in the Appendix and summarized in Figs. S1–S2.

Molecular data

We employed a publicly available nuclear dataset that was obtained through anchored hybrid enrichment (AHE) (Lemmon et al 2012) and was first used to resolve the

phylogeny of Varanidae (Brennan et al. 2021). The dataset is available at https:/dx.doi.org/10.5061/dryad.tx95x69t8 and was supplemented with sequences of the AHE loci extracted from a recently published genome of *V. komodoensis* (Lind et al. 2019) using custom scripts available at https://github.com/IanGBrennan/mitoGenome_Assembly. We included representatives of all living species (9) and subspecies (5) belonging to the LAMc and an outgroup (*V. timorensis*). All species were represented by a single individual, except for *V. gouldii* (6 individuals) and *V. panoptes* (7 individuals). Voucher numbers, locality details, and proportion of missing data for the sequenced samples are specified in Table S1. We obtained alignments for a total of 388 nuclear loci. To minimize the impacts that incomplete taxon sampling, missing data, and low loci informativeness can have on phylogenetic inference and the detection of hybridization, we generated two subsets of the data for downstream analyses. The first (Subset 1) contains all loci with at least one sequence per species (n = 337). The second dataset used in downstream analyses (Subset 2) contains 40 loci from Subset 1 with little missing data and a high number of informative sites. Alignments in Subsets 1 and 2 average 1,654 bp and 1,607 bp length; 4.40% and 5.88% segregating sites; and 6.42% and 3.82% missing data, respectively.

Mitochondrial genomes were obtained for most individuals from raw reads generated incidentally by the AHE capture and sequencing approach, using code available at https://github.com/IanGBrennan/mitoGenome_Assembly, and obtained from GenBank for *V. komodoensis* (GenBank accession numbers [GB] in Table S1). We used a publicly available mitochondrial genome of *V. niloticus* (GB AB185327) as reference for sequence assembly and alignment. The proportion of missing data for each sample is specified in Table S1. For the mitochondrial introgression test (see below), we downloaded additional sequences of the NADH dehydrogenase subunit 2 gene (*ND2*) for the LAMc and an outgroup (*V. acanthurus*) from GenBank (GB in Table S2).

Phylogenomics

Many of the methods we employed to test for hybridization rely on individual gene trees and a species-level phylogeny. Thus, we inferred individual trees for each locus in Subset 1. To evaluate mito-nuclear discordance, we obtained the maternal phylogeny based on the mitochondrial genomes. Tree inference was performed using maximum likelihood in IQ-TREE 1.7 (Nguyen et al. 2015; see Appendix). Node support was obtained by performing 1,000 ultrafast bootstrap replicates (Hoang et al. 2018). In the presence of ILS, it is generally accepted that methods based on the multi-species coalescent (MSC) recover interspecific relationships more accurately than concatenation approaches (Edwards et al. 2007; Mendes and Hahn 2018). While full Bayesian

implementation of the MSC can be prohibitively inefficient for large datasets, the development of approaches based on the MSC that summarize gene trees to estimate species trees has improved the scalability of coalescent methods (Mirarab et al. 2014; Rabiee et al. 2019). In order to maximize the sampling of loci while accounting for ILS, we used the summary method ASTRAL-III 5.6.3 (Zhang et al. 2018) to estimate the species tree of the LAMc. We specified the maximum likelihood gene trees of Subset 1 obtained with IQ-TREE as input for ASTRAL and performed multi-locus bootstrapping (Seo 2008) based on the ultrafast bootstrap trees of each locus.

To temporally frame our results and perform morphological analyses that take an ultrametric tree as input we time-calibrated the ASTRAL species tree in MCMCTree as implemented in the PAML 4.8 package (Yang 2007). MCMCTree is a Bayesian method that estimates divergence times on a fixed topology. Its use of approximate likelihood calculation permits the efficient analysis of large alignments (dos Reis and Yang 2011), compared to computationally demanding Bayesian methods such as BEAST2 (Bouckaert et al. 2014) or MrBayes (Ronquist et al. 2012). We used a concatenated alignment of Subset 1 as input for MCMCTree, choosing the individuals with the lowest proportion of missing data for those species with multiple individuals. We first estimated the branch lengths of the ASTRAL tree in BASEML as implemented in PAML. To calibrate the tree, we specified a minimum age of 3.6 Ma for the divergence between *V. komodoensis* and *V. varius*, based on the oldest known *V. komodoensis* fossils (Hocknull et al. 2009; Brennan et al. 2021). Fossil calibration of the root is not straightforward given the uncertain phylogenetic placement of early Australian varanids. Thus, we based the prior for the root age on the molecular-only tree inferred by Brennan et al. (2021), specifying a uniform prior with upper and lower bounds of 23.8 Ma and 17.8 Ma, respectively. To calculate the proportion of loci supporting each branch, we first obtained an individual-level tree with ASTRAL-III 5.6.3 (Zhang et al. 2018), using the maximum likelihood gene trees of Subset 1 as input. We then annotated this tree with gene concordance factors in IQ-TREE 1.7 (Nguyen et al. 2015).

Reticulation

To characterize phylogenetic discordance and identify clusters of gene trees supporting particular topologies, we estimated the distribution of gene trees in phylogenetic tree space for Subset 1 using the 'treespace 1.1.3.2' (Jombart et al. 2017) package in R 3.5.3 (R Core Team 2019). We rooted the maximum likelihood gene trees on *V. timorensis*, calculated the number of tree clusters based on the gap statistic (Tibshirani et al. 2001) in the 'cluster 2.1' (Maechler et al. 2019) R package, and found the geometric median tree for each cluster in 'treespace 1.1.3.2' (Jombart et al. 2017). Our phylogenetic

analyses revealed both gene tree–gene tree and gene tree–species tree incongruence (see Results). Introgression and ILS are the main sources of phylogenetic conflict in protein-coding eukaryote genes (Mallet et al. 2016). To evaluate whether the conflict is partially caused by introgression while accounting for ILS, we performed phylogenetic network inference based on two methods: one based on unrooted quartets of taxa and implemented in SNaQ (Solís-Lemus and Ané 2016), and one based on rooted triplets of taxa and implemented in PhyloNet 3.6.10 (Than et al. 2008). To minimize the effects that taxon sampling can have on network inference (Karimi et al. 2020), we based the analyses on the maximum likelihood gene trees including at least one representative per species (Subset 1). To minimize potential biases caused by missing data and low sequence variation (Mason et al. 2019), we also analysed Subset 2 (see below). Branch lengths in SNaQ are measured in coalescent units and we therefore specified the uncalibrated ASTRAL species tree as starting tree. For the four analyses (SNaQ and PhyloNet for each of the two subsets), the maximum number of reticulations was set to 5. The results of the SNaQ analysis of Subset 1 are conservative (i.e. they infer a single reticulation) and are the most congruent with the ABBA-BABA and morphological results (see Results). Thus, we obtained bootstrap values for this network by performing 100 bootstrap replicates based on the ultrafast bootstrap trees of loci in Subset 1. Additional details are found in the Appendix.

The possibility of nuclear introgression was further evaluated using ABBA-BABA tests (Green et al. 2010). Consider a tree with topology (((taxon 1, taxon 2), taxon 3), Outgroup)). Under ILS, there should be an equal frequency of alleles showing the "ABBA" and "BABA" patterns ($D = 0$; each letter represents an allele for each of the four taxa, respectively). An excess of either pattern is indicative of introgression ($D \neq 0$) (Green et al. 2010). We extracted single nucleotide polymorphisms (SNPs) from the full AHE dataset (388 loci) by keeping only biallelic sites without missing data using SeATTLE (Pavón-Vázquez and Pavón-Vázquez 2019) and the 'phrynomics 2.0' (Leaché et al. 2015) R package. We reconstructed the allelic phases of the SNPs in fastPHASE 1.4 (Scheet and Stephens 2006), using species as "subpopulation labels" and default settings. Based on the estimated phylogenetic networks (Results), we performed post-hoc analyses testing for introgression in every three-taxon combination of the Komodo dragon with members of an Australian clade (hereafter called the Australian clade) comprising *V. giganteus*, *V. gouldii*, *V. mertensi*, *V. panoptes*, *V. rosenbergi*, and *V. spenceri*. We specified *V. timorensis* as outgroup. Additionally, we tested if more SNP variants are shared between *V. komodoensis* and the members of the Australian clade than between the latter and the Komodo dragon's sister species, *V. varius*. The ABBA-BABA tests were performed in the 'evobiR 1.2' (Blackmon and Adams 2015) R package. We ran the analyses twice for each taxon set, firstly using allele frequencies and

secondly the majority consensus sequence for each species. To assess significance and account for the non-independence of SNPs (given that more than one could come from a single locus), we performed 1,000 jackknife replicates with the largest possible block size (i.e., half the number of SNPs present in each dataset). The number of SNPs was 4,624–5,738 ($\bar{x}$ = 5,187) and 4,562–5,148 ($\bar{x}$ = 4,851) in the allele frequency and consensus sequence analyses, respectively.

As a final test of hybridization in the LAMc, we used a simulation approach to evaluate whether the observed mito-nuclear discordance was more congruent with ILS or introgression. We compared the observed genetic distances for a fraction of the maternally inherited mitochondrial genome to the distances obtained through simulations under the MSC (a null-model of ILS and divergence) (Joly et al. 2009). To maximize intraspecific sampling and control for alignment ambiguity, our analyses were based on the protein coding *ND2* gene (1,039 bp). Given that realistic sequence simulation depends on accurate estimation of population parameters, we downloaded additional sequences of the LAMc from GenBank. We calculated the minimum uncorrected genetic distances between species pairs (*p*-min) for the empirical alignment and for 1,000 alignments simulated in MCcoal (Rannala and Yang 2003), and used simulated values of *p*-min as a null distribution for significance testing (Joly et al. 2009), controlling for the false discovery rate as a result of multiple testing (Benjamini and Hochberg 1995). Additional details on the choice of priors and parameters are found in the Appendix.

Morphology

Ancient hybridization does not only leave an imprint on the genome, but can also leave a trace detectable in present day phenotypes (Karimi et al. 2020). To test if introgressive hybridization left an imprint on the phenotype of the LAMc, one of us (C.J.P.V.) recorded 20 external linear measurements (Table S3) for 107 adult specimens belonging to the LAMc, including snout-vent length (SVL). After accounting for sexual dimorphism (Appendix), our dataset contained 88 specimens, averaging 9.78 specimens per species. All statistical analyses were based on the residuals of a linear regression of each log-transformed trait against the log-transformed SVL, which is commonly used as a proxy for body size in reptiles (e.g., Meiri 2007, 2008; Pincheira-Donozo and Tregenza 2011). To initially identify what effect reticulation could have had on the morphology of the LAMc, we performed both conventional principal component analysis (PCA) and phylogenetic PCA (phyloPCA) on the residuals and overlaid the time-calibrated species tree on the PCA plots using the “phylomorphospace” function of the R package ‘phytools 0.6-99’ (Revell 2009, 2012).

We tested whether phenotypic variation in the LAMc is more consistent with a bifurcating tree or a reticulated network by fitting different evolutionary models in PhyloNetworks (Solís-Lemus et al. 2017). First, we time-calibrated the network obtained from the SNaQ analysis of Subset 1 (which is the most consistent with the ABBA-BABA and morphological results; see Results) based on the branch lengths of individual gene trees following Bastide et al. (2018) and Karimi et al. (2020). We fitted four basic Brownian motion (BM) models to the size-corrected traits and the first two principal components obtained with the PCA and phyloPCA: 1) both parental taxa contribute to the hybrid phenotype with magnitude proportional to their relative genetic contributions (describing morphological intermediacy); 2) same as (1), but an evolutionary shift occurs following hybridization (describing transgressive evolution); 3) an evolutionary shift occurred in the same taxa as in (2), but did not involve hybridization (shifted BM in a bifurcating tree); and 4) a single-rate model in a bifurcating tree. To account for uncertainty in the estimation of parental genetic contributions and for the possibility that phenotypic and genetic contributions were not proportional, we also fitted models 1 and 2 to networks where the contribution of each parent was set to 25%, 50%, and 75%, respectively. To eliminate the possibility that changes in fit could be attributed to changes in branch lengths, we used the backbone phylogeny extracted from the calibrated network to test the tree-like models. We compared the models based on the Akaike Information Criterion (AIC), Akaike weights (AICw), and difference in AIC (ΔAIC).

To test whether *V. komodoensis* and sand monitors are more similar to each other than expected given the phylogeny, we used a recently developed method that was originally designed to evaluate evolutionary convergence and is implemented in the "search.conv" function of the R package 'RRphylo 2.4.7' (Castiglione et al. 2018, 2019). The method employs the angles between phenotypic vectors as a measure of similarity. Importantly for our study, "search.conv" allows the specification of ancestral states (see below). We implemented the state categorization approach, classifying the taxa for which similarity was being tested under the same state ("hybrid"). We used the 19 size-corrected traits, first two PCs, and first two phyloPCs independently to compare *V. komodoensis* with the sand monitor clade and also with each individual sand monitor species, randomly shuffling the "hybrid" state across the species 1,000 times to assess significance.

The "search.conv" function depends on ancestral state reconstruction. Inferring the morphology of the most recent common ancestor (MRCA) of sand monitors through conventional ancestral character reconstruction could be biased if the phenotypes of living sand monitors show signs of past hybridization. Thus, we aimed to reconstruct the phenotype of the ancestral sand monitor with which *V. komodoensis* hybridized through phylogenetic imputation (Fig. S2), which infers terminal and ancestral phenotypes in the

presence of missing data based on an evolutionary model and the phylogeny. We deleted all the morphological data of sand monitors and inferred the character states of their MRCA under BM. We used the 'Rphylopars 0.2.9' package (Goolsby et al. 2017), which can incorporate intraspecific variation and correlation between characters. Additional details on the phylogenetic imputation are found in the Appendix. We refer to the taxon whose morphology was reconstructed through imputation as the reticulation-free MRCA. We specified the morphology of the reticulation-free MRCA as the ancestral phenotype of sand monitors and repeated the "search.conv" analyses comparing *V. komodoensis* and the sand monitor clade. The ancestral morphology of other nodes was inferred with the "RRphylo" function, which is the same function used internally by "search.conv".

While our species tree is well-supported and concordant with previous studies (Brennan et al. 2021), there is uncertainty in divergence dates. We assessed the sensitivity of "search.conv" to branch length uncertainty by repeating analyses on a sample of 100 trees with branch lengths based on the MCMCTree credibility intervals (see Appendix). We also performed a test of morphological intermediacy based on the count of individual characters that are intermediate between the alleged parental lineages in the putative hybrid taxa (Wilson 1992). Additional details are found in the Appendix.

Biogeography

To evaluate the biogeographic plausibility of hybridization between *V. komodoensis* and sand monitors we reconstructed the ancestral ranges of the LAMc. We ran our ancestral range reconstruction analyses on the time-calibrated species tree. We also modified the aforementioned tree in order to incorporate our knowledge of the past distribution of the Komodo dragon as indicated by its fossil record. The Komodo dragon is the only living member of the LAMc with a rich fossil record from outside its current range whose taxonomic identity has been rigorously assessed (Hocknull et al 2009). We added known fossils as tips of the tree basing their ages on previous palaeontological studies (Hocknull et al 2009; Price et al. 2015) (Table S4).

We used likelihood-based models to infer ancestral distributions in discrete geographic areas using the 'BioGeoBEARS 1.1.2' (Matzke 2013) R package. We divided the range of the LAMc into nine discrete areas (see Results and Appendix) and assigned each species to specific areas based on the Atlas of Living Australia (2019) online database and relevant literature (Appendix). We ran analyses under the DEC and DEC+J models, implementing a likelihood-ratio tests for model selection (Matzke 2014). Additionally, we used the R package 'rase 0.3-3' to estimate ancestral ranges in a

Bayesian framework (Quintero et al. 2015). This method uses a BM diffusion model to estimate ancestral ranges based on polygonal distributions that can be irregular and/or discontinuous, thus bypassing the biases associated with the categorisation of geographic space into discrete units. See Appendix for more details on the ancestral range reconstruction.

Patterns of range expansion and local extinction are difficult to infer from extant only records and geographically isolated fossils. To understand this process in the Komodo dragon we estimated its present and past potential distribution based on its realized climatic niche. We extracted climate data for contemporary and fossil records (Table S5) and used it to model the species distribution using generalized linear models (GLM). We also tested whether the climatic niche of the Komodo dragon has remained stable over time. Additional details are found in the Appendix.

Results

Phylogenomics

The interspecific relationships recovered in our species tree were concordant with most trees inferred by Brennan et al. (2021) (Figs. 1, S3). The New Guinean *V. salvadorii* was recovered as sister to the rest of the members of the LAMc. A group comprising *V. komodoensis* and *V. varius* is sister to a primarily Australian clade containing the remaining species (i.e., the Australian clade). A clade that includes *V. giganteus* and *V. mertensi* is sister to the sand monitors. Within the sand monitors, *V. spenceri* is sister to the remaining species and *V. rosenbergi* is sister to a clade comprising *V. gouldii* and *V. panoptes*. Multi-locus bootstrap values were high (100% for all nodes). In contrast, concordance factors were low, smaller than 50% in most cases (Fig. 1). Our species tree differs topologically from trees based on fewer nuclear loci (Vidal et al. 2002, Pyron et al. 2013) and mitochondrial trees (Ast 2001; Fitch et al. 2006), including our own (Fig. S4). Diversification of the LAMc appears to have occurred primarily during the Miocene (Fig. 1). Divergence between *V. komodoensis* and *V. varius* occurred ~8 Ma (mean 7.54 Ma, 95% CI 4.6–11.6 Ma). The basal split within sand monitors was estimated to have occurred ~10 Ma (mean 9.93 Ma, 95% CI 6.3–14.8 Ma).

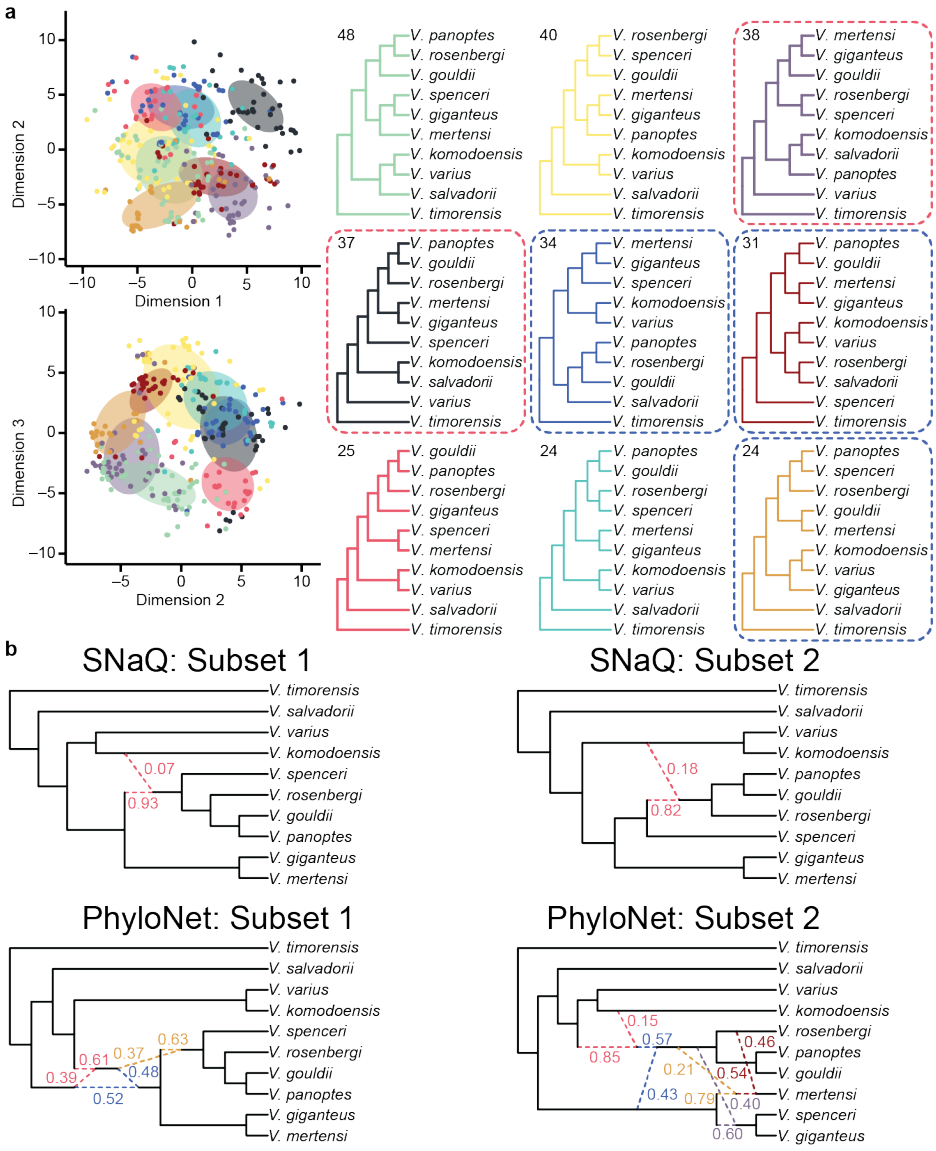

Figure 2. Molecular evidence of hybridization in the large Australasian monitors clade. a) Clusters of gene trees identified through multidimensional scaling of phylogenetic tree space; different colors are used for each cluster; individual gene trees and 95% confidence ellipses for each cluster are plotted to the left, and the median tree for each cluster is plotted to the right; the number of trees assigned to each cluster is shown next to each median tree; red dotted lines indicate trees where *V. komodoensis* is more closely related to sand monitors than to its sister species, while blue dotted lines indicate trees where *V. komodoensis* disrupts the monophyly of the Australian clade. b) Phylogenetic networks inferred for the large Australasian monitors clade; reticulation events are represented by the dotted lines, with numbers indicating the proportion of alleles inherited from each of the involved taxa; analyses were based on either 337 loci with all species represented (Subset 1) or 40 informative loci with little missing data (Subset 2).

Reticulation

Exploration of phylogenetic tree space revealed nine clusters of gene trees supporting different relationships (Fig. 2a). In two of the median trees *V. komodoensis* is more

closely related to sand monitors than to *V*. *varius* and in three of them *V*. *komodoensis* (sometimes accompanied by its sister species *V*. *varius* and *V*. *salvadorii*) disrupts the monophyly of the Australian clade. The backbone trees recovered by SNaQ were concordant with our other trees based on the AHE data for the LAMc, while the PhyloNet analysis differed mainly in the positions of *V*. *salvadorii* and *V*. *spenceri* (Fig. 2b). All network analyses detected reticulation involving the clade comprising *V*. *komodoensis* and *V*. *varius* and the Australian clade, but there was disagreement on exactly which species were involved (Fig. 2b). The SNaQ analysis of Subset 1 detected a single reticulation involving *V*. *komodoensis* and a common ancestor of sand monitors. In more than half of the bootstrap replicates of this network *V*. *komodoensis* was inferred as the origin of gene flow and sand monitors as the hybrid clade (Fig. S5). The SNaQ analysis of Subset 2 supports reticulation between a common ancestor of *V*. *komodoensis* and *V*. *varius* and an ancestor of sand monitors excluding *V*. *spenceri*. The PhyloNet analysis of Subset 1 identified three reticulations, all involving the Australian clade and the *V*. *komodoensis* + *V*. *varius* lineage. The PhyloNet analysis of Subset 2 detected five reticulations. One of them involved *V*. *komodoensis* and a common ancestor of three sand monitors. The other reticulations are found within the Australian clade. Significant deviation of *D* from 0 in our ABBA-BABA analyses was mostly observed for the tests implicating introgression between the Komodo dragon and sand monitors, to the exclusion of other members of the Australian clade and *V*. *varius* (Table S6). The other significant result was that based on the majority consensus sequences and implicating introgression between *V*. *komodoensis* and *V*. *gouldii*, to the exclusion of *V*. *panoptes*. Mitochondrial introgression was only detected between *V*. *gouldii* and *V*. *panoptes*, and only before correcting for multiple testing (Table S7).

Morphology

The PCA and phyloPCA were mostly congruent with each other (Fig. 3; see Table S8 for loadings). The highly arboreal and phylogenetically divergent *V*. *salvadorii* is morphologically divergent from the other members of the LAMc. Sand monitors are morphologically intermediate between the other members of the Australian clade (*V*. *giganteus* and *V*. *mertensi*) and *V*. *komodoensis*. The reticulated MRCA of sand monitors is intermediate between *V*. *komodoensis* and the reticulation-free MRCA.

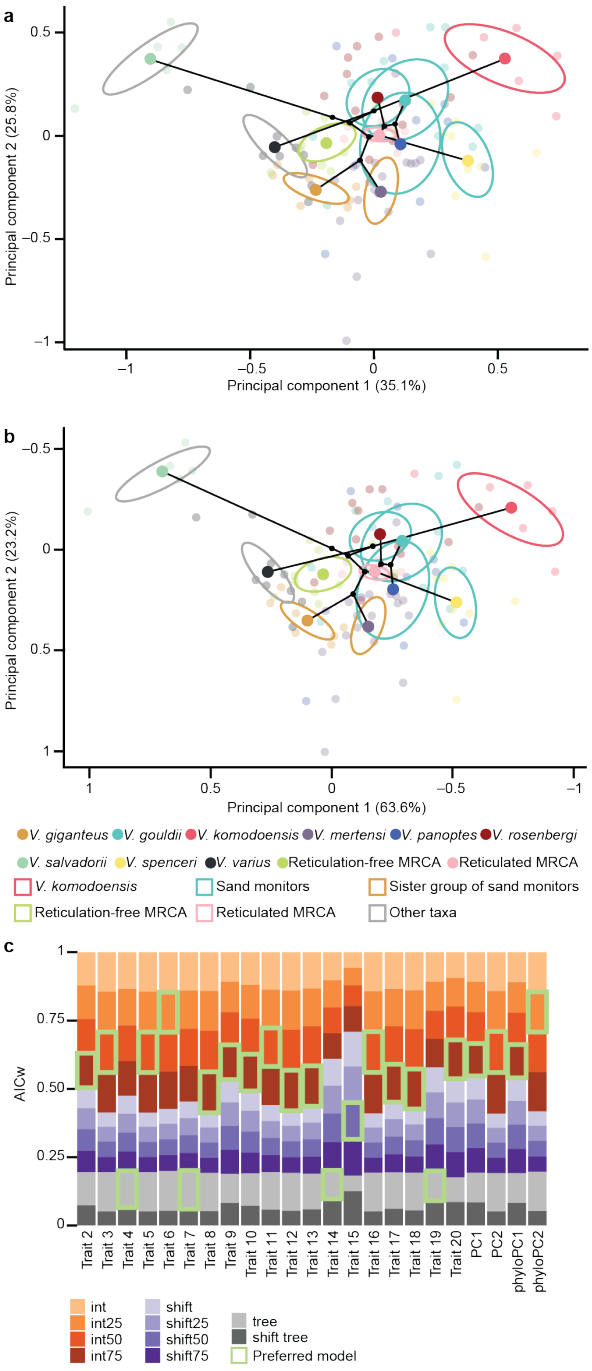

Figure 3. Morphological evidence of hybridization in the large Australasian monitors clade. a) Principal component analysis (PCA) of morphological data; taxa match Fig. 1, with the addition of the most recent common ancestor of sand monitors as inferred from the traits of living taxa (reticulated MRCA) and as inferred from the phylogeny and the traits of other taxa (reticulation-free MRCA); each small translucent point represents a specimen and large opaque points the average morphology for each taxon; 95% confidence ellipses are plotted for each taxon; the nuclear phylogeny is shown in black, with each circle representing the average morphology for each node. b) Phylogenetic PCA of morphological data; axes are reversed to ease comparison with conventional PCA. c) Akaike weights (AICw) of evolutionary models describing morphological intermediacy (int), a transgressive shift (shift), shifted Brownian motion on a tree (shift tree), and single-rate Brownian motion on a tree (tree); the first two models were fitted on the network obtained from the SNaQ analysis of Subset 1, specifying the relative genetic contribution of *V. komodoensis* as 7%. (empirical value), 25%, 50%, or 75% (see Table S3 for character coding).

Evolutionary models where *V. komodoensis* contributed to the variation observed in sand monitors were favored for 15 of 19 characters, the conventional PCs, and the phyloPCs (Fig. 3). For 14 traits and all PCs, the best scoring models were those where sand monitors are intermediate between the parental lineages, with a greater contribution of *V. komodoensis* than that estimated by SNaQ. Transgressive evolution was the best model for one trait, while conventional BM in a bifurcating tree was favored for four traits. The AICw and ΔAIC of the best models were relatively low. However, regardless of the uncertainty in genetic contributions, intermediacy models were preferred over tree-like models for most traits (Table S9).

The "search.conv" analyses revealed multiple instances of greater than expected similarity with *V. komodoensis*, most commonly involving *V. gouldii* but also implicating *V. rosenbergi* and the sand monitor clade as a whole (Table S10). The phenotype of the MRCA of sand monitors inferred through ancestral state reconstruction is more similar to *V. komodoensis* than the reticulation-free MRCA (Fig. 3). Remarkably, most of the "search.conv" results performed on the species tree where the reticulation-free MRCA was specified as the ancestral phenotype of sand monitors were significant. This is likely the result of sand monitors "travelling" a larger phenotypic distance from the reticulation-free MRCA towards *V. komodoensis* than from the reticulated MRCA, which is more similar to *V. komodoensis*. Results were mostly robust to branch-length uncertainty (Table S10).

Most of the character count tests revealed that there is a significant proportion of characters in sand monitors that are intermediate between *V. giganteus*/*V. mertensi* and *V. komodoensis* (Tables S11–S13). The only exceptions were the tests that evaluated whether *V. rosenbergi* and *V. spenceri* are intermediate between *V. komodoensis* and *V. mertensi*. The test evaluating the intermediacy of the reticulated MRCA with respect to *V. komodoensis* and the reticulation-free MRCA was significant.

Biogeography

The DEC model could not be rejected in favor of the DEC+J model in either of our 'BioGeoBEARS' analyses and we therefore present the results of the former (Tables S14–S15). All our biogeographic analyses suggest that the LAMc originated in the northern portion of the Australian craton, which encompasses southern New Guinea and the northern half of Australia (Figs. 4, S6–S7). Most analyses identified northern Australia as the place of origin of *V. komodoensis*. However, the 'BioGeoBEARS' analysis based exclusively on current distributions suggests that *V. komodoensis* and *V. varius* diverged through vicariance from a MRCA distributed in the Lesser Sunda Islands and the Australian tropical grasslands (Figs. 4a, S6). Both 'BioGeoBEARS' and 'rase'

identified the area occupied today by the Australian tropical grasslands as the most likely ancestral range for sand monitors (Figs. 4, S6–S7).

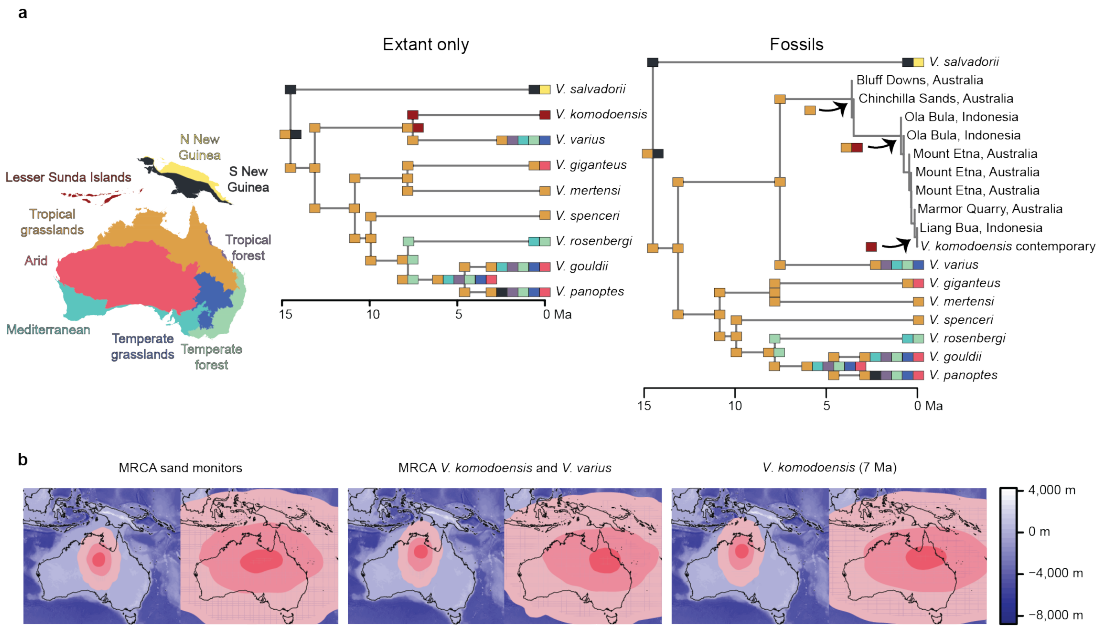

Figure 4. Geographic distribution of the large Australasian monitors in space and time. a) Ancestral ranges inferred from current distribution in discrete areas (left); ancestral ranges are shown by the colored rectangles on each node of the tree including only contemporary records (middle) and fossil records of *V. komodoensis* (right); arrows indicate shifts into particular ranges; uncertainty in ancestral ranges is presented in Fig. S6. b) Ancestral ranges based on polygonal distributions; results are shown in pairs for the analysis including only contemporary records (left) and fossil records of *V. komodoensis* (right); different shades of red are used for 5% (darkest), 50%, and 95% (lightest) posterior kernel density; sea depth/elevation is indicated in order to highlight areas that are currently underwater but that can become exposed during glacial periods.

The area of suitable habitat for the Komodo dragon was smaller for the present than for most of our historic reconstructions, except for a warm period in the Pliocene (~ 3.03–3.26 Ma). All past models show portions of northern mainland Australia as suitable habitat, while in the present the potential distribution becomes largely restricted to the Sunda Islands (Fig. S8a). Furthermore, the past and present climatic niches of *V. komodoensis* appear to overlap broadly (Fig. S8b). We estimated $D = 0.09$ and $I = 0.28$. The null hypothesis of equivalent niches could not be rejected using either statistic ($p = 0.998$ for both). Overall, our results suggest that the realized niche of *V. komodoensis* has remained relatively stable through time and support its past presence in northern Australia (see Appendix).

Discussion

We discuss how the approach used here offers insight into the nature, effects, and implications of reticulation in the large Australasian monitors clade (LAMc). Discussion on the diversification and systematics of the LAMc and the evolutionary history of the Komodo dragon is found in the Appendix.

Taxa involved in reticulation

Phylogenetic conflict in the LAMc is partially driven by hybridization. Evidence of phylogenetic incongruence includes the relatively low gene concordance factors and the detection of multiple gene tree clusters supporting different topologies. The disagreement between the inferred phylogenetic networks could reflect analytical differences, but also low and/or conflicting signal in the estimated gene trees (Mason et al. 2019). However, all networks detected hybridization between the *V*. *komodoensis* + *V*. *varius* lineage and sand monitors. In a majority of the bootstrap replicates of the SNaQ network of Subset 1, *V*. *komodoensis* was inferred to be the source of gene flow and a common ancestor of sand monitors the receiver. Furthermore, ABBA-BABA tests suggest that neither the Komodo dragon's sister taxon, *V*. *varius*, or the common ancestor of this clade is the source of introgression. Additionally, the *D* statistic was significant for tests involving all individual sand monitor species. Molecular data are unable to exclude other closely related and extinct relatives of the Komodo dragon such as the megalania *V*. *priscus* or other unidentified fossil monitors from north-eastern Australia as the source of introgression (Hocknull et al. 2020), but, given megalania's immense size, copulation with sand monitors seems unlikely. It is more plausible that hybridization involved *V*. *komodoensis*, of which the smallest sexually mature individuals are similar in size to large sand monitors (~1.5 m) (Auffenberg 1981). Introgression between *V*. *komodoensis* and an ancestral sand monitor is the most plausible reticulation event within the LAMc and this hypothesis is also supported by the results of the phenotypic analyses.

The reticulation event in Fig. 1 seems temporally plausible as the credibility intervals of the ages of the MRCA of sand monitors and *V*. *komodoensis* + *V*. *varius* overlap broadly (Figs. 1, S3), the divergence between *V*. *komodoensis* and *V*. *varius* has been recovered as older than the MRCA of sand monitors in some analyses (Brennan et al. 2021), and introgression is known to adversely impact phylogenetic tree dating (Leaché et al. 2014; Drovetski et al. 2015) and could be responsible for the older mean age estimate of the MRCA of sand monitors with respect to *V*. *komodoensis*. Alternatively, a

less parsimonious explanation would involve several instances of hybridization between *V. komodoensis* and the sand monitor lineage.

Nature and effects of reticulation

Hybridization has been detected across many squamate families, and has been identified as a cause of polyploidy, parthenogenesis, and unisexuality (Fujita and Moritz 2009; Neaves and Baumann 2011). However, prior evidence for hybridization in Varanidae is limited. Brennan et al. (2021) found that an individual of *V. bengalensis* showed mixed ancestry with a distantly related *Varanus* clade and suggested that the conserved chromosomal number in Varanidae could facilitate hybridization (Kinga and King 1975). Here, we show compelling evidence for hybridization in monitor lizards. The relatively low proportion of alleles coming from the Komodo dragon that was inherited by sand monitors is more consistent with introgressive hybridization than with hybrid speciation (Fig. 2). The apparent absence of mitochondrial introgression could be due to our limited sampling, but it could also suggest that backcrossing was male biased. This could be due to selection against hybrid females (Michell et al. 2016). Alternatively, it has been suggested that hybridization will commonly involve males of the larger species and females of the smaller species, reflecting female preferences or mechanical limitations to mating (Grant and Grant 1997; Wirtz 1999). This is consistent with the inferred role of the large Komodo dragon as the source of gene flow (Fig. S5d).

Facultative parthenogenesis (non-obligate asexual reproduction) has been reported for the Komodo dragon, the sand monitor *V. panoptes*, and other varanids outside the LAMc (Lenk et al. 2005; Watts et al. 2006; Iannucci et al. 2019). Vertebrate parthenogenesis is often associated with polyploidy, which is in turn often associated with hybridization (Mallet 2008). However, all the parthenogenetic varanid individuals for which ploidy has been tested are diploid (Iannucci et al. 2019). Nonetheless, polyploidy has been recently reported for one individual of a normally diploid species, *V. albigularis* (Iannucci et al. 2019). Thus, it seems possible that future studies with wide sampling of individuals could reveal a link between parthenogenesis, polyploidy, and hybridization in *Varanus*.

Patterns of morphological variation in the LAMc are consistent with hybridization involving *V. komodoensis* and sand monitors. Sand monitors are morphologically intermediate between their sister clade and the Komodo dragon (Fig. 3; Appendix). While support was not decisive, evolutionary models involving a contribution of *V. komodoensis* in the phenotype of sand monitors were preferred for most characters. In most cases, the preferred model was that implying intermediacy. Furthermore, the “search.conv” analyses revealed several instances of greater than expected similarity between sand

monitors and the Komodo dragon. Convergence cannot be ruled out as the single explanation for the intermediacy of sand monitors and their similarity with the Komodo dragon. However, hybridization appears to be behind the apparent convergence given the molecular evidence for introgression. Furthermore, considering a bifurcating phylogeny, the Komodo dragon is equally closely related to sand monitors and *V. giganteus*, another large terrestrial monitor that mainly feeds on vertebrates (Horn and King 2004). However, *V. giganteus* is less similar to the Komodo dragon than sand monitors (Fig. 3).

Most studies documenting long-term effects of hybridization report the adaptive introgression of discretized traits (e.g., The *Heliconius* Genome Consortium 2012; Jones et al. 2018; Meier et al. 2017; Karimi et al. 2020). Backcrossing of hybrid individuals with the parental species is expected to sway the phenotype closer to the parental morphology and away from intermediacy (Wilson 1992). However, our results suggest that hybridization can result in long-term morphological intermediacy. Hybrid intermediacy is the result of epistasis or heterozygosity for genes with incomplete dominance (Masello et al. 2019). While increased hybrid fitness is most commonly associated with the production of extreme phenotypes (transgressive segregation), intermediacy also can result in a selective advantage (Masello et al. 2019). If intermediacy increases fitness and backcrossing occurs, intermediacy could become widespread in the parental species through selection (Delph and Kelly 2014; Masello et al. 2019). Alternatively, genetic drift can cause intermediacy to become widespread if it does not significantly alter fitness and hybridization is pervasive (Haygood et al. 2003; Mallet 2007).

Geographic and Temporal Location of Reticulation

Biogeographic reconstruction can provide support for reticulation hypotheses when the ranges of parental lineages are inferred to overlap or be adjacent (Burbrink and Gehara 2018). Our biogeographic analyses suggest that the co-ocurrence of *V. komodoensis* and ancestral sand monitors in northern Australia was likely. The only exception is the 'BioGeoBEARS' analysis ignoring fossil evidence. The 'rase' analyses suggest that the hybridizing taxa occurred close to a transition zone between arid and tropical environments. This region likely experienced a dynamic history of habitat expansion and contraction as aridification of Australia accelerated in the Miocene, supporting pockets of mesic habitat surrounded by arid habitats (Morton et al. 1995; Fujita et al. 2010; Oliver et al. 2014). This could promote the secondary contact of previously isolated lineages.

One important implication of our study is the presence of *V. komodoensis* in continental Australia. Hocknull et al. (2009) assigned Pliocene and Miocene fossils from

northeastern Australia to *V. komodoensis*. Our results provide independent evidence for the past presence of the Komodo dragon in Australia as Northern Australia was recovered consistently as the ancestral range of sand monitors. Thus, the Komodo dragon had to occur in the region for hybridization to happen, as supported by most of our biogeographic analyses. The exception is the 'BioGeoBEARS' analysis which does not incorporate the fossil record. Thus, we agree with Hocknull et al. (2009) and propose an Australian origin of *V. komodoensis* followed by immigration into the Lesser Sunda Islands.

Accurate time-calibration of reticulation events remains challenging. Most divergence dating approaches do not incorporate gene flow into the analytical framework (Leaché et al. 2014; Brubrink and Gehara 2018). Recently, Bastide et al. (2018) and Karimi et al. (2020) presented the method employed here to time-calibrate phylogenetic networks based on pairwise phylogenetic distances on gene trees. However, it has several limitations: branch length units are not intuitive, it can create polytomies and negative branch lengths, suffers from identifiability issues, and assumes clock-like rates (Bastide et al. 2018). In this study we relied on a time-calibrated bifurcating tree to temporally frame our results. While gene flow can negatively impact tree dating (Leaché et al. 2014), in the LAMc the proportion of introgressed genes appears to be small and the backbone phylogeny is well supported (Figs. 1, S5). Considering the time of origin of the Komodo dragon and sand monitors (see Results), hybridization appears to have occurred in the late Miocene. In Australia, this time period is characterized by decreasing temperatures and increasing aridity (Mao and Retallack 2019), which may have promoted secondary contact.

Conclusions

The present study showcases how accounting for hybridization and using several lines of evidence can inform diverse aspects of evolutionary inference in an iconic group of large predatory lizards including Earth's largest living lizard, the Komodo dragon. *Varanus komodoensis* likely hybridized with a common ancestor of sand monitors in northern Australia, which left an imprint on the genotype and phenotype of living sand monitors. Our results demonstrate that the signs of ancient hybridization can be recovered from contemporary data even when hybridization is followed by speciation and suggest that the Komodo dragon originated in northern Australia and emigrated to the Lesser Sunda Islands before becoming locally extinct in Australia.

Supplementary Material

The AHE data underlying this article are available in the Dryad Digital Repository at https://dx.doi.org/10.5061/dryad.tx95x69t8. The Komodo dragon genome is available in the National Center for Biotechnology Information (NCBI) at https://www.ncbi.nlm.nih.gov/, and can be accessed with accession SJPD00000000. Custom scripts for the assembly of mitochondrial genomes and extraction of the AHE loci from the genome are available in GitHub at https://github.com/IanGBrennan. The morphological data are available in the Appendix.

Funding

This work was supported by an Australian Research Council grant to J.S.K. Support for the graduate education of C.J.P.V. and I.G.B. was awarded by the Australian Government Research Training Program.

Acknowledgments

We thank A. Allison, A.P. Amey, W. Böhme, U. Bott, R.D. Bray, P.D. Campbell, P.J. Couper, M. Cugnet, G.M. Dally, K. de Queiroz, P. Doughty, A. Drew, M. Flecks, M.E. Hagemann, M.R. Hutchinson, L. Joseph, C. Kovach, S. Mahony, D. Rödder, J.J.L. Rowley, J.W. Streicher, N. Vidal, and A.H. Wynn for facilitating specimen examination in their respective institutions; C. Ané, J-F. Flot, P.Y. Novikova, L.J. Revell, and E.A. Pavón Vázquez for their help with bioinformatics; M. Arvizu Meza for her support during specimen examination; D. Esquerré and O. Jiménez Robles for suggestions on the morphological and climatic niche analyses, respectively; D. Esquerré, J. Fenker, S. Paphatmethin, M. Pepper, L.G. Tedeschi, and S. Tiatragul for comments on drafts of this manuscript; A.L. Lind and K.S. Pollard for allowing us to use genomic data they generated; and C. Solís Lemus and three anonymous reviewers for offering suggestions that greatly improved this manuscript. Illustrations in Fig. 1 were based on photographs by D. Esquerré (*V. gouldii* and *V. komodoensis*), R. Gilbert (*V. giganteus*), and J.L. Ugalde Trejo (*V. salvadorii*).

References

Arnold M.L., Kunte K. 2017. Adaptive genetic exchange: a tangled history of admixture and evolutionary innovation. Trends Ecol. Evol. 32:601–611.

Ast J.C. 2001. Mitochondrial DNA evidence and evolution in Varanoidea (Squamata). Cladistics 17:211–226.

Atlas of Living Australia. 2019. Available from: http://www.ala.org.au (accessed 1 April 2019).

Auffenberg W. 1981. The behavioral ecology of the Komodo monitor. Gainesville: University Presses of Florida.

Barton N., Hewitt G. 1989. Adaptation, speciation and hybrid zones. Nature 341:497–503.

Bastide P., Solís-Lemus C., Kriebel R., William Sparks K., Ané C. 2018. Phylogenetic comparative methods on phylogenetic networks with reticulations. Syst. Biol. 67:800–820.

Benjamini Y., Hochberg Y. Controlling the false discovery rate: a practical and powerful approach to multiple testing. J. R. Stat. Soc. B 57:289–300.

Blackmon H., Adams R.H. 2015. EvobiR: tools for comparative analyses and teaching evolutionary biology. Available from: https://doi.org/10.5281/zenodo.30938.

Bouckaert R., Heled J., Kühnert D., Vaughan T., Wu C., Xie D., Suchard M.A., Rambaut A., Drummond A.J. 2014. BEAST 2: a software platform for Bayesian evolutionary analysis. PLoS Comput. Biol. 10:e1003537.

Brennan I.G., Lemmon A.R., Lemmon E.M., Portik D.M., Weijola V., Welton L., Donnellan S.C., Keogh J.S. 2021. Phylogenomics of monitor lizards and the role of competition in dictating body size disparity. Syst. Biol. 70:120–132.

Burbrink F.T., Gehara M. 2018. The biogeography of deep time phylogenetic reticulation. Syst. Biol. 67:743–755.

Cao Z., Liu X., Ogilvie H.W., Yan Z., Nakhleh L. 2019. Practical aspects of phylogenetic network analysis using PhyloNet. BioRxiv 746362.

Castiglione S., Serio C., Tamagnini D., Melchionna M., Mondanaro A., Di Febbraro M., Profico A., Piras P., Barattolo F., Raia P. 2019. A new, fast method to search for morphological convergence with shape data. PLoS ONE 14:e0226949.

Castiglione S., Tesone G., Piccolo M., Melchionna M., Mondanaro A., Serio C., Di Febbraro M., Raia P. 2018. A new method for testing evolutionary rate variation and shifts in phenotypic evolution. Methods Ecol. Evol. 2018:181–10.

Chen L., Wolf A.B., Fu W., Li L., Akey J.M. 2020. Identifying and interpreting apparent Neanderthal ancestry in African individuals. Cell 180:677–687.

Ciofi C., Beaumont M.A., Swingland I.R., Bruford M.W. 1999. Genetic divergence and units for conservation in the Komodo dragon *Varanus komodoensis*. Proc. R. Soc. Lond. B 66:2269–2274.

Conrad J.L., Ast J.C., Montanari S., Norell M.A. 2011. A combined evidence phylogenetic analysis of Anguimorpha (Reptilia: Squamata). Cladistics 27:230–277.

Darwin C. 1859. On the origin of species by means of natural selection, or the preservation of favoured races in the struggle for life. London: John Murray.

Delph L.F., Kelly J.K. 2014. On the importance of balancing selection in plants. New Phytol. 201:45–56.

Dos Reis M., Yang Z. 2011. Approximate likelihood calculation on a phylogeny for Bayesian estimation of divergence times. Mol. Biol. Evol. 28:2161–2172.

Drovetski S.V., Semenov G., Red'kin Y.A., Sotnikov V.N., Fadeev I.V., Koblik E.A. 2015. Effects of asymmetric nuclear introgression, introgressive mitochondrial sweep, and purifying selection on phylogenetic reconstruction and divergence estimates in the pacific clade of *Locustella* warblers. PLoS One 10:e0122590.

Edwards S.V., Liu L., Pearl D.K. 2007. High-resolution species trees without concatenation. P. Natl. Acad. Sci. USA 104:5936–5941.

Fitch A.J., Goodman A.E., Donnellan S.C. 2006. A molecular phylogeny of the Australian monitor lizards (Squamata: Varanidae) inferred from mitochondrial DNA sequences. Aust. J. Zool. 54:253–269.

Fry B.G., Wroe S., Teeuwisse W., van Osch M.J.P., Moreno K., Ingle J., McHenry C., Ferrara T., Clausen P., Scheib H., Winter K.L., Greisman L., Roelants K., van der Weerd L., Clemente C.J., Giannakis E., Hodgson W.C., Luz S., Martelli P., Krishnasamy K., Kochva E., Kwok H.F., Scanlon D., Karas J., Citron D.M., Goldstein E.J.C., Mcnaughtan J.E., Norman J.A. 2009. A central role for venom in predation by *Varanus komodoensis* (Komodo Dragon) and the extinct giant *Varanus* (*Megalania*) *priscus*. P. Natl. Acad. Sci. USA 106:8969–8974.

Fujita M.K., McGuire J.A., Donnellan S.C., Moritz, C.M. 2010. Diversification at the arid-monsoonal interface: Australia-wide biogeography of the Bynoe's gecko (*Heteronotia binoei*; Gekkonidae). Evolution 64:2293–2314.

Fujita M.K., Moritz C. 2009. Origin and evolution of parthenogenetic genomes in lizards: current state and future directions. Cytogenet. Genome Res. 127:261–272.

Goolsby E.W., Bruggeman J., Ané C. 2017. Rphylopars: fast multivariate phylogenetic comparative methods for missing data and within-species variation. Methods Ecol. Evol. 8:22–27.

Grant P.R., Grant B.R. 1997. Hybridization, sexual imprinting, and mate choice. Am. Nat. 149:1–28.

Green R.E., Krause J., Briggs A.W., Maricic T., Stenzel U., Kircher M., Patterson N., Li H., Zhai W., Fritz M.H., Hansen N.F., Durand E.Y., Malaspinas A., Jensen J.D., Marques-Bonet T., Alkan C., Prüfer K., Meyer M., Burbano H.A., Good J.M., Schultz R., Aximu-Petri A., Butthof A., Höber B., Höffner B., Siegemund M., Weihmann A., Nusbaum C., Lander E.S., Russ C., Novod N., Affourtit J., Egholm M., Verna C., Rudan P., Brajkovic D., Kucan Ž., Gušic I., Doronichev V.B., Golovanova L.V., Lalueza-Fox C., de la Rasilla M., Fortea J., Rosas A., Schmitz R.W., Johnson P.L.F., Eichler E.E., Falush D., Birney E., Mullikin J.C., Slatkin M., Nielsen R., Kelso J., Lachmann M., Reich D., Pääbo S. 2010. A draft sequence of the Neandertal genome. Science 328:710–722.

Harrison R.G., Larson E.L. 2014. Hybridization, introgression, and the nature of species boundaries. J. Hered. 105:795–809.

Haygood R., Ives A.R., Andow D.A. 2003. Consequences of recurrent gene flow from crops to wild relatives. Proc. R. Soc. Lond. B 270:1879–1886.

Hoang D.T., Chernomor O., von Haeseler A., Minh B.Q., Vinh L.S. 2018. UFBoot2: Improving the ultrafast bootstrap approximation. Mol. Biol. Evol. 35:518–522.

Hocknull S.A., Lewis R., Arnold L.J., Pietsch T., Joannes-Boyau R., Price G.J., Moss P., Wood R., Dosseto A., Louys J., Olley J., Lawrence, R.A. 2020. Extinction of eastern Sahul megafauna coincides with sustained environmental deterioration. Nat. Comm. 11:1–14.

Hocknull S.A., Piper P.J., van den Bergh G.D., Due R.A., Morwood M.J., Kurniawan I. 2009. Dragon's paradise lost: palaeobiogeography, evolution and extinction of the largest-ever terrestrial lizards (Varanidae). PLoS ONE 4:e724.

Horn H.-G., King D.R. 2004. *Varanus giganteus*. In: Pianka E., King D., editors. Varanoid lizards of the world. Bloomington: Indiana University Press. p. 335–354.

Iannucci A., Altmanová M., Ciofi C., Ferguson-Smith M., Milan M., Pereira J.C., Pether J., Rehák I., Rovatsos M., Stanyon R., Velenský P., Ráb P., Kratochvíl L., Johnson Pokorná M. 2019. Conserved sex chromosomes and karyotype evolution in monitor lizards (Varanidae). Heredity 123:215–227.

IUCN 2019. 2019. The IUCN Red List of Threatened Species. Version 2019-2. Available from: http://www.iucnredlist.org (accessed 3 July 2019).

Joly S., McLenachan P.A., Lockhart P.J. 2009. A statistical approach for distinguishing hybridization and incomplete lineage sorting. Am. Nat. 174:54–70.

Jombart T., Kendall M., Almagro-Garcia J., Colijn C. 2017. Treespace: statistical exploration of landscapes of phylogenetic trees. Mol. Ecol. Resour. 17:1385–1392.

Jones M.R., Mills L.S., Alves P.C., Callahan C.M., Alves J.M., Lafferty D.J.R., Jiggins F.M., Jensen J.D., Melo-Ferreira J., Good J.M. 2018. Adaptive introgression underlies polymorphic seasonal camouflage in snowshoe hares. Science 360:1355–1358.

Karimi N., Grover C.E., Gallagher J.P., Wendel J.F., Ané C., Baum D.A. 2020. Reticulate evolution helps explain apparent homoplasy in floral biology and pollination in baobabs (*Adansonia*; Bombacoideae; Malvaceae). Syst. Biol. 69:462–478.

Kinga M., King D. 1975. Chromosomal evolution in the lizard genus *Varanus* (Reptilia). Aust. J. Biol. Sci. 28:89–108.

Lamichhaney S., Berglund J., Almén M.S., Maqbool K., Grabherr M., Martinez-Barrio A., Promerová M., Rubin C.-J., Wang C., Zamani N., Grant B.R., Grant P.R., Webster M.T., Andersson L. 2015. Evolution of Darwin's finches and their beaks revealed by genome sequencing. Nature 518:371–375.

Lampert K.P., Schartl M. 2008. The origin and evolution of a unisexual hybrid: *Poecilia formosa*. Philos T. R. Soc. B 363:2901–2909.

Leaché A.D., Banbury B.L., Felsenstein J., Nieto-Montes de Oca A., Stamatakis A. 2015. Short tree, long tree, right tree, wrong tree: new acquisition bias corrections for inferring SNP phylogenies. Syst. Biol. 6:1032–1047.

Leaché A.D., Harris R.B., Rannala B., Yang Z. 2014. The influence of gene flow on species tree estimation: a simulation study. Syst. Biol. 63:17–30.

Lemmon A.R., Emme S.A., Lemmon E.M. 2012. Anchored hybrid enrichment for massively high-throughput phylogenomics. Syst. Biol. 61:727–744.

Lenk P., Eidenmueller B., Staudter H., Wicker R., Wink M. 2005. A parthenogenetic *Varanus*. Amphibia-Reptilia 26:507–514.

Li G., Davis B.W., Eizirik E., Murphy W.J. 2016. Phylogenomic evidence for ancient hybridization in the genomes of living cats (Felidae). Genome Res. 26:1–11.

Lin L., Wiens J.J. 2017. Comparing macroecological patterns across continents: evolution of climatic niche breadth in varanid lizards. Ecography 40:960–970.

Lind A.L., Lai Y.Y.Y., Mostovoy Y., Holloway A.K., Iannucci A., Mak A.C.Y., Fondi M., Orlandini V., Eckalbar W.L., Milan M., Rovatsos M., Kichigin I.G., Makunin A.I., Johnson Pokorná M., Altmanová M., Trifonov V.A., Schijlen E., Kratochvíl L., Fani R., Velenský P., Rehák I., Patarnello T., Jessop T.S., Hicks J.W., Ryder O.A., Mendelson III J.R., Ciofi C., Kwok P., Pollard K.S., Bruneau B.G. 2019. Genome of the Komodo dragon reveals adaptations in the cardiovascular and chemosensory systems of monitor lizards. Nat. Ecol. Evol. 3:1241–1252.

Maechler M., Rousseeuw P., Struyf A., Hubert M., Hornik K. 2019. Cluster: cluster analysis basics and extensions. R package version 2.1.0. Available from: https://CRAN.R-project.org/package=cluster.

Mallet J. 2005. Hybridization as an invasion of the genome. Trends Ecol. Evol. 20:229–237.

Mallet J. 2007. Hybrid speciation. Nature 446:279–283.

Mallet J. 2008. Hybridization, ecological races and the nature of species: empirical evidence for the ease of speciation. Philos T. R. Soc. B 363:2971–2986.

Mallet J., Besansky N., Hahn M.H. 2016. How reticulated are species? BioEssays 38:140–149.

Mao X., Retallack G. 2019. Late Miocene drying of central Australia. Palaeogeogr. Palaeoclim. Palaeoecol. 514:292–304.

Margono B.A., Potapov P.V., Turubanova S., Stolle F., Hansen M.C. 2014. Primary forest cover loss in Indonesia over 2000–2012. Nat. Clim. Change 4:730–735.

Masello J.F., Quillfeldt P., Sandoval-Castellanos E., Alderman R., Calderón L., Cherel Y., Cole T.L., Cuthbert R.J., Marin M., Massaro M., Navarro J., Phillips R.A., Ryan P.G., Shepherd L.D., Suazo C.G., Weimerskirch H., Moodley Y. 2019. Additive traits lead to feeding advantage and reproductive isolation, promoting homoploid hybrid speciation. Mol. Biol. Evol. 36:1671–1685.

Mason A.J., Grazziotin F.G., Zaher H., Lemmon A.R., Lemmon E.M., Parkinson C.L. 2019. Reticulate evolution in nuclear Middle America causes discordance in the phylogeny of palm-pitvipers (Viperidae: *Bothriechis*). J. Biogeogr. 46:833–844.

Matzke N.J. 2013. Probabilistic historical biogeography: new models for founder-event speciation, imperfect detection, and fossils allow improved accuracy and model-testing. Front. Biogeogr. 5:242–248.

Matzke N.J. 2014. Model selection in historical biogeography reveals that founder-event speciation is a crucial process in island clades. Syst. Biol. 63:951–970.

Mendes F.K., Hahn M.W. 2018. Why concatenation fails near the anomaly zone. Syst. Biol. 67:158–169.

Meier J.I., Marques D.A., Mwaiko S., Wagner C.E., Excoffier L., Seehausen O. 2017. Ancient hybridization fuels rapid cichlid fish adaptive radiations. Nat. Commun. 8:14363.

Meiri S. 2007. Size evolution in island lizards. Global Ecol. Biogeogr. 16:702–708.

Meiri S. 2008. Evolution and ecology of lizard body sizes. Global Ecol. Biogeogr. 17:724–734.

Meyer B.S., Matschiner M., Salzburger W. 2017. Disentangling incomplete lineage sorting and introgression to refine species-tree estimates for Lake Tanganyika cichlid fishes. Syst. Biol. 66:531–550.

Mirarab S., Reaz R., Bayzid Md.S., Zimmermann T., Swenson M.S., Warnow T. 2014. ASTRAL: genome-scale coalescent-based species tree estimation. Bioinformatics 30:i541–i548.

Mitchell S.M., Muehlbauer L.K., Freedberg S. 2016, Nuclear introgression without mitochondrial introgression in two turtle species exhibiting sex-specific trophic differentiation. Ecol Evol. 6: 3280–3288.

Molnar R.E. 2004. Dragons in the dust: the paleobiology of the giant monitor lizard *Megalania*. Bloomington: Indiana University Press.

Morton S.R., Short J., Barker R.D. 1995. Refugia for biological diversity in arid and semi-arid Australia. Canberra: Department of the Environment, Sport and Territories.

Neaves W.B., Baumann, P. 2011. Unisexual reproduction among vertebrates. Trends Genet. 27:81–88.

Nguyen L-T., Schmidt H.A., von Haeseler A., Minh B.Q. 2015. IQ-TREE: a fast and effective stochastic algorithm for estimating maximum-likelihood phylogenies. Mol. Biol. Evol. 32:268–274.

Oliver P.M., Smith K.L., Laver R.J., Doughty P., Adams M. 2014. Contrasting patterns of persistence and diversification in vicars of a widespread Australian lizard lineage (the *Oedura marmorata* complex). J. Biogeogr. 41:2068–2079.

Page R.D.M., Charleston M.A. 1997. From gene to organismal phylogeny: reconciled trees and the genetree/species tree problem. Mol. Phylogenet. Evol. 7:231–240.

Patton A.H., Margres M.J., Epstein B., Eastman J., Harmon L.J. Storfer A. 2020. Hybridizing salamanders experience accelerated diversification. Sci. Rep. 10:1–12.

Pavón-Vázquez E.A., Pavón-Vázquez C. J. 2019. SeATTLE: sequence alignment transformation into a table for later edition. Available from: https://github.com/CarlosPavonV/seattle.

Pianka E., King D, editors. 2004. Varanoid lizards of the world. Bloomington: Indiana University Press.

Pincheira-Donoso D., Tregenza T. 2011. Fecundity selection and the evolution of reproductive output and sex-specific body size in the *Liolaemus* lizard adaptive radiation. Evol. Biol. 38:197–207.

Price G.J., Louys J., Cramb J., Feng Y., Zhao J., Hocknull S.A., Webb G.E., Nguyen A.D., Joannes-Boyau R. 2015. Temporal overlap of humans and giant lizards (Varanidae; Squamata) in Pleistocene Australia. Quaternary Sci. Rev. 125:98–105.

Pyron R.A., Burbrink F.T., Wiens J.J. 2013. A phylogeny and revised classification of Squamata, including 4161 species of lizards and snakes. BMC Evol. Biol. 13:93.

Quintero I., Keil P., Jetz W., Crawford F.W. 2015. Historical biogeography using species geographical ranges. Syst. Biol. 64:1059–1073.

R Core Team. 2019. R: A language and environment for statistical computing, Vienna, Austria. Available from: https://www.R-project.org/.

Rabiee M., Sayyari E., Mirarab S. 2019. Multi-allele species reconstruction using ASTRAL. Mol. Phylogenet. Evol. 130:286–296.

Rannala B., Yang Z. 2003. Bayes estimation of species divergence times and ancestral population sizes using DNA sequences from multiple loci. Genetics 164:1645–1656.

Revell L.J. 2009. Size-correction and principal components for interspecific comparative studies. Evol. 63:3258–3268.

Revell L.J. 2012. Phytools: an R package for phylogenetic comparative biology (and other things). Methods Ecol. Evol. 3:217–223.

Ronquist F., Teslenko M., van der Mark P., Ayres D.L., Darling A., Höhna S., Larget B., Liu L., Suchard M.A., Huelsenbeck J.P. 2012. MrBayes 3.2: efficient bayesian

phylogenetic inference and model choice across a large model space. Syst. Biol. 61:539–542.

Scheet P., Stephens M. 2006. A fast and flexible statistical model for large-scale population genotype data: applications to inferring missing genotypes and haplotypic phase. Am. J. Hum. Genet. 78:629–644.

Seo, T.K. 2008. Calculating bootstrap probabilities of phylogeny using multilocus sequence data. Mol. Biol. Evol. 25:960–971.

Solís-Lemus C., Ané C. 2016. Inferring phylogenetic networks with maximum pseudolikelihood under incomplete lineage sorting. PLoS Genet. 12:e1005896.

Solís-Lemus C., Bastide P., Ané C. 2017. PhyloNetworks: a package for phylogenetic networks. Mol. Biol. Evol. 34:3292–3298.

Stebbins G.L. 1959. The role of hybridization in evolution. P. Am. Philos. Soc. 103:231–251.

Taylor S.A., Larson E.L. 2019. Insights from genomes into the evolutionary importance and prevalence of hybridization in nature. Nat. Ecol. Evol. 3:170–177.

Than C., Ruths D., Nakhleh L. 2008. PhyloNet: a software package for analyzing and reconstructing reticulate evolutionary relationships. BMC Bioinformatics 9:322.

The *Heliconius* Genome Consortium. Butterfly genome reveals promiscuous exchange of mimicry adaptations among species. Nature 487:94–98.

Tibshirani R., Walther G., Hastie T. 2001. Estimating the number of clusters in a data set via the gap statistic. J. R. Statist. Soc. B 63:411–423.

Uetz P., Freed P., Hošek J., editors. 2019. The Reptile Database. Available from: http://www.reptile-database.org (accessed 5 July 2019).

Vidal N., Marin J., Sassi J., Battistuzzi F.U., Donnellan S., Fitch A.J., Fry B.G., Vonk F.J., Rodriguez de la Vega R.C., Couloux A., Hedges S.B. 2012. Molecular evidence for an Asian origin of monitor lizards followed by Tertiary dispersals to Africa and Australasia. Biol. Lett. 8:853–855.

Villanea F.A., Schraiber J.G. 2019. Multiple episodes of interbreeding between Neanderthal and modern humans. Nature Ecol. Evol. 3:39–44.

Watts P.C., Buley K.R., Sanderson S., Boardman W., Ciofi C., Gibson R. 2006. Parthenogenesis in Komodo dragons. Nature 444:1021–1022.

Wilson P. 1992. On inferring hybridity from morphological intermediacy. Taxon 41:11–23.

Wirtz P. 1999. Mother species–father species: unidirectional hybridization in animals with female choice. Anim. Behav. 58:1–12.

Yang Z. 2007. PAML 4: phylogenetic analysis by maximum likelihood. Mol. Biol. Evol. 24:1586–1591.

Zhang C., Rabiee M., Sayyari E., Mirarab S. 2018. ASTRAL-III: polynomial time species tree reconstruction from partially resolved gene trees. BMC Bioinformatics 19:153.

CHAPTER IV

Geographic sorting of genetic and phenotypic variation through gene flow and selection in a monitor lizard species complex

GEOGRAPHIC SORTING OF GENETIC AND PHENOTYPIC VARIATION THROUGH GENE FLOW AND SELECTION IN A MONITOR LIZARD SPECIES COMPLEX

Carlos J. Pavón-Vázquez[1,2], Damien Esquerré[1], Paul Doughty[3], Stephen C. Donnellan[4,5], and J. Scott Keogh[1]

[1]Division of Ecology and Evolution, Research School of Biology, Australian National University, Canberra, ACT 2601, Australia

[2]E-mail: cjpvunam@gmail.com

[3]Department of Terrestrial Zoology, Western Australian Museum, Welshpool, WA 6016, Australia

[4]School of Biological Sciences, University of Adelaide, Adelaide, SA 5005, Australia

[5]South Australian Museum, Adelaide SA 5000, Australia

Abstract

Selection and gene flow are two major factors shaping geographic patterns of genetic and phenotypic variation, with effects that are usually conflicting. Gene flow is predicted to prevent local adaptation by replacing locally adapted alleles. Taxa with wide distributions spanning a variety of environmental conditions offer an exceptional opportunity to evaluate the effects of local adaptation and gene flow, and assess how they act together to geographically sort genetic and phenotypic variation. Here, we address these issues by characterizing phylogeographic structure and phenotypic variation in the monitor lizards of the *Varanus acanthurus* species complex. This group has a wide distribution in Australia that encompasses a wide environmental gradient between the arid interior and the northern monsoonal tropics. We obtained thousands of single nucleotide polymorphisms, mitochondrial sequences, linear morphometric data, geometric morphometric data, and climatic data from throughout the range of the *V. acanthurus* complex. We used our data to uncover evidence for gene flow and local adaptation, and to evaluate species limits. We identified multiple contact zones between populations, but also signs of local adaptation. Variation in some loci is correlated with climate. Furthermore, body size is positively correlated with precipitation and temperature. Finally, we identified the need for taxonomic revision in the group, including the identification of an undescribed species. Interspecific relationships are uncertain, likely as a result of rapid and recent speciation. Our study shows that local adaptation

can occur despite extensive gene flow, and offers insight into the ecological and evolutionary consequences of spatiotemporal climatic variation in northern Australia.

Keywords: Admixture, Australia, biogeography, local adaptation, species delimitation, *Varanus*

Taxa with large geographic ranges are exposed to a wide variety of environmental conditions. Natural selection will then promote the emergence of local adaptation, with individuals native to a region showing higher fitness than immigrants (Lenormand 2002; Kawecki and Ebert 2004). Local adaptation can proceed in two ways: through changes in the direction of selection for individual alleles across regions, or when the intensity of selection for several polymorphic loci differs between regions (Lenormand 2002). In fact, it seems like the response to environmental variation is usually polygenic (Pritchard and Di Rienzo 2010). In practice, local adaptation is often inferred by detecting genotypic and phenotypic differentiation between areas with dissimilar conditions or across environmental gradients (Savolainen et al. 2013). When local adaptation occurs, it can have a large impact on the ecology and evolutionary trajectory of populations (Blanquart et al. 2013), allowing range expansions and contractions (Kirkpatrick and Barton 1997), shaping ecological interactions (Kaltz and Shykoff 1998), and promoting speciation (Lenormand et al. 2012).

Gene flow is another major force moulding the geographic distribution of genetic and phenotypic variation (Slatkin 1987). Gene flow is classically considered a homogenizing agent that keeps populations and species genetically and phenotypically similar (Mayr 1942; Slatkin 1985). It is predicted that gene flow prevents local adaptation by promoting the replacement of locally adapted alleles by non-adaptive or maladaptive alleles (gene swamping) (Lenormand 2002). Migration is even theorized to have catastrophic, self-reinforcing effects on fitness. The introduction of locally maladapted alleles can decrease fitness and consequently density in contact zones, increasing the relative proportion of immigrants versus residents if migration persists, which will then again reduce density (migration meltdown) (Kawecki et al. 1997; Lenormand 2002). A similar effect is achieved when there is selection against hybrids and density is thus reduced in contact zones (hybrid sink effect) (Barton 1986; Lenormand 2002).

Recent empirical research has challenged the notion that gene flow prevents local adaptation (Milano et al. 2014; Brauer et al. 2018; Miller et al. 2019). A variety of mechanisms and scenarios are thought to make local adaptation with gene flow possible, and there are ways in which gene flow may actually promote local adaptation. Through

the introduction of new alleles, gene flow can increase genetic standing variation upon which selection can act (Barrett and Schluter 2008; Tigano and Friesen 2016). Adaptive introgression can introduce new alleles that increase fitness locally (Tigano and Friesen 2016; Leroy et al. 2020). On the other hand, genomic architecture can protect adapted loci from the homogenising effects of gene flow if adapted loci are found in areas of low recombination or if chromosomic rearrangements or epigenetic modifications reduce recombination (Tigano and Friesen 2016).

In Australia, two large biomes with contrasting environmental conditions share a long common border. These are the northern monsoonal tropics and the central arid zone (Byrne 2011). Rainfall in the Australian arid zone, particularly on the northern portion, is remarkably unpredictable compared to other arid regions on Earth, and there is large seasonal variation in temperature (Morton et al. 2011; Oliver et al. 2014). In contrast, the monsoonal tropics have a marked rainy season in the summer, and temperatures are generally hot (Bowman et al. 2009). Despite their dissimilar climate, many taxa are present in both biomes (Fujita et al. 2010; Oliver et al. 2014). With no major physical barriers between these two regions, these taxa are distributed over wide environmental gradients (Bowman et al. 2009). This makes this transitional zone an ideal location to study the interaction between adaptation, gene flow, and the environment.

Monitor lizards (Squamata: Varanidae: *Varanus*) are a conspicuous and widespread component of the Australian terrestrial fauna. The miniaturized subgenus *Odatria* is the most diverse group of monitors in Australia, accounting for 19 of the 30 species that are present in the country (Wilson and Swan 2017). The spiny-tailed monitor (*V. acanthurus*) is a specialized member of *Odatria* that shelters in crevices and burrows within rocky outcrops, using its tail to block them (Dryden 2004). The species shows notable morphological variation across its wide range encompassing the arid zone and monsoonal tropics, and has been accordingly divided into three subspecies: *V. a. acanthurus* from monsoonal environments in the Kimberley region in north-eastern Western Australia and surroundings; *V. a. brachyurus*, with a wide distribution in the arid and semi-arid regions of Western Australia, the Northern Territory, and Queensland; and *V. a. insulanicus*, from islands off the Northern Territory, specifically Groote Eylandt and the Wessel group (Dryden 2004; Cogger 2014; Wilson and Swan 2017). *Varanus acanthurus* has been considered to represent either a widespread and variable species (Storr 1980) or a species complex (King and Horner 1987). Molecular analyses have shown that *V. a. insulanicus* is more closely related to *V. baritji*, from the monsoonal Top End region in the Northern Territory, than to other *V. acanthurus* (Fitch et al. 2006; Brennan et al. 2021). Furthermore, *V. storri storri* from north-eastern Queensland appears to be more closely related to *V. acanthurus* and *V. baritji* than to *V. storri*

ocreatus, from north-western Queensland, the Kimberley region, and adjacent areas in the Northern Territory (Thompson et al. 2008).

In this study we use genome-wide single nucleotide polymorphisms (SNPs) and mitochondrial DNA sequences to characterize phylogeographic structure in a clade containing the closely related *V*. *acanthurus*, *V*. *baritji*, and *V*. *s*. *storri*. We evaluated the possibility of gene flow between populations and tested whether precipitation and/or temperature covary geographically with genetic and phenotypic variation. Furthermore, we discuss how geographic structure reflects past environmental change in Australia. Finally, we combined our molecular data with linear and geometric morphometric data to assess species limits, proposing a new taxonomic framework for this morphologically variable species complex.

Materials and Methods

Molecular sampling

We genotyped individuals in the *V*. *acanthurus* complex using the DArTseq (Diversity Array Technology sequencing) platform designed by Diversity Arrays Technology, Canberra (DArT). This is a low cost approach based on a combination of complexity reduction using restriction enzymes, filtering by fragment size, and sequencing (Kilian et al. 2012; Georges et al. 2018). The generated data includes thousands of SNPs and their associated flanking regions. Most fragments are 69 bp long and come from coding regions (Petroli et al. 2012). DArTseq data has been used before to evaluate gene flow, phylogeographic structure, species limits, and local adaptation (Melville et al. 2017; Brauer et al. 2018; Georges et al. 2018; Aguirre-Liguori et al. 2019; Chaplin et al. 2020; Walters et al. 2020). The complexity reduction procedure was optimized for our dataset, sequencing performed in an Illumina Hiseq2500 sequencer, and the genome of *V*. *komodoensis* used as reference for mapping (Lind et al. 2019).

We generated two sets of DArTseq data, given that the number of retrieved SNPs is reduced when distantly related taxa are included in the SNP calling pipeline. First, the DArT pipeline was run for 169 individuals of the *V*. *acanthurus* complex (*V*. *acanthurus*, *V*. *baritji*, and *V*. *s*. *storri*), obtaining a total of 202,570 SNPs. We used the 'dartR 1.8.3' R package (Gruber et al. 2018) to filter our dataset as follows (in order). We dropped those SNPs with reproducibility < 0.99, that were missing in more than 85% of samples, were found in the same fragment as other SNPs (to avoid linkage), and whose minor allele was found exclusively in a single individual. Subsequently, we deleted individuals with more than 70% missing data. After filtering, the dataset contained 17,277 SNPs and

162 individuals (Fig. 1; Table S1): 144 of *V. acanthurus*, 15 of *V. baritji*, and three of *V. s. storri*. We used this dataset for most downstream analyses, except for those requiring outgroups, and refer to it as the population SNP dataset. The second dataset includes two individuals from each of nine populations in the *V. acanthurus* complex, one individual of *V. s. ocreatus*, two individuals of the outgroup, *V. varius*, and comprises 197,326 SNPs. We selected individuals of the *V. acanthurus* complex showing little admixture with other populations. The number of populations and admixture were estimated using the first dataset (see below). We applied the same filters specified above except for the individual filtering, obtaining 14,542 SNPs for 21 individuals (Table S1). We used this dataset in those analyses requiring outgroup specification and refer to it as the phylogenetic SNP dataset.

We also obtained partial sequences of the mitochondrial gene coding for the NADH dehydrogenase subunit 4 protein (*ND4*). Our sampling included 172 individuals (Fig. 1): 158 of *V. acanthurus*, two of *V. baritji*, one of *V. s. storri*, six of *V. s. ocreatus*, two each of *V. kingorum* and *V. primordius*, and one of the outgroup *V. caudolineatus*. Nine sequences were obtained from GenBank, while the others were obtained following the protocol described in Fitch et al. (2006) (Table S1). Amplified PCR products were purified and sequenced on an AB 3730xl DNA Analyzer at the Genome Discovery Unit, ACRF Biomolecular Resource Facility, The John Curtin School of Medical Research, Australian National University. We aligned the sequences using the MUSCLE algorithm (Edgar 2004). The final alignment consisted of 600 bp.

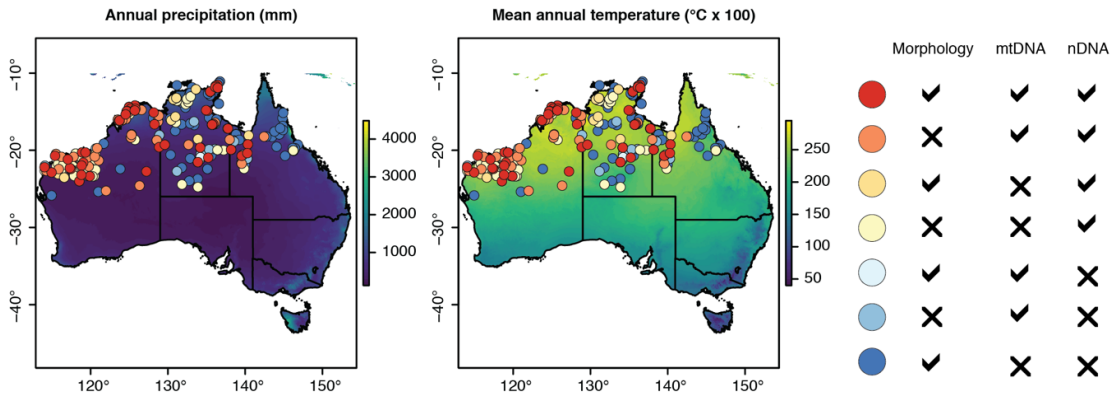

Figure 1. Geographic sampling of individuals in the *V. acanthurus* complex. Localities are coloured based on the type of data available. Lines represent state and territory limits. Maps depict variables representing annual trends in precipitation and temperature.

Population structure

Analyses of population structure were performed on the population SNP dataset. First,

we estimated ancestry coefficients using sNMF (Frichot et al. 2014). This is a computationally efficient but accurate method based on sparse nonnegative matrix factorization and least-squares optimization (Frichot et al. 2014). We ran the analyses on the 'LEA 2.8.0 R' package (Frichot and François 205). First, we tested 18 combinations of the α and tolerance parameters, choosing that with the lowest cross-entropy. In these test runs, we performed ten repetitions for each value of K (number of populations) between one and ten. We then performed 100 repetitions for each of the aforementioned values of K with the best combination of α (100) and tolerance (0.0001). We obtained the optimal value of K and individual ancestry coefficients from the run with the lowest cross-entropy. We also characterized population structure by performing principal component analysis (PCA) with the "gl.pcoa" function of 'dartR'.

Isolation by distance (IBD) appears to be common in nature (Sexton et al. 2014). We characterized patterns of IBD by evaluating the correlation between geographic and genetic distance. We measured geographic distance as the natural logarithm of the Euclidean distance between collecting localities in the Mercator projection. Analyses of IBD usually employ F_{ST} / 1 – F_{ST} as measure of genetic distance, but in our study most localities are represented by a single individual. Thus, we calculated the more appropriate $\hat{a}$ statistic in genepop v. 1.1.7 (Rousset, 2000) and used it as our measure of genetic distance (Rousset, 2000). We then performed a Mantel test to evaluate the correlation between geographic and genetic distance using the "gl.ibd" function of the 'dartR' package. We performed this test on all the samples together and independently on three sets of populations identified by sNMF that cluster together on the PCA.

Demographic statistics

To infer demographic processes for each population identified by sNMF, we calculated two statistics: observed heterozygosity (*Ho*) and Tajima's *D* (Tajima 1989). Heterozygosity is expected to be higher in populations with admixture or large effective sizes. Tajima's *D* indicates whether populations have an excess ($D < 0$) or deficit ($D > 0$) of rare alleles, as expected from population expansion and contraction, respectively. We conducted these analyses on the raw SNP dataset, filtered only to exclude the individuals that were not included on the sNMF analyses and loci with low reproducibility (< 0.99). This resulted on the retention of 150,448 loci. We used 'dartR' to calculate the observed heterozygosity. Considering that estimates could be biased because our dataset only includes variable loci, we estimated the number of invariable loci based on a Poisson distribution and adjusted *Ho* accordingly. We estimated Tajima's *D* with the 'snpR 1.1.2.0' R package (Hemstrom and Jones 2021).

Gene flow

For each pairwise combination of populations identified by sNMF that either cluster together in the PCA or spatially overlap (as revealed by sNMF), we evaluated the presence of hybrids with NewHybrids 1.1 (Anderson and Thompson 2002). This software uses Markov chain Monte Carlo (MCMC) to compute the posterior probability that individuals belong to user-defined hybrid categories based on their genotype frequencies (Anderson and Thompson 2002). We specified the default categories: pure members of each population, F1 hybrids, F2 hybrids, and backcrosses of F1 hybrids with each parental population. For each pairwise comparison, we first deleted individuals of the non-focal populations from the population SNP dataset, then deleted loci with more than 85% missing data, and subsequently selected 200 loci randomly for analysis due to computational limits. We ran NewHybrids with default settings for 10,000 burn-in sweeps and 10,000 post-burn-in sweeps.

Additionally, we used TreeMix 1.13 (Pickrell and Pritchard 2012) to infer a population tree with migration edges (m). This software relies on allele frequency data and a Gaussian approximation to genetic drift (Pickrell and Pritchard 2012). We performed the analyses on the phylogenetic SNP dataset (which contains two individuals from each population identified by sNMF), specified *V. varius* as outgroup, a block size of 500 SNPs, and ran five independent analyses for each value of *m* between one and five. We used the 'OptM 0.1.3' R package (Fitak 2019) to select the optimal value of *m* as suggested by the bent cable model, which produced the best fit based on the Akaike Information Criterion (AIC). We verified that the five independent replicates for the selected value of *m* produced consistent results.

Influence of climate on genetic and phenotypic differentiation

We identified candidate loci under environmental selection through a genotype-environment association (GEA) approach. Specifically, we implemented redundancy analysis (RDA), which displays low rates of type I and II errors and is robust to variation in population structure, demographic history, sampling design, and sample size (Forester et al. 2018). We based the analysis on the population SNP dataset and performed the analysis in the 'vegan 2.5.6' R package (Oksanen et al. 2019) following the approach of Brauer et al. (2018). For each collecting locality, we extracted 19 variables describing variation in temperature and precipitation from a raster with resolution of 0.5' (Fick and Hijmans 2017). We then performed PCA separately for the variables describing variation in temperature (bioclimatic variables 1–11) and precipitation (12–19). We removed the principal components (PCs) with eigenvalues < 1, that did not contribute significantly to the model (identified with the "ordistep" function of 'vegan'), and were highly correlated

(those with variance inflation factor > 10) (Dyer et al. 2010; Brauer et al. 2018). In this way, we performed the RDA analysis on two PCs for temperature and two for precipitation, conditioned on geographic origin specified as sampling coordinates. We conducted an analysis of variance with 1,000 permutations to assess the significance of the model, of each RDA axis, and the marginal significance of the environmental PCs. We identified as candidates those loci with scores greater than three standard deviations from the mean locus scores of each significant RDA axis. We mapped the candidate loci using the genome of *V. komodoensis* (Lind et al. 2019) as reference. Additionally, we used Blast2GO (Götz et al. 2008) with default settings as implemented in OmicsBox 1.4.0 to map and functionally annotate the candidate loci.

Additionally, we tested whether climate is an important driver of phylogeographic structure. We used the 'Sunder 0.0.4' R package (Botta et al. 2015) to compare the effects of environmental and geographic distance in genetic differentiation. 'Sunder' is an extension of the method proposed by Bradburd et al. (2013), which surpasses autocorrelation issues affecting Mantel tests by implementing a model where covariance decreases exponentially with geographic and environmental distance. 'Sunder' extends the method by modifying the covariance model and incorporating a model selection step to evaluate whether models with or without environmental effects better fit the data (Botta et al. 2015). The method also produces posterior distributions of statistics describing the contribution of geographic and environmental distance to genetic covariance (β_D and β_E, respectively). We used custom scripts (available at https://github.com/CarlosPavonV/RandomMolR) to collapse localities separated by less than 3 km into a single site, obtain the allele counts per site, and obtain the geographic distances between sites (natural logarithm of orthodromic distance). We specified environmental distances as the Euclidean distance between each PC retained in the RDA analysis. We normalized the geographic and environmental distances by dividing them by their respective standard deviation (Bradburd et al. 2013). For each environmental PC, we ran the MCMC for 10,000 iterations, with a thinning of 20, and using 10% of pairs (collecting sites × loci) as validation set in the cross-validation procedure.

We also tested whether variation in body size correlates with climate. Specifically, we tested the heat balance and water availability hypotheses. The heat balance hypothesis is based on Bergmann's (1847) rule and predicts a negative relationship between body size and temperature because of increased heat conservation in larger organisms (Olalla-Tárraga and Rodríguez 2007). On the other hand, the water availability hypothesis suggests that drier conditions promote larger body sizes because of increased tolerance to desiccation (Ashton 2002). We recorded snout-vent length (SVL), a commonly used proxy for body size in reptiles, for 172 adult specimens of the *V.*

acanthurus complex: 127 of *V. acanthurus*, 28 of *V. baritji*, and 17 of *V. s. storri*. Using the "procD.lm" function of the 'geomorph 3.0.3' R package (Adams and E. Otarola-Castillo 2013), we verified that there was no sexual dimorphism in body size (see below). For each collecting locality, we obtained the mean annual temperature (in °C × 100), annual precipitation (in mm), and mean SVL in case that more than one specimen came from the same locality. All analyses were performed in R 3.6.2 (R Core Team 2019). We fitted a linear model using generalized least squares (GLS) to test for correlation between the natural logarithms of SVL and each climatic variable. To account for spatial autocorrelation, we also fitted GLS models with the following spatial correlation structures (using the collecting coordinates): exponential, Gaussian, rational quadratics, and spherical. We compared models based on the sample-size-corrected AIC (AICc). Additionally, we used the 'hier.part' package (Mac Nally and Walsh 2004) to perform hierarchical partitioning (Chevan and Sutherland 1991), calculating the relative contribution of each log-transformed climatic variable to the variance in log-transformed SVL. Hierarchical partitioning analysis fits multiple regression models and averages the effect of each variable based on a given goodness-of-fit measure. We specified the quasi-Poisson family and R^2 as the goodness-of-fit measure.

Phylogenetics

We reconstructed an individual-level phylogeny of the *V. acanthurus* complex based on the SNP data through two approaches: maximum likelihood analysis of the concatenated SNPs and quartet analysis based on the coalescent. Both analyses were performed on the population SNP dataset. We ran the maximum likelihood analysis on IQ-TREE 1.6.8 (Nguyen et al. 2015). We randomly assigned one or other allele for heterozygous positions and deleted 146 sites that were rendered invariable in the process. We evaluated models that incorporate ascertainment bias correction (Lewis 2001) with ModelFinder (Kalyaanamoorthy et al. 2017) and executed the analysis under the TVM+F+ASC+R5 model, which was selected based on the Bayesian information criterion (BIC). We obtained support values through 1,000 ultrafast bootstrap replicates (Hoang et al. 2018). We performed analyses under the coalescent in SVDquartets (Chifman and Kubatko 2014) as implemented in PAUP* 4.0 (Swofford 2003). We used ambiguity codes for heterozygous sites and obtained support values through 1,000 bootstrap replicates. We rooted the IQ-TREE and SVDquartets trees based on the topology of a species tree obtained through Bayesian analysis under the multi-species coalescent (see below).

We reconstructed the relationships between the populations in the *V. acanthurus* complex by building species trees using two approaches: quartet analysis and Bayesian

estimation under the multi-species coalescent. We performed both analyses on the phylogenetic SNP dataset, assigning individuals to the populations identified by sNMF, and rooting the trees on *V. varius*. We used SVDquartets to obtain a species tree through quartet analysis, using ambiguity codes for heterozygous sites and obtaining support values through 1,000 bootstrap replicates. We performed Bayesian inference under the multi-species coalescent with SNAPP (Bryant et al. 2012) as implemented in BEAST 2.5.1 (Bouckaert et al. 2019). We obtained a neighbour-joining tree using the "gl.tree.nj" function of 'dartR' to be used as starting tree in SNAPP. Same as for IQ-TREE, we randomly resolved heterozygous positions and deleted 35 sites rendered invariable. After dropping sites with only missing data in one or more species, 2,361 SNPs were retained. We used a ruby script to instruct SNAPP to estimate divergence dates (Stange et al. 2018). We applied a secondary calibration for the root age, specifying a normal distribution prior with a mean of 20.56 Ma and standard deviation of 1.5 Ma based on Brennan et al. (2021). We performed two independent analyses with 500,000 generations sampled every 250 generations. We determined the burn-in and confirmed adequate sampling and convergence with Tracer 1.6 (Rambaut et al. 2014). We specified 10% burn-in, combined the runs, and obtained the maximum clade credibility (MCC) tree with mean node heights.

Finally, we obtained the mitochondrial tree through maximum likelihood with IQ-TREE. We used PartitionFinder 2 (Lanfear et al. 2017) to get the best fitting partitioning scheme and substitution model based on the BIC. We obtained support values through 1,000 ultrafast bootstrap replicates (Hoang et al. 2018) and rooted the tree on *V. caudolineatus*.

Taxonomy

Historically, species delimitation has been constrained by the adopted species concepts and what features they use to define species (e.g., studies adopting the biological species concept would rely on the actual or potential production of fertile offspring to delimit species). However, it is now evident that the criteria used by each of these concepts are often violated (e.g., some deeply divergent lineages can produce fertile offspring, and not all members of a species may interbreed with each other as seen in ring species). The general lineage species concept attempts to unify the underlying rationale of previous concepts, defining species as independently evolving metapopulation lineages (De Queiroz 1998, 2007). Under this concept, the problems of species conceptualization and delimitation become more independent. Species are treated as hypothesis and features that would be considered as defining traits of species under other concepts, such as reproductive isolation or morphological divergence, are

seen as evidence supporting the hypothesis (De Queiroz, 1998, 2007; Pante et al., 2015). In this study, we adopt the general lineage species concept. Our taxonomic recommendations take into account evidence coming from molecular and morphological data. Particularly, we evaluated species limits between populations/metapopulations by testing for: fixed allelic differences (which are considered strong indicators of restricted gene flow) (Georges et al. 2018), genetic divergence while accounting for gene flow (Jackson et al. 2017; Leaché et al. 2019), and morphometric differentiation (which indicates restricted gene flow and/or ecological divergence) (Esquerré et al. 2019). We also took into account the geographic patterns of admixture obtained with sNMF and NewHybrids. We consider that the sympatry or close proximity of individuals belonging to different populations without evidence of admixture supports the species-level divergence between them, as does the presence of both pure and admixed individuals in a certain region or the geographical restriction of hybrids (i.e., an hybrid zone). On the other hand, we consider that geographic clines of admixture where one genetic makeup gradually gives way to another is more consistent with a single species showing geograhic structure but unified by extensive gene flow (Chambers and Hillis 2020; Marshall et al. 2021).

Molecular species delimitation

We evaluated whether there are fixed differences in the population SNP dataset between the populations identified by sNMF. We used the "gl.fixed.diff" function of 'dartR', which performs pairwise comparisons between operational taxonomic units (OTUs) and assesses the significance of the results through simulation to control for false positives arising from sampling error (Georges et al. 2018). We performed 1,000 simulation repetitions where we identified true positives based on a threshold of 0.02 for the true minor allele frequency. We repeated the analysis after removing two individuals from Limmen National Park, Northern Territory, that had mixed ancestry from many populations according to sNMF. We considered the groups of populations showing significant fixed differences as OTUs for another fixed difference analysis and as putative species for downstream analyses.

We estimated the genealogical divergence index (GDI) between the groups of populations showing fixed differences to quantify their degree of genetic divergence (Jackson et al. 2017). The GDI takes values between 0 and 1, where 0 indicates a single panmictic population and 1 indicates complete isolation between OTUs (Jackson et al. 2017). Values below 0.2 are considered as strong support for a single species, values between 0.2 and 0.7 are ambiguous, and values above 0.7 indicate strong support for species-level divergence (Jackson et al. 2017; Leaché et al. 2019). The GDI for each

OTU is calculated with the formula $1 - e^{-2\tau AB / \theta A}$, where τAB is the divergence time between OTUs A and B, and θA is the ancestral effective population size of OTU A (Leaché et al. 2019). We used BPP 4.2 (Flouri et al. 2018) to obtain a posterior distribution of divergence times, ancestral population sizes, and consequently the GDI. Due to computational limits, we selected 500 loci at random from the population SNP dataset. We fixed the topology based on the species tree inferred by SNAPP. Based on the genetic distances between and within putative species, we specified inverse gamma (IG) priors for the ancestral population size (θ_0; IG (3, 0.002)) and root age (τ_0; IG (3, 0.005)). We ran the MCMC for 32,000 burn-in iterations and 2 million post-burn-in iterations sampled every second iteration. We analysed the results in Tracer and accordingly deleted 75% of samples from the post-burn-in stage. We ran a second analysis to verify the consistency of the results.

Morphological sampling

We obtained four morphological datasets to evaluate whether there is phenotypic differentiation between the putative species: SVL, linear morphometric data describing body shape, and geometric morphometric data describing head shape in dorsal and lateral view. All individuals included in the morphometric analyses were adults. We recorded SVL and 17 external measurements describing body shape for 172 specimens (Fig. 1; Table S2). Additionally, we obtained photographs of the head for 169 and 170 specimens in dorsal and lateral view, respectively (Fig. 1; Tables S3–S4).

Some body measurements could not be recorded for all individuals (e.g., individuals with incomplete tails, missing fingers), in which case we used random forest training to input missing data. We performed the imputation in 'missForest 1.4' (Stekhoven and Bühlmann 2012), including putative species, sex, and SVL as predictors. Downstream analyses of SVL were performed on the natural logarithm of SVL. For the body shape dataset, we used log-shape ratios to correct for differences in body size. We calculated size as the geometric mean of all the measurements, divided each trait by size, and obtained the natural logarithm of the resulting ratios for downstream analyses (Mosimann, 1970).

We digitalized and processed the geometric morphometric data in 'geomorph'. We digitized 13 landmarks and 20 semi-landmarks in dorsal view (Fig. S1A), sliding the semi-landmarks based on the minimization of bending energy. For the lateral view, we digitized 10 landmarks (Fig. S1B). We removed the effects of size, location, and orientation through generalized Procrustes analysis (GPA) (Gower 1975). For the dorsal view, we took bilateral symmetry into account for the GPA and used the symmetric component of shape in subsequent analyses.

For each dataset and putative species, we used the "procD.lm" function of 'geomorph' to test for significant sexual dimorphism with 1,000 permutations. We only detected sexual dimorphism in body shape. Since our sampling is male biased, we removed the females of the putative species showing significant sexual dimorphism, resulting in a total sample size of 116 individuals.

Morphological divergence

We performed analyses of variance to test whether the putative species are morphologically divergent. For SVL and each other linear measurement, we performed ANOVA and then used Tukey's honest significant differences (HSD) as post-hoc test. We also performed multivariate analyses on the body measurements as a whole and the head shape datasets using the "advanced.procD.lm" function of 'geomorph'. We tested the influence of clade on morphological variation based on a multivariate linear model, assessing significance through 10,000 iterations. We visualized morphological differences using boxplots (SVL) and PCA plots (other datasets).

Results

Population structure

The sNMF analyses with the lowest cross-entropy were those where $K = 9$ (Fig. 2A). The distributions of three populations show broad correspondence with the known ranges of *V. s. storri*, *V. baritji*, and *V. a. insulanicus* (Fig. 2B; Table S5), but some individuals in the mainland north-eastern Top End were grouped with *V. a. insulanicus*. The other six populations are distributed as follows (Fig. 2B): the Selwyn Range in the Northern Territory-Queensland border, Cape Crafword region, widespread in the arid and semi-arid regions of central Australia, Kimberley region (except for Maret Islands), Maret Islands, and Pilbara region. Many populations show admixture where they come close or into contact (Figs. 2A, B). Specifically, there is considerable admixture between *Varanus a. insulanicus* and *V. baritji*; between the populations in the Kimberley and Maret Islands; and between the Selwyn Range and widespread populations, Pilbara, and Kimberley. Individuals from the Limmen National Park in the south-eastern Top End show mixed ancestry from several populations. Three clusters are readily identifiable in the plot of the first two PCs (Fig. 2C). One corresponds to *V. a. insulanicus* + *V. baritji*, another to *V. s. storri* and the population from Cape Crawford, and the last one to the remaining populations. In the latter cluster, structure is apparent within the widespread and Kimberley populations. PC3 more clearly distinguishes *V. s. storri* from the Cape

Crawford population and these two from the rest (Fig. S2). Thus, the populations in the *V. acanthurus* complex can be grouped into four main clusters: *V. s. storri* (SS), the Cape Crawford population (CC), *V. baritji* and *V. a. insulanicus* (BI), and the rest of the populations corresponding to *V. a. acanthurus* and *V. a. brachyurus* (AB).

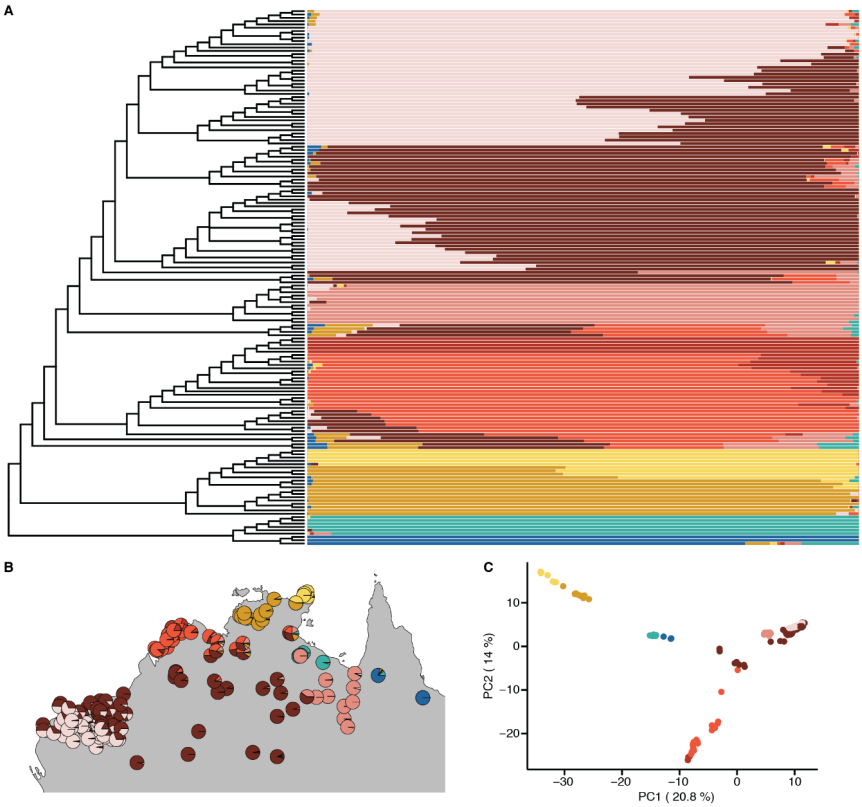

Figure 2. Geographic structure in the *V. acanthurus* complex. A) Ancestry coefficients estimated by sNMF; the tree was obtained from the analyses of a SNP dataset with SVDquartets (see Fig. 6); branch lengths are arbitrary. B) Geographic distribution of genetic structure as inferred by sNMF; each circle represents an individual. C) Principal component analysis of the population SNP dataset; individuals are coloured according to which population has the largest contribution in their ancestry coefficients.

All the Mantel tests we performed were significant (Table S6), suggesting that IBD is an important driver of genetic divergence. However, visual exploration of the data revealed that, for similar geographic distances, genetic differentiation is usually higher between the four identified clusters than within them (Fig. 3). When comparing groups of closely related populations independently, we also found that for a similar geographic distance between-population genetic distance is higher than within-population distance (Fig. S3). This suggests some degree of reproductive isolation between populations.

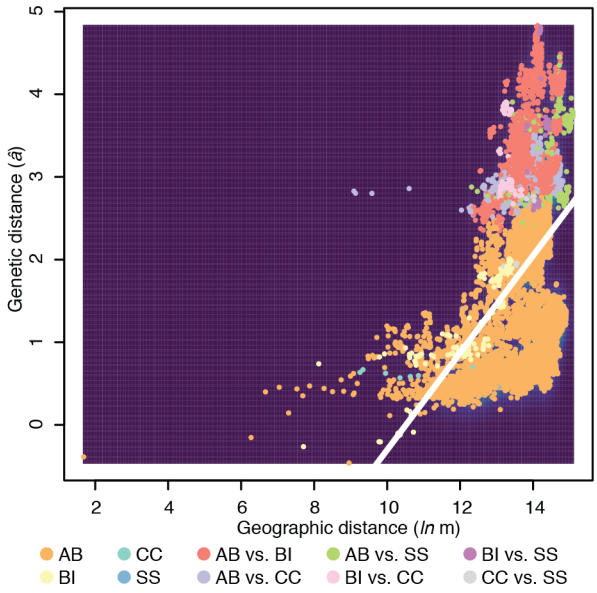

Figure 3. Isolation by distance in the *V. acanthurus* complex. Each point represents a pairwise comparison between individuals belonging to four distinct population clusters. The white line was obtained through linear regression. The background colour indicates kernel density.

Table 1. Demographic statistics for populations in the *V. acanthurus* complex. The observed heterozygosity (*Ho*) was adjusted to account for the absence of invariant loci (adjusted *Ho*).

Population	Individuals	*Ho*	Adjusted *Ho*	Tajima's *D*
Cape Crawford	6	0.0145	0.0126	0.0491
Kimberley	26	0.0172	0.015	–1.0478
Maret Islands	5	0.0179	0.0157	0.1021
Pilbara	38	0.0174	0.0152	–1.2446
Selwyn Range	12	0.017	0.0149	–0.4124
V. a. insulanicus	8	0.0191	0.0167	–0.2109
V. baritji	12	0.0194	0.017	–0.5893
V. s. storri	3	0.0185	0.0161	1.01
Widespread	52	0.0176	0.0153	–1.3635

Demographic statistics

The estimated *Ho* varied little between populations, but southern populations from arid and semi-arid environments show lower values in general (Table 1). Tajima's *D* is positive in *V. s. storri*, CC, and the Maret Islands population, being highest in the former. Other populations show negative Tajima's *D*, with the widespread population showing the lowest values.

Gene flow

NewHybrids identified multiple individuals as hybrids between the sNMF populations (Fig. 4A; Table S7). F2 hybrids were identified between *V. a. insulanicus* and *V. baritji*, and also between the widespread population and the Pilbara, Kimberley, and Selwyn Range populations. Multiple individuals from the transition between the arid zone and the Australian monsoonal tropics where identified as hybrids in more than one pairwise population comparison. The analyses did not identify any F1 hybrids.

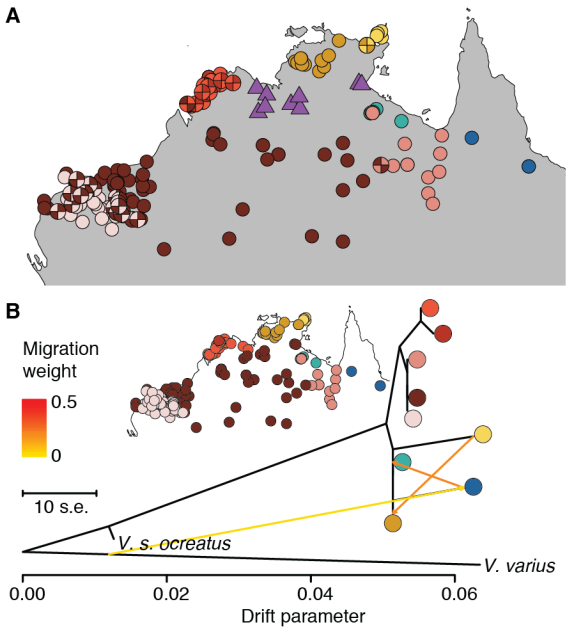

Figure 4. Gene flow in the *V. acanthurus* complex. A) Results of hybrid identification with NewHybrids; pie charts indicate F2 hybrids between two populations; triangles indicate individuals that were identified as hybrids in more than one pairwise comparison between populations. B) Population tree with migration edges obtained with TreeMix; coloured circles indicate the populations in the *V. acanthurus* complex, whose distribution is indicated in the inset; the migration edges are coloured according to their weight; horizontal branch lengths are proportional to estimated genetic drift; the scale bar shows ten times the average standard error in the sample covariance matrix.

The AIC favoured a model where the change point is at $m = 2.73$ (Fig. S4; Table S8); i.e., a population tree with tree migration edges was favoured (Fig. 4B). In this tree, *V. s. ocreatus* is outside the *V. acanthurus* complex. Within the complex, two main clades were identified. One includes *V. s. storri*, *V. baritji*, *V. a. insulanicus*, and the Cape Crawford population. *Varanus a. insulanicus* is sister to a clade in which *V. baritji* and *V. s. storri* are sister to the exclusion of the Cape Crawford population. The other main clade is equivalent to the AB cluster. In that clade, the Kimberley and Maret Islands populations form a clade that is sister to a clade where the Pilbara and widespread populations are sister to each other, to the exclusion of the Selwyn Range population. Migration was

identified between *V. a. insulanicus* and *V. baritji*, between *V. s. storri* and the Cape Crawford population, and between *V. s. storri* and the outgroup, *V. varius*.

Influence of climate on genetic and phenotypic differentiation

The first and second PCs of the precipitation variables explain 62.22% and 22.42% of variance, respectively. In the case of the temperature variables, the first and second PCs account for 70.05% and 20.25% of variance, respectively. The RDA model was significant (F = 6.325, DF = 4, p = 0.001) and spatial structure accounted for 21.31% of genetic variance, while the environmental data accounted for 11.04% of variance after accounting for spatial structure. The marginal effect of each environmental PC was significant (precipitation PC1: F = 8.83, DF = 1, p = 0.001; precipitation PC2: F = 3.67, DF = 1, p = 0.001; temperature PC1: F = 5.53, DF = 1, p = 0.001; temperature PC2: F = 1.6, DF = 1, p = 0.047). The first four RDA axes were significant (RDA1: F = 16.38, DF = 1, p = 0.001, variance explained (VE) = 64.72%; RDA2: F = 5.21, DF = 1, p = 0.001, VE = 20.61%; RDA3: F = 2.26, DF = 1, p = 0.004, VE = 8.92%; RDA4: F = 1.45, DF = 1, p = 0.03, VE = 5.74%). We identified a total of 979 candidate loci, of which 399 were outliers for RDA1, 104 for RDA2, 245 for RDA3, and 322 for RDA4 (Fig. 5A). Among the candidate loci, 305 were more strongly correlated with precipitation PC1 than the other variables, 54 with precipitation PC2, 560 with temperature PC1, and 60 with temperature PC2 (Table S9). The genomic location of the candidate loci based on the genome of *V. komodoensis* is given in Table S9. Mapping and annotation of most candidate loci was unsuccessful (Table S10).

In the 'Sunder' analyses, the model where genetic differentiation is explained by geographical distance alone was favoured for all environmental PCs (Fig. 5B). Under the model where both geographic and environmental distances have an effect on genetic differentiation, the posterior means of β_D were smaller than those of β_E (Table S11). This indicates that genetic covariance decreases slowly as environmental distance increases (with respect to geographic distance), i.e., that the effect of geographical distance on genetic divergence is greater than the effect of environmental distance (Botta et al. 2015).

The linear models with no spatial autocorrelation were favoured by the AICc when testing the relationship between body size and climate. We found a significant positive relationship between body size and annual precipitation (F = 16.93, DF = 1, p = 0.0001), and also with mean annual temperature (F = 17.89, DF = 1, p < 0.0001) (Fig. 5C). The hierarchical partitioning analysis revealed that annual precipitation and annual mean temperature explain independently 48.19% and 51.81% of body size variance, respectively (Fig. 5D).

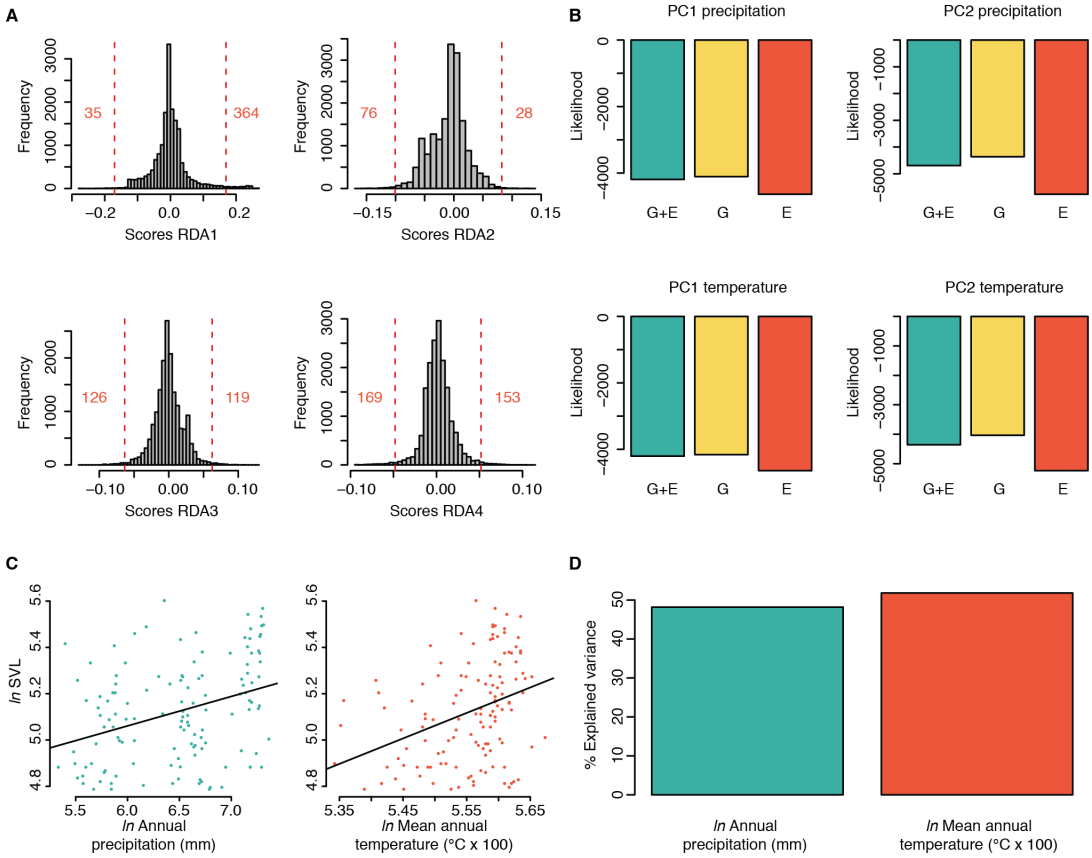

Figure 5. Signatures of local adaptation in the *V. acanthurus* complex. A) Histograms of locus scores for each RDA axis; the number of candidate loci with scores more than three standard deviations away from the mean (vertical dotted lines) are indicated in red. B) Likelihood of models where genetic distance is driven by geographic distance (G), environmental distance (E), or both (G+E), for each environmental principal component; note the negative likelihood values; i.e., shorter bars indicate models with higher likelihoods. C) Linear regression of body size against environmental variables. D) Percentage of variance in body size explained by environmental variables based on hierarchical partitioning.

Phylogenetics

In the individual-level nuclear trees (Figs. 6, S5–S6), a clade that includes CC and SS appears as sister to the clade that includes BI and AB (note that the trees were rooted according to the SNAPP topology). Each of these four major clades was strongly supported, but the relationships between them are not in the SVDquartets tree. The population from Cape Crawford and *V. s. storri* were consistently recovered as monophyletic. The individuals assigned to *V. a. insulanicus* constitute a clade, but they are nested within a paraphyletic *V. baritji*. Within AB, the widespread population is not monophyletic. The individuals in the Maret Islands form a clade that is nested within individuals from the Kimberley population. The Selwyn Range population is monophyletic, but is nested within individuals assigned to the widespread population.

The population from the Pilbara is rendered paraphyletic by few individuals from the widespread population.

Both species trees recover a monophyletic *V. acanthurus* complex to the exclusion of *V. s. ocreatus* (Fig. 6, S7); i.e., *V. storri* is not monophyletic. The SVDquartets species tree recovers two major clades. One includes CC + SS and *V. baritji* + *V. a. insulanicus* (BI). The other clade corresponds to AB and shows the populations from the Kimberley and Maret Islands as sister to each other, and this group as sister to a clade that includes the Selwyn Range, widespread, and Pilbara populations. The latter two were recovered as sisters. The SNAPP species tree differs by placing CC + SS as sister to AB + BI. The mean age for the most recent common ancestor (MRCA) of the *V. acanthurus* complex was 1.33 Ma (95% highest posterior density (HPD) 1.1–1.57). The deepest split between individual populations in the complex was between CC and SS (mean = 1.15 Ma, 95% HPD 0.95–1.41). The mean age of the split between AB and BI was 1.26 Ma (95% HPD 1.03–1.47). Other divergences within the complex were inferred to be more recent than 1 Ma.

Same as the nuclear species trees, the mitochondrial tree (Fig. 6, S8) recovers a monophyletic *V. acanthurus* complex that excludes *V. s. ocreatus*. The latter appears as sister to a clade that includes the *V. acanthurus* complex and the closely related species *V. kingorum* and *V. primordius*. Within the strongly supported *V. acanthurus* complex, a clade that includes the individuals that were assigned to the *V. a. insulanicus* population by sNMF appears as sister to the rest. An individual without nuclear data but that comes from the same locality as genotyped *V. baritji* is nested within *V. a. insulanicus*. CC and SS appear again as monophyletic and sister to each other, with AB as sister to both. Within AB, a clade that includes most of the individuals from the Kimberley and Maret Islands populations is sister to the rest. Some individuals in this clade are from the Pilbara region, and a few samples from the widespread population are nested within the Kimberley + Maret Islands clade. A clade that contains most of the individuals from the Pilbara appears as sister to a clade that includes three main subclades: one that includes individuals from the eastern Pilbara (including some that were assigned to the widespread population by sNMF), one that includes the individuals from the Selwyn Range population, and another one that includes most individuals from the widespread population plus some from the Maret Islands and the Pilbara.

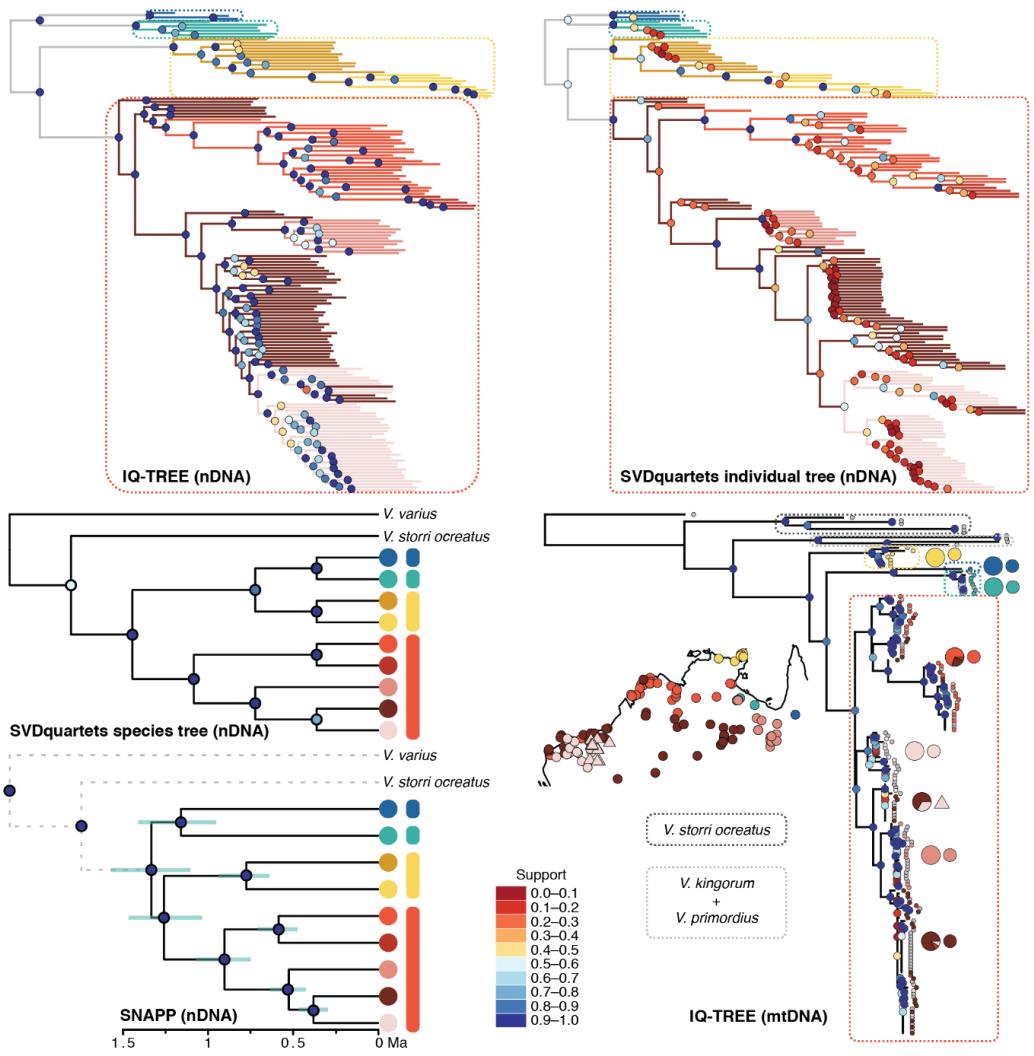

Figure 6. Phylogenetic relationships in the *V. acanthurus* complex. Branch lengths are arbitrary for SVDquartets, proportional to substitutions per site for IQ-TREE, and proportional to time for SNAPP. Circles in nodes indicate support values: ultrafast bootstrap for IQ-TREE, bootstrap for SVDquartets, and posterior probabilities for SNAPP. The dotted rectangles in the individual-level trees and vertical bars in the species trees indicate putative species (see Fig. 7). In the individual-level nuclear trees, branches are coloured based on their population assignment by sNMF. In the species trees, populations are indicated by the circles in the tips. In the SNAPP tree, dotted branches were shortened for visualization purposes and the horizontal blue bars indicate the 95% highest posterior density of divergence times. In the mitochondrial tree, population assignments by sNMF for individuals with nuclear data are shown by the circles at the tips; pie charts indicate the proportion of individuals belonging to each population within each major clade; and symbols next to pie charts were used to map the geographic distribution of each major clade.

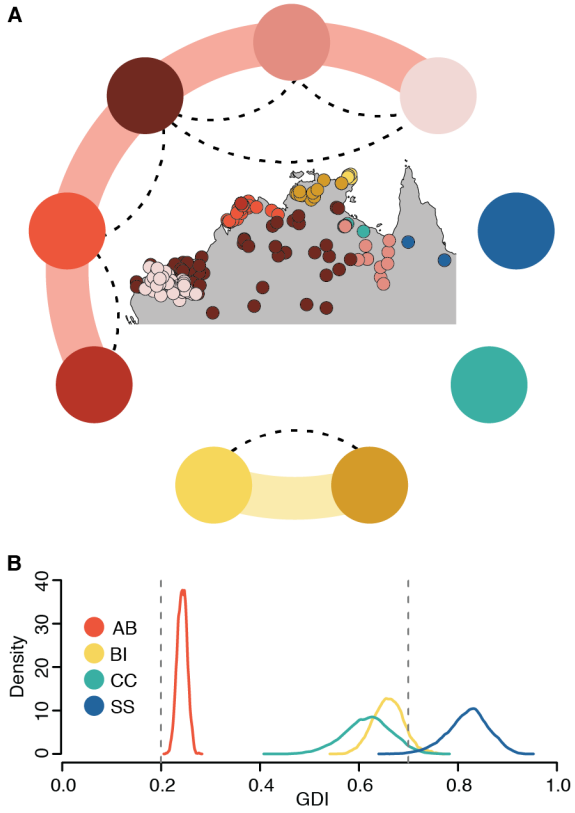

Figure 7. Species limits in the *V. acanthurus* complex. A) Results of the fixed difference analysis; populations are indicated by circles; dotted lines connect populations with no significant fixed differences; the arched bands connect populations that are directly or indirectly connected by gene flow as suggested by the absence of significant fixed differences; i.e., putative species. B) Posterior distribution of the genealogical divergence index (GDI) between putative species; GDI values below 0.2, between 0.2 and 0.7, and above 0.7 are considered as strong evidence against species-level divergence, ambiguous, and strong evidence for species-level divergence, respectively.

Molecular species delimitation

The fixed difference analysis (Fig. 7A) revealed that there are fixed differences between most populations identified by sNMF, except for the widespread and Pilbara populations (Tables S12–S13). The Cape Crawford population and *V. s. storri* have significant fixed differences with each other and every other population (Tables S12–S14). The differences between *V. a. insulanicus* and *V. bairtji* are not significant, but each of them showed significant differences with every other population. Within AB, differences were not significant between the widespread population and every other population, except for the one from the Maret Islands. Differences were also non-significant between the Pilbara and Selwyn Range populations, and between the Kimerley and Maret Islands populations. Thus, we identified four population clusters that are apparently isolated from each other. Results did not qualitatively differed when removing the individuals from Limmen National Park. The fixed difference analysis performed on the four clusters—

equivalent to AB, BI, CC, and SS—revealed significant fixed differences between them (Table S14).

The GDI suggests that the *V. acanthurus* compex comprises more than one species (Fig. 7B). The GDI was highest and above 0.7 for SS, supporting its species-level status. For the remaining clusters, GDI estimates are ambiguous. Among these, mean estimates are higher for BI, followed by CC, and lowest for AB.

Morphological divergence

The ANOVA coupled with HSD revealed significant differences in SVL between the following pairs of putative species (larger taxon indicated by *): AB and BI* (p adjusted for multiple testing (p_{adj}) = 0.009); AB* and SS (p_{adj} = 0.002); BI* and CC (p_{adj} = 0.009); and BI* and SS (p_{adj} < 0.0001) (Fig. 8; Table S15). We also found significant differences between the putative species in most linear measurements describing body shape (Tables S15). The closely related CC and SS significantly differ in relative head depth (p_{adj} = 0.002), hand width (p_{adj} = 0.02), toe IV length (p_{adj} = 0.04), and foot width (p_{adj} = 0.046). The multivariate analyses revealed that most taxa differ significantly in body shape, except for AB and CC (Table S15). Similarly, the PCA of the body shape variables (Fig. 8) shows that mean PC1 scores differ markedly between putative species, except for AB and CC. Based on the variable contributions to PC1, individuals in SS tend to have shorter necks and longer fingers than the other taxa. On the other hand, BI individuals have longer necks and shorter fingers. PC1 scores for AB and CC are intermediate between SS and BI.

The multivariate analyses of dorsal head shape revealed that all pairs of putative species differ significantly (Table S15). The PCA plot (Fig. 8) shows that individuals assigned to SS have large eyes, snouts that are short and narrow, and broad heads posteriorly. The mean head shape of AB is similar, but with a narrower head posteriorly. On the other hand, BI has on average small eyes, a snout that is broad and long, and a narrow head posteriorly. On average, CC individuals have broad heads posteriorly and an eye length and snout shape that are intermediate between AB + SS and BI.

Lateral head shape differs significantly between the following pairs: AB-BI, AB-SS, BI-SS, and CC-SS (Table S15). The PCA plot (Fig. 8) shows that individuals assigned to SS have relatively long eyes and heads that are dorsally-compressed posteriorly. On average, individuals in BI have smaller eyes and less dorsally-compressed heads. Eye length is intermediate between SS and BI in AB and CC, while they have deeper heads.

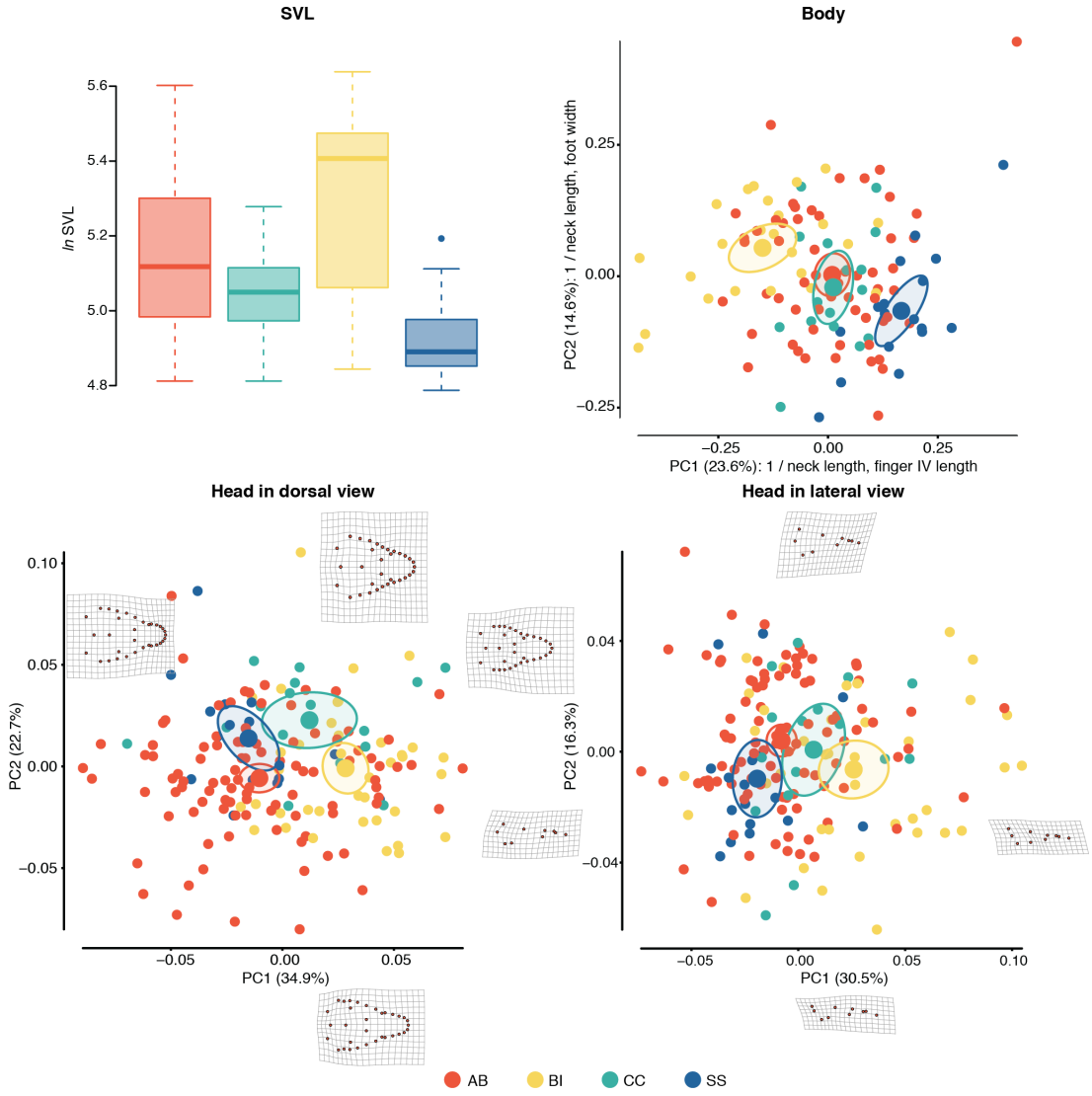

Figure 8. Morphological variation in the *V. acanthurus* complex. Colours indicate putative species. Boxplots show variation in body size. In the principal component (PC) plots, small points represent individuals, large points represent the mean PC scores per species, and circles indicate 95% confidence ellipses. For body shape, the two variables with the greatest contribution to each PC are indicated. For head shape, the landmark configuration and deformation grids (with respect to mean shape) are shown for the individuals at the extremes of each PC.

Discussion

We found evidence for local adaptation with gene flow in the *V. acanthurus* complex. Additionally, we identified meta-populations that may represent distinct species. Below, we elaborate on the relative importance of gene flow, local adaptation, and climate in the geographic sorting of genetic diversity and body size. Next, we discuss what historical processes may be responsible for the observed patterns of geographic structure. Finally,

we propose a new taxonomic framework for the group based on our molecular and morphological analyses.

Gene flow, adaptation, and climate

Our analyses suggest that gene flow has been more common within putative species than between species. The Kimberley, Selwyn Range, and Pilbara populations are widely allopatric but there appears to be gene flow between each of these and the widespread population from the arid and semi-arid regions of central Australia. Thus, connectivity and cohesion within AB seems to be maintained by the widespread population. The smallest Tajima's *D* was found in this population and heterozygosity is lower than in other more geographically restricted populations (Table 1). This suggests that the widespread population experienced a recent range expansion, consistent with other biogeographic and geological evidence for the steady expansion of the arid biome in Australia from the Miocene (Byrne et al. 2008, 2011). The Pilbara population, which is also found in the arid zone, has the second lowest Tajima's *D* (Table 1). Thus, it seems like aridification could have promoted the secondary contact of previously isolated populations through the range expansion of arid-adapted lineages. Multiple populations appear to have come into contact in the transition zone between arid and monsoonal environments (Figs. 2, 4). Here, individuals show elevated admixture between the widespread, Kimberley, and Selwyn Range populations. Some individuals even show a relatively high admixture proportion from *V*. *baritji*. Ecotones can persist as hybrid zones when hybrids have a selective advantage in intermediate habitats (Moore 1977; Ford et al. 1987). The transition zone supported pockets of mesic habitat throughout its recent history (Morton et al. 1995; Fujita et al. 2010; Oliver et al. 2014), laying conditions for secondary contact as mesic habitats expand or as lineages adapt to arid conditions. The region has been identified as a likely point of secondary contact before (Ford et al. 1987; Pavón-Vázquez et al. 2021). Climate driven instances of secondary contact appear to be common in Australia (Strasburg and Kearney 2005; Kearney et al. 2006; Ansari et al. 2019), reinforcing the role of aridification as one of the main factors shaping diversity patterns in the continent.

Gene flow between the Kimberley and Maret Islands populations, and between *V*. *a*. *insulanicus* and *V*. *baritji* has likely occurred during glacial periods of low sea levels. During these periods, northern Australia becomes connected with New Guinea and many of the islands in the Top End and Kimberley merge with the mainland (Voris 2000). TreeMix suggested gene flow between *V*. *a*. *insulanicus* and *V*. *baritji*, and between CC and *V*. *s*. *storri* (Fig. 4B). However, this could just reflect phylogenetic uncertainty instead of actual migration, where the close relationship between these two pairs recovered by

the other methods is identified as gene flow by TreeMix. Indeed, NewHybrids did not identify any hybrids between CC and *V. s. storri* (Fig. 4A) and they are separated by a well-known biogeographic barrier (see below). Recent gene flow between *V. s. storri* and *V. varius* as suggested by TreeMix seems extremely unlikely considering the huge size difference between these taxa and could be an artefact of incomplete lineage sorting. Mean adult SVL in *V. s. storri* is approximately 14 cm, while *V. varius* matures at around 40 cm SVL (Carter 1999).

Despite evidence for gene flow in the *V. acanthurus* complex, we found signatures of environmental influence on genotypic and phenotypic variation. This is not surprising considering the wide distribution of the group that spans monsoonal and arid environments. Furthermore, climate likely imposed strong selective pressure given the seemingly pivotal role of aridifcation in the evolutionary history of the complex. The RDA identified multiple candidate loci, most of them having a strong relationship with temperature. Our results align with an emerging paradigm where large molecular datasets are revealing that local adaptation can occur in the presence of gene flow if selection is strong (Brauer et al. 2018), even in systems approaching panmixia (Miller et al. 2019). The RDA approach is generally robust under a variety of demographic scenarios (Forester et al. 2018). However, our approach is unable to falsify some alternative scenarios. For example, environmental variables may be covarying with temperature and precipitation. Another possible confounding phenomenon is allele surfing, where otherwise rare alleles increase their frequency through successive founder events during range expansions (Ricklefs and Bermingham 2002). However, allele surfing may provide opportunity for adaptation to occur through soft selective sweeps (Gralka et al. 2016).

Phenotypic variation in body size appears to be influenced by climate. Our analyses revealed a significant positive correlation of SVL with both precipitation and temperature. Thus, the water availability and heat balance hypotheses were falsified. A positive correlation between body size and temperature has been documented in both ectotherms and endotherms (Yom-Tov 2006; Hileman et al. 2017; Wei et al. 2018). It has been proposed that this pattern may be caused by a non-adaptive process, where precipitation increases plant productivity, which in turn can increase prey abundance (Hileman et al. 2017; Wei et al. 2018). A positive relationship between body size and temperature appears to be common in squamates (Ashton and Feldman 2003). Similarly to precipitation, temperature may be positively correlated with productivity. Furthermore, elevated temperatures during development have been shown to increase body size in squamates (Arnold and Peterson 1989). Alternatively, selection on body size for thermoregulation may be relaxed in warmer environments (Shine and Madsen 1996). This would allow squamates to become larger in order to access the benefits of

increased body sizes, such as reduced predation and better competitive performance (Peters 1983; Ashton and Feldman 2003). Our approach does not allow us to rule out alternative explanations, such as correlation between the tested climatic variables and other environmental variables, or correlation between body size and another trait being environmentally selected (Cushman et al. 1993; Gaston and Blackburn 2000; Vinarski 2014). Thus, the positive relationship between SVL, precipitation, and temperature in the *V. acanthurus* complex could be the result of adaptation, aptation, plasticity, or a combination of these.

While we found evidence for climate imposing selection on several loci and a significant correlation between climate and body size, it seems like broader patterns of genetic divergence are mainly driven by other factors. Geographic distance seems to be having a stronger influence on genetic divergence than environmental distance (Fig. 5). Thus, adaptation to climatic conditions was probably not the main driver of diversification in the group; i.e., there is no evidence for ecological divergence. Instead, it seems like divergence within populations is mainly caused by IBD, while divergence between populations and between putative species seems to be the result of habitat contractions and the appearance of geographic features acting as barriers to gene flow (see below).

Biogeography

The relationships between the putative species in the *V. acanthurus* complex are ambiguous. The TreeMix, SVDquartets, SNAPP, and mitochondral topologies do not agree with each other (Figs. 4, 6). This is likely a result of the rapid and recent radiation of the *V. acanthurus* complex, where molecular markers may not have evolved fast enough compared to divergence in order to provide sufficient phylogenetic signal (Giarla and Esselstyn 2015; Leaché et al. 2016). The inferred dates for the splits between putative species in the complex are close to each other temporally and the credibility intervals overlap broadly (Fig. 6). There are less than 200 kyr between the basal split in the complex and the most recent speciation event (between *V. s. storri* and the Cape Crawford population). Alternatively, phylogeny may be obscured by admixture. However, our analyses suggest gene flow between putative species has been limited and all putative species are monophyletic in both the SNP and mitochondrial trees (Fig. 6).

Despite the phylogenetic uncertainty, patterns observed in the *V. acanthurus* complex offer insight into the biogeography of northern Australia. A close relationship between the complex and *V. kingorum*, *V. primordius*, and *V. s. ocreatus* is supported by our mitochondrial analyses and by other phylogenetic studies (e.g., Fitch et al. 2006; Vidal et al. 2012; Brennan et al. 2021). All of these taxa are distributed in the monsoonal tropics of northern Australia. *Varanus kingorum* is known from the Ord River region in Western

Australia and adjacent Northern Territory; *V. primordius* from the eastern Top End; and *V. s. ocreatus* from the Kimberley region and adjacent parts of the Northern territory, plus the semi-arid ranges in the border between the Northern Territory and Queensland (Wilson and Swan 2017). The *V. acanthurus* complex itself is more diverse in the monsoonal tropics, where the *V. a. insulanicus*, *V. baritji*, *V. s. storri*, Cape Crawford, Kimberley, Maret Islands, and Selwyn Range populations occur. Thus, it seems likely that the *V. acanthurus* complex has a northern Australian origin. This is further supported by the relatively high observed heterozygosity of most northern populations compared to southern populations (Table 1).

The importance of the monsoonal tropics of Australia as a hotspot of richness and endemism is supported by studies on multiple taxa (González-Orozco et al. 2011; Catullo et al. 2014; Moritz et al. 2016; Braby et al. 2020), and particularly saxicolous taxa such as the *V. acanthurus* complex (Potter et al. 2012; Laver et al. 2018). This is likely the result of long-term persistence in the monsoonal tropics, and particularly in mesic refugial areas such as the rocky escarpments in the Top End and Kimberley (Fujita et al. 2010; Laver et al. 2018; Oliver et al. 2019). Diversification of the clade including the *V. acanthurus* complex, *V. kingorum*, *V. primordius*, and *V. s. ocreatus* mimics that of co-distributed taxa. Diversification in the group started in the Miocene (Brennan et al. 2021) and continued into the Pleistocene, as in *Petrogale* rock wallabies (Potter et al. 2012) and multiple gecko lineages (Oliver et al. 2017). This time period in Australia is characterized by a general trend of increasing aridity and fragmentation of mesic habitats (Byrne et al. 2008, 2011), with mesic-adapted lineages becoming isolated in refugia and occasional invasion of the arid zone from the tropics (Fujita et al. 2010; Moritz et al. 2016), such as the widespread *V. acanthurus* population.

Phylogeographic structure within the *V. acanthurus* complex is also concordant with previously identified patterns. A wide extension of clay flats at the western base of the Cape York Peninsula, known as the Carpentarian Gap, has been demonstrated to be an important biogeographic barrier (Jennings and Edwards 2005; Bowman et al. 2009; Catullo et al. 2014). Isolation between the closely related Cape Crawford population and *V. s. storri* seems to be driven by this geographic feature. The Cape Crawford area has been identified before as a centre of endemism (Potter et al. 2016; Oliver et al. 2019). Within AB, endemic lineages were identified in the Kimberley, Pilbara, and Selwyn Range. These regions, with their numerous escarpments and gorges, have been previously identified as important mesic refugia in the face of increasing aridification (Fujita et al. 2010; Pepper et al. 2013; Catullo et al. 2014; Oliver et al. 2014). However, our analyses suggest that gene flow has prevented speciation of the lineages occurring there. It seems like gene flow is mainly driven by the expansion of the arid-adapted widespread population, which shows admixture with all the other populations of AB with

which it comes into contact. Despite their recent isolation, the islands off the Top End and Kimberley have been recently recognized as important centres of endemic diversity, likely because they have acted as refugia (Moritz et al. 2016; Laver et al. 2018; Oliver et al. 2019). In the *V. acanthurus* complex, *V. a. insulanicus* plus the Kimberley and Maret Islands populations occur in these islands. Gene flow has likely occurred between them and mainland populations when sea levels have been low, preventing speciation. However, there is some degree of differentiation between them and mainland populations. In particular, the islands in the Kimberley seem to host deeply divergent lineages (Fig. S2).

Taxonomy

Our study revealed some necessary changes to the taxonomy of *V. acanthurus* and closely related taxa. First, our study confirmed that *V. storri* is not monophyletic. Both our nuclear and mitochondrial trees show *V. s. storri* is more closely related to other species in the *V. acanthurus* complex than to *V. s. ocreatus*. In fact, our mitochondrial tree shows that *V. kingorum* and *V. primordius* are more closely related to *V. s. storri* than *V. s. ocreatus*. Thus, *V. s. ocreatus* should be elevated to the species level. Morphologically, *V. s. ocreatus* is distinguished from *V. s. storri* by having enlarged scales under the distal portion of the hindlimbs, fewer scales around midbody, fewer transversal rows of ventral scales, and a longer tail and limbs (Storr 1980). Specimens can also be identified based on their collecting localities, as the taxa occur east (*V. s. storri*) and west (*V. s. ocreatus*) of the Carpentarian Gap (Wilson and Swan 2017).

The population from the Cape Crawford area and *V. s. storri* were recovered as sisters in most of our analyses. We found that these lineages are reciprocally monophyletic (Fig. 6), show significant fixed differences, NewHybrids did not identify hybrids between them, the GDI of *V. s. storri* is high (Fig. 7), and both populations are morphometrically distinct (Fig. 8). Likewise, CC has a bright yellow gular region (vs cream or white in *V. s. storri*) and a well-defined dark postocular stripe (vs usually faint or ill-defined) (Fig. 9). Finally, the lineages are separated by the clay plains in the Carpentarian Gap, a well-documented biogeographic barrier (Kearns et al. 2011; Smith et al. 2011; Catullo et al. 2014). Our molecular and morphological analyses suggest that both CC and *V. s. storri* are distinct to other members of the *V. acanthurus* complex. Even when the Selwyn Range population comes close to CC (~ 8 km) in McArthur, Northern Territory, we did not find any evidence for gene flow between them, or between either CC or *V. s. storri* and BI. Thus, we consider that *V. s. storri* should be elevated to the species level and that the population from Cape Crawford represents an undescribed species.

We found that *V. acanthurus* is not monophyletic, as the subspecies *V. a. insulanicus* is more closely related to *V. baritji*. We found evidence for high gene flow between *V. a. insulanicus* and *V. baritji* (Figs. 2, 4) in Donydji, north-eastern Top End. Additionally, they are not reciprocally monophyletic (Fig. 6) and we did not detect significant fixed differences between them (Fig. 7). Morphologically, *V. a. insulanicus* differs from *V. baritji* by having alternating pale and dark longitudinal stripes on the neck (King and Horner 1987). However, the dorsal pattern of *V. a. insulanicus* is more similar to that of *V. baritji* (barred) than to other *V. acanthurus* (ocelli) (King and Horner 1987). Some degree of morphological differentiation in offshore island populations is not surprising (Keogh et al. 2007; Roulin and Salamin 2010), and photographic evidence indicates that individuals with a colour pattern similar to *V. a. insulanicus* inhabit eastern portions of Kakadu National Park in the mainland. We could not obtain molecular data for specimens from Groote Eylandt, the type locality of *V. a. insulanicus* (Mertens 1958). However, photographic evidence and our own examination of the type series show that their coloration is similar to that of *V. a. insulanicus* from the Wessel group and *V. baritji*. Additionally, reciprocal monophyly (Fig. 6), fixed allelic differences, a relatively high GDI (though inconclusive) (Fig. 7), and morphological differentiation (Figs. 8–9; Table S15) with other taxa in the *V. acanthurus* complex suggest that *V. a. insulanicus* + *V. baritji* are distinct from other populations in the complex. The sNMF (Fig. 2) and NewHybrids (Fig. 4; Table S7) analyses suggest there is some admixture between *V. a. insulanicus* + *V. baritji* and AB in the southern Top End (particularly in Limmen National Park). However, gene flow seems to be geographically restricted and in the admixed individuals the genetic contribution of *V. a. insulanicus* + *V. baritji* seems to be minimal compared to other populations in AB. Thus, we consider that *V. a. insulanicus* and *V. baritji* should be synonymized, with the former having priority (Mertens 1958), and that together they represent a distinct species.

AB is the clade with the widest distribution and notable morphological variation has been noted previously. Individuals from Barrow Island, off the coast of the Pilbara region, are miniaturized (Storr 1980; Case and Schwaner 1993). Individuals from the southern Pilbara are miniaturized and have a brick red background coloration. However, our analyses revealed that individuals from Barrow Island and the southern Pilbara are nested within a clade that includes other samples from the Pilbara. Individuals from the Kimberley, Maret Islands, and Selwyn Range populations have a thicker reticulum and darker coloration. Some individuals in the Selwyn Range population have bright yellow gular regions, and occasionally a bright yellow dorsal background colour (Schmida 2020). However, there is considerable admixture where the different populations identified by sNMF come into contact (Figs. 2, 4A), individuals assigned to the different populations interleave with each other in the nuclear and mitochondrial trees (Fig. 6),

and there are no significant fixed differences that would suggest that any population is reproductively isolated (Fig. 7A). Thus, we consider that *V. acanthurus* should be regarded as a monotypic and morphologically variable species.

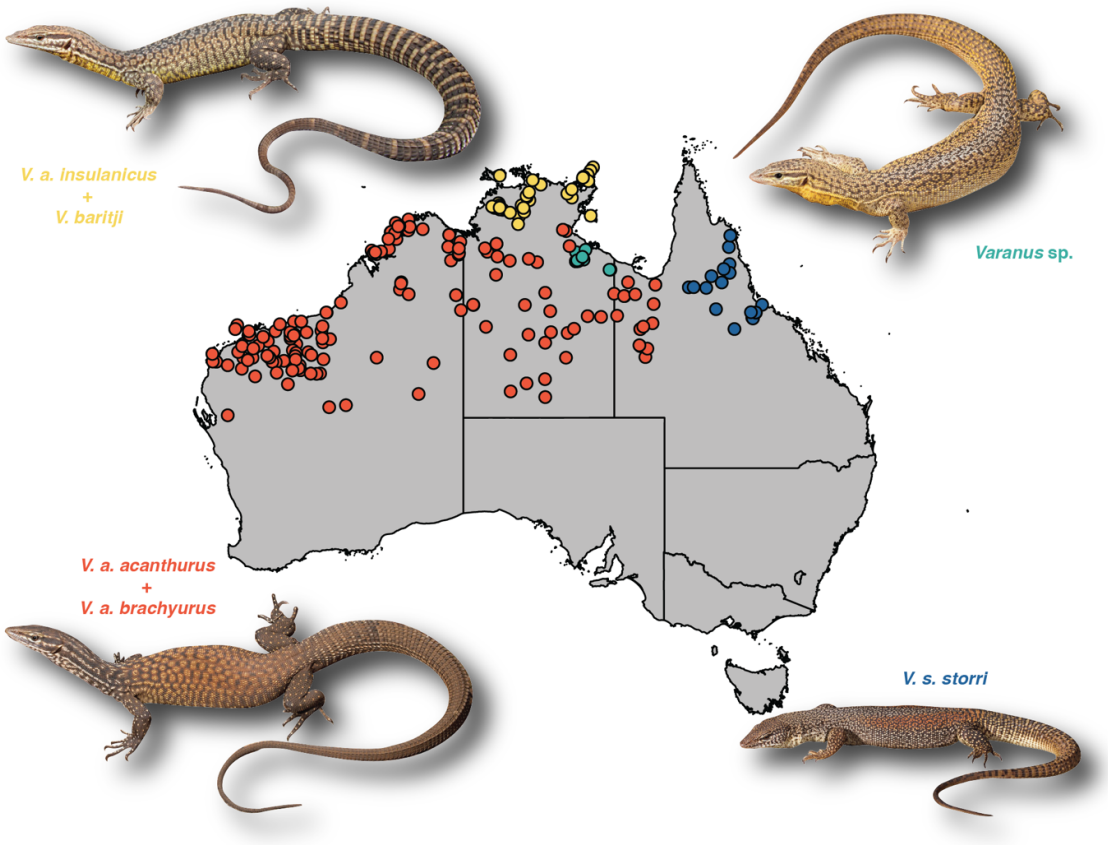

Figure 9. Geographic distribution of species in the *V. acanthurus* complex. Multiple sources of evidence support the distinctness of these four lineages. We show taxon names under the current taxonomy. Only localities with sequenced or morphologically examined individuals are mapped. Lines indicate state borders. Photographs by Stephen M. Zozaya.

Conclusions

Our study demonstrates that local adaptation may arise in the presence of extensive gene flow. Even when climate-imposed selection dictates allelic frequencies in some loci, isolation by distance, habitat contractions, and the presence of geographic barriers to gene flow are the main drivers of divergence and speciation in the *V. acanthurus* complex. The fragmentation of mesic environments and expansion of arid habitats as a result of aridification has been the main driving force behind the diversification of the group, dictating patterns of gene flow and isolation. Finally, the *V. acanthurus* complex

was found to be integrated by four genetically divergent and morphologically diagnosable taxa, including one undescribed species.

Acknowledgments

We thank A.P. Amey, R.D. Bray, P.D. Campbell, P.J. Couper, G.M. Dally, P. Doughty, A. Drew, M.R. Hutchinson, L. Joseph, C. Kovach, S. Mahony, J. Melville, J.J.L. Rowley, J.W. Streicher, S. South, J. Sumner, A. Velasco Castrillón, and J. Worthington Wilmer for the support provided during specimen examination in their respective institutions and for the loan of tissue samples; M. Arvizu Meza for helping with specimen examination; R.A. Catullo, J. Fenker, and B.Q. Minh for methodological suggestions; C. Correa Ospina, T. Cripps, and A. Kilian for their help with sequencing; A. de Laive, C.J. Jolly, B. Schembri, and S.M. Zozaya for sharing relevant photographs; J. Dobry for sharing SNP data for *V. s. storri*; and A.J. Fitch and M. Pepper for performing most mitochondrial sequencing. This work was supported by grants from the Australian Capital Territory Herpetological Association to C.J.P.V. and the Australian Research Council to J.S.K. Support for the graduate education of C.J.P.V. was awarded by the Australian Government Research Training Program.

Literature Cited

Adams, D. C., & Otárola-Castillo, E. (2013). geomorph: an R package for the collection and analysis of geometric morphometric shape data. Methods Ecol. Evol., 4(4), 393–399.

Aguirre-Liguori, J. A., Gaut, B. S., Jaramillo-Correa, J. P., Tenaillon, M. I., Montes-Hernández, S., García-Oliva, F., Hearne, S. J., and Eguiarte, L. E. (2019). Divergence with gene flow is driven by local adaptation to temperature and soil phosphorus concentration in teosinte subspecies (*Zea mays parviglumis* and *Zea mays mexicana*). Mol. Ecol., 28(11), 2814–2830.

Anderson, E. C., & Thompson, E. A. (2002). A model-based method for identifying species hybrids using multilocus genetic data. Genetics, 160(3), 1217–1229.

Ansari, M. H., Cooper, S. J. B., Schwarz, M. P., Ebrahimi, M., Dolman, G., Reinberger, L., Saint, K. M., Donnellan, S. C., Bull, M. C., & Gardner, M. G. (2019). Plio-Pleistocene diversification and biogeographic barriers in southern Australia

reflected in the phylogeography of a widespread and common lizard species. Mol. Phylogenet. Evol., 133, 107–119.

Arnold, S. J., & Peterson, C. R. (1989). A test for temperature effects on the ontogeny of shape in the garter snake *Thamnophis sirtalis*. Physiol. Zool., 62(6), 1316–1333.

Ashton, K. G. (2011). Do amphibians follow Bergmann's rule? Can. J. Zool., 80, 708–716.

Ashton, K. G., & Feldman, C. R. (2003). Bergmann's rule in nonavian reptiles: turtles follow it, lizards and snakes reverse it. Evolution, 57(5), 1151–1163.

Barrett, R. D. H., & Schluter, D. (2008). Adaptation from standing genetic variation. Trends Ecol. Evol., 23(1), 38–44.

Barton, N. H. (1986). The effects of linkage and density-dependent regulation on gene flow. Heredity, 57(3), 415–426.

Bergmann, C. (1847). Ueber die verhältnisse der wärmeökonomie der thiere zu ihrer grösse. Göttinger Studien, 1, 595–708.

Blanquart, F., Kaltz, O., Nuismer, S. L., & Gandon, S. (2013). A practical guide to measuring local adaptation. Ecol. Lett., 16(9), 1195–1205.

Botta, F., Eriksen, C., Fontaine, M. C., & Guillot, G. (2015). Enhanced computational methods for quantifying the effect of geographic and environmental isolation on genetic differentiation. Methods Ecol. Evol., 6(11), 1270–1277.

Bouckaert, R., Heled, J., Kühnert, D., Vaughan, T., Wu, C.-H., Xie, D., Suchard, M. A., Rambaut, A., & Drummond, A. J. (2014). BEAST 2: A software platform for bayesian evolutionary analysis. PLoS Comput. Biol., 10(4), e1003537.

Bowman, D. M. J. S., Brown, G. K., Braby, M. F., Brown, J. R., Cook, L. G., Crisp, M. D., Ford, F., Haberle, S., Hughes, J., Isagi, Y., Joseph, L., McBride, J., Nelson, G., & Ladiges, P. Y. (2010). Biogeography of the Australian monsoon tropics. J. Biogeogr., 37(2), 201–216.

Braby, M. F., Williams, M. R., Coppen, R. A. M., Williams, A. A. E., & Franklin, D. C. (2020). Patterns of species richness and endemism of butterflies and day-flying moths in the monsoon tropics of northern Australia. Biol. Conserv., 241, 108357.

Bradburd, G. S., Ralph, P. L., & Coop, G. M. (2013). Disentangling the effects of geographic and ecological isolation on genetic differentiation. Evolution, 67(11), 3258–3273.

Brauer, C. J., Unmack, P. J., Smith, S., Bernatchez, L., & Beheregaray, L. B. (2018). On the roles of landscape heterogeneity and environmental variation in determining population genomic structure in a dendritic system. Mol. Ecol., 27(17), 3484–3497.

Brennan, I. G., Lemmon, A. R., Lemmon, E. M., Portik, D. M., Weijola, V., Welton, L., Donnellan, S. C., & Keogh, J. S. (2021). Phylogenomics of monitor lizards and the role of competition in dictating body size disparity. Syst. Biol., 70(1), 120–132.

Bryant, D., Bouckaert, R., Felsenstein, J., Rosenberg, N. A., & RoyChoudhury, A. (2012). Inferring species trees directly from biallelic genetic markers: bypassing gene trees in a full coalescent analysis. Mol. Biol. Evol., 29(8), 1917–1932.

Byrne, M., Steane, D. A., Joseph, L., Yeates, D. K., Jordan, G. J., Crayn, D., Aplin, K., Cantrill, D. J., Cook, L. G., Crisp, M. D., Keogh, J. S., Melville, J., Moritz, C., Porch, N., Sniderman, J. M. K., Sunnucks, P., & Weston, P. H. (2011). Decline of a biome: evolution, contraction, fragmentation, extinction and invasion of the Australian mesic zone biota. J. Biogeogr., 38(9), 1635–1656.

Byrne, M., Yeates, D. K., Joseph, L., Kearney, M., Bowler, J., Williams, M. A. J., Cooper, S., Donnellan, S. C., Keogh, J. S., Leys, R., Melville, J., Murphy, D. J., Porch, N., & Wyrwoll, K.-H. (2008). Birth of a biome: insights into the assembly and maintenance of the Australian arid zone biota. Mol. Ecol., 17(20), 4398–4417.

Carter, D. B. (1999). Reproductive cycle of the lace monitor (*Varanus varius*). Mertensiella, 11, 137–147.

Case, T. J., & Schwaner, T. D. (1993). Island/mainland body size differences in Australian varanid lizards. Oecologia, 94(1), 102–109.

Catullo, R. A., Lanfear, R., Doughty, P., & Keogh, J. S. (2014). The biogeographical boundaries of northern Australia: evidence from ecological niche models and a multi-locus phylogeny of *Uperoleia* toadlets (Anura: Myobatrachidae). J. Biogeogr., 41(4), 659–672.

Chambers, E. A., & Hillis, D. M. (2020). The multispecies coalescent over-splits species in the case of geographically widespread taxa. Syst. Biol., 69(1), 184–193.

Chaplin, K., Sumner, J., Hipsley, C. A., & Melville, J. (2020). An integrative approach using phylogenomics and high-resolution x-ray computed tomography for species delimitation in cryptic taxa. Syst. Biol., 69(2), 294–307.

Chevan, A., & Sutherland, M. (1991). Hierarchical Partitioning. Am. Stat., 45(2), 90–96.

Chifman, J., & Kubatko, L. (2014). Quartet inference from snp data under the coalescent model. Bioinformatics, 30(23), 3317–3324.

Cogger, H. G. (2018). Reptiles and amphibians of Australia. CSIRO publishing.

Cushman, J. H., Lawton, J. H., & Manly, B. F. J. (1993). Latitudinal patterns in European ant assemblages: variation in species richness and body size. Oecologia, 95(1), 30–37.

De Queiroz, K. (1998). The general lineage concept of species, species criteria, and the process of speciation: a conceptual unification and terminological recommendations. In: Howard, D. J., & Berlocher, S. H. (eds.). Endless forms: species and speciation. Oxford University Press.

De Queiroz, K. (2007). Species concepts and species delimitation. Syst. Biol., 56(6), 879–886.

https://doi.org/10.1080/10635150701701083.

Dryden, G. (2004). *Varanus acanthurus*. In: Pianka, E. R., & King, D. R. (eds.). Varanoid lizards of the world. Indiana University Press.

Dyer, R. J., Nason, J. D., & Garrick, R. C. (2010). Landscape modelling of gene flow: improved power using conditional genetic distance derived from the topology of population networks. Mol. Ecol., 19(17), 3746–3759.

Edgar, R. C. (2004). MUSCLE: multiple sequence alignment with high accuracy and high throughput. Nucleic Acids Res., 32(5), 1792–1797.

Esquerré, D., Ramírez-Álvarez, D., Pavón-Vázquez, C. J., Troncoso-Palacios, J., Garín, C. F., Keogh, J. S., & Leaché, A. D. (2019). Speciation across mountains: Phylogenomics, species delimitation and taxonomy of the *Liolaemus leopardinus* clade (Squamata, Liolaemidae). Mol. Phylogenet. Evol., 139, 106524.

Fick, S. E., & Hijmans, R. J. (2017). WorldClim 2: new 1-km spatial resolution climate surfaces for global land areas. Int. J. Climatol., 37(12), 4302–4315.

Fitak, R. R. (2019). optM: an R package to optimize the number of migration edges using threshold models. R package version 0.1.3. Available at: https://CRAN.R-project.org/package=optM.

Fitch, A. J., Goodman, A. E., & Donnellan, S. C. (2006). A molecular phylogeny of the Australian monitor lizards (Squamata : Varanidae) inferred from mitochondrial DNA sequences. Aust. J. Zool., 54(4), 253–269.

Flouri, T., Jiao, X., Rannala, B., & Yang, Z. (2018). Species tree inference with BPP using genomic sequences and the multispecies coalescent. Mol. Biol. Evol., 35(10), 2585–2593.

Ford, J. (1987). Hybrid zones in Australian birds. Emu - Austral Ornithology, 87(3), 158–178.

Forester, B. R., Lasky, J. R., Wagner, H. H., & Urban, D. L. (2018). Comparing methods for detecting multilocus adaptation with multivariate genotype–environment associations. Mol. Ecol., 27(9), 2215–2233.

Frichot, E., & François, O. (2015). LEA: An R package for landscape and ecological association studies. Methods Ecol. Evol., 6(8), 925–929.

Frichot, E., Mathieu, F., Trouillon, T., Bouchard, G., & François, O. (2014). Fast and efficient estimation of individual ancestry coefficients. Genetics, 196(4), 973–983.

Fujita, M. K., McGuire, J. A., Donnellan, S. C., & Moritz, C. (2010). Diversification and persistence at the arid–monsoonal interface: Australia-wide biogeography of the Bynoe's Gecko (*Heteronotia binoei*; Gekkonidae). Evolution, 64(8), 2293–2314.

Gaston, K. J., & Blackburn, T. M. (2000). Pattern and Process in Macroecology. Blackwell Publishing.

Georges, A., Gruber, B., Pauly, G. B., White, D., Adams, M., Young, M. J., Kilian, A., Zhang, X., Shaffer, H. B., & Unmack, P. J. (2018). Genomewide SNP markers breathe new life into phylogeography and species delimitation for the problematic short-necked turtles (Chelidae: *Emydura*) of eastern Australia. Mol. Ecol., 27(24), 5195–5213.

Giarla, T. C., & Esselstyn, J. A. (2015). The challenges of resolving a rapid, recent radiation: empirical and simulated phylogenomics of Philippine shrews. Syst. Biol., 64(5), 727–740.

González-Orozco, C. E., Laffan, S. W., & Miller, J. T. (2011). Spatial distribution of species richness and endemism of the genus *Acacia* in Australia. Aust. J. Bot., 59(7), 601–609.

Götz, S., García-Gómez, J. M., Terol, J., Williams, T. D., Nagaraj, S. H., Nueda, M. J., Robles, M., Talón, M., Dopazo, J., & Conesa, A. (2008). High-throughput functional annotation and data mining with the Blast2GO suite. Nucleic Acids Res., 36(10), 3420–3435.

Gower, J. C. (1975). Generalized procrustes analysis. Psychometrika, 40(1), 33–51.

Gralka, M., Stiewe, F., Farrell, F., Möbius, W., Waclaw, B., & Hallatschek, O. (2016). Allele surfing promotes microbial adaptation from standing variation. Ecol. Lett., 19(8), 889–898.

Gruber, B., Unmack, P. J., Berry, O. F., & Georges, A. (2018). DARTR: An R package to facilitate analysis of SNP data generated from reduced representation genome sequencing. Mol. Ecol. Resour., 18(3), 691–699.

Hemstrom, W., & Jones, M. (2021). snpR: user friendly population genomics for SNP datasets with categorical metadata. Authorea.

Hileman, E. T., King, R. B., Adamski, J. M., Anton, T. G., Bailey, R. L., Baker, S. J., Bieser N. D., Bell Jr, T. A., Bissell, K. M., Bradke, D. R., Campa III, H., Casper, G. S., Cedar, K., Cross, M. D., DeGregorio, B. A., Dreslik, M. J., Faust, L. J., Harvey, D. S., Hay, R. W., Jellen, B. C., Johnson, B. D., Johnson, G., Kiel, B. D., Kingsbury, B. A., Kowalski, M. J., Lee, Y. M., Lentini, A. M., Marshall, J. C., Mauger, D., Moore, J. A., Paloski, R. A., Phillips, C. A., Pratt, P. D., Preney, T., Prior, K. A., Promaine, A., Redmer, M., Reinert, H. K., Rouse, J. D., Shoemaker, K. T., Sutton, S., VanDeWalle, T. J., Weatherhead, P. J., Wynn, A., & Yagi, A. (2017). Climatic and geographic predictors of life history variation in Eastern Massasauga (*Sistrurus catenatus*): a range-wide synthesis. PLoS One, 12, e0172011.

Hoang, D. T., Chernomor, O., von Haeseler, A., Minh, B. Q., & Vinh, L. S. (2018). UFBoot2: Improving the ultrafast bootstrap approximation. Mol. Biol. Evol., 35(2), 518–522.

Jackson, N. D., Carstens, B. C., Morales, A. E., & O'Meara, B. C. (2017). species delimitation with gene flow. Syst. Biol., 66(5), 799–812.

Jennings, W. B., & Edwards, S. V. (2005). Speciational history of Australian grass finches (*Poephila*) inferred from thirty gene trees. Evolution, 59(9), 2033–2047.

Kaltz, O., & Shykoff, J. A. (1998). Local adaptation in host–parasite systems. Heredity, 81(4), 361–370.

Kalyaanamoorthy, S., Minh, B. Q., Wong, T. K. F., von Haeseler, A., & Jermiin, L. S. (2017). ModelFinder: fast model selection for accurate phylogenetic estimates. Nat. Methods, 14(6), 587–589.

Kawecki, T. J., & Ebert, D. (2004). Conceptual issues in local adaptation. Ecol. Lett., 7(12), 1225–1241.

Kawecki, T. J., Barton, N. H., & Fry, J. D. (1997). Mutational collapse of fitness in marginal habitats and the evolution of ecological specialisation. J. Evol. Biol., 10(3), 407–429.

Kearney, M., Blacket, M. J., Strasburg, J. L., & Moritz, C. (2006). FAST-TRACK: Waves of parthenogenesis in the desert: evidence for the parallel loss of sex in a grasshopper and a gecko from Australia. Mol. Ecol., 15(7), 1743–1748.

Kearns, A. M., Joseph, L., Omland, K. E., & Cook, L. G. (2011). Testing the effect of transient Plio-Pleistocene barriers in monsoonal Australo-Papua: did mangrove habitats maintain genetic connectivity in the Black Butcherbird? Mol. Ecol., 20(23), 5042–5059.

Keogh, J. S., Scott, I. A. W., & Hayes, C. (2005). Rapid and repeated origin of insular gigantism and dwarfism in Australian tiger snakes. Evolution, 59(1), 226–233.

Kilian, A., Wenzl, P., Huttner, E., Carling, J., Xia, L., Blois, H., Caig, V., Heller-Uszynska, K., Jaccoud, D., Hopper, C., Aschenbrenner-Kilian, M., Evers, M., Peng, K., Cayla, C., Hok, P., & Uszynski, G. (2012). Diversity arrays technology: a generic genome profiling technology on open platforms. Methods Mol. Biol., 888, 67–89.

King, M., & Horner, P. (1987). A new species of monitor (Platynota: Reptilia) from northern Australia and a note on the status of *Varanus acanthurus insulanicus* Mertens. The Beagle, 4(1), 73–79.

Kirkpatrick, M., & Barton, N. H. (1997). Evolution of a species' range. Am. Nat., 150(1), 1–23

Lanfear, R., Frandsen, P. B., Wright, A. M., Senfeld, T., & Calcott, B. (2017). PartitionFinder 2: New Methods for Selecting Partitioned Models of Evolution for Molecular and Morphological Phylogenetic Analyses. Mol. Biol. Evol., 34(3), 772–773.

Laver, R. J., Doughty, P., & Oliver, P. M. (2018). Origins and patterns of endemic diversity in two specialized lizard lineages from the Australian Monsoonal Tropics (*Oedura* spp.). J. Biogeogr., 45(1), 142–153.

Leaché, A. D., Banbury, B. L., Linkem, C. W., & Nieto-Montes de Oca, A. (2016). Phylogenomics of a rapid radiation: is chromosomal evolution linked to increased diversification in north american spiny lizards (genus *Sceloporus*)? BMC Evol. Biol., 16(1), 1–16.

Leaché, A. D., Zhu, T., Rannala, B., & Yang, Z. (2019). The spectre of too many species. Syst. Biol., 68(1), 168–181.

Lenormand, T. (2002). Gene flow and the limits to natural selection. Trends Ecol. Evol., 17(4), 183–189.

Lenormand, T. (2012). From Local Adaptation to Speciation: Specialization and Reinforcement. Int. J. Ecol., 2012, 11.

Leroy, T., Louvet, J.-M., Lalanne, C., Le Provost, G., Labadie, K., Aury, J-M., Delzon, S., Plomion, C., & Kremer, A. (2020). Adaptive introgression as a driver of local adaptation to climate in European white oaks. New Phytol., 226(4), 1171–1182.

Lewis, P. O. (2001). A likelihood approach to estimating phylogeny from discrete morphological character data. Syst. Biol., 50(6), 913–925.

Lind, A. L., Lai, Y. Y. Y., Mostovoy, Y., Holloway, A. K., Iannucci, A., Mak, A. C. Y., Fondi, M., Orlandini, V., Eckalbar, W. L., Milan, M., Rovatsos, M., Kichigin, I. G., Makunin, A. I., Pokorná, M. J., Altmanová, M., Trifonov, V. A., Schijlen, E., Kratochvíl, L., Fani, R., Velenský, P., Rehák, I., Patarnello, T., Jessop, T. S., Hicks, J. W., Ryder, O. A., Mendelson III, J. R., Ciofi, C., Kwok, P-Y., Pollard, K. S., & Bruneau, B. G. (2019). Genome of the Komodo dragon reveals adaptations in the cardiovascular and chemosensory systems of monitor lizards. Nat. Ecol. Evol., 3(8), 1241–1252.

Marshall, T. L., Chambers, E. A., Matz, M. V., & Hillis, D. M. (2021). How mitonuclear discordance and geographic variation have confounded species boundaries in a widely studied snake. Mol. Phylogenet. Evol., 162, 107194.

Mayr, E. (1942). Systematics and the origin of species, from the viewpoint of a zoologist. Harvard University Press.

Melville, J., Haines, M. L., Boysen, K., Hodkinson, L., Kilian, A., Date, K. L. S., Potvin, D. A., & Parris, K. M. (2017). Identifying hybridization and admixture using SNPs: application of the DArTseq platform in phylogeographic research on vertebrates. R. Soc. Open Sci., 4(7).

Mertens, R. (1958). Bemerkungen über die Warane Australiens. Senckenbergiana Biologica, 39, 229–264.

Milano, I., Babbucci, M., Cariani, A., Atanassova, M., Bekkevold, D., Carvalho, G. R., Espiñeira, M., Fiorentino, F., Garofalo, G., Geffen, A. J., Hansen, J. H., Helyar, S. J., Nielsen, E. E., Ogden, R., Patarnello, T., Stagioni, M., FishPopTrace Consortium, Tinti, F., & Bargelloni, L. (2014). Outlier SNP markers reveal fine-scale genetic structuring across European hake populations (*Merluccius merluccius*). Mol. Ecol., 23(1), 118–135.

Miller, A. D., Hoffmann, A. A., Tan, M. H., Young, M., Ahrens, C., Cocomazzo, M., Rattray A., Ierodiaconou, D. A., Treml, E., & Sherman, C. D. H. (2019). Local and regional scale habitat heterogeneity contribute to genetic adaptation in a commercially important marine mollusc (*Haliotis rubra*) from southeastern Australia. Mol. Ecol., 28(12), 3053–3072.

Moore, W. S. (1977). An evaluation of narrow hybrid zones in vertebrates. Q. Rev. Biol., 52(3), 263–277.

Moritz, C., Fujita, M. K., Rosauer, D., Agudo, R., Bourke, G., Doughty, P., Palmer, R., Pepper, M., Potter, S., Pratt, R., Scott, M., Tonione, M., & Donnellan, S. (2016).

Multilocus phylogeography reveals nested endemism in a gecko across the monsoonal tropics of Australia. Mol. Ecol., 25(6), 1354–1366.

Morton, S. R., Short, J., & Barker, R. D. (1995). Refugia for biological diversity in arid and semi-arid australia: a report to the Biodiversity Unit of the Department of Environment, Sport and Territories. Deptartment of Environment, Sport and Territories.

Morton, S. R., Stafford Smith, D. M., Dickman, C. R., Dunkerley, D. L., Friedel, M. H., McAllister, R. R. J., Reid, J. R. W., Roshier, D. A., Smith, M. A., Walsh, F. J., Wardel, G. M., Watson, I. W., & Westoby, M. (2011). A fresh framework for the ecology of arid Australia. J. Arid Environ., 75(4), 313–329.

Mosimann, J. E. (1970). Size allometry: size and shape variables with characterizations of the lognormal and generalized gamma distributions. J. Am. Stat. Assoc., 65(330), 930–945.

Nally, R. M., & Walsh, C. J. (2004). Hierarchical partitioning public-domain software. Biodivers. Conserv., 13(3), 659–660.

Nguyen, L.-T., Schmidt, H. A., von Haeseler, A., & Minh, B. Q. (2015). IQ-TREE: a fast and effective stochastic algorithm for estimating maximum-likelihood phylogenies. Mol. Biol. Evol., 32(1), 268–274.

Oksanen, J., Blanchet, F. G., Friendly, M., Kindt, R., Legendre, P., McGlinn, D., Minchin, P. R., O'Hara, R. B., Simpson, G. L., Solymos, P., Stevens, M. H. H., Szoecs, E., & Wagner, H. (2019). vegan: Community ecology package. R package version 2.5-6. Available at: https://CRAN.R-project.org/package=vegan.

Olalla-Tárraga, M. Á., & Rodríguez, M. Á. (2007). Energy and interspecific body size patterns of amphibian faunas in Europe and North America: anurans follow Bergmann's rule, urodeles its converse. Global Ecol. Biogeogr., 16(5), 606–617.

Oliver, P. M., Ashman, L. G., Bank, S., Laver, R. J., Pratt, R. C., Tedeschi, L. G., & Moritz, C. C. (2019). On and off the rocks: persistence and ecological diversification in a tropical Australian lizard radiation. BMC Evol. Biol., 19(1), 1–15.

Oliver, P. M., Couper, P. J., & Pepper, M. (2014). Independent transitions between monsoonal and arid biomes revealed by systematic revison of a complex of Australian geckos (*Diplodactylus*; Diplodactylidae). PLoS One, 9(12), e111895.

Oliver, P. M., Laver, R. J., De Mello Martins, F., Pratt, R. C., Hunjan, S., & Moritz, C. C. (2017). A novel hotspot of vertebrate endemism and an evolutionary refugium in tropical Australia. Divers. Distrib., 23(1), 53–66.

Pavón-Vázquez, C. J., Brennan, I. G., & Keogh, J. S. (2021). A comprehensive approach to detect hybridization sheds light on the evolution of Earth's largest lizards. Syst. Biol., syaa102.

Pepper, M., Doughty, P., & Keogh, J. S. (2013). Geodiversity and endemism in the iconic Australian Pilbara region: a review of landscape evolution and biotic response in an ancient refugium. J. Biogeogr., 40(7), 1225–1239.

Peters, R. H. (1983). The ecological implications of body size. Cambridge University Press.

Petroli, C. D., Sansaloni, C. P., Carling, J., Steane, D. A., Vaillancourt, R. E., Myburg, A. A., Bonfim da Silva Jr., O., Pappas Jr., G. J., Kilian, A., & Grattapaglia, D. (2012). Genomic characterization of DArT markers based on high-density linkage analysis and physical mapping to the *Eucalyptus* genome. PLoS One, 7(9), e44684.

Pickrell, J. K., & Pritchard, J. K. (2012). Inference of Population Splits and Mixtures from Genome-Wide Allele Frequency Data. PLos Genet., 8(11), e1002967.

Potter, S., Bragg, J. G., Peter, B. M., Bi, K., & Moritz, C. (2016). Phylogenomics at the tips: inferring lineages and their demographic history in a tropical lizard, *Carlia amax*. Mol. Ecol., 25(6), 1367–1380.

Potter, S., Cooper, S. J. B., Metcalfe, C. J., Taggart, D. A., & Eldridge, M. D. B. (2012). Phylogenetic relationships of rock-wallabies, *Petrogale* (Marsupialia: Macropodidae) and their biogeographic history within Australia. Mol. Phylogenet. Evol., 62(2), 640–652.

Pritchard, J. K., & Di Rienzo, A. (2010). Adaptation - not by sweeps alone. Nat. Rev. Genet., 20838407.

R Core Team (2019). R: A language and environment for statistical computing. R Foundation for Statistical Computing, Vienna, Austria. Available at: https://www.R-project.org/.

Rambaut, A., Suchard, M. A., Xie, D., & Drummond, A. J. (2014). Tracer v1.6. Available at: http://beast.bio.ed.ac.uk/Tracer.

Ricklefs, R. E., & Bermingham, E. (2002). The concept of the taxon cycle in biogeography. Global Ecol. Biogeogr., 11(5), 353–361.

Roulin, A., & Salamin, N. (2010). Insularity and the evolution of melanism, sexual dichromatism and body size in the worldwide-distributed barn owl. J. Evol. Biol., 23(5), 925–934.

Rousset. (2000). Genetic differentiation between individuals. J. Evol. Biol., 13(1), 58–62.

Savolainen, O., Lascoux, M., & Merilä, J. (2013). Ecological genomics of local adaptation. Nat. Rev. Genet., 14(11), 807–820.

Schmida, G. (2020). A photographic guide to Australian monitors. Blurb.

Sexton, J. P., Hangartner, S. B., & Hoffmann, A. A. (2014). Genetic isolation by environment or distance: which pattern of gene flow is most common? Evolution, 68(1), 1–15.

Shine, R., & Madsen, T. (1996). Is thermoregulation unimportant for most reptiles? an example using water pythons (*Liasis fuscus*) in tropical Australia. Physiol. Zool., 69(2), 252–269.

Slatkin, M. (1985). Gene Flow in Natural Populations. Annu. Rev. Ecol. Syst., 16(1), 393–430.

Slatkin, M. (1987). Gene flow and the geographic structure of natural populations. Science, 236(4803), 787–792.

Smith, K. L., Harmon, L. J., Shoo, L. P., & Melville, J. (2011). Evidence of constrained phenotypic evolution in a cryptic species complex of agamid lizards. Evolution, 65(4), 976–992.

Stange, M., Sánchez-Villagra, M. R., Salzburger, W., & Matschiner, M. (2018). Bayesian divergence-time estimation with genome-wide single-nucleotide polymorphism data of sea catfishes (Ariidae) supports Miocene closure of the Panamanian Isthmus. Syst. Biol., 67(4), 681–699.

Stekhoven, D. J., & Bühlmann, P. (2012). MissForest—non-parametric missing value imputation for mixed-type data. Bioinformatics, 28(1), 112–118.

Storr, G. M. (1980). The monitor lizards (genus *Varanus* Merrem, 1820) of Western Australia. Rec. West. Aust. Mus., 8(2), 237–293.

Strasburg, J. L., & Kearney, M. (2005). Phylogeography of sexual *Heteronotia binoei* (Gekkonidae) in the Australian arid zone: climatic cycling and repetitive hybridization. Mol. Ecol., 14(9), 2755–2772.

Swofford, D. L. (2003) PAUP*. Phylogenetic analysis using parsimony and other methods. Version 4. Sinauer Associates.

Tajima, F. (1989). Statistical method for testing the neutral mutation hypothesis by DNA polymorphism. Genetics, 123(3), 585–595.

Thompson, G. G., Clemente, C. J., Withers, P. C., Fry, B. G., & Norman, J. A. (2009). Is body shape of varanid lizards linked with retreat choice? Aust. J. Zool., 56(5), 351–362.

Tigano, A., & Friesen, V. L. (2016). Genomics of local adaptation with gene flow. Mol. Ecol., 25(10), 2144–2164.

Vidal, N., Marin, J., Sassi, J., Battistuzzi, F. U., Donnellan, S., Fitch, A. J., Fry, B. G., Vonk, F. J., Rodriguez de la Vega, R. C., Couloux, A., & Hedges, S. B. (2012). Molecular evidence for an Asian origin of monitor lizards followed by Tertiary dispersals to Africa and Australasia. Biol. Lett., 8(5), 853–855.

Vinarski, M. V. (2014). On the applicability of Bergmann's rule to ectotherms: The state of the art. Biol. Bull. Rev., 4(3), 232–242.

Voris, H. K. (2000). Maps of Pleistocene sea levels in Southeast Asia: shorelines, river systems and time durations. J. Biogeogr., 27(5), 1153–1167.

Walters, S. J., Robinson, T. P., Byrne, M., Wardell-Johnson, G. W., & Nevill, P. (2020). Contrasting patterns of local adaptation along climatic gradients between a sympatric parasitic and autotrophic tree species. Mol. Ecol., 29(16), 3022–3037.

Wei, X., Yan, L., Zhao, C., Zhang, Y., Xu, Y., Cai, B., Jiang, N., & Huang, Y. (2018). Geographic variation in body size and its relationship with environmental gradients in the Oriental Garden Lizard, *Calotes versicolor*. Ecol. Evol., 8(9), 4443–4454.

Wilson, S. K., & Swan, G. (2017). A complete guide to reptiles of Australia. Reed New Holland.

Yom-Tov, Y., & Geffen, E. (2006). Geographic variation in body size: the effects of ambient temperature and precipitation. Oecologia, 148(2), 213–218.

SYNTHESIS

In this thesis, we accompanied monitor lizards through their evolutionary history. Our journey began roughly 120 million years ago (Ma), when dinosaurs still roamed the planet. Around this time, monitor lizards and their closest living relative, the Borneo earless monitor, split from the Chinese crocodile lizard somewhere in Asia (Brennan et al. 2021; Chapter I). The last common ancestor of the Borneo earless monitor and monitor lizards lived around 70 Ma (Lin and Wiens 2017), approximately at the same time that *Tyrannosaurus rex* started stalking the North American forests (Johnson 2008). There are notable biological differences between the lizard cousins. The Borneo earless monitor is a sluggish inhabitant of riparian habitats that lacks external ears and a pineal eye, and has small eyes and limbs (Pianka 2004). On the other hand, monitor lizards are notable among reptiles for their aerobic capacity and adaptability, have external ears and a pineal eye—or two in the case of the extinct *Saniwa ensidens* (Smith et al 2018)—and generally have large eyes and limbs (Pianka and King 2004). Monitor lizards were particularly successful at colonizing new areas (even remote islands) and forming new species (Chapter I), while the Borneo earless monitor is the sole representative of its family. The notable ecomorphological differentiation between these two was likely the result of an evolutionary shift in developmental rates, with monitor lizards showing a "juvenile-like" appearance compared with the Borneo earless monitor (Chapter II).

The most recent common ancestor of extant varanids lived around 33 Ma (Brennan et al. 2021), when mammals had already replaced non-avian dinosaurs as the dominant group in terrestrial ecosystems. This ancestral varanid probably originated in either Asia or Africa (Holmes et al. 2010; Vidal et al. 2012; Brennan et al. 2021; Chapter I). Varanid diversity in these regions remained relatively low, but the collision of Australia and Asia 25 Ma provided a unique evolutionary opportunity for varanids (Chapter I). This allowed monitors to colonise Australia, Melanesia, and the newly formed Philippine archipelago. Prompted by a combination of the dynamic environmental and geological history of the region and interspecific competition, varanid richness and ecomorphological diversity exploded in Indo-Australasia (Chapter I).

The notable diversification of varanids was made possible by evolutionary shifts in ontogenetic development (Chapter II). Shifts in the direction of ontogenetic change differentiated the major clades within Varanidae, while the morphological differences between closely related species were mainly driven by changes in the timing and rate of development (Chapter II). The ontogenetic lability of varanids also enabled them to specialize ecologically. The highly arboreal members of the *Hapturosaurus* subgenus

show ontogenetic trajectories that differ markedly from those of other varanids, becoming more gracile as they grow. In contrast, many varanid species become more robust as adults, likely because juveniles are more arboreal than adults (Chapter II).

As varanids diversified in Indo-Australasia, several lineages became true giants. One of them was the Komodo dragon from Indonesia, Earth's largest lizard. For many years, the Komodo dragon was considered a quintessential example of insular giantism. However, fossil evidence indicates that the species may have originated in mainland Australia (Hocknull et al. 2009), before migrating to Indonesia and becoming locally extinct in Australia. Additional evidence for the Australian origin of the Komodo dragon is found in an odd place, in the genotypes and phenotypes of Australian sand monitors (Chapter III). Living sand monitors are more similar genetically and morphologically to the Komodo dragon than expected based on the relationships between them and their close relatives. This suggests that the Komodo dragon hybridized with an ancestral sand monitor, indicating that the Komodo dragon once lived in Australia (Chapter III), since it split from around 8 Ma and at least until 150 thousand years ago (Hocknull 2005; Hocknull et al. 2009). There, the Komodo dragon was a remarkable member of an already spectacular ecosystem that included the marsupial lion, an even larger monitor lizard, terrestrial crocodiles, and perhaps even the first humans to arrive in Australia (Hocknull et al. 2009; Scanlon 2014; Price et al. 2015).

It is in Pleistocene Australia that our evolutionary journey comes to an end. As mentioned above, in this continent varanids started interacting with their environments in novel ways (Chapter I). One specialized group is the spiny-tailed monitors (*Varanus acanthurus* complex), which have adapted to life in rocky escarpments, sheltering under large rocks or in crevices (Dryden 2004). The range of these varanids includes the northern Australian monsoonal tropics, the arid interior, and the transitional zone between these two. Despite extensive gene flow between most populations in the complex, the genotypes and phenotypes of these lizards exhibit signs of local adaptation (Chapter IV). This adaptability has allowed spiny-tailed monitors to expand their range from the mild monsoonal tropics into the harsh Australian outback. Some of the populations in the complex appear to be reproductively isolated from each other, representing distinct species. One of this is an undescribed species with a restricted range in the Gulf of Carpentaria (Chapter IV). If we do not want this evolutionary odyssey to end, we must take action to protect this spectacular lizards from the threats posed by human activities.

By following monitor lizards in their pilgrimage across space and time we learned that the characterisation of individual-level and population-level processes can improve our understanding of macroevolutionary dynamics and speciation. Analysing molecular,

phenotypic, and environmental data with recently developed analytical tools, I found evidence for the following: ecological and geographical context shape lineage diversification dynamics and phenotypic evolution; postnatal ontogenetic development may be subject to selection and explains interspecific patterns of morphological variation; ancient hybridization has long-lasting effects on genetic and phenotypic variation; and gene flow, local adaptation, and the environment act together to geographically sort genetic and phenotypic variation, ultimately preventing or promoting speciation. The large datasets and results generated here will likely facilitate the use of varanids as an evolutionary model in future studies. Additionally, the approaches used in this thesis can become a guideline for additional research on the processes happening at the interface between micro- and macroevolution, ultimately improving our understanding on how the diversity of life on Earth came to be.

REFERENCES

Auffenberg, W. 1981. The behavioral ecology of the Komodo monitor. University Press of Florida, Gainesville.

Barrett, R. D. H., & Schluter, D. 2008. Adaptation from standing genetic variation. Trends Ecol. Evol. 23:38–44.

Brennan, I. G., Lemmon, A. R., Lemmon, E. M., Portik, D. M., Weijola, V., Welton, L., Donnellan, S. C., & Keogh, J. S. 2021. Phylogenomics of monitor lizards and the role of competition in dictating body size disparity. Syst. Biol. 70:120–132.

Christian, A., & Garland, T. 1996. Scaling of Limb Proportions in Monitor Lizards (Squamata: Varanidae). J. Herpetol. 30:219–230.

Clemente, C. J., Withers, P. C., Thompson, G., & Lloyd, D. 2011. Evolution of limb bone loading and body size in varanid lizards. J. Exp. Biol. 214:3013–3020.

Cogger, H. G., & Heatwole, H. 1981. The Australian reptiles: origins, biogeography, distribution patterns and island evolution. In: A. Keast (Ed.), Ecological biogeography of Australia. Springer, The Hague.

Collar, D. C., Schulte II, J. A., & Losos, J. B. 2011. Evolution of extreme body size disparity in monitor lizards (*Varanus*). Evolution 65:2664–2680.

Condamine, F. L., Romieu, J., & Guinot, G. 2019. Climate cooling and clade competition likely drove the decline of lamniform sharks. Proc. Natl. Acad. Sci. U.S.A. 116:20584–20590.

Darwin, C. 1859. On the origin of species by means of natural selection, or the preservation of favoured races in the struggle for life. John Murray, London.

Doughty, P., Kealley, L., Fitch, A., & Donnellan, S. C. 2014. A new diminutive species of *Varanus* from the Dampier Peninsula, western Kimberley region, Western Australia. Rec. West. Aust. Mus. 29:128–140.

Dryden, G. 2004. *Varanus acanthurus*. In: Pianka, E. R., & King, D. R. (Eds.), Varanoid lizards of the world. Indiana University Press, Bloomington.

Erwin, D. H. 2000. Macroevolution is more than repeated rounds of microevolution. Evol. Dev. 2:78–84.

Esquerré, D., Sherratt, E., & Keogh, J. S. 2017. Evolution of extreme ontogenetic allometric diversity and heterochrony in pythons, a clade of giant and dwarf snakes. Evolution 71:2829–2844.

Gould, S. J., & Lewontin, R. C. 1979. The spandrels of San Marco and the Panglossian paradigm: a critique of the adaptationist programme. Proc. R. Soc. Lond. B Biol. Sci. 205:581–598.

Grant, P. R., & Grant, B. R. 2019. Hybridization increases population variation during adaptive radiation. Proc. Natl. Acad. Sci. U.S.A. 116:23216–23224.

Gray, J. A., Sherratt, E., Hutchinson, M. N., & Jones, M. E. H. (2019). Changes in ontogenetic patterns facilitate diversification in skull shape of Australian agamid lizards. BMC Evol. Biol. 19:7.

Harmon, L. J., Andreazzi, C. S., Débarre, F., Drury, J., Goldberg, E. E., Martins, A. B., Melián, C. J., Narwani, A., Nuismer, S. L., Pennell, M. W., Rudman, S. M., Seehausen, O., Silvestro, D., Weber, M., & Matthews, B. 2019. Detecting the macroevolutionary signal of species interactions. J. Evol. Biol. 32:769–782.

Hedrick, P. W. 2011. Genetics of populations. Jones and Bartlett Publishers, Sudbury.

Hembry, D. H., & Weber, M. G. 2020. Ecological interactions and macroevolution: a new field with old roots. Annu. Rev. Ecol. Evol. Syst. 51:215–243.

Hocknull, S. A. 2005. Ecological succession during the late Cainozoic of central eastern Queensland: extinction of a diverse rainforest community. Mem. Queensland Mus. 51:39–122.

Hocknull, S. A., Piper, P. J., van den Bergh, G. D., Due, R. A., Morwood, & M. J., Kurniawan, I. 2009. Dragon's paradise lost: palaeobiogeography, evolution and extinction of the largest-ever terrestrial lizards (Varanidae). PLoS ONE 4:e724.

Holmes, R. B., Murray, A. M., Attia, Y. S., Simons, E. L., & Chatrath, P. 2010. Oldest known *Varanus* (Squamata: Varanidae) from the Upper Eocene and Lower Oligocene of Egypt: support for an African origin of the genus. Palaeontology 53:1099–1110.

Huxley, J. 1942. Evolution: the modern synthesis. Allen and Unwin, London.

Johnson, K. 2008. How old is *T. rex*? Challenges with the dating of terrestrial strata deposited during the Maastrichtian stage of the Cretaceous period. In: Larson, P., & Carpenter, K. (Eds.), *Tyrannosaurus rex*, the tyrant king. Indiana University Press, Bloomington.

Kingsolver, J. G., & Pfennig, D. W. 2004. Individual-level selection as a cause of Cope's rule of phyletic size increase. Evolution 58:1608–1612.

Klingenberg, C. P. 2010. There's something afoot in the evolution of ontogenies. BMC Evol. Biol. 10:221.

Klingenberg, C. P. 2016. Size, shape, and form: concepts of allometry in geometric morphometrics. Dev. Genes Evol. 226:113–137.

Koch, A., Ziegler, T., Böhme, W., Arida, E., & Auliya, M. 2013. Pressing problems: distribution, threats, and conservation status of the monitor lizards (Varanidae: *Varanus* spp.) of Southeast Asia and the Indo-Australian Archipelago. Herpetol. Conserv. Biol. 8:1–62.

Lamichhaney, S., Berglund, J., Almén, M. S., Maqbool, K., Grabherr, M., Martinez-Barrio, A., Promerová, M., Rubin, C.-J., Wang, C., Zamani, N., Grant, B. R., Grant, P. R., Webster, M. T., & Andersson, L. 2015. Evolution of Darwin's finches and their beaks revealed by genome sequencing. Nature 518:371–375.

Lin, L.-H., & Wiens, J. J. 2017. Comparing macroecological patterns across continents: evolution of climatic niche breadth in varanid lizards. Ecography 40:960–970.

Mallet, J. 2007. Hybrid speciation. Nature 446:279–283.

Mayr, E. 1942. Systematics and the origin of species, from the viewpoint of a zoologist. Harvard University Press, Cambridge.

Meier, J. I., Marques, D. A., Mwaiko, S., Wagner, C. E., Excoffier, L., & Seehausen, O. 2017. Ancient hybridization fuels rapid cichlid fish adaptive radiations. Nat. Commun. 8:14363.

Molnar, R. E. 2004. Dragons in the dust: the paleobiology of the giant monitor lizard Megalania. Indiana University Press, Bloomington.

Mora, C., Tittensor, D. P., Adl, S., Simpson, A. G., & Worm, B. 2011. How many species are there on Earth and in the ocean? PLoS Biol. 9:e1001127.

Müller, G. B. 2007. Evo–devo: extending the evolutionary synthesis. Nat. Rev. Genet. 8:943–949.

Openshaw, G. H., & Keogh, J. S. 2014. Head shape evolution in monitor lizards (*Varanus*): interactions between extreme size disparity, phylogeny and ecology. J. Evol. Biol. 27:363–373.

Openshaw, G. H., D'Amore, D. C., Vidal-García, M., & Keogh, J. S. 2017. Combining geometric morphometric analyses of multiple 2D observation views improves interpretation of evolutionary allometry and shape diversification in monitor lizard (*Varanus*) crania. Biol. J. Linn. Soc. 120:539–552.

Pedersen, R. Ø., Sandel, B., & Svenning, J.-C. 2014. Macroecological evidence for competitive regional-scale interactions between the two major clades of mammal carnivores (Feliformia and Caniformia). PLoS One 9:e100553.

Pianka, E. R. 1995. Evolution of body size: varanid lizards as a model system. Am. Nat. 146:398–414.

Pianka, E. 2004. *Lanthanotus borneensis*. In: Pianka, E. R., & King, D. R. (Eds.), Varanoid lizards of the world. Indiana University Press, Bloomington.

Pianka, E. R., & King, D. R. (Eds.). 2004. Varanoid lizards of the world. Indiana University Press, Bloomington.

Price, G. J., Louys, J., Cramb, J., Feng, Y., Zhao, J., Hocknull, S. A., Webb, G. E., Nguyen, A. D., & Joannes-Boyau, R. 2015. Temporal overlap of humans and giant lizards (Varanidae; Squamata) in Pleistocene Australia. Quaternary Sci. Rev. 125:98–105.

Ruse, M. 2009. The history of evolutionary thought. In: Ruse, M., & Travis, J. (Eds.), Evolution: the first four billion years. The Belknap Press of Harvard University Press, London.

Scanlon, J. D. 2014. Giant terrestrial reptilian carnivores of Cenozoic Australia. In: Glen, A. S., & Dickman, C. R. (Eds.), Carnivores of Australia: past, present and future. CSIRO Publishing, Collingwood.

Schuett, G. W., Reiserer, R. S., & Earley, R. L. 2009. The evolution of bipedal postures in varanoid lizards. Biol. J. Linn. Soc. 97:652–663.

Simons, A. M. 2002. The continuity of microevolution and macroevolution. J. Evol. Biol. 15:688–701.

Simpson, G. G. 1944. Tempo and mode in evolution. Columbia University Press, New York, NY.

Slatkin, M. 1985. Gene flow in natural populations. Annu. Rev. Ecol. Syst. 16:393–430.

Smith, K. T., Bhullar, B.-A. S., Köhler, G., & Habersetzer, J. 2018. The only known jawed vertebrate with four eyes and the bauplan of the pineal complex. Curr. Biol. 28:1101–1107.

Thompson, G. G., & Withers, P. C. 1997. Comparative morphology of Western Australian varanid lizards (Squamata: Varanidae). J. Morphol. 233:127–152.

Thompson, G. G., Clemente, C. J., Withers, P. C., Fry, B. G., & Norman, J. A. 2009. Is body shape of varanid lizards linked with retreat choice? Aust. J. Zool. 56:351–362.

Thomson, J. A. 1917. On growth and form. Nature 100:21–22.

Uetz, P., Freed, P. & Hošek, J. (Eds.). 2020. The Reptile Database. Available at: http://www.reptile-database.org.

Vidal, N., Marin, J., Sassi, J., Battistuzzi, F. U., Donnellan, S., Fitch, A. J., Fry, B. G., Vonk, F. J., Rodriguez de la Vega, R. C., Couloux, A., & Hedges, S. B. 2012. Molecular evidence for an Asian origin of monitor lizards followed by Tertiary dispersals to Africa and Australasia. Biol. Lett. 8:853–855.

Wilson, S. K., & Swan, G. 2017. A complete guide to reptiles of Australia. Reed New Holland, Sydney.

SUPPLEMENTARY MATERIAL*

*Supplementary tables available at: https://doi.org/10.5281/zenodo.5168793

CHAPTER I

Supplementary Materials and Methods

Taxonomic background

Varanus griseus caspius was treated as a full species by Brennan et al. (2021), but pending a more rigorous study on the widespread and polytypic *V. griseus* here we consider it as a single evolutionary unit. Eidenmüller et al. (2017) showed that *V. prasinus* is polyphyletic. Thus, we consider the samples from the vicinities of the type locality of western Papua New Guinea as true *V. prasinus*, including *V. reisingeri* which was recently relegated as a subspecies of *V. prasinus* (Bucklitsch et al. 2016), and excluded other samples of *V. prasinus* from our sampling pending a more rigorous taxonomic assessment of the group. Populations in the *V. indicus* complex from the Solomon Islands apparently represent an undescribed lineage (Weijola et al. 2019). While additional specific diversity may be present within the lineage (Weijola et al. 2019), in this study we conservatively consider it as a single species (*Varanus* sp. Solomon Islands). Three species closely related to *V. chlorostigma* have been recently described or resurrected: *V. bennetti*, *V. colei*, and *V. tsukamotoi* (Böhme et al. 2019; Weijola et al. 2020). Divergence of these species from topotypic *V. chlorostigma* is fairly recent (< 2 Ma) (Weijola et al. 2019), and their recognition would force us to acknowledge other populations currently allocated to *V. chlorostigma* as separate species. Thus, for the purposes of this study, we have analyzed *V. bennetti*, *V. colei*, *V. chlorostigma*, and *V. tsukamotoi* as a single evolutionary unit (*V. chlorostigma*). Species limits in the Australo-Papuan populations of the *V. timorensis* complex are ill-defined, and we have considered all of them under *V. scalaris* (Smith et al. 2004). The subspecies *V. acanthurus insulanicus* is consistently recovered as sister to *V. baritji* and is apparently more distantly related to other populations of *V. acanthurus* (Fitch et al. 2006; Brennan et al. 2021; Pavón-Vázquez et al. in prep.). Thus, we consider *V. a. insulanicus* as a distinct evolutionary unit.

Phylogenetics

Our tree is mainly based on the extant-only phylogeny of Brennan et al. (2021). We based the phylogenetic position and divergence dates of *Lanthanotus borneensis*, *V. dumerilii*, and *V. nebulosus* on another recently published multi-locus phylogeny (Lin and Wiens 2017). The most complete phylogenies of the *Euprepiosaurus* and *Hapturosaurus* subgenera and the *salvator* complex in the *Soterosaurus* subgenus have been published

independently from each other and some of the relationships and/or divergence dates are in conflict with those of Brennan et al. (2021). Thus, we estimated a time-calibrated phylogeny for each of these subgenera using available molecular data and based our dating on the phylogeny of Brennan et al. (2021), subsequently binding the trees to our backbone phylogeny. All analyses were conducted in BEAST 2.5.1 (Bouckaert et al. 2014).

The phylogeny of *Euprepiosaurus* was based on sequences of the *16S* and *ND4* mitochondrial loci (Table S1). We assigned each locus to its own partition and selected substitution models based on the Bayesian information criterion using ModelFinder (Kalyaanamoorthy et al. 2017). The best-fitting models were TIM3e+I (*16S*) and TN+F+G4 (*ND4*). We built a species tree specifying a relaxed log-normal clock model and a Yule tree model. We included *V. prasinus* as outgroup and specified a normal distribution for the root-age prior ($\bar{x}$ = 13.02, σ = 0.001). We ran two independent analyses for 1,000 million generations with sampling every 25,000 iterations. We verified convergence and adequate sampling for every parameter (effective sample size > 200), combined the runs, deleted 10% of samples as burnin, and extracted the maximum clade credibility (MCC) tree with mean branch lengths.

The phylogeny of *Hapturosaurus* was based on unique haplotypes of *16S* (Table S1). The sequence of *V. bogerti* comes from Eidenmüller et al. (2017). The best-fitting model was TIM2e+I. We specified a relaxed log-normal clock model and a Yule tree model. We included *V. chlorostigma* as outgroup and specified a normal distribution for the root-age prior ($\bar{x}$ = 13.02, σ = 0.001). We ran two independent analyses for 100 million generations with sampling every 5,000 iterations and obtained the MCC tree. For downstream analyses, we only kept one individual per species (all species were monophyletic).

Finally, the phylogeny of the *salvator* complex was based on 4 nuclear loci (*PRLR* and anonymous nuclear loci L44, L52, and L74) and a mitochondrial fragment containing *ND1*, *ND2*, and associated tRNAs (available at https://doi.org/10.5061/dryad.m0n61). The best-fitting models were F81+F (L44), HKY+F+I (L52), and JC (L74 and *PRLR*). Due to mixing problems, we chose a relatively simple model for the mitochondrial fragment (HKY+F) and specified a strict molecular clock. We built a species tree based on the Yule model. We included *V. rudicollis* as outgroup and specified a normal distribution for the root-age prior ($\bar{x}$ = 5.95, σ = 0.001). We ran two independent analyses for 1,000 million generations with sampling every 50,000 iterations and obtained the MCC tree.

Morphological data

All of the specimens in our phenotypic datasets were adults, except for three individuals, each one belonging to the species *V. bogerti*, *V. rasmusseni*, and *V. zugorum*. These taxa are exceedingly rare in collections and only one adult of *V. bogerti* and none of the other species were available. In the case of linear measurements, we imputed missing data (i.e., from specimens having incomplete tails and/or toes, or traits not recorded in the literature for *V. bitatawa*, *V. mabitang*, and *V. semotus*) using random forest training in 'missForest 1.4' (Stekhoven and Bühlmann 2012), including species and sex as predictors. Due to practical reasons, large specimens of larger species are rare in collections. Therefore, the mean body size in our sample may not be representative of body size variation in the wild and there is systematic bias towards smaller sizes in larger species compared to smaller species. Furthermore, reptiles show indeterminate growth and thus SVL is correlated with age, and thus some authors advocate for the use of maximum SVL in reptile comparative studies (e.g. Stamps and Andrews 1992; Greer 2001; Sherratt et al. 2018). Thus, we based our analyses on maximum SVL. We tested for sexual dimorphism in the linear measurements for each species in which each sex was represented by at least three specimens. We compared the sexes through an analysis of variance using the 'procD.lm' function of the 'geomorph 3.0.3' R package (Adams and Otarola-Castillo 2013), assessing significance by performing 1,000 permutations. Since our sampling is biased towards males, we discarded females for those species in which sexual dimorphism was significant at the 95% confidence level.

When taking the head photographs, we tried to keep position and orientation as consistent as possible. Digitalization and processing of the landmark data was performed in 'geomorph 3.0.3' (Adams and Otarola-Castillo 2013). For the dorsal view we digitized 13 landmarks and 20 semi-landmarks, sliding the semi-landmarks based on the minimization of bending energy. For the lateral view we digitized 10 landmarks. In damaged specimens, we estimated the position of missing landmarks per species using the thin-spline method (Gunz et al. 2009). Same as for the linear measurements, we tested for sexual dimorphism in the Procrustes aligned coordinates and removed females of the sexually dimorphic species. After removing females of the sexually dimorphic species, we repeated the generalized Procrustes analysis.

Biogeography

We reconstructed the biogeographic history of monitor lizards using the maximum likelihood implementation of the 'BioGeoBEARS 1.1.2' (Matzke 2013) R package. We divided the range of monitor lizards into seven biogeographic regions, primarily based on the zoogeographic realms of Holt et al. (2013). Monitor lizards are only marginally

distributed in the Palearctic and Sino-Japanese realms, and the species present there are more widely distributed in the Saharo-Arabian and Oriental realms, respectively. Thus, we considered the former realms as part of the latter. We considered the Philippines east of Huxley's Line as a separate biogeographic unit given their oceanic origin (Hall 1996, 1998) and high levels of endemicity, including monitor lizards in the *Philippinosaurus* and *Soterosaurus* subgenera. We also considered the islands of eastern Melanesia (including the Solomon Islands and islands of northeastern Papua New Guinea) as a separate unit, given their biogeographic uniqueness as part of the Vitiaz Arc (Ewart 1988; Lucky and Sarnat 2010), including the presence of endemic monitor lizards in the *Euprepiosaurus* and *Solomonsaurus* subgenera.

We tested three main biogeographic models (Matzke 2014): Dispersal-Extinction-Cladogenesis (DEC) (Ree and Smith 2008), and the likelihood implementations of the Dispersal-Vicariance Analysis (DIVALIKE) (Ronquist 1997) and BayArea models (BAYAREALIKE) (Landis et al. 2013). In addition to the basic implementation, for each of the models we incorporated free parameters corresponding to founder-event speciation (*j*), dispersal probability as a function of distance (*x*), and both *j* and *x*, resulting in a total of 12 models. We accounted for plate tectonics and island surfacing by performing a time-stratified analysis with 14 time slices: 2.5 Ma, 5–40 Ma with 5 Ma increases, and 60–140 Ma with 20 Ma increases. To estimate *x*, we calculated the minimum distance between regions for each time slice using GPlates 2.2.0 (Müller et al. 2018). Additionally, we incorporated matrices specifying which areas are allowed at each time slice. Insular regions were only allowed after their time of emergence. Areas incorporating two or more regions were only allowed when the distance between each of their components was below the median. We considered the model with the lowest sample-size corrected Akaike Information Criterion (AICc) as the preferred model, and then compared it against nested models using likelihood ratio tests (LRT).

Supplementary Discussion

Biogeography of Varanidae

The model with the lowest AICc was DEC+*j*+*x*, and LRT also favored this model (p against DEC, DEC+*j*, and DEC+*x* < 0.001). Thus, it seems like dispersal mediated by distance has been an important component of the varanid biogeographic history. The maximum likelihood solution (Fig. S3) suggests an African origin of crown varanids, consistent with the northern African location of the earliest *Varanus* fossils (Holmes et al. 2010). Other studies have suggested an Asian origin (Vidal et al. 2012; Brennan et

al. 2021), a result supported by the presence of the closest relatives of Varanidae, *Lanthanotus* and *Shinisaurus*, in Southeast Asia. Our results suggest that *Varanus* colonized Indo-Australasia, particularly Melanesia, from Africa early in their evolutionary history. Cenozoic direct dispersal between Indo-Australasia and Africa is considered to be unlikely (Schodde 2006; Moyle et al. 2016), but has been confirmed in other taxa (Bergh and Linder 2009; Heinicke et al. 2013). As noted by Brennan et al. (2021), these results echo the findings of other studies showing the persistence of old endemic lineages in Melanesia (Heads 2011; Oliver et al. 2017, 2018). However, the uncertainty in our results should be noted (Fig. S3). It seems like additional fossils and/or methodological progress are necessary to confidently locate the geographic origin of Varanidae.

New Guinea and the Philippines appear to have been important stepping stones as monitors expanded their range northwestwardly in Australasia and into mainland Asia in the late Oligocene and early Miocene. A role of islands in Australasia as sources of colonization has been proposed for other taxa (Keogh 1998; Rowe et al. 2019). However, the crown age of the Papuan and Malesian radiations is younger than the inferred timing of their initial colonization. Perhaps the proto-Papuan and proto-Philippine archipelagos provided opportunity for dispersal early in their emergence but conditions for lineage persistence and diversification appeared later. A fundamental role for dispersal in the diversification of varanids is reinforced by the support for a biogeographic model including the *j* parameter and by our DREaD analyses (Fig. 3b). Subsequently, varanid diversification appears to have been mainly driven by the radiation of single clades within particular regions in Indo-Australasia, with limited exchange between these regions. This contrasts with the patterns in other taxa where biotic exchange within Indo-Australasia appears to have been pervasive (Moyle et al. 2016; Morinaka et al. 2017; Rowe et al. 2019). The limited secondary colonization could be a result of competitive exclusion by incumbent taxa (see Main Text). Furthermore, few taxa moved into the Oriental realm, with one lineage (Oriental clade) moderately diversifying and expanding its range in the region until coming in contact with the Afro-Arabian clade to the west (Fig. 1).

Supplementary Figures

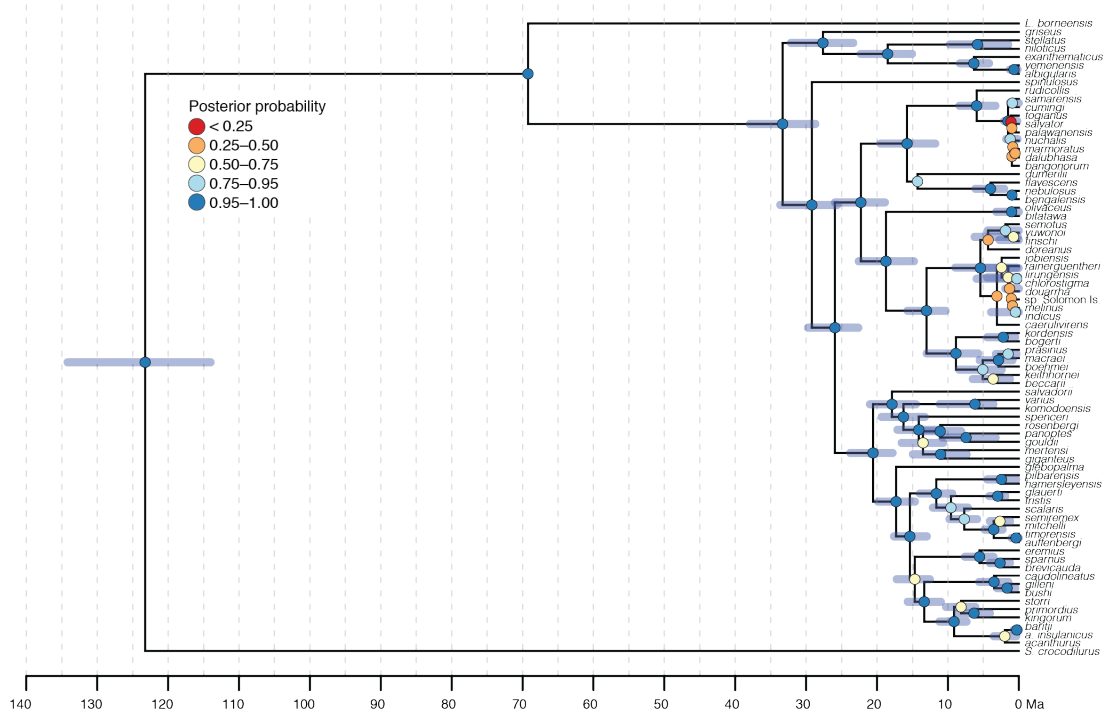

Figure S1. Time-calibrated phylogeny of Varanidae and closely related taxa. Nodes are colored based on their posterior probability. Bars denote the 95% highest posterior density of divergence times (not shown for sections of the tree based on Lin and Wiens (2017) and nodes with posterior probability < 0.50).

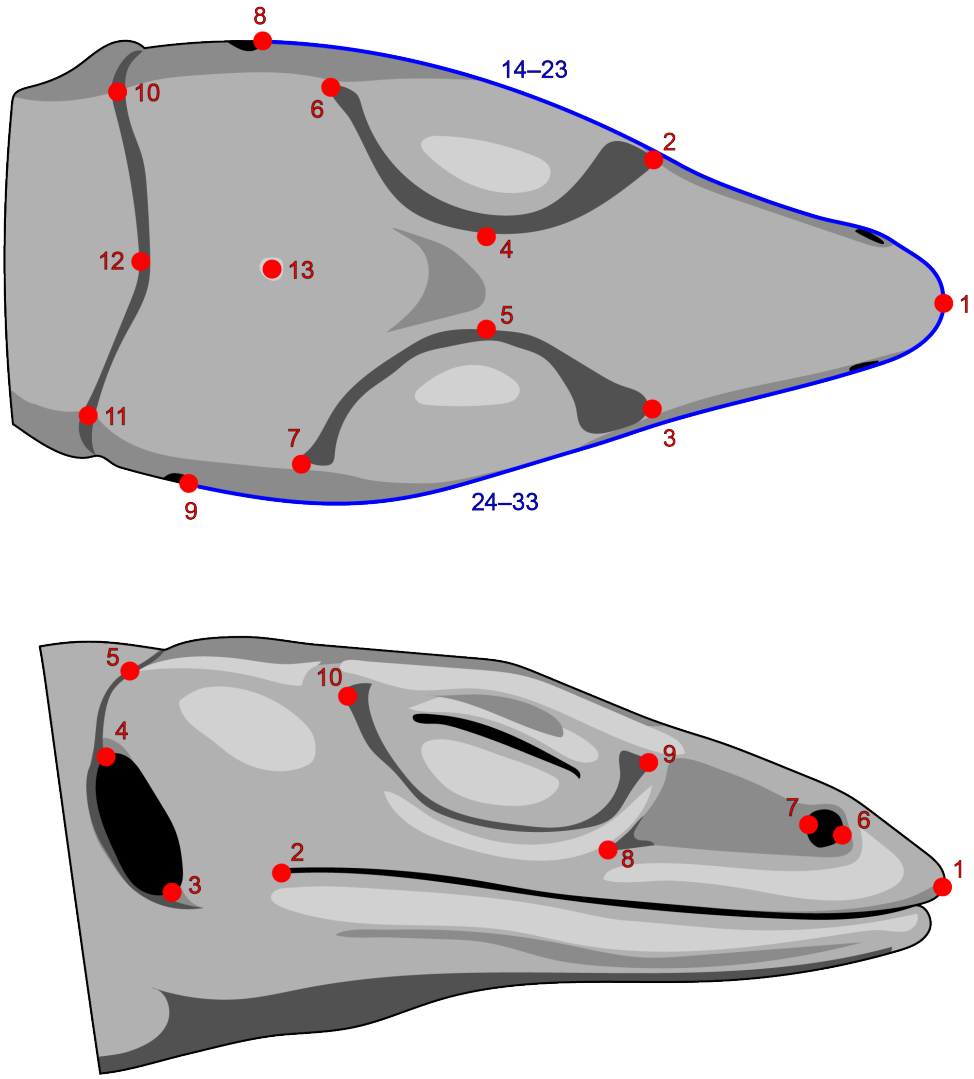

Figure S2. Landmark configuration for head shape in dorsal (top) and lateral (bottom) view. The blue lines indicate sliding semi-landmarks.

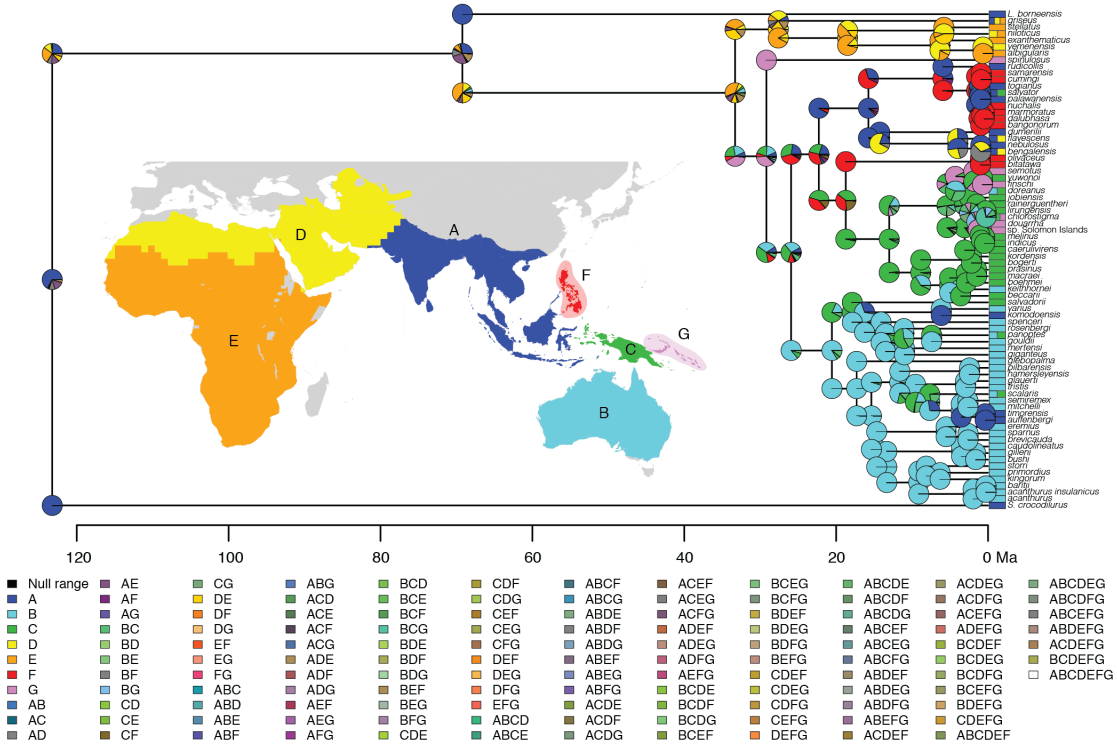

Figure S3. Ancestral range reconstruction of Varanidae and closely related taxa.

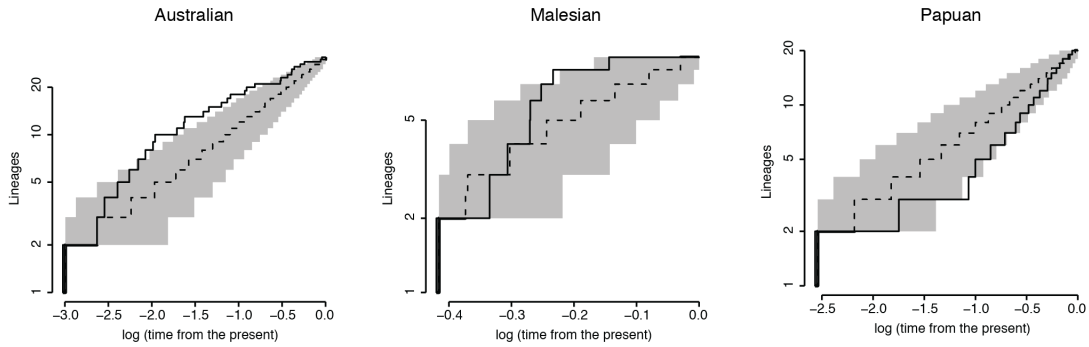

Figure S4. Lineage-through-time plots. The solid lines represent the empirical estimates of lineages through time. The shaded areas represent 95% confidence intervals of 1,000 simulations performed under a pure-birth process. The dashed lines represent the median of the simulations.

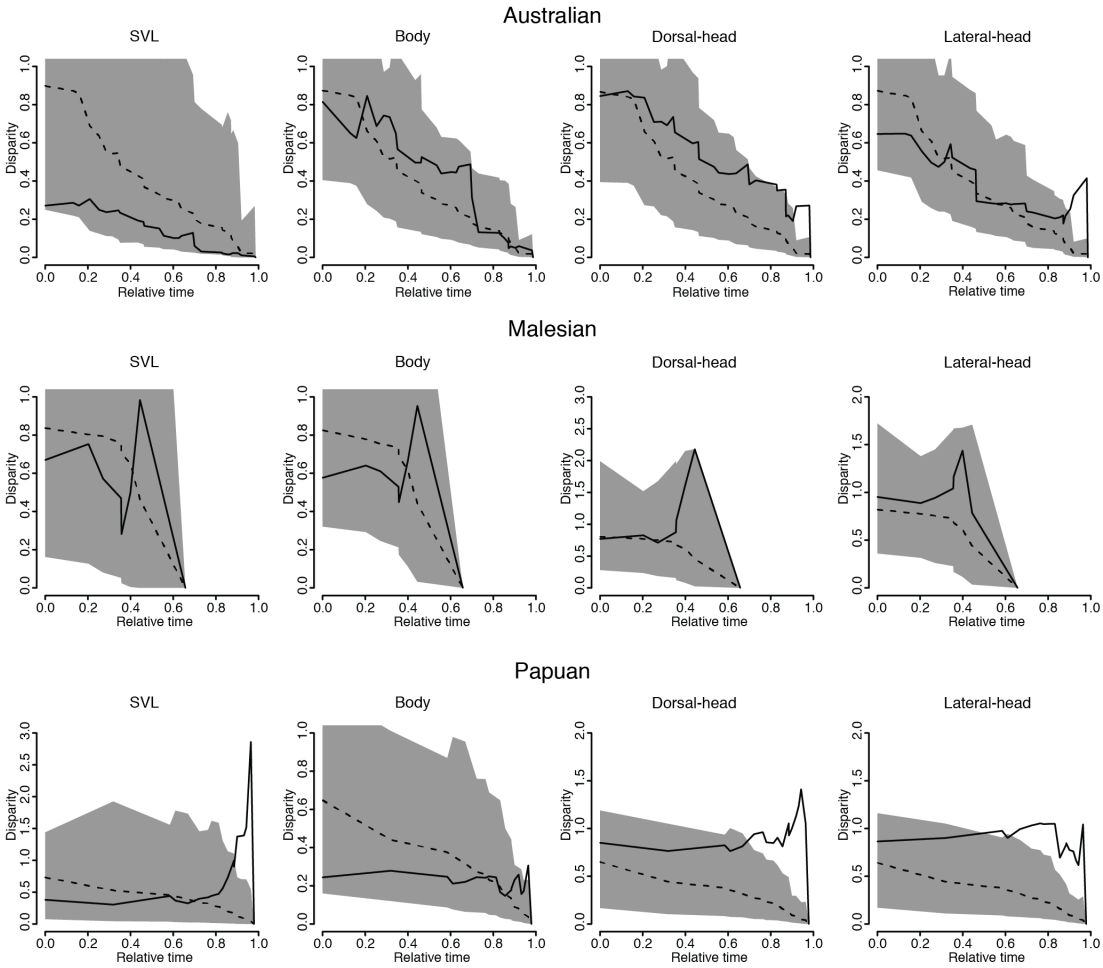

Figure S5. Disparity-through-time plots. The solid lines represent the empirical estimates of disparity through time. The shaded areas represent 95% confidence intervals of 2,500 simulations performed under Brownian motion using the rank envelope method. The dashed lines represent the median of the simulations.

Literature Cited*

*Includes references in Supporting Tables.

Adams, D.C., and E. Otárola-Castillo. 2013. geomorph: an R package for the collection and analysis of geometric morphometric shape data. Methods Ecol. Evol. 4:393–399.

Bergh, N. G., and H. P. Linder. 2009. Cape diversification and repeated out-of-southern-Africa dispersal in paper daisies (Asteraceae–Gnaphalieae). Mol. Phylogenet. Evol. 51:5–18.

Böhme, W., H. J. Jacobs, T. Koppetsch, and A. Schmitz. 2019. The Kei Islands monitor lizard (Squamata: Varanidae: *Varanus*: *Euprepiosaurus*) as a distinct morphological, taxonomic, and conservation unit. Russ. J. Herpetol. 26:272–280.

Bouckaert, R., J. Heled, D. Kühnert, T. Vaughan, C. Wu., D. Xie, M. A. Suchard, A. Rambaut, and A. J. Drummond. 2014. BEAST 2: a software platform for Bayesian evolutionary analysis. PLoS Comput. Biol. 10:e1003537.

Brennan, I. G., A. R Lemmon, E. M. Lemmon, D. M. Portik, V. Weijola, L. Welton, S. C. Donnellan, and J. S. Keogh. 2021. Phylogenomics of monitor lizards and the role of competition in dictating body size disparity. Syst. Biol. 70:120–132.

Bucklitsch, Y., W. Boehme, and A. Koch. 2016. Scale morphology and micro-structure of monitor lizards (Squamata: Varanidae: *Varanus* spp.) and their allies: implications for systematics, ecology, and conservation. Zootaxa 4153:1–192.

Eidenmüller, B., A. Koch, J. Köhler, and R. Wicker. New findings on the relationships among New Guinea tree monitor lizards of the *Varanus prasinus* (Schlegel, 1839) complex. Hepetozoa 30:9–20.

Ewart, A. 1988. Geological history of the Fiji–Tonga–Samoan region of the SW Pacific, and some palaeogeographic and biogeographic implications. *In* J. P. Duffels (ed.). The cicadas of the Fiji, Samoa and Tonga Islands, their taxonomy and biogeography (Homeoptera, Cicadoidea). Scandinavian Science Press, Leiden, ZH.

Fitch, A. J., A. E. Goodman, and S. C. Donnellan. 2006. A molecular phylogeny of the Australian monitor lizards (Squamata: Varanidae) inferred from mitochondrial DNA sequences. Aust. J. Zool. 54:253–269.

Greer, A. E. 2001. Distribution of maximum snout-vent length among species of scincid lizards. J. Herpetol. 35:383–395.

Gunz, P., P. mitteroecker, S. Neubauer, G. W. Weber, and F. L. Bookstein. 2009. Principles for the virtual reconstruction of hominin crania. J. Hum. Evol. 57:48–62.

Hall, R. 1996. Reconstructing Cenozoic SE Asia. Geol. Soc. Spec. Publ. 106:153–184.

Hall, R. 1998. The plate tectonics of Cenozoic SE Asia and the distribution of land and sea. *In* Hall, R., and J. D. Holloway. Biogeography and geological evolution of SE Asia. Backhuys Publishers, Leiden, ZH.

Heads, M. 2011. Old taxa on young islands: a critique of the use of island age to date island-endemic clades and calibrate phylogenies. Syst. Biol. 60:204–218.

Heinicke, M. P., J. D. Daza, E. Greenbaum, T. R. Jackman, and A. M. Bauer. 2014. Phylogeny, taxonomy and biogeography of a circum-Indian Ocean clade of leaf-toed geckos (Reptilia: Gekkota), with a description of two new genera. Syst. Biodivers. 12: 23–42.

Holmes, R. B., A. M. Murray, Y. S. Attia, E. L. Simons, and P. Chatrath. 2010. Oldest known *Varanus* (Squamata: Varanidae) from the Upper Eocene and Lower Oligocene of Egypt: support for an African origin of the genus. Palaeontology 53:1099–1110.

Holt, B. G., J. P. Lessard, M. K. Borregaard, S. A. Fritz, M. B. Araújo, D. Dimitrov, P-H. Fabre, C. H. Graham, G. R. Graves, K. A. Jønsson, D. Nogués-Bravo, Z. Wang, R. J. Whittaker, J. Fjeldså, and C. Rahbek. 2013. An update of Wallace's zoogeographic regions of the world. Science 339:74–78.

Kalyaanamoorthy, S., B. Q. Minh, T. K. F. Wong, A. von Haeseler, and L. S. Jermiin. 2017. ModelFinder: fast model selection for accurate phylogenetic estimates. Nat. Methods 14:587–589.

Keogh, J. S. 1998. Molecular phylogeny of elapid snakes and a consideration of their biogeographic history. Biol. J. Linn. Soc. 63:177–203.

Koch, A., M. Auliya, A. Schmitz, U. Kuch, and W. Böhme. 2007. Morphological studies on the systematics of South East Asian water monitors (*Varanus salvator* complex): nominotypic populations and taxonomic overview. Mertensiella 16:109–180.

Landis, M. J., N. J. Matzke, B. R. Moore, and J. P. Huelsenbeck. 2013. Bayesian analysis of biogeography when the number of areas is large. Syst. Biol. 62:789–804.

Lin, L., and J. J. Wiens. 2017. Comparing macroecological patterns across continents: evolution of climatic niche breadth in varanid lizards. Ecography 40:960–970.

Lucky, A., and E. M. Sarnat. 2010. Biogeography and diversification of the Pacific ant genus *Lordomyrma* Emery. J. Biogeogr. 37:624–634.

Matzke, N. J. 2013. Probabilistic historical biogeography: new models for founder-event speciation, imperfect detection, and fossils allow improved accuracy and model-testing. Front. Biogeogr. 5:242–248.

Matzke, N. J. 2014. Model selection in historical biogeography reveals that founder-event speciation is a crucial process in island clades. Syst. Biol. 63:951–970

Meiri, S. 2018. Traits of lizards of the world: variation around a successful evolutionary design. Global Ecol. Biogeogr. 27:1168-1172.

Morinaka, S., N. Minaka, T. Miyata, and S. Hoshizaki. 2017. Phylogeography of the *Delias hyparete* species group (Lepidoptera: Pieridae): complex historical dispersals into and out of Wallacea. Biol. J. Linn. Soc. 121:576-591.

Moyle, R. G., C. H. Oliveros, M. J. Andersen, P. A. Hosner, B. W. Benz, J. D. Manthey, S. L. Travers, R. M. Brown, and B. C. Faircloth. 2016. Tectonic collision and uplift of Wallacea triggered the global songbird radiation. Nat. Comm. 7:12709.

Müller, R. D., J. Cannon, X. Qin, R. J. Watson, M. Gurnis, S. Williams, T. Pfaffelmoser, M. Seton, S. H. J. Russell, and S. Zahirovic. 2018. GPlates: building a virtual Earth through deep time. Geochem. Geophy. Geosy. 19:2243–2261.

Oliver, P. M., R. M. Brown, F. Kraus, E. Rittmeyer, S. L. Travers, and C. D. Siler. 2018. Lizards of the lost arcs: mid-Cenozoic diversification, persistence and ecological marginalization in the West Pacific. Proc. Roy. Soc. B Biol. Sci. 285:20171760.

Oliver, P. M., S. L. Travers, J. Q. Richmond, P. Pikacha, and R. N. Fisher. 2018. At the end of the line: independent overwater colonizations of the Solomon Islands by a hyperdiverse trans-Wallacean lizard lineage (*Cyrtodactylus*: Gekkota: Squamata). Zool. J. Linn. Soc. 182:681–694.

Ree, R. H., and S. A. Smith. 2008. Maximum likelihood inference of geographic range evolution by dispersal, local extinction, and cladogenesis. Syst. Biol. 57:4–14.

Ronquist, F. 1997. Dispersal-vicariance analysis: a new approach to the quantification of historical biogeography. Syst. Biol. 46:195–203.

Rowe, K. C., A. S. Achmadi, P. H. Fabre, J. J. Schenk, S. J. Steppan, and J. A. Esselstyn. 2019. Oceanic islands of Wallacea as a source for dispersal and diversification of murine rodents. J. Biogeogr. 46:2752–2768.

Schodde, R. 2006. Australia's bird fauna today—origins and evolutionary development. *In* Merrick, J. R., M. Archer, G. M. Hickey, and M. S. Y. Lee. (eds.). Evolution and biogeography of Australasian vertebrates. Auscipub, Oatlands, NSW.

Sherratt, E., A. R. Rasmussen, and K. L. Sanders. 2018. Trophic specialization drives morphological evolution in sea snakes. Roy. Soc. Open Sci. 5:172141.

Smith, L. A., S. S. Sweet, and D. R. King. 2004. *Varanus scalaris*. *In* Pianka, E. R., and D. R. King (eds.). Varanoid Lizards of the World. Indiana University Press, Bloomington, IN.

Stamps, J. A., and R. M. Andrews. 1992. Estimating asymptotic size using the largest individuals per sample. Oecologia, 92:503–512.

Stekhoven, D.J., and P. Bühlmann. 2012. MissForest—non-parametric missing value imputation for mixed-type data. Bioinformatics 28:112–118.

Vidal, N., J. Marin, J. Sassi, F. U. Battistuzzi, S. Donnellan, A. J. Fitch, B. G. Fry, F. J. Vonk, R. C. Rodriguez de la Vega, A. Couloux, and S. B. Hedges. 2012. Molecular evidence for an Asian origin of monitor lizards followed by Tertiary dispersals to Africa and Australasia. Biol. Lett. 8:853–855.

Weijola, V., V. Vahtera, A. Koch, A. Schmitz, and F. Kraus. 2020. Taxonomy of Micronesian monitors (Reptilia: Squamata: *Varanus*): endemic status of new species argues for caution in pursuing eradication plans. Roy. Soc. Open Sci. 7:200092.

Weijola, V., V. Vahtera, C. Lindqvist, and F. Kraus. 2019. A molecular phylogeny for the Pacific monitor lizards (*Varanus* subgenus *Euprepiosaurus*) reveals a recent and rapid radiation with high levels of cryptic diversity. Zool. J. Linn. Soc. 186:1053–1066.

Ziegler, T., W. Böhme, and A. Schmitz. 2007. A new species of the *Varanus indicus* group (Squamata, Varanidae) from Halmahera Island, Moluccas: morphological and molecular evidence. Zoosyst. Evol. 83:109–119.

CHAPTER II

Supporting Materials and Methods

Supporting Materials and Methods

The taxonomic framework, phylogeny, morphological data processing, and ancestral range reconstruction are based on an unpublished study on the diversification of Varanidae (Pavón-Vázquez et al., under review). The phylogeny was trimmed to match our sampling.

Taxonomic background

Varanus griseus caspius was treated as a full species by Brennan et al. (2021), but pending a more rigorous study on the widespread and polytypic *V. griseus* here we consider it as a single evolutionary unit. Eidenmüller et al. (2017) showed that *V. prasinus* is polyphyletic. Thus, we consider the samples from the vicinities of the type locality of western Papua New Guinea as true *V. prasinus*, including *V. reisingeri* which was recently relegated as a subspecies of *V. prasinus* (Bucklitsch et al. 2016), and excluded other samples of *V. prasinus* from our sampling pending a more rigorous taxonomic assessment of the group. Populations in the *V. indicus* complex from the Solomon Islands apparently represent an undescribed lineage (Weijola et al. 2019). While additional specific diversity may be present within the lineage (Weijola et al. 2019), in this study we conservatively consider it as a single species (*Varanus* sp. Solomon Islands). Three species closely related to *V. chlorostigma* have been recently described or resurrected: *V. bennetti*, *V. colei*, and *V. tsukamotoi* (Böhme et al. 2019; Weijola et al. 2020). Divergence of these species from topotypic *V. chlorostigma* is fairly recent (< 2 Ma) (Weijola et al. 2019), and their recognition would force us to acknowledge other populations currently allocated to *V. chlorostigma* as separate species. Thus, for the purposes of this study, we have analyzed *V. bennetti*, *V. colei*, *V. chlorostigma*, and *V. tsukamotoi* as a single evolutionary unit (*V. chlorostigma*). Species limits in the Australo-Papuan populations of the *V. timorensis* complex are ill-defined, and we have considered all of them under *V. scalaris* (Smith et al. 2004). The subspecies *V. acanthurus insulanicus* is consistently recovered as sister to *V. baritji* and is apparently more distantly related to other populations of *V. acanthurus* (Fitch et al. 2006; Brennan et al.

2021; Pavón-Vázquez et al. in prep.). Thus, we excluded individuals of *V*. *a*. *insulanicus* from our sample of *V*. *acanthurus*.

Morphological data

The linear measurements that we recorded to characterize body shape were: head length (along dorsal midline, between tip of snout and anterior edge of tympanum), head width (at level of anterior edge of tympanum), head depth (at level of middle of eyes), neck length (between anterior edge of tympanum and gular fold), body length (between gular fold and vent), hip width (width of pelvic gridle measured at level of middle of hindlimbs), tail length (between vent and tip of tail), tail width (measured at level of one third of tail length from vent), and tail depth (measured at level of one third of tail length from vent) (Fig. S1). The measurements used to characterize limb shape were: upper arm length (between base of forelimb and elbow), lower arm length (between elbow and wrist), hand length (between wrist and base of finger IV), hand width (perpendicular to base of finger V), finger IV length (between base of finger and proximal edge of claw), upper leg length (between base of hindlimb and knee), lower leg length (between knee and ankle), foot length (between ankle and base of toe IV), foot width (perpendicular to base of toe V), and toe IV length (between base of toe and proximal edge of claw) (Fig. S1). The landmarks describing head shape are: tip of snout, anterior edges of supraocular semicircles, medial edges of supraocular semicircles, posterior edges of supraocular semicircles, anterior edges of tympanum, posterior edges of nuchal fold, and anterior edge of nuchal fold (Fig. S1). Ten sliding semi-landmarks were placed on each side between the tip of the snout and the anterior edge of the tympanum (Fig. S1). *Lanthanotus* lacks an external tympanum, but a depression covered with scales smaller than surrounding osteoderms indicates the position of the auricular organs (Maisano et al. 2002).

We imputed missing data (i.e., from specimens having incomplete tails and/or toes) using random forest training in 'missForest 1.4' (Stekhoven and Bühlmann 2012), including species and sex as predictors. To account for relatedness in data imputation, we performed the procedure separately for *Shinisaurus*, *Lanthanotus*, and each varanid subgenus. Due to practical reasons, large specimens of larger species are rare in collections. Therefore, the mean body size in our sample may not be representative of body size variation in the wild and there is systematic bias towards smaller sizes in larger species compared to smaller species. Furthermore, reptiles show indeterminate growth and thus snout-vent-length (SVL) is correlated with age, and thus some authors advocate for the use of maximum SVL in reptile comparative studies (e.g. Stamps and Andrews 1992; Greer 2001; Sherratt et al. 2018). Thus, we based our analyses on

maximum SVL instead of mean SVL. We tested for sexual dimorphism in the linear measurements for each species in which each sex was represented by at least three specimens. We compared the sexes through an analysis of variance using the 'procD.lm' function of the 'geomorph 3.0.3' R package (Adams and Otarola-Castillo 2013), assessing significance by performing 1,000 permutations. Since our sampling is biased towards males, we discarded females for those species in which sexual dimorphism was significant at the 95% confidence level.

When taking the head photographs, we tried to keep position and orientation as consistent as possible. Digitalization and processing of the landmark data was performed in 'geomorph 3.0.3' (Adams and Otarola-Castillo 2013). In damaged specimens, we estimated the position of missing landmarks per species using the thin-spline method (Gunz et al. 2009). Same as for the linear measurements, we tested for sexual dimorphism in the Procrustes aligned coordinates and removed females of the sexually dimorphic species. After removing females of the sexually dimorphic species, we repeated the generalized Procrustes analysis.

Phylogenetics

The tree is mainly based on the extant-only phylogeny of varanids presented by Brennan et al. (2021). This phylogeny was based on 60 nuclear exons obtained through anchored hybrid enrichment (Lemmon et al. 2012). We based the phylogenetic position and divergence dates of *Lanthanotus borneensis*, *V. dumerilii*, and *V. nebulosus* on another recently published multi-locus phylogeny (Lin and Wiens 2017). The most complete phylogenies of the *Euprepiosaurus* and *Hapturosaurus* subgenera and the *salvator* complex in the *Soterosaurus* subgenus have been published independently from each other and some of the relationships and/or divergence dates are in conflict with those of Brennan et al. (2021). Thus, we estimated a time-calibrated phylogeny for each of these subgenera using available molecular data and based our dating on the phylogeny of Brennan et al. (2021), subsequently binding the trees to our backbone phylogeny. All analyses were conducted in BEAST 2.5.1 (Bouckaert et al. 2014).

The phylogeny of *Euprepiosaurus* was based on sequences of the *16S* and *ND4* mitochondrial loci (Table S5). We assigned each locus to its own partition and selected substitution models based on the Bayesian information criterion using ModelFinder (Kalyaanamoorthy et al. 2017). The best-fitting models were TIM3e+I (*16S*) and TN+F+G4 (*ND4*). We built a species tree specifying a relaxed log-normal clock model and a Yule tree model. We included *V. prasinus* as outgroup and specified a normal distribution for the root-age prior ($\bar{x}$ = 13.02, σ = 0.001). We ran two independent analyses for 1,000 million generations with sampling every 25,000 iterations. We verified

convergence and adequate sampling for every parameter (effective sample size > 200), combined the runs, deleted 10% of samples as burnin, and extracted the maximum clade credibility (MCC) tree with mean branch lengths.

The phylogeny of *Hapturosaurus* was based on unique haplotypes of *16S* (Table S5). The sequence of *V. bogerti* comes from Eidenmüller et al. (2017). The best-fitting model was TIM2e+I. We specified a relaxed log-normal clock model and a Yule tree model. We included *V. chlorostigma* as outgroup and specified a normal distribution for the root-age prior ($\bar{x}$ = 13.02, σ = 0.001). We ran two independent analyses for 100 million generations with sampling every 5,000 iterations and obtained the MCC tree. For downstream analyses, we only kept one individual per species (all species were monophyletic).

Finally, the phylogeny of the *salvator* complex was based on 4 nuclear loci (*PRLR* and anonymous nuclear loci L44, L52, and L74) and a mitochondrial fragment containing *ND1*, *ND2*, and associated tRNAs (available at https://doi.org/10.5061/dryad.m0n61). The best-fitting models were F81+F (L44), HKY+F+I (L52), and JC (L74 and *PRLR*). Due to mixing problems, we chose a relatively simple model for the mitochondrial fragment (HKY+F) and specified a strict molecular clock. We built a species tree based on the Yule model. We included *V. rudicollis* as outgroup and specified a normal distribution for the root-age prior ($\bar{x}$ = 5.95, σ = 0.001). We ran two independent analyses for 1,000 million generations with sampling every 50,000 iterations and obtained the MCC tree.

Stochastic mapping of habitat use

We reconstructed the evolution of habitat use in Paleoanguimorpha through stochastic character mapping based on maximum likelihood. We used the “make.simmap” function of ‘phytools 0.7.62’ (Revell 2012) and specified a model with equal rates of transition between states. We obtained 1,000 stochastic maps and randomly selected one stochastic map for the model-fitting analyses.

Biogeography

We limited competition to sympatric taxa when fitting the matching competition and diversity dependent models. This required us to reconstruct the biogeographic history of Paleoanguimorpha. We used the maximum likelihood implementation of the ‘BioGeoBEARS 1.1.2’ (Matzke 2013) R package. We divided the range of paleoanguimorphs into seven biogeographic regions, primarily based on the zoogeographic realms of Holt et al. (2013). These lizards are only marginally distributed in the Palearctic and Sino-Japanese realms, and the species present there are more widely distributed in the Saharo-Arabian and Oriental realms, respectively. Thus, we

considered the former realms as part of the latter. We considered the Philippines east of Huxley's Line as a separate biogeographic unit given their oceanic origin (Hall 1996, 1998) and high levels of endemicity, including varanids in the *Philippinosaurus* and *Soterosaurus* subgenera. We also considered the islands of eastern Melanesia (including the Solomon Islands and islands of northeastern Papua New Guinea) as a separate unit, given their biogeographic uniqueness as part of the Vitiaz Arc (Ewart 1988; Lucky and Sarnat 2010), including the presence of endemic varanids in the *Euprepiosaurus* and *Solomonsaurus* subgenera.

We tested three main biogeographic models (Matzke 2014): Dispersal-Extinction-Cladogenesis (DEC) (Ree and Smith 2008), and the likelihood implementations of the Dispersal-Vicariance Analysis (DIVALIKE) (Ronquist 1997) and BayArea models (BAYAREALIKE) (Landis et al. 2013). In addition to the basic implementation, for each of the models we incorporated free parameters corresponding to founder-event speciation (*j*), dispersal probability as a function of distance (*x*), and both *j* and *x*, resulting in a total of 12 models. We accounted for plate tectonics and island surfacing by performing a time-stratified analysis with 14 time slices: 2.5 Ma, 5–40 Ma with 5 Ma increases, and 60–140 Ma with 20 Ma increases. To estimate *x*, we calculated the minimum distance between regions for each time slice using GPlates 2.2.0 (Müller et al. 2018). Additionally, we incorporated matrices specifying which areas are allowed at each time slice. Insular regions were only allowed after their time of emergence. Areas incorporating two or more regions were only allowed when the distance between each of their components was below the median. We considered the model with the lowest sample-size corrected Akaike Information Criterion (AICc) as the preferred model, and then compared it against nested models using likelihood ratio tests (LRT). The model with the lowest AICc was DEC+*j*+*x*, and LRT also favored this model (*p* against DEC, DEC+*j*, and DEC+*x* < 0.001). We obtained 50 stochastic maps from the reconstruction based on the preferred model and randomly selected one stochastic map for the model-fitting analyses.

Supporting Figures

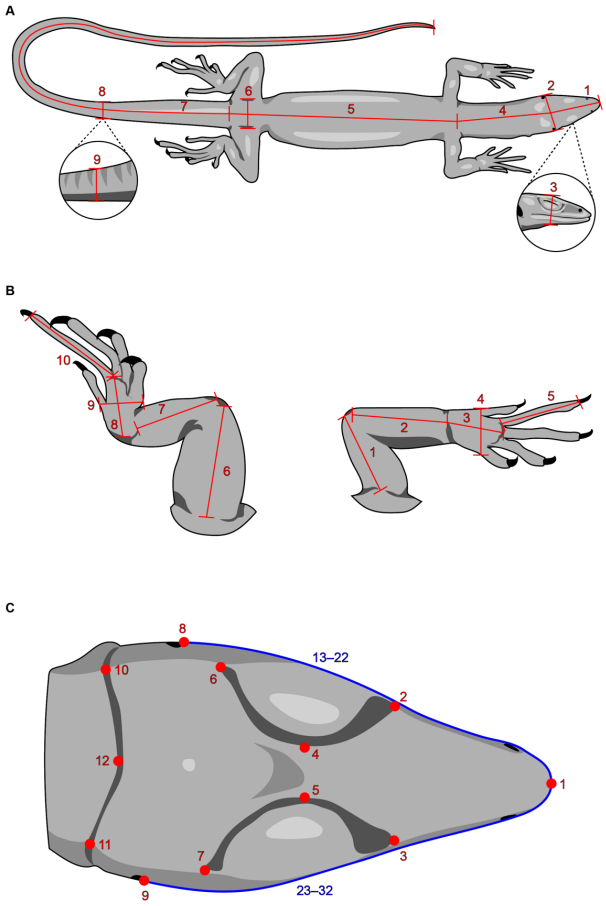

Figure S1. Morphometric data. A) Linear measurements describing body shape: head length (1), head width (2), head depth (3), neck length (4), body length (5), hip width (6), tail length (7), tail width (8), and tail depth (9). B) Linear measurements describing limb shape: upper arm length (1), lower arm length (2), hand length (3), hand width (4), finger IV length (5), upper leg length (6), lower leg length (7), foot length (8), foot width (9), and toe IV length (10). C) Landmark configuration used to characterize head shape: tip of snout (1), anterior edges of supraocular semicircles (2–3), medial edges of supraocular semicircles (4–5), posterior edges of supraocular semicircles (6–7), anterior edges of tympanum (8–9), posterior edges of nuchal fold (10–11), and anterior edge of nuchal fold (12); the blue lines indicate sliding semi-landmarks (13–32).

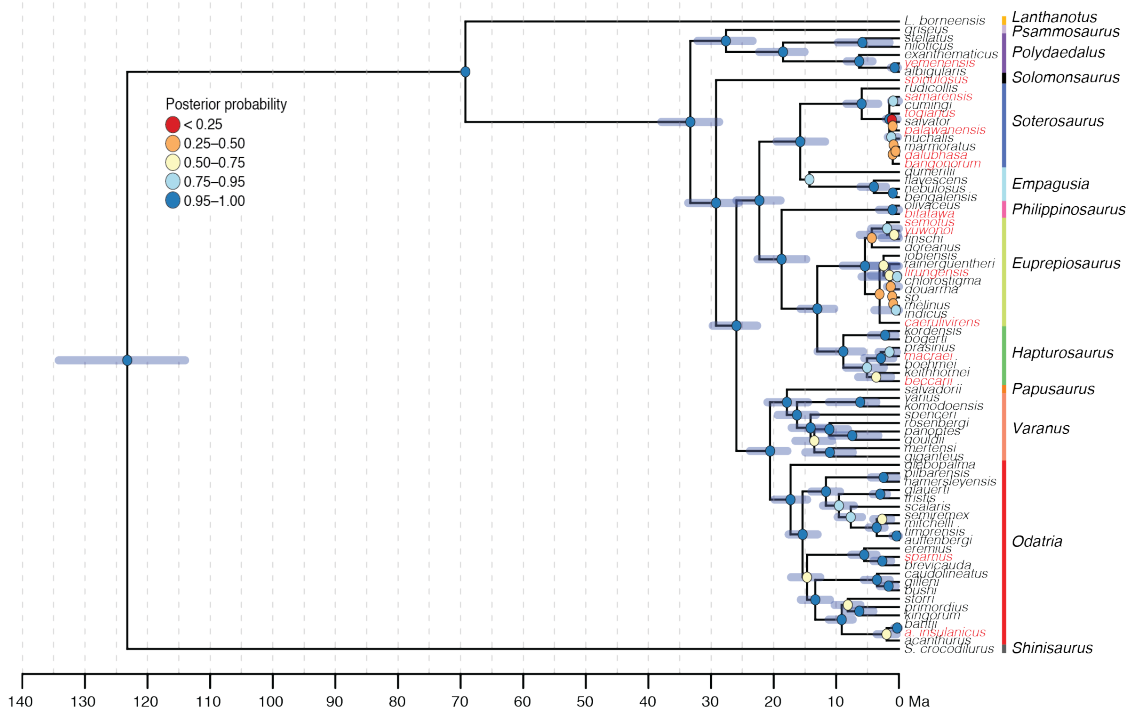

Figure S2. Time-calibrated phylogeny of Paleoanguimorpha from Pavón-Vázquez et al. (under review). Nodes are colored based on their posterior probability. Blue bars denote the 95% highest posterior density of divergence times (not shown for sections of the tree based on Lin and Wiens (2017) and nodes with posterior probability < 0.50). Taxa in red were excluded from the ontogenetic analyses.

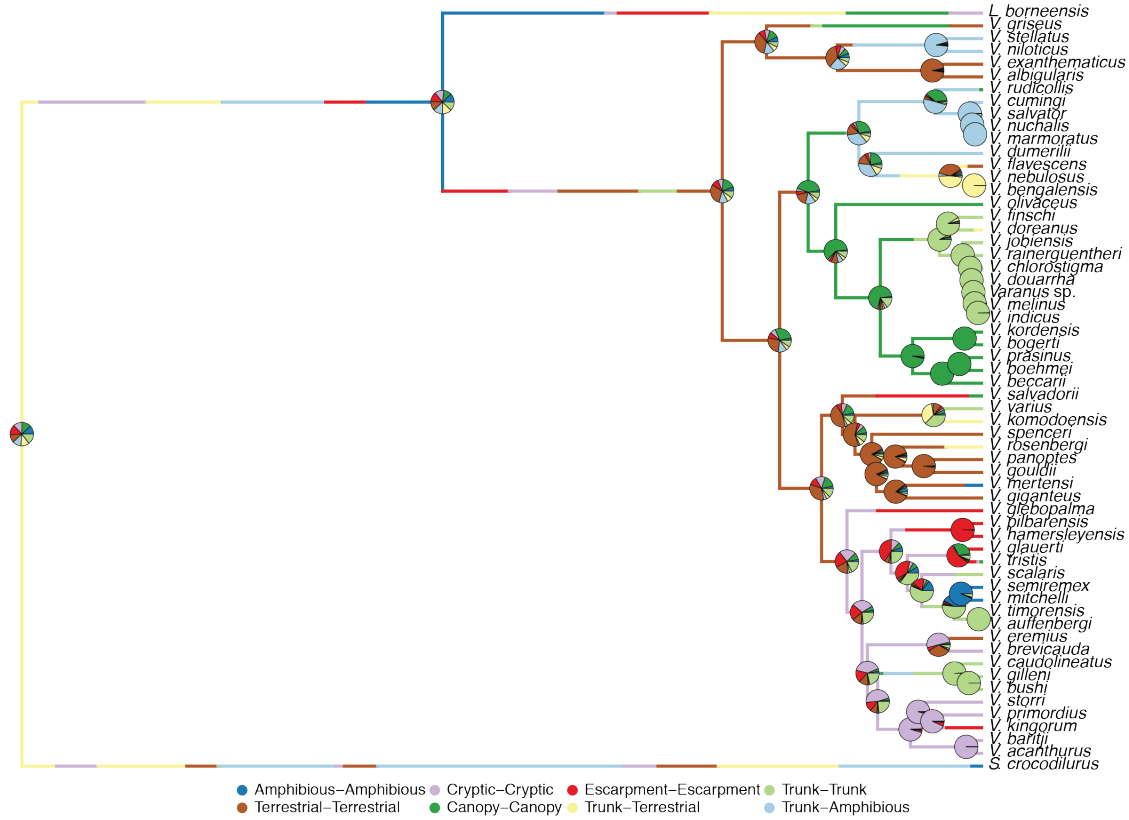

Figure S3. Stochastic character mapping of habitat use in Paleoanguimorpha. Branches are colored based on a single stochastic map used in downstream analyses. Pie charts indicate uncertainty in the reconstruction based on 1,000 stochastic maps.

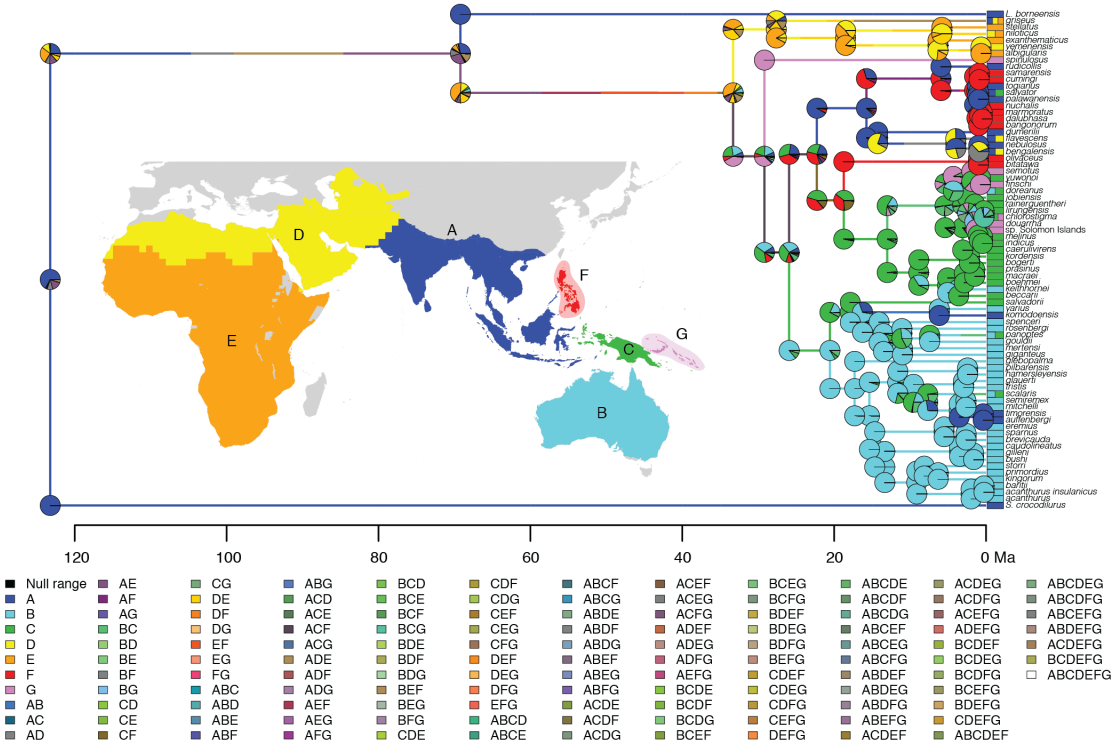

Figure S4. Ancestral range reconstruction of Paleoanguimorpha from Pavón-Vázquez et al. (under review). Branches are colored based on a single stochastic map used in downstream analyses.

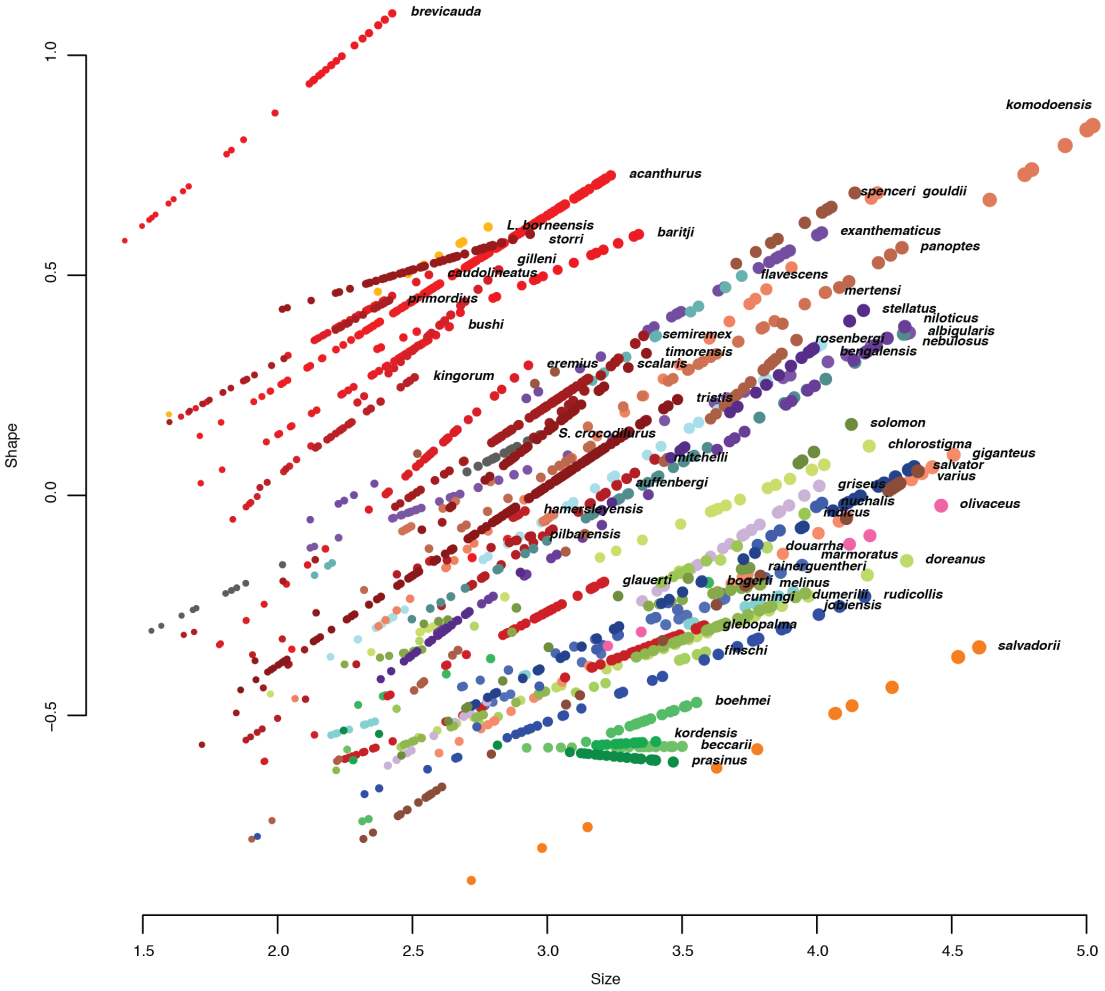

Figure S5. Ontogenetic change in body shape with size (taken from the homogeneity of slopes test). The horizontal axis represents size (log-transformed geometric mean of linear measurements) and the vertical axes the first principal component of the predicted shape. Points represent individuals. Similar colors are used for species belonging to the same genus/subgenus.

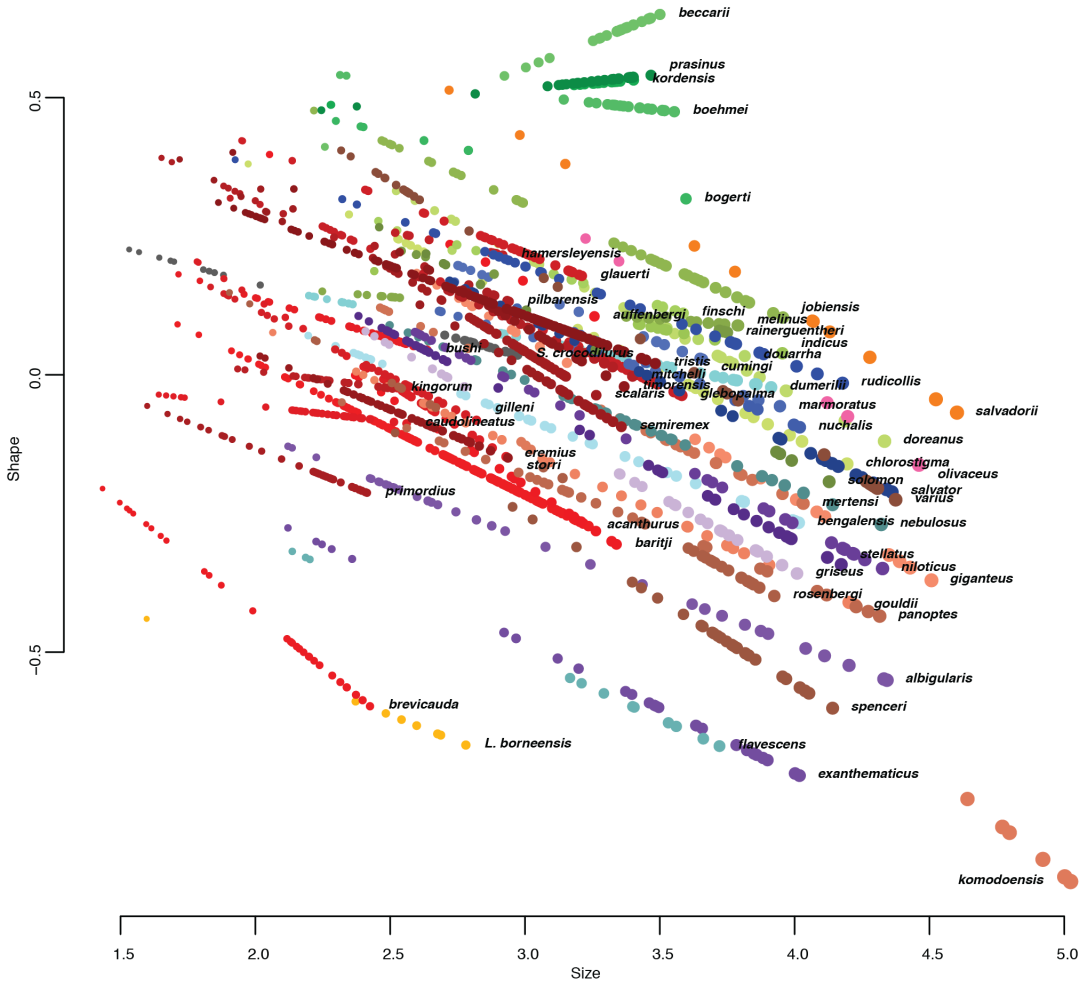

Figure S6. Ontogenetic change in limb shape with size (taken from the homogeneity of slopes test). The horizontal axis represents size (log-transformed geometric mean of linear measurements) and the vertical axes the first principal component of the predicted shape. Points represent individuals. Similar colors are used for species belonging to the same genus/subgenus.

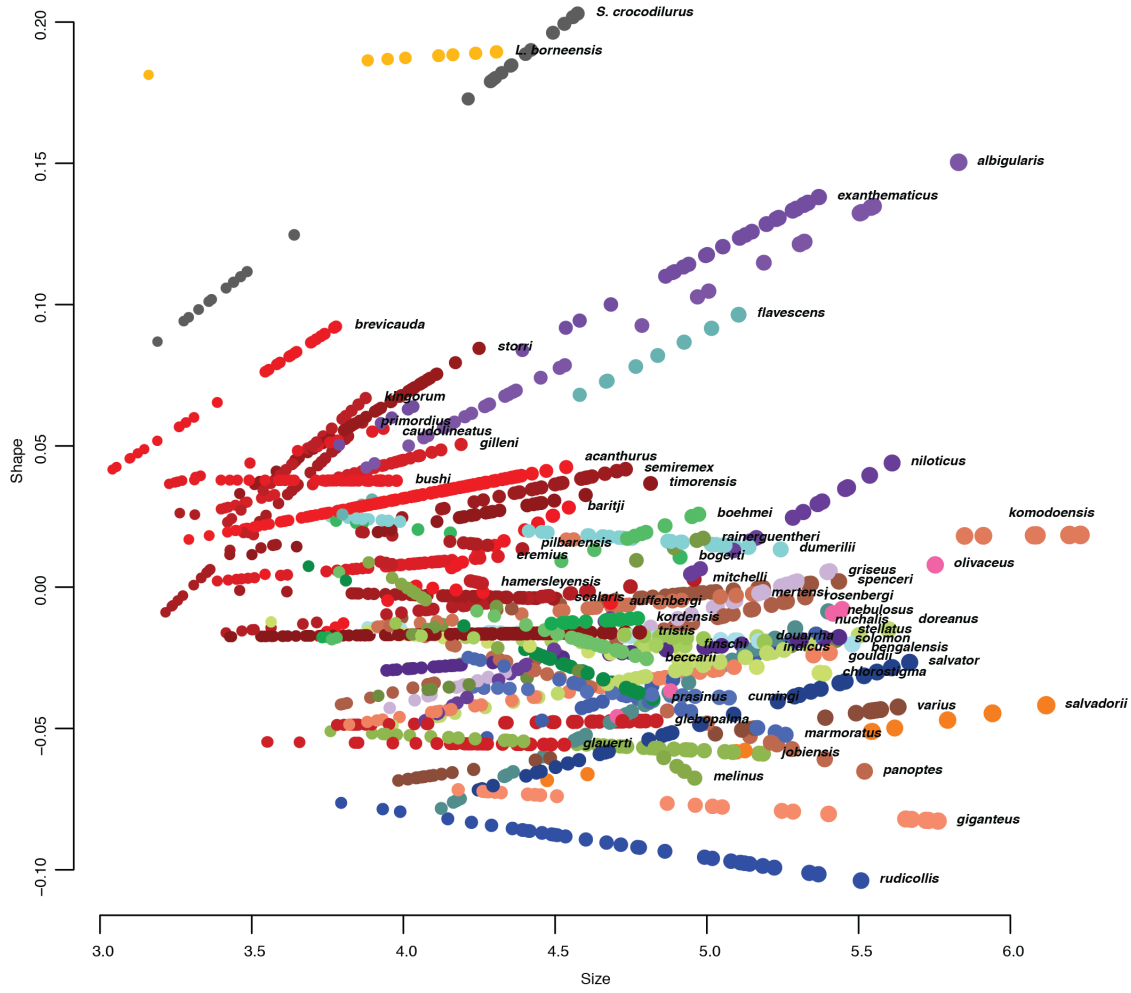

Figure S7. Ontogenetic change in head shape with size (taken from the homogeneity of slopes test). The horizontal axis represents size (log-transformed centroid size) and the vertical axes the first principal component of the predicted shape. Points represent individuals. Similar colors are used for species belonging to the same genus/subgenus.

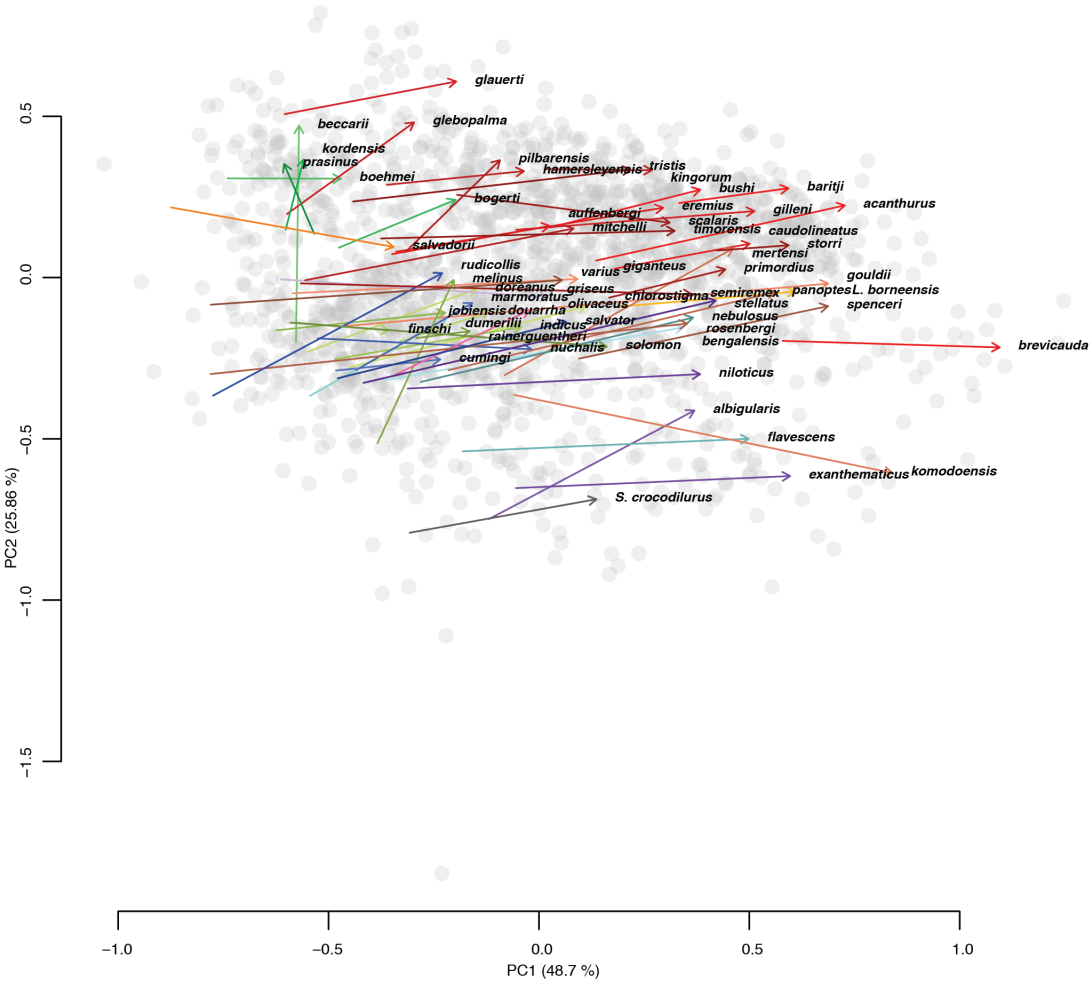

Figure S8. Ontogenetic change of body shape in morphospace (taken from the phenotypic trajectory analysis). The horizontal and vertical axes represent the first and second principal components of the variables describing shape, respectively. Trajectories go from mean juvenile shape to mean adult shape Similar colors are used for species belonging to the same genus/subgenus. Gray points represent individuals.

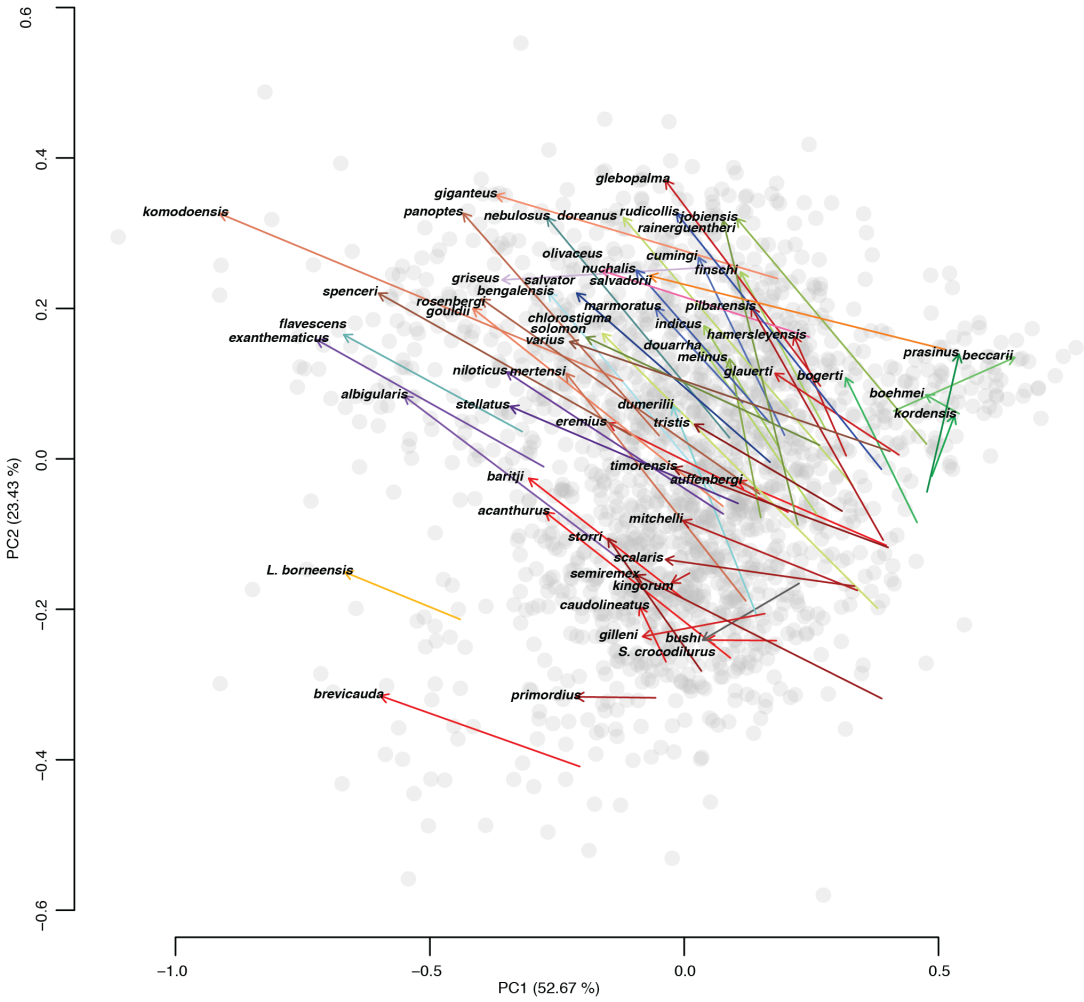

Figure S9. Ontogenetic change of limb shape in morphospace (taken from the phenotypic trajectory analysis). The horizontal and vertical axes represent the first and second principal components of the variables describing shape, respectively. Trajectories go from mean juvenile shape to mean adult shape Similar colors are used for species belonging to the same genus/subgenus. Gray points represent individuals.

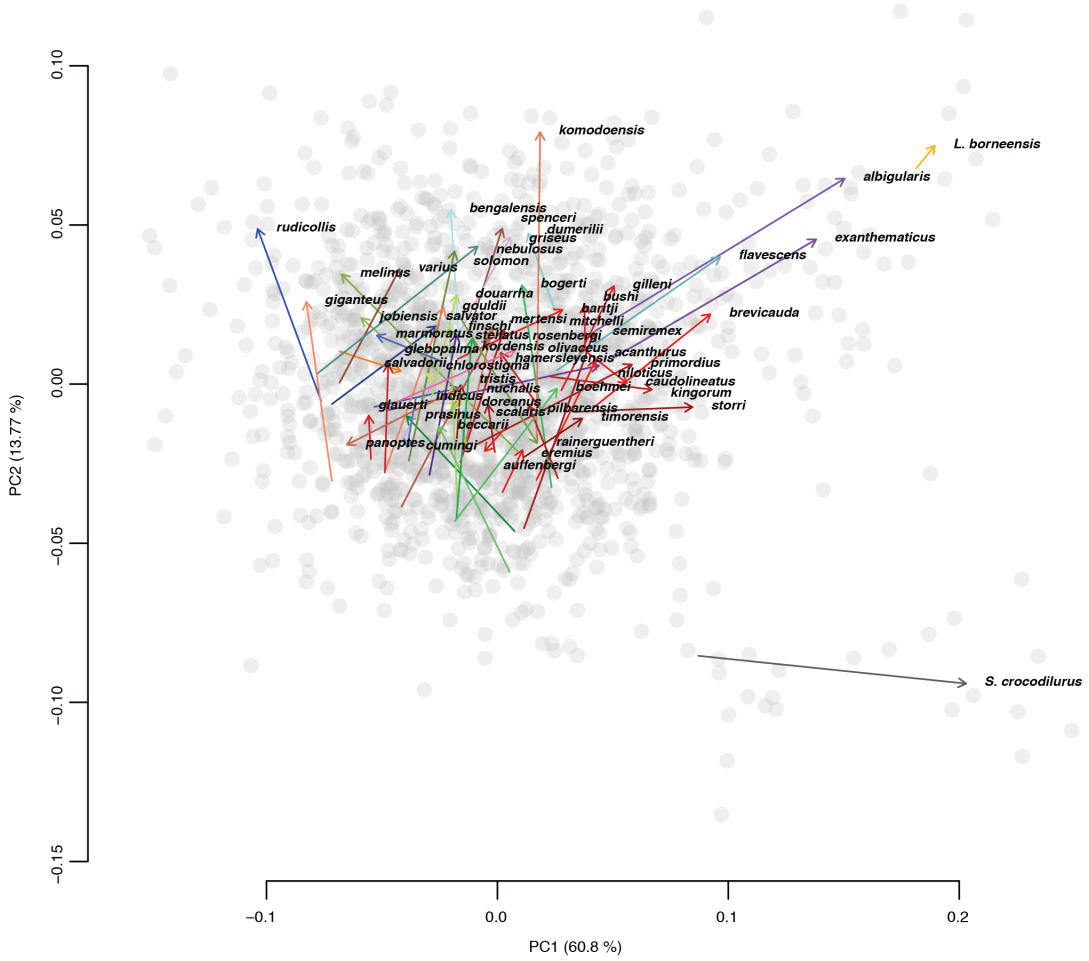

Figure S10. Ontogenetic change of head shape in morphospace (taken from the phenotypic trajectory analysis). The horizontal and vertical axes represent the first and second principal components of the variables describing shape, respectively. Trajectories go from mean juvenile shape to mean adult shape Similar colors are used for species belonging to the same genus/subgenus. Gray points represent individuals.

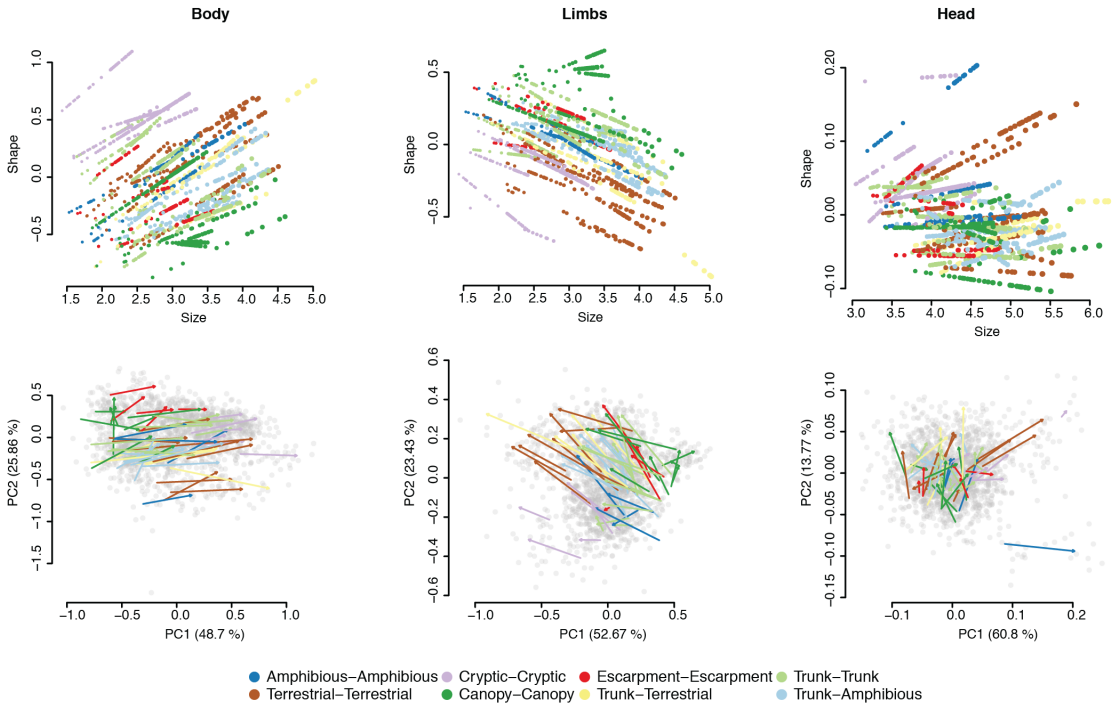

Figure S11. Ontogenetic allometric trajectories colored by habitat use. The top row shows ontogenetic change in the predicted shape (from the homogeneity of slopes test) and the bottom row shows the results of the phenotypic trajectory analyses.

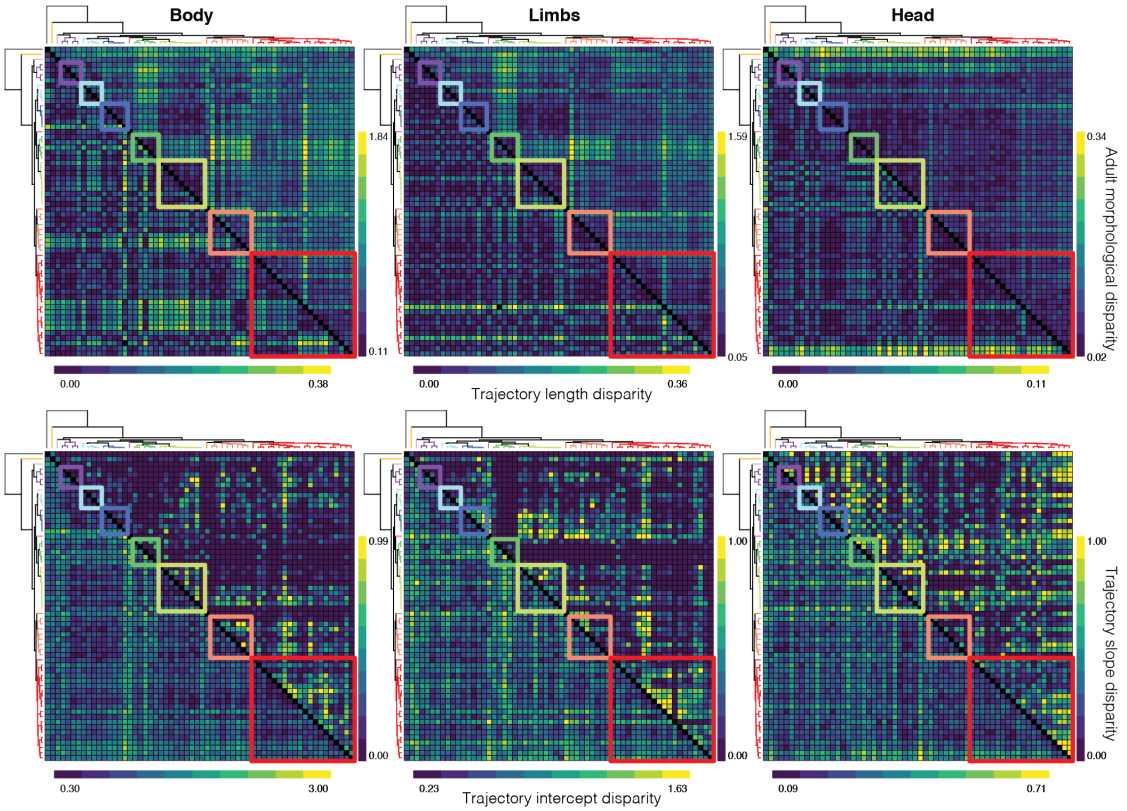

Figure S12. Morphological and ontogenetic disparity. Each grid is a square matrix where cells represent a pairwise comparison between species (diagonal in black). The phylogenetic tree depicting interspecific relationships is shown in the axes. Squares with colored borders indicate comparisons within clades (colors follow Fig. 2). For each species pair, we characterized morphological disparity as the Euclidean distance between the predicted adult phenotypes, disparity in trajectory lengths as the absolute difference between the estimated lengths, disparity in trajectory slopes as degrees, and disparity in trajectory intercepts as the Euclidean distance between intercepts.

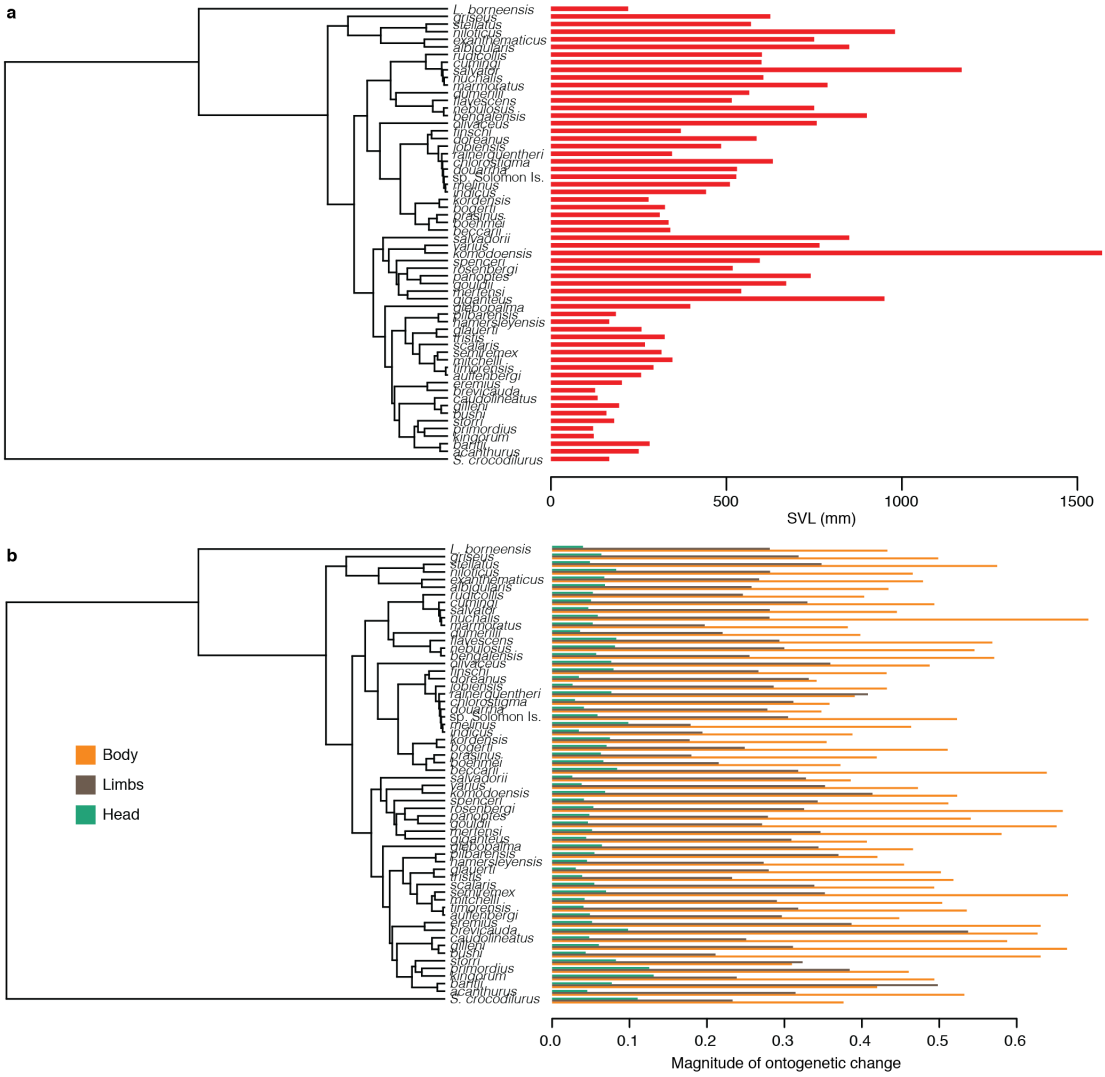

Figure S13. Relationship between body size and the magnitude of ontogenetic shape change. a) Maximum snout-vent length, a commonly used proxy for body size (SVL). b) Magnitude of ontogenetic shape change for each of the analyzed datasets.

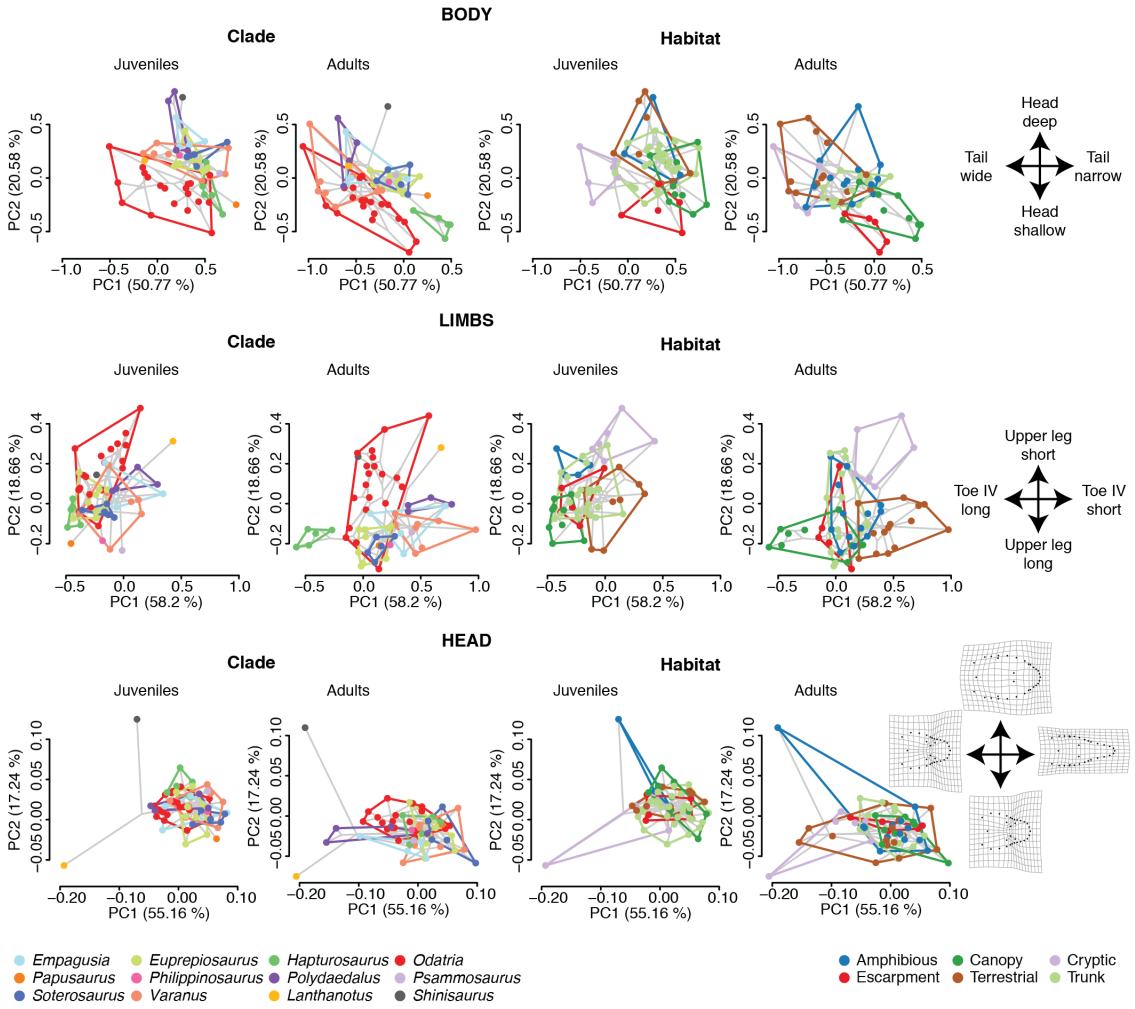

Figure S14. Phylomorphospace of juvenile and adult paleoanguimorphs. Axes represent the first and second principal components of the morphological data. Points (representing mean values per species) and convex hulls are colored by either clade or habitat use. For the linear measurements, the diagrams on the right indicate change in the traits that contribute the most to variation along each axis. For head shape, deformation grids show the head shape at the extremes of each axis and how they differ from the mean head shape.

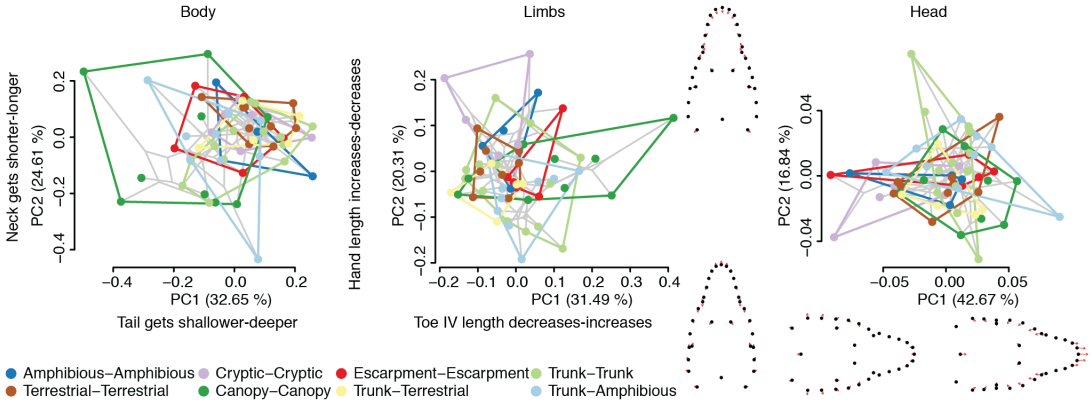

Figure S15. Phyloallomspace of Paleoanguimorpha. Axes correspond to the first two principal components (PCs) of the slopes of the ontogenetic allometric trajectories. The phylogenetic tree and inferred ancestral conditions (nodes) are shown in light gray. For the linear measurements, we show the trait whose slope contributes majorly to each PC and how it changes ontogenetically at the lower and upper extremes of each axis (separated by dash, in that order). For head shape, we show the average landmark configuration of juveniles of the species at each extreme (black points) and how landmarks move as each species grows (red arrows). Convex hulls are shown for each habitat use category.

Literature Cited*

*Includes references in Supporting Tables.

Adams, D.C., and E. Otárola-Castillo. 2013. geomorph: an R package for the collection and analysis of geometric morphometric shape data. Methods Ecol. Evol. 4:393–399.

Aplin, K. P., A. J. Fitch, and D. J. King. 2006. A new species of *Varanus* Merrem (Squamata: Varanidae) from the Pilbara region of Western Australia, with observations on sexual dimorphism in closely related species. Zootaxa 1313:1–38.

Böhme, W., H. J. Jacobs, T. Koppetsch, and A. Schmitz. 2019. The Kei Islands monitor lizard (Squamata: Varanidae: *Varanus*: *Euprepiosaurus*) as a distinct morphological, taxonomic, and conservation unit. Russ. J. Herpetol. 26:272–280.

Bouckaert, R., J. Heled, D. Kühnert, T. Vaughan, C. Wu., D. Xie, M. A. Suchard, A. Rambaut, and A. J. Drummond. 2014. BEAST 2: a software platform for Bayesian evolutionary analysis. PLoS Comput. Biol. 10:e1003537.

Brennan, I. G., A. R Lemmon, E. M. Lemmon, D. M. Portik, V. Weijola, L. Welton, S. C. Donnellan, and J. S. Keogh. 2020. Phylogenomics of monitor lizards and the role of competition in dictating body size disparity. Syst. Biol. 70:120–132.

Bucklitsch, Y., W. Boehme, and A. Koch. 2016. Scale morphology and micro-structure of monitor lizards (Squamata: Varanidae: *Varanus* spp.) and their allies: implications for systematics, ecology, and conservation. Zootaxa 4153:1–192.

del Canto, R. 2007. Notes on the occurrence of *Varanus auffenbergi* on Roti Island. Biawak 1:24–25.

Eidenmüller, B., A. Koch, J. Köhler, and R. Wicker. New findings on the relationships among New Guinea tree monitor lizards of the *Varanus prasinus* (Schlegel, 1839) complex. Hepetozoa 30:9–20.

Ewart, A. 1988. Geological history of the Fiji–Tonga–Samoan region of the SW Pacific, and some palaeogeographic and biogeographic implications. *In* J. P. Duffels (ed.). The cicadas of the Fiji, Samoa and Tonga Islands, their taxonomy and biogeography (Homeoptera, Cicadoidea). Scandinavian Science Press, Leiden, ZH.

Fitch, A. J., A. E. Goodman, and S. C. Donnellan. 2006. A molecular phylogeny of the Australian monitor lizards (Squamata: Varanidae) inferred from mitochondrial DNA sequences. Aust. J. Zool. 54:253–269.

Greer, A. E. 2001. Distribution of maximum snout-vent length among species of scincid lizards. J. Herpetol. 35:383–395.

Gunz, P., P. mitteroecker, S. Neubauer, G. W. Weber, and F. L. Bookstein. 2009. Principles for the virtual reconstruction of hominin crania. J. Hum. Evol. 57:48–62.

Hall, R. 1996. Reconstructing Cenozoic SE Asia. Geol. Soc. Spec. Publ. 106:153–184.

Hall, R. 1998. The plate tectonics of Cenozoic SE Asia and the distribution of land and sea. *In* Hall, R., and J. D. Holloway. Biogeography and geological evolution of SE Asia. Backhuys Publishers, Leiden, ZH.

Holt, B. G., J. P. Lessard, M. K. Borregaard, S. A. Fritz, M. B. Araújo, D. Dimitrov, P-H. Fabre, C. H. Graham, G. R. Graves, K. A. Jønsson, D. Nogués-Bravo, Z. Wang, R. J. Whittaker, J. Fjeldså, and C. Rahbek. 2013. An update of Wallace's zoogeographic regions of the world. Science 339:74–78.

Jacobs, H. J. 2003. A further new emerald tree monitor lizard of the *Varanus prasinus* species group from Waigeo, West Irian (Squamata: Sauria: Varanidae). Salamandra 39:65–74.

Kalyaanamoorthy, S., B. Q. Minh, T. K. F. Wong, A. von Haeseler, and L. S. Jermiin. 2017. ModelFinder: fast model selection for accurate phylogenetic estimates. Nat. Methods 14:587–589.

Landis, M. J., N. J. Matzke, B. R. Moore, and J. P. Huelsenbeck. 2013. Bayesian analysis of biogeography when the number of areas is large. Syst. Biol. 62:789–804.

Lemmon, A. R., S. A. Emme, and E. Moriarty Lemmon. 2012. Anchored hybrid enrichment for massively high-throughput phylogenomics. Syst. Biol. 61:727–744.

Lin, L., and J. J. Wiens. 2017. Comparing macroecological patterns across continents: evolution of climatic niche breadth in varanid lizards. Ecography 40:960–970.

Lucky, A., and E. M. Sarnat. 2010. Biogeography and diversification of the Pacific ant genus *Lordomyrma* Emery. J. Biogeogr. 37:624–634.

Maryan, B., P. M. Oliver, A. J. Fitch, and M. O'Connell. 2014. Molecular and morphological assessment of *Varanus pilbarensis* (Squamata: Varanidae), with a description of a new species from the southern Pilbara, Western Australia. Zootaxa 3768:139–158.

Matzke, N. J. 2013. Probabilistic historical biogeography: new models for founder-event speciation, imperfect detection, and fossils allow improved accuracy and model-testing. Front. Biogeogr. 5:242–248.

Matzke, N. J. 2014. Model selection in historical biogeography reveals that founder-event speciation is a crucial process in island clades. Syst. Biol. 63:951–970.

McCoy, M. 2006. Reptiles of the Solomon Islands. Pensoft Publishers, Sofia, SOF.

Meiri, S. 2018. Traits of lizards of the world: variation around a successful evolutionary design. Global Ecol. Biogeogr. 27:1168-1172.

Müller, R. D., J. Cannon, X. Qin, R. J. Watson, M. Gurnis, S. Williams, T. Pfaffelmoser, M. Seton, S. H. J. Russell, and S. Zahirovic. 2018. GPlates: building a virtual Earth through deep time. Geochem. Geophy. Geosy. 19:2243–2261.

Pianka, E., and D. R. King (eds.). 2004. Varanoid lizards of the world. Indiana University Press, Bloomington, IN.

Ree, R. H., and S. A. Smith. 2008. Maximum likelihood inference of geographic range evolution by dispersal, local extinction, and cladogenesis. Syst. Biol. 57:4–14.

Revell, L. J. 2012. phytools: an R package for phylogenetic comparative biology (and other things). Methods Ecol. Evol. 3:217–223.

Ronquist, F. 1997. Dispersal-vicariance analysis: a new approach to the quantification of historical biogeography. Syst. Biol. 46:195–203.

Sabaj M.H. 2019. Standard symbolic codes for institutional resource collections in herpetology and ichthyology: an online reference. Version 7.1 (21 March 2019). Available at http://www.asih.org/. Accessed December 1, 2020.

Sherratt, E., A. R. Rasmussen, and K. L. Sanders. 2018. Trophic specialization drives morphological evolution in sea snakes. Roy. Soc. Open Sci. 5:172141.

Smith, L. A., S. S. Sweet, and D. R. King. 2004. *Varanus scalaris*. *In* Pianka, E. R., and D. R. King (eds.). Varanoid Lizards of the World. Indiana University Press, Bloomington, IN.

Stamps, J. A., and R. M. Andrews. 1992. Estimating asymptotic size using the largest individuals per sample. Oecologia, 92:503–512.

Stekhoven, D.J., and P. Bühlmann. 2012. MissForest—non-parametric missing value imputation for mixed-type data. Bioinformatics 28:112–118.

van Schingen, M., C. T. Pham, H. A. Thi, T. Q. Nguyen, M. Bernardes, M. Bonkowski, and T. Ziegler. 2015. First ecological assessment of the endangered crocodile

lizard, *Shinisaurus crocodilurus*, Ahl, 1930 in Vietnam: microhabitat characterization and habitat selection. Herpetol. Conserv. Biol. 10:948–958.

Weijola, V. S-Å. 2010. Geographical distribution and habitat use of monitor lizards of the north Moluccas. Biawak 4:7–23.

Weijola, V., and S. S. Sweet. 2015. A single species of mangrove monitor (*Varanus*) occupies Ambon, Seram, Buru and Saparua, Moluccas, Indonesia. Amphib. Reptile Conserv. 9:14–23.

Weijola, V., F. Kraus, V. Vahtera, C. Lindqvist, and S. C. Donnellan. 2017. Reinstatement of *Varanus douarrha* Lesson, 1830 as a valid species with comments on the zoogeography of monitor lizards (Squamata: Varanidae) in the Bismarck Archipelago, Papua New Guinea. Austr. J. Zool. 64:434-451.

Weijola, V., V. Vahtera, A. Koch, A. Schmitz, and F. Kraus. 2020. Taxonomy of Micronesian monitors (Reptilia: Squamata: *Varanus*): endemic status of new species argues for caution in pursuing eradication plans. Roy. Soc. Open Sci. 7:200092.

Weijola, V., V. Vahtera, C. Lindqvist, and F. Kraus. 2019. A molecular phylogeny for the Pacific monitor lizards (*Varanus* subgenus *Euprepiosaurus*) reveals a recent and rapid radiation with high levels of cryptic diversity. Zool. J. Linn. Soc. 186:1053–1066.

CHAPTER III

Supplementary Materials and Methods

Molecular data

Noting that the AHE dataset was generated to infer the phylogeny of all monitor lizards (Varanidae), we optimized the alignment of each locus for our focal taxon using the MUSCLE algorithm (Edgar 2004). To obtain Subset 2, we ranked loci based on their number of parsimony informative sites and amount of missing data. We assigned a score ranging from 1 for the highest ranked loci in each category to 337 (number of loci in Subset 1) for the lowest ranked. Then we summed the scores for each locus and selected the 40 loci with the best (i.e., lowest) sum of scores.

Phylogenomics

We obtained individual gene trees for the nuclear loci and the matrilineal phylogeny based on the mitochondrial genomes in IQ-TREE 1.7 (Nguyen et al. 2015). The substitution models and partitioning scheme were selected using the Bayesian Information Criterion (BIC) in ModelFinder (Kalyaanamoorthy et al. 2017) and PartitionFinder (Lanfear et al. 2016), respectively. In the case of the nuclear genes, the starting partitioning scheme assigned each codon position to a different partition. In the case of the mitochondrial genomes, we included outgroups *V. niloticus*, *V*. *palawanensis*, and *V*. *timorensis*.

We used the -a option in ASTRAL-III 5.6.3 (Zhang et al. 2018) to map all individuals to their respective species for species tree inference. To estimate branch lengths in the ASTRAL species tree we used BASEML, running analyses for 2,000 burnin iterations and 200,000 post-burnin iterations sampled every 10 generations. For the MCMCTree analyses, we specified a relaxed log-normal clock with independent rates, HKY+G as substitution model, 2,000 burnin iterations, and 2,000,000 post-burnin iterations sampled every 100 generations. We performed the BASEML-MCMCTree procedure twice to evaluate mixing and convergence.

We also time-calibrated the individual-level tree obtained in ASTRAL with BASEML and MCMCTree (Yang 2007). We used the concatenated alignment of Subset 1 as input and specified the same priors and parameters employed to calibrate the species tree (see main text), but increasing chain lengths (BASEML: 5,000 burnin iterations, 500,000

post-burnin iterations, 10 thinning; MCMCTree: 10,000 burnin iterations, 5,000,000 post-burnin iterations, 100 thinning).

Reticulation

Phylogenetic tree space for Subset 1 was explored using the 'treespace 1.1.3.2' (Jombart et al. 2017) package in R 3.5.3 (R Core Team 2019). The gene trees were those obtained in IQ-TREE 1.7 (Nguyen et al. 2015). For species represented by more than one individual (*V. gouldii* and *V. panoptes*), we kept the samples with fewer missing data and removed the rest.

For the SNaQ analysis of Subset 1, the quartet concordance factors used to infer reticulation were obtained from the maximum likelihood gene trees. For Subset 2, they were obtained from a random sample of ten ultrafast bootstrap trees for each loci taken from the IQ-TREE analyses. We deleted quartets containing more than one individual per species. For each subset, we ran six SNaQ analyses, allowing between 0 and 5 hybridization events (h). The best scoring network/tree under a given value of h was used as starting network/tree under $h + 1$. We specified 10 runs for each value of h and chose the optimal number of h based on the slope heuristic of the pseudo-likelihood compared amongst the best-scoring networks for each value of h (Solís-Lemus and Ané 2016). Bootstrapping in PhyloNetworks (Solís-Lemus et al. 2017) does not allow more than one sample per species. Thus, for each ultrafast bootstrap tree in Subset 1 we kept the samples of *V. gouldii* and *V. panoptes* with fewer missing data using the 'ape 5.3' package (Paradis and Schliep 2018).

The PhyloNet analyses were based on the maximum pseudo-likelihood implementation that takes rooted gene trees as input (Yu and Nakhleh 2015). We included all individuals and assigned them to their respective species using the '-a' option. The analysis of Subset 1 was based on the individual maximum likelihood gene trees. For the analysis of Subset 2, network inference was based on a random sample of ten ultrafast bootstrap trees for each loci taken from the IQ-TREE analyses. The trees were rooted on the outgroup *V. timorensis* in R 3.5.3 (R Core Team 2019) using the 'ape 5.3' package (Paradis and Schliep 2018). For both analyses, the maximum number of hybridizations was set to 5 and other options were set to their default values. We chose the best-scoring network based on its log-probability.

For our mitochondrial introgression tests, we first estimated the ancestral population sizes (θ) and divergence times (τ) based on the time-calibrated species tree in BPP 3.3 (Yang 2015). We specified a gamma distribution with shape (α) = 2 and scale (β) = 2,000 as prior for θ, and with $\alpha = 2$ and $\beta = 6.33$ as prior for the root age (τ_0). We based the

prior for θ on the mean uncorrected pairwise genetic distance (*p*-distance) between the concatenated AHE sequences of *V*. *panoptes* (the species with the largest number of sequenced individuals), and the prior for τ_0 on the mitochondrial *p*-distance between *V*. *komodoensis* and *V*. *varius* and the divergence dates in the time-calibrated species tree. For both priors, we considered the effective population size of the mitochondria to be one-fourth the size of the nuclear. BPP analyses consisted of two runs with a burnin period of 10,000 iterations, followed by a post-burn-in period of 100,000 iterations sampled every second iteration. Second, we simulated 1,000 mitochondrial alignments under the multi-species coalescent in MCcoal (Rannala and Yang 2003), based on the time-calibrated species tree and following a clock model with independent branch rates. We based the values of θ and τ on the BPP results and ran ModelFinder (Kalyaanamoorthy et al. 2017) on the *ND2* alignment to estimate the parameters for the substitution model. Lastly, we evaluated whether the observed minimum uncorrected genetic distances between species (*p*-min) were smaller than expected under the multi-species coalescent, which would suggest the existence of mitochondrial introgression. A maximum likelihood tree of the *ND2* alignment was obtained in IQ-TREE and is shown in Fig. S3b.

Morphology

All statistical analyses were performed in R 3.5.3 (R Core Team 2019). We used random forest training to predict missing values (e.g., due to incomplete tails), including species and sex as predictors in 'missForest 1.4' (Stekhoven and Bühlmann 2012). We log-transformed the data and performed a linear regression of each log-corrected trait against the log-corrected SVL. We tested for sexual dimorphism in the residuals by performing an analysis of variance in 'geomorph 3.0.3' (Adams and Otarola-Castillo 2013) and assessed significance through 1,000 permutations. Since our dataset contained more males than females, we discarded females for the species showing significant sexual dimorphism (*V*. *spenceri*). Our final dataset consisted of 88 specimens: 7 of *V*. *giganteus*, 11 of *V*. *gouldii*, 6 of *V*. *komodoensis*, 18 of *V*. mertensi, 10 of *V*. *panoptes*, 13 of *V*. *rosenbergi*, 5 of *V*. *salvadorii*, 9 of *V*. *spenceri*, and 9 of *V*. *varius*. After removing females of *V*. *spenceri*, we repeated the regression of each log-corrected trait against log-SVL. All analyses were based on the residuals of the regression. We performed the phylogenetic PCA on the covariance matrix under a Brownian motion (BM) model in 'phytools' (Revell 2012).

To fit models of morphological evolution we time-calibrated the SNaQ network of Subset 1 based on the maximum likelihood gene trees using code available at https://github.com/nkarimi/Adansonia_HybSeq (Karimi et al. 2020). The pipeline does

not allow more than one sample per species. Thus, for each gene tree we kept the samples of *V. gouldii* and *V. panoptes* with fewer missing data using the 'ape 5.3' package (Paradis and Schliep 2018).

We used the time-calibrated species tree in phylogenetic imputation. The accuracy of imputation methods can be compromised by sampling biases, low phylogenetic signal of traits, and long terminal branches (Swenson 2013; Molina-Venegas et al. 2018). However, the method implemented in 'Rphylopars' is among few that optimize imputation based on evolutionary models and accounts for intraspecific variation and correlation between traits (Goolsby et al. 2017). It has also been shown to perform comparatively well under different conditions (Nakagawa and de Villemereuil 2019). We simulated intraspecific variation in each character for the reticulated and reticulation-free MRCA of sand monitors by taking ten values (the rounded mean sample size for each species in our morphological dataset) at random from a normal distribution with mean and standard deviation equal to those estimated in 'Rphylopars' (Goolsby et al. 2017) for each character and taxa (Fig. S1). We used the "predict" function of the R built-in 'stats 3.6.2' package to get the PCA scores of the nine simulated individuals in the reticulated and reticulation-free MRCA. To get the phylogenetic PCA scores of each individual, including the nine simulated individuals in the reticulated and reticulation-free MRCA, we used the "scores" function of 'phytools' (Revell 2012).

To evaluate the sensitivity of the "search.conv" (Castiglione et al. 2019) method to branch length uncertainty we obtained a sample of 100 trees using a script available at https://github.com/CarlosPavonV/RandomMolR. These trees have the same topology as the species-tree but had differing branch lengths within the 95% confidence intervals of the divergence dates estimated with MCMCTree. The "overfitRR" function of the RRphylo 2.4.7' package (Castiglione et al. 2018) tests the robustness of RRphylo results by shuffling and removing tips across the tree. However, it is time consuming and does not incorporate information on node support or branch length confidence intervals to perform shuffling. Therefore, we modified the "search.conv" function to store the null distribution of phenotypic angles and then compare them to the angles inferred for our sample of 100 trees.

Multivariate intermediacy can arise from divergence without reticulation (Wilson 1992). One way to evaluate if intermediacy is caused by hybridization is to count the individual characters that are significantly different between the supposed parental taxa and intermediate for the presumably hybrid taxon (Wilson 1992). To test whether ancient hybridization resulted in morphological intermediacy we performed a test based on character counts (Wilson 1992). We first identified the characters that differ significantly between *V. komodoensis* and *V. giganteus*/*V. mertensi* using ANOVA and Tukey's test

of honest significant differences as post-hoc test. Among those characters that differed significantly, we identified those for which the mean value for each species of sand monitor is intermediate between *V. komodoensis* and *V. giganteus*/*V. mertensi*. Significance was assessed by comparing the number of intermediate and non-intermediate characters in a one-sided sign test (Wilson 1992).

We also performed the character count procedure by specifying *V. komodoensis* and the reticulation-free MRCA as hybridizing taxa and the reticulated MRCA as the putative hybrid taxon. If the morphology of living sand monitors shows signs of hybridization with the Komodo dragon, we expected the character states of the reticulated MRCA to be intermediate for those traits that differ between *V. komodoensis* and the reticulation-free MRCA.

Biogeography

For the 'BioGeoBEARS 1.1.2' (Matzke 2013) analyses we divided the study area into nine discrete regions. Given their isolation from other regions where members of the LAMc occur, we categorized the Lesser Sunda Islands as an independent area. We divided New Guinea into a southern and northern area on either side of the Central Range. This mountain range has been identified as an important biogeographic barrier, particularly for lowland taxa (Tallowin et al. 2014). Our Australian area divisions are based on the terrestrial biome division of Olson et al. (2001) and follow the nomenclature of Cardillo et al. (2017). There are only a few records of a single member of the LAMc (*V. varius*) from the "Montane Grasslands and Shrublands." Thus, we followed Cardillo et al. (2017) and merged that biome with the surrounding Temperate Forest. We restricted the list of possible states to represent historically plausible scenarios by specifying an area adjacency matrix (Table S15). For the analyses of the tree including the Komodo dragon fossils, we used the fossil tips as "hooks" (tips with zero-length branches), meaning that no cladogenetic events are recorded but that information on distribution is inputted for *V. komodoensis* at particular times. We acknowledged uncertainty on past distributions by specifying the areas in which the fossils were found as hard-presences and the rest of the areas as regions of possible occurrence. If there was temporal overlap for occurrence in several areas, we specified all the occupied areas at that particular time as hard-presences for the relevant tips. We used the time-calibrated species tree in the analysis based on contemporary records only.

For the rase 0.3-3' (Quintero et al. 2015) analyses, we compiled distribution records for each species in the LAMc. The records from Australia were obtained from the Atlas of Living Australia, and we only included those with associated museum specimens (Atlas of Living Australia 2019). Records of *V. komodoensis*, *V. panoptes horni*, and *V.*

salvadorii were obtained from relevant literature (Böhme 1988; Ciofi et al. 1999; Sastrawan and Ciofi 2002; Horn et al. 2007; Hocknull et al. 2009). The number of records totalled 15,760, with 40–8,433 ($\bar{x}$ = 1,748.56) records per species. Polygons depicting the distribution of each species were built from these records in R. We used the same trees employed in the discrete area analyses for the 'rase' analyses based on fossil and contemporary records, respectively. For the analysis including fossil records, we specified an "additive distribution" for *V. komodoensis*, meaning that the distribution of the species was assumed to have expanded through time with the addition of more recent records, with some exceptions implying local extinction: the species was assumed to have become locally extinct in Australia sometime between 0.15–0.33 Ma and its current distribution was based on contemporary records only. For each fossil locality, we generated ten randomly located points from a normal distribution with the mean equal to the latitude/longitude of each fossil record and a standard deviation of 1. The analysis including fossils consisted of 50,000 generations, with sampling every 10 generations, and 10% burn-in. The analysis based only on contemporary records was the same, except that it consisted of 10,000 generations. Post-processing and evaluation of the MCMC was made with the R package 'coda 0.19-2' (Plummer et al. 2006). Note that ancestral ranges inferred by 'rase' often fall in the centre of the combined tip ranges, a common behaviour of methods based on BM (Lemey et al. 2010).

To estimate the potential distribution of *V. komodoensis* through time, we extracted climatic data for 92 contemporary presence/absence records (Ciofi et al. 1999; Sastrawan and Ciofi 2002) (Table S5) from the Bioclim database (Hijmans et al. 2005) and from PaleoClim (Brown et al. 2018) for 6 fossil yielding localities (climatic dataset in parentheses): Liang Bua, Indonesia (Greenlandian) (Fordham et al. 2017); Tangi Talo (Ola Bula), Indonesia (MIS19) (Brown et al. 2018); Mount Etna, Australia (MIS19) (Brown et al. 2018); Marmor Quarry, Australia (MIS19) (Brown et al. 2018); Chinchilla Sand, Australia (mid-Pliocene) (Hill 2015); and Bluff Downs, Australia (M2) (Dollan et al. 2015) (Table S4). We removed tightly correlated climatic variables (Pearson's $r > 0.85$, or $r < -0.85$), thus basing our analyses on eight variables: annual mean temperature (BIO1), temperature seasonality (BIO4), mean temperature of wettest quarter (BIO8), mean temperature of driest quarter (BIO9), mean temperature of warmest quarter (BIO10), precipitation of driest month (BIO14), precipitation seasonality (BIO15), and precipitation of warmest quarter (BIO18). We generated 104,000 background points (pseudo-absences), 100,000 for the present and 1,000 for each past time slice, acknowledging that the fossil records may be unrepresentative of the past distribution of the species (i.e., the species may have been present in areas where fossils did not form/have not been discovered). We randomly selected points from each time slice for model training (~ 80% of points) and testing (~ 20% of points). Model training was based on 36 presence

records and 46,376 absences/pseudo-absences. We used 7 presence records and 11,594 pseudo-absence points for model evaluation. We evaluated six models, differing in their error distributions and link functions, and conducted all subsequent analyses on the model with a binomial error distribution and logistic link function based on its area under the receiver operating characteristic curve (Fielding and Bell 1997). For each time slice, we transformed the output of the model to a presence/absence matrix, based on a threshold that maximizes sensitivity (true positive rate) and specificity (true negative rate) (Liu et al. 2016). We then calculated the surface of the area where the species was estimated to be present.

We visualized the niche overlap between the contemporary and fossil records of *V. komodoensis* by performing PCA on the dataset used for GLM training and using the niceOverPlot function (Fernández-López 2017) in R 3.5.3 (R Core Team 2019). Using the same dataset, we employed the 'ecospat 3.0' (Di Cola et al. 2017) R package to estimate Schoener's *D* (Schoener 1968) and Warren's *I* (Warren et al. 2008) and to conduct a niche equivalency test (Schoener 1968).

Supplementary Discussion

Diversification of the large Australasian monitors clade

Our results suggest that the LAMc originated during the Middle Miocene in northern Sahul, understood as the area comprising northern Australia and southern New Guinea (Figs. 4, S6–S7). Northern portions of present-day New Guinea likely remained as isolated islands for much of the Cenozoic, while southern New Guinea has been more stable as part of the Australian craton (Toussaint et al. 2014). Thus, if the LAMc was distributed in New Guinea early in its evolutionary history, it seems likely that it was in the south and this is in agreement with our results (Figs. 4, S6–S7). The LAMc belongs to a clade that also includes the predominantly Australian subgenus *Odatria* (Brennan et al. 2021), a diverse group of small-sized monitors. The ancestors of both subgenera likely invaded the Australopapuan region from southeast Asia (Vidal et al. 2012; Brennan et al. 2021). Thus, it seems reasonable that early in their evolutionary history the LAMc occupied the northern portion of Sahul that is closer to Asia. Our age estimate for the most recent common ancestor (MRCA) of the LAMc and *Odatria* is roughly consistent with the age of the earliest varanid fossils from Australia, coming from the Oligocene-Miocene boundary of central (Estes 1984) and north-central Australia (Scanlon 2014). The taxonomic affinities of these fossils are uncertain. Given our divergence time

estimates, they could represent an early member of either subgenus or a stem representative of the LAMc + *Odatria* lineage.

Vicariance was probably responsible for the split between *V. salvadorii* and the remaining members of the LAMc, with the latter former becoming restricted to southern New Guinea and the latter to northern Australia (Figs. 4, S6–S7). The *V. salvadorii* lineage likely persisted in the part of the Australian craton that is now southern New Guinea, before spreading to other parts of New Guinea as accretion occurred later in the Miocene (Tallowin et al. 2014; Toussaint et al. 2014). Presently, *V. salvadorii* does not occur in Australia. This may seem surprising, given that Australia and New Guinea have been intermittently connected as recently as 17,000 years ago (Pepper et al. 2017). In fact, *Varanus panoptes* likely invaded New Guinea during one of those episodes in the Pleistocene (Figs. 4, S6–S7). However, *V. emeritus* from the Pleistocene of southeastern Queensland is remarkably similar to *V. salvadorii* (Molnar 2004). Furthermore, while the phylogenetic position of the extinct *V. priscus* within the LAMc is uncertain, it is sometimes recovered as sister to *V. salvadorii* (Brennan et al. 2021). Thus, persistence or re-invasion of Australia by *V. salvadorii* or a close relative posteriorly to the Middle Miocene cannot be ruled out.

We dated most remaining speciation events in the LAMc to the Middle and Late Miocene (Figs. 1, S3), except for the split between *V. gouldii* and *V. panoptes* in the Pliocene. Later stages of the Miocene were characterized in Australia by a sharp increase in aridity that fragmented mesic habitats, dictating diversification dynamics across several taxa (Martin 2006; Byrne et al. 2008, 2011; Brennan and Oliver 2017; Brennan and Keogh 2018). Diversification of the LAMc appears to have primarily occurred in central or north-central Australia. Our biogeographic analyses based on discrete areas support that it occurred primarily in the north, in the region occupied today by tropical grasslands. The ‘rase’ analyses suggest that several speciation events occurred farther south, in the present day transition zone between arid and tropical environments (Figs. 1, 4, S6–S7). This region may have experienced a dynamic history of environmental mosaicism as the continent aridified, promoting diversification. Recent research has also recognized the importance of the highlands in the arid-tropical transition zone for lineage persistence, which supported pockets of mesic habitat that served as refugia (Morton et al. 1995; Fujita et al. 2010; Oliver et al. 2014). Even today, five species belonging to the LAMc are distributed in the region and come into contact in the Selwyn Range, along the northern border between the Northern Territory and Queensland (Fig. 1).

Ecological speciation may have also played an important role in the diversification of the LAMc, given that most speciation events in the LAMc appear to have occurred within

the Australian tropical grasslands and that there is broad overlap in the present distributions of the members of the LAMc (Fig. 1). In fact, interspecific interactions appear to have influenced body size evolution in Australian monitors (Brennan et al. 2021). The ecological disparity between some sister species is remarkable given their relatively recent divergence: *V. varius* is heavily arboreal, its sister *V. komodoensis* is terrestrial and considerably larger; *V. mertensi* is medium-sized and semi-aquatic, its sister *V. giganteus* is terrestrial and large (Auffenberg 1981; Pianka and King 2004; Cogger 2014). Conclusive evidence for sympatric speciation remains elusive (Martin et al. 2015), but Australian monitors seem to be a suitable model to address this issue.

Systematics of the large australasian monitors clade

The phylogeny of the LAMc supported by the AHE data differs from that recovered in other studies using nuclear data (Vidal et al. 2012; Pyron et al. 2013; Lin and Wiens 2017), which may have been misled by a combination of ILS and introgression. This highlights how phylogenetic studies can benefit from using a large number of loci and accounting for ILS and reticulation. In our study, ILS seems to be solely responsible for the discordance between the mitochondrial and species trees.

All members of the LAMc except for *V. salvadorii* have been historically assigned to the subgenus *Varanus* (Böhme 2003; Bucklitsch et al. 2016). Our own mitochondrial trees and previous studies based on fewer loci suggest that *V. salvadorii* is nested within the subgenus *Varanus*. Despite the seeming paraphyly of the subgenus *Varanus* with respect to *V. salvadorii*, the monotypic subgenus *Papusaurus* is commonly used in the literature to accommodate the latter species (Böhme 2003; Bucklitsch et al. 2016). However, our analyses of the AHE dataset support the monophyly of the subgenus *Varanus* with respect to *Papusaurus*. Thus, the future use of *Papusaurus* is justified, especially considering the ecological and morphological distinctness of *V. salvadorii* (Fig. 3).

Our sampling allows us to discern patterns of infraspecific genetic structure in *V. gouldii* and *V. panoptes*. Our results do not support the reciprocal monophyly of the subspecies of *V. gouldii*: *V. g. flavirufus* from the Australian arid zone and *V. g. gouldii* from semiarid, mesic, and tropical regions of Australia (Fig. S3). This species is remarkable for the degree of colour variation exhibited throughout its range and may represent a species complex (Storr 1980; Thompson 2004; Cogger 2014). On the other hand, *V. panoptes horni* from southern New Guinea renders *V. p. panoptes* from northern Australia paraphyletic, while *Varanus p. rubidus* from northwestern Western Australia appears to be more divergent (Fig. S3). This is consistent with studies in other taxa showing that the divergence between northern Australian and southern New Guinean

populations is fairly shallow (Pepper et al. 2017; Natusch et al. 2020). Furthermore, we found evidence of mitochondrial introgression between *V. gouldii* and *V. panoptes*, which could be expected given their close relationship and broad sympatry. However, there is no locality data for the mtDNA samples of *V. gouldii* that are nested within *V. panoptes* (Fig. S4) and the taxonomic identity of the associated individuals could not be morphologically verified. Dense geographic sampling seems necessary to resolve the taxonomy of *V. gouldii* and *V. panoptes*.

Evolutionary history of the Komodo dragon

Sheltered in remote islands of the Indonesian archipelago, the emblematic Komodo dragon was formally described in the early 20th century (Ouwens 1912), more than 150 years after the beginning of formal taxonomy. Since then, its evolution and natural history have generated widespread interest. Traditionally, the large size of *V. komodoensis* has been attributed to either insular giantism or to specialization for preying on extinct dwarf elephants of the genus *Stegodon*, which inhabited the Lesser Sundas during the Pleistocene (Auffenberg 1981). However, the earliest fossils assignable to *V. komodoensis* come from north-eastern Australia and already show the characteristic large size of this species (Hocknull et al. 2009). Furthermore, other extinct and extant members of the LAMc attain large sizes close to 2 m, including the sister species of the Komodo dragon, *V. varius*. This suggests that the large size of *V. komodoensis* could be better explained by phyletic giantism (Hocknull et al. 2009), possibly coupled with the effects of interspecific competition with other monitors in the diverse monitor communities of northern Australia. Competition appears to have had a major role in body size divergence among Australian varanids (Brennan et al. 2021).

Most of our biogeographic analyses include northern Australia as part of the Komodo dragon's ancestral range. Taken together, our results suggest that *V. komodoensis* diverged from *V. varius* during the Late Miocene (~ 8 Ma), originating in the northern half of Australia, likely in the continent's north-east given the fossil evidence (Fig. 4; Hocknull et al. 2009). From there, the Komodo dragon expanded its range westward, hybridizing with an ancestor of sand monitors somewhere in northern Australia during the Miocene, then crossing Weber's line and reaching Flores ~900 thousand years ago (ka) (Hocknull et al. 2009). Flores and Komodo have probably been isolated from other land masses for all of the Quaternary, maybe since the Cretaceous (Auffenberg 1980; van den Bergh et al. 2001). Thus, the arrival of the Komodo dragon likely involved overwater dispersal aided by low sea levels (van den Bergh et al. 2001; Hocknull et al. 2009). Fossil remains suggest that the species may have crossed Wallace's line reaching Java during the

middle Pleistocene, but it has not been possible to confirm the fossils' taxonomic identity (Hocknull et al. 2009).

There is ongoing debate about the relative importance of human arrival and climate change in Australian megafaunal extinctions (Wroe et al. 2013; Hocknull et al. 2020). While our models suggest that the Komodo dragon could have inhabited Sahul as recently as the Holocene (Fig. S8), the most recent confidently identified fossils have been dated to ~330 thousand years old (kyr), with a possibly younger record of ~150 kyr from Marmor Quarry (Hocknull 2005; Hocknull et al. 2009; Price et al. 2009; Price et al. 2015). However, fossils of varanids within the size range of *V. komodoensis* have been recovered from ~50 kyr deposits in eastern Australia, within the time frame of human arrival (Price et al. 2015).

The biotic interactions that *V. komodoensis* has experienced throughout its history merit special attention. The Komodo dragon is a relict of faunal assemblages that included other vertebrates remarkable for their size and ecology. The Komodo dragon was contemporary with other members of the Australian megafauna, some of which were the original prey of *V. komodoensis*, but also large marsupial carnivores of the families Thylacinidae and Thylacoleonidae, giant madtsoiid snakes, and terrestrial mekosuchine crocodilians (Scanlon 2014). The coexistence with marsupial predators may be explained by differences in activity times: monitors are diurnal and marsupials are mainly crepuscular or nocturnal (Brennan et al. 2021). The coexistence with other large reptilian predators is superficially more surprising, but ecosystems are able to sustain large numbers of ectotherms, which have lower energetic requirements than endotherms (Currie and Fritz 1993). Today, the Komodo dragon is only sympatric with one other monitor species, the large *V. salvator*. However, in Australia, *V. komodoensis* coexisted with other varanids including the giant megalania, *V. priscus* (Hocknull 2009). Thus, character displacement could help explain the colossal size of *V. priscus*, considering that smaller size categories were probably already represented by *V. komodoensis*, *V. varius*, sand monitors, and the dwarf monitors of the subgenus *Odatria*. After colonizing the Indonesian archipelago, the Komodo dragon may have also coexisted with two extinct species of large monitor in the Sunda Islands, *V. bolkayi* from Java and *V. hooijeri* from Flores (Molnar 2004). In Flores, *V. komodoensis* also coexisted with the small *Homo floresiensis*, which could have been prey, but also either hunted or scavenged the lizards (van den Bergh et al. 2009). The Komodo dragon also found new prey items in the form of *Stegodon*, giant tortoises, and/or large scavenging birds (Auffenberg 1981; van den Bergh et al. 2001; Shine and Somaweera 2019). Following their extinction ~50 ka, there was a long period where large prey items wouldn't be available for the Komodo dragon until the human-mediated introduction of large mammals ~10 ka (Shine and Somaweera 2019), which presently constitute the bulk of the dragon's diet (Auffenberg

1981). A combination of biotic and abiotic circumstances coupled with the lizard's behavioral, developmental, and ecological flexibility likely enabled it to survive during this period (Shine and Somaweera 2019).

In Wallacea, the Komodo dragon survived the arrival of a group of animals known for its ability to dramatically alter its environment and promote species extinction: hominids. The appearance of hominid artifacts in Flores ~800 ka coincides with a major faunal turnover, with the Komodo dragon being the sole survivor among terrestrial tetrapods (van den Bergh et al. 2001). *Homo floresiensis* first appeared in Flores ~190 ka and then was replaced by modern humans ~50 ka (Sutikna et al. 2016). This evidences the lizard's ability to coexist with hominids to a certain degree. However, our results suggest that the distribution of *V. komodoensis* is constrained by climate and that its realized niche has remained relatively stable through time. Our niche models suggest that the past climatic niche of *V. komodoensis* overlaps with its current niche. Furthermore, the climate of northern Australia during the Miocene appears to have been more arid but still monsoonal (Herold et al. 2011), a type of climate still preferred by the species today (Auffenberg 1981).

The introduction of *V. komodoensis* into Australia has been suggested before, originally as an ecological substitute of the extinct *V. priscus* (Flannery 1994) and later as a return of the Komodo dragon to its original range (Scanlon 2014). Considering the dragon's vulnerability to the current climate emergency (Jones et al. 2020), this possibility may need to be considered to ensure the survival of the species. Lundgren et al. (2020) showed that introduced herbivores can restore late Pleistocene ecological functions. The return of a species to its original range may seem even more justifiable, but there needs to be careful consideration regarding the public's response, the ecological impact that a top predator may have on a community whose composition has changed since the last time the species was part of it, the availability of suitable habitat, and the chances of establishing a breeding population given the current Australian climate. Regardless of the exact timing of the Komodo dragon's extinction in Australia, our models suggest that current climatic conditions in Australia are not optimal for the species.

Unfortunately, the survival of the Komodo dragon is threatened by prey poaching, habitat loss, and illegal trafficking (Ciofi et al. 1999; Daley 2019). This is particularly alarming because this lizard's small geographic range and trophic position as an apex predator make it especially vulnerable (Cardillo et al. 2004). Furthermore, while a role for human activities in the extirpation of *V. komodoensis* from Australia cannot be ruled out, our results suggests that climate change was a major factor and that colonisation of Wallacea allowed the species to persist, evidencing the vulnerability of this species to

climate change. Jones et al. (2020) used climate and demographic modelling to project the range and abundance of the Komodo dragon into the future, predicting a dramatic reduction in its range and abundance. Thus, protecting the current habitat of *V. komodoensis* from direct disturbance may not be enough to secure the future persistence of the species. With well-conserved habitat becoming increasingly rare in the Indonesian archipelago (Margono et al. 2014), dispersal may not save this iconic reptile from the current climate crisis.

Supplementary Figures

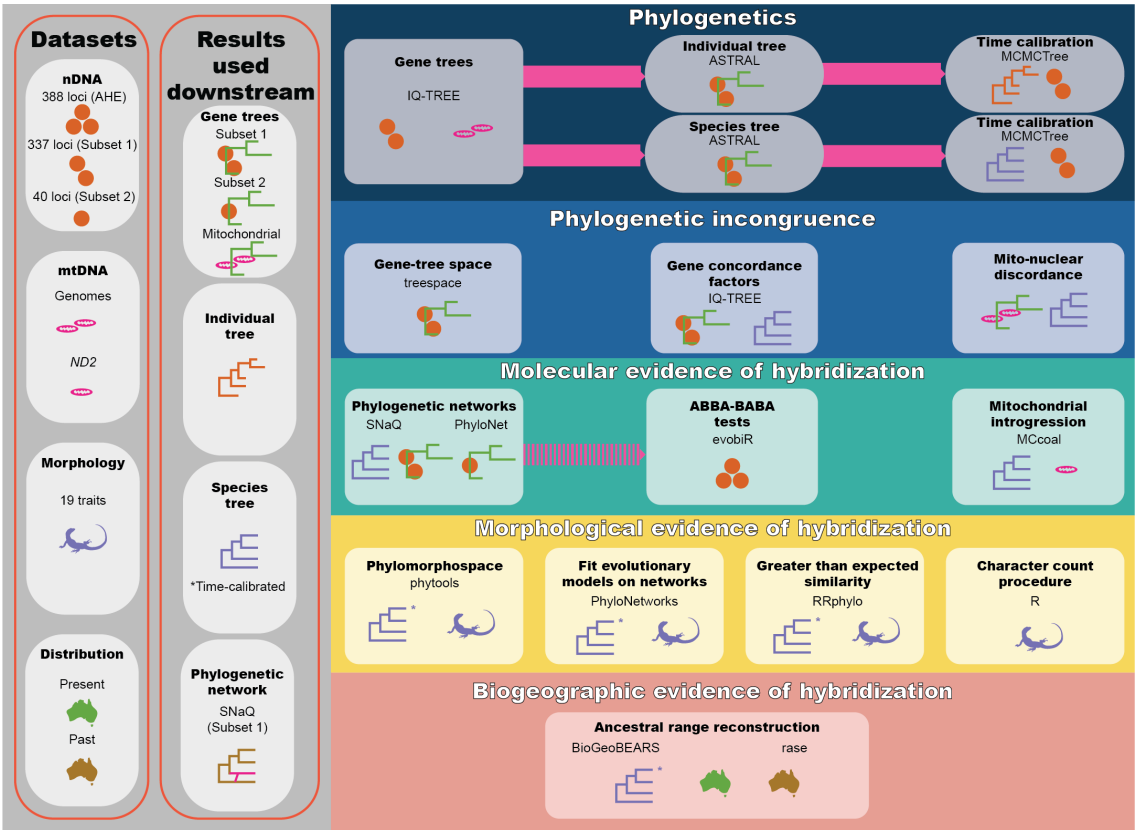

Figure S1. Summary of the approach implemented here to detect ancient hybridization in the LAMc. Data transformation and filtering procedures are not shown. Major stages of the approach are shown in the coloured panels. Individual analyses, the software used to perform them, and the data and results of previous analyses necessary to run each analysis are shown within each panel. Broad solid pink arrows indicate results that are used as input for other analyses in the same stage, while broad dashed pink arrows indicate results that informed the design of other analyses (post-hoc tests).

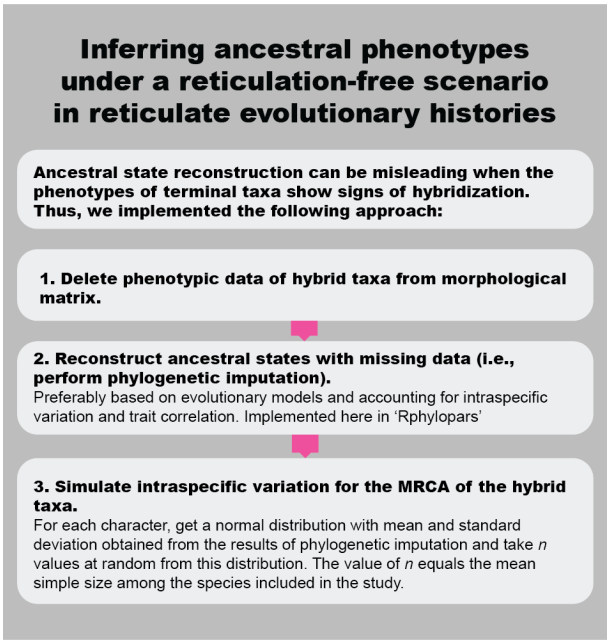

Figure S2. Summary of the general approach used to infer the ancestral morphology of sand monitors under a reticulation-free scenario.

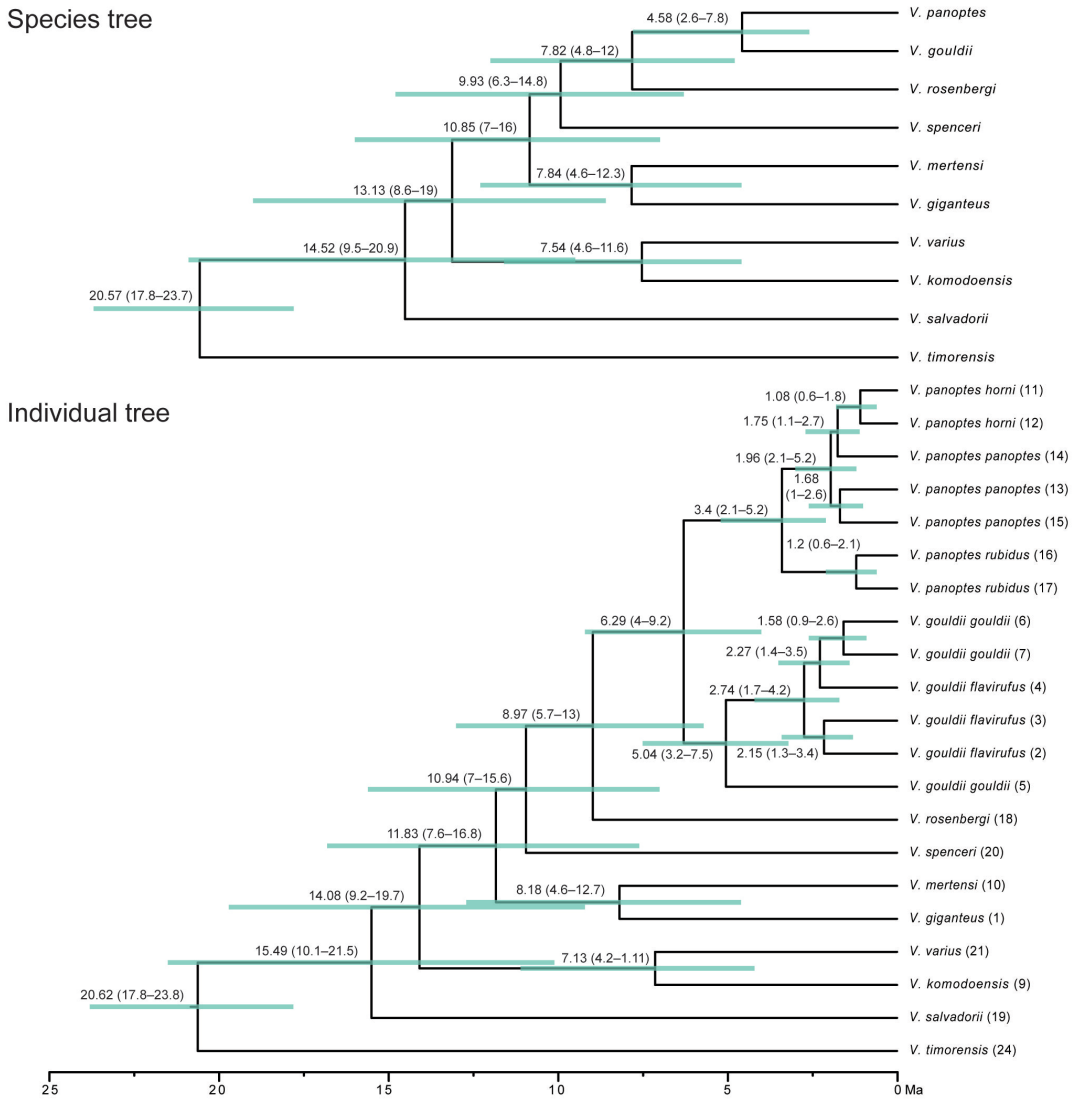

Figure S3. Divergence times in the large Australasian monitors clade (LAMc). Blue bars represent the 95% confidence interval (CI) for divergence dates. Numbers in nodes indicate the mean for the divergence times with the 95% CI in parentheses. Samples in the individual tree are numbered following Table S1.

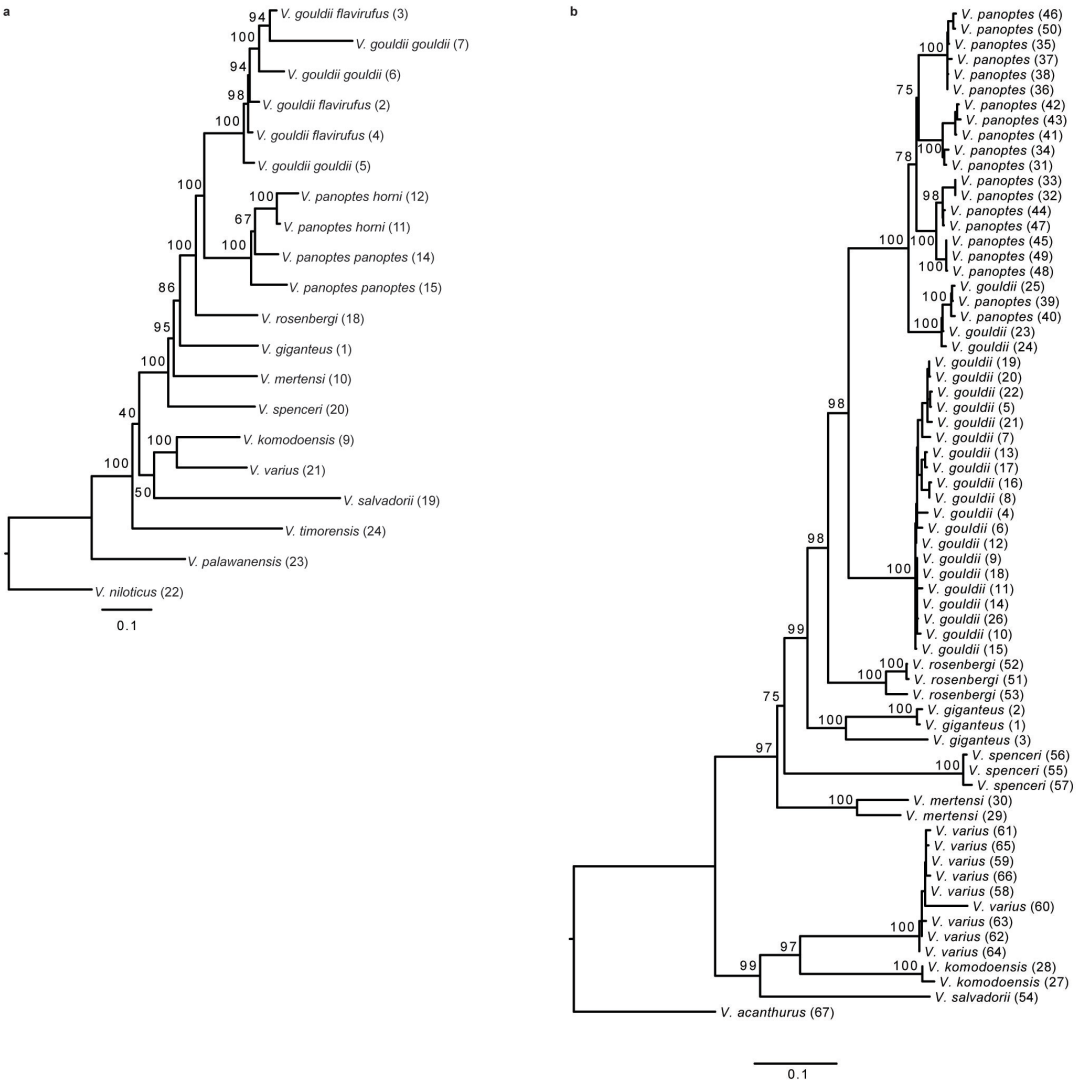

Figure S4. Mitochondrial phylogeny of the LAMc. a) Tree based on the mitochondrial genomes; sample numbering follows Table S1; numbers at nodes are ultrafast bootstrap values; the scale bar represents substitutions per branch length unit. b) Tree based on the NADH dehydrogenase subunit 2 gene (*ND2*); sample numbering follows Table S2; numbers at nodes are ultrafast bootstrap values; the scale bar represents substitutions per branch length unit.

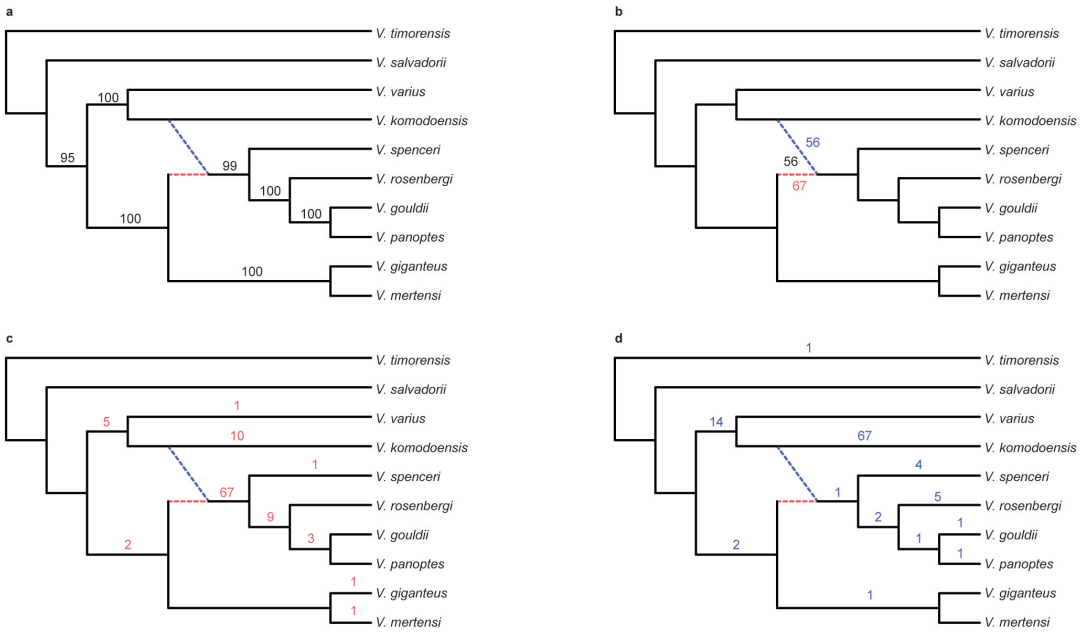

Figure S5. Bootstrap support for the network of Subset 1 obtained with SNaQ. a) Bootstrap values of tree edges. b) Bootstrap values of major hybrid edge (red), minor hybrid edge (blue), and the reticulation event (black). c) Proportion of bootstrap networks where each internal/terminal node appears as the hybrid lineage. d) Proportion of bootstrap networks where each internal/terminal node appears as the source of gene flow.

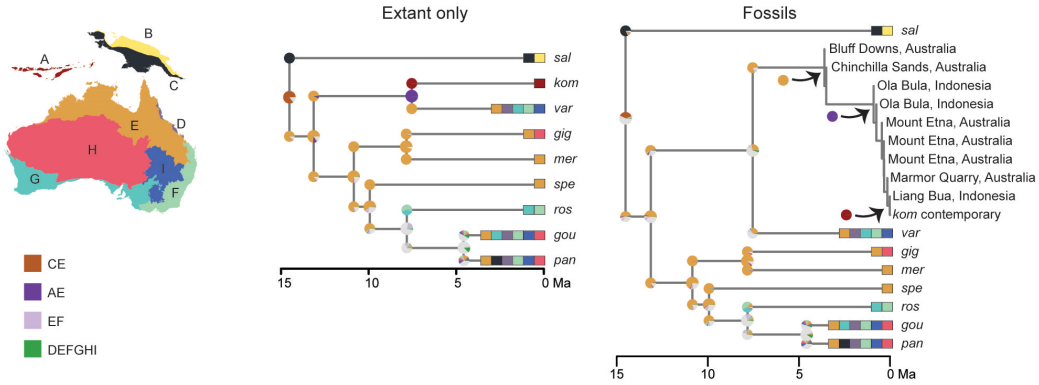

Figure S6. Ancestral range reconstruction of the LAMc using 'BioGeoBears' based on contemporary records only and including fossil records of *V. komodoensis*. Grey was used for ranges encompassing more than one area and not found in the maximum likelihood estimates presented in Fig. 4.

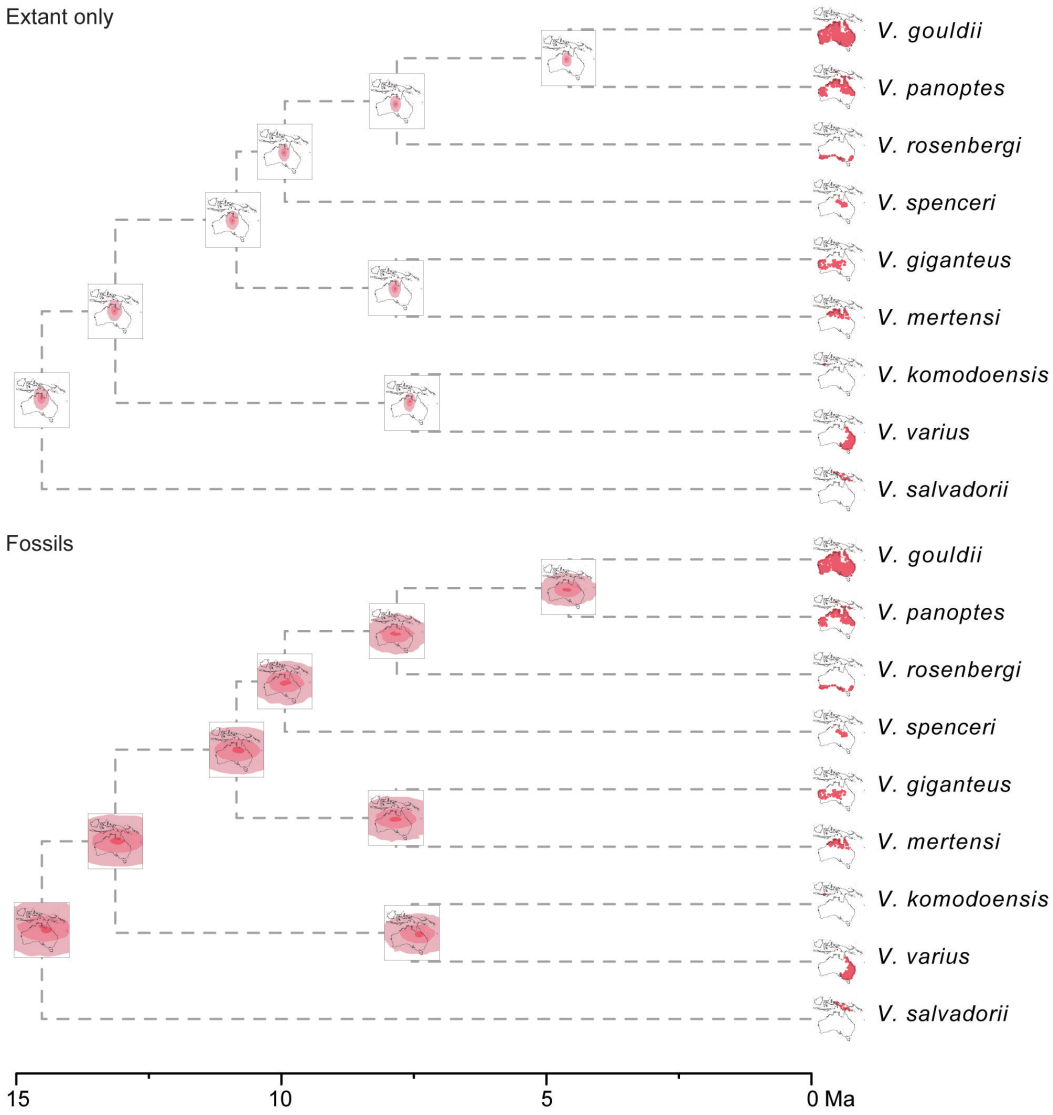

Figure S7. Ancestral range reconstruction of the LAMc using 'rase' based on contemporary records only and including fossil records of *V. komodoensis*. Different shades of red are used for 5% (darkest), 50%, and 95% (lightest) posterior kernel density. Note that including fossils increases uncertainty, but results in ancestral range estimates that are more congruent with the fossil record in *V. komodoensis*.

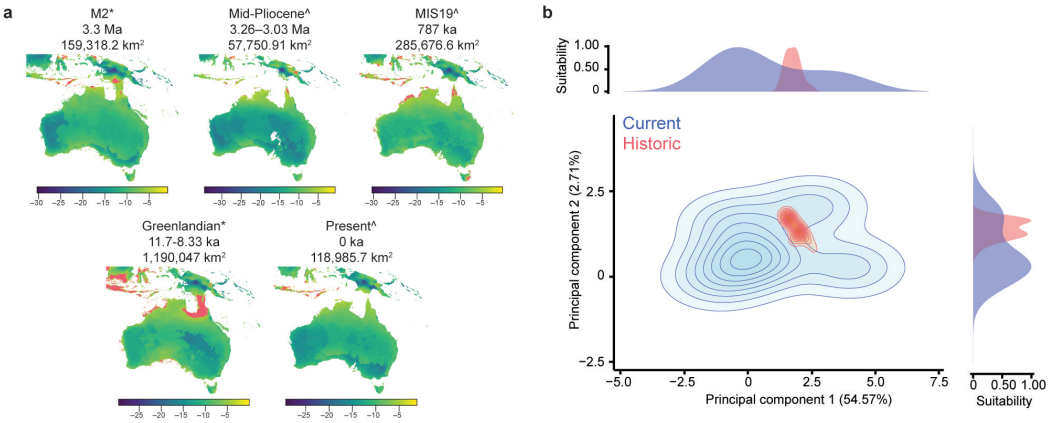

Figure S8. Climatic niche modelling in *V. komodoensis*. a) Suitable area for the Komodo dragon through time based on its realised climatic niche and inferred from contemporary and fossil records; an asterisk (*) and a carat (^) are used for cold and warm periods, respectively; colour denotes suitability, with red areas indicating presence and the surface of the presence area indicated to the right. b) Principal component analysis of climatic data for fossil and contemporary records of *V. komodoensis*; contour lines, shading, and histograms indicate suitability along the climatic space.

Supplementary References

*Includes references in supplementary tables.

Adams D.C., Otárola-Castillo E. 2013. geomorph: an R package for the collection and analysis of geometric morphometric shape data. Methods Ecol. Evol. 4:393–399.

Atlas of Living Australia. 2019. Available from: http://www.ala.org.au (accessed 1 April 2019).

Auffenberg W. 1980. The herpetofauna of Komodo, with notes on adjacent areas. B. Florida St. Mus. Biol. Sci. 25: 37–158.

Auffenberg W. 1981. The behavioral ecology of the Komodo monitor. Gainesville: University Presses of Florida.

Böhme W. 2003. Checklist of the living monitor lizards of the world (family Varanidae). Zool. Verhandelingen 341:3–43.

Böhme W. 1988. Der Arguswaran (*Varanus panoptes* Storr, 1980) auf Neuguinea: *V. panoptes horni* ssp. n. Salamandra 24:87–101.

Brennan I.G., Keogh J.S. 2018. Miocene biome turnover drove conservative body size evolution across Australian vertebrates. Proc. R. Soc. B 285:20181474.

Brennan I.G., Lemmon A.R., Lemmon E.M., Portik D.M., Weijola V., Welton L., Donnellan S.C., Keogh J.S. 2021. Phylogenomics of monitor lizards and the role of competition in dictating body size disparity. Syst. Biol. 70:120–132.

Brennan I.G., Oliver P.M. 2017. Mass turnover and recovery dynamics of a diverse Australian continental radiation. Evolution 71:1352–1365.

Brown J.L., Hill D.J., Dolan A.M., Carnaval A.C., Haywood A.M. 2018. PaleoClim, high spatial resolution paleoclimate surfaces for global land areas. Sci. Data. 5:180254.

Bucklitsch Y., Boehme W., Koch A. 2016. Scale morphology and micro-structure of monitor lizards (Squamata: Varanidae: *Varanus* spp.) and their allies: implications for systematics, ecology, and conservation. Zootaxa 4153:1–192.

Byrne M., Steane D.A., Joseph L., Yeates D.K., Jordan G.J., Crayn D., Aplin K., Cantrill D.J., Cook L.G., Crisp M.D., Keogh J.S., Melville J., Moritz C., Porch N., Sniderman J.M.K., Sunnucks P., Weston P.H. 2011. Decline of a biome: evolution, contraction, fragmentation, extinction and invasion of the Australian mesic zone biota. J. Biogeogr. 38:1635–1656.

Byrne M., Yeates D.K., Joseph L., Kearney M., Bowler J., Williams M.A., Cooper S., Donnellan S.C., Keogh J.S., Leys R., Melville J., Murphy D.J., Porch N., Wyrwoll K.H. 2008. Birth of a biome: insights into the assembly and maintenance of the Australian arid zone biota. Mol. Ecol. 17:4398–4417.

Cardillo M., Purvis A., Sechrest W., Gittleman J.L., Bielby J., Mace G.M. 2004. Human population density and extinction risk in the world's carnivores. PLoS Biol. 2:e197.

Cardillo M., Weston P.H., Reynolds Z.K.M., Olde P.M., Mast A.R., Lemmon E.M., Lemmon A.R., Bromham L. 2017. The phylogeny and biogeography of *Hakea* (Proteaceae) reveals the role of biome shifts in a continental plant radiation. Evolution 71:1928–1943.

Castiglione S., Serio C., Tamagnini D., Melchionna M., Mondanaro A., Di Febbraro M., Profico A., Piras P., Barattolo F., Raia P. 2019. A new, fast method to search for morphological convergence with shape data. PLoS ONE 14:e0226949.

Castiglione S., Tesone G., Piccolo M., Melchionna M., Mondanaro A., Serio C., Di Febbraro M., Raia P. 2018. A new method for testing evolutionary rate variation and shifts in phenotypic evolution. Methods Ecol. Evol. 2018:181–10.

Ciofi C., Beaumont M.A., Swingland I.R., Bruford M.W. 1999. Genetic divergence and units for conservation in the Komodo dragon *Varanus komodoensis*. Proc. R. Soc. Lond. B 66:2269–2274.

Cogger H.G. 2014. Reptiles & amphibians of Australia. Collingwood: CSIRO publishing.

Currie D.J., Fritz J.T. 1993. Global patterns of animal abundance and species energy use. Oikos 67:56–68.

Daley J. 2019. Indonesia considers closing Komodo Island because poachers keep stealing the dragons. Available from: https://www.smithsonianmag.com/smart-news/there-be-no-dragons-indonesia-considers-closing-komodo-island-tourists-180971877/.

Dawson L., Muirhead J., Wroe S. 1999. The Big Sink Fauna: a lower Pliocene mammalian fauna from the Wellington Caves complex, Wellington, New South Wales. Rec. West. Aust. Mus. Supp. 57:265–290.

Di Cola V., Broennimann O., Petitpierre B., Breiner F.T., D'Amen M., Randin C., Engler R., Pottier J., Pio D., Dubuis A., Pellissier L., Mateo R.G., Hordijk W., Salamin N., Guisan A. 2017. Ecospat: an R package to support spatial analyses and modeling of species niches and distributions. Ecography 40:774–787.

Dolan A.M., Haywood A.M., Hunter S.J., Tindall J.C., Dowsett H.J., Hill D.J., Pickering S.J. 2015. Modelling the enigmatic Late Pliocene Glacial Event—Marine Isotope Stage M2. Global Planet. Change 128:47–60.

Edgar, R.C. 2004. MUSCLE: multiple sequence alignment with high accuracy and high throughput. Nucleic Acids Res. 32:1792–1797.

Estes R. 1984. Fish, amphibians and reptiles from the Etadunna Formation, Miocene of South Australia. Aust. Zool. 21:335–343.

Fernández-López J. 2017. NiceOverPlot, or when the number of dimensions does matter. Available from: https://allthiswasfield.blogspot.com.es/2017/05/niceoverplot-or-when-number-of.html.

Fielding A.H., Bell J.F. 1997. A review of methods for the assessment of prediction errors in conservation presence/absence models. Environ. Conserv. 24:38–49.

Flannery, T. 1994. The future eaters: an ecological history of the Australasian lands and people. Port Melbourne: Reed Books.

Fordham D.A, Saltré F., Haythorne S., Wigley T.M.L., Otto-Bliesner B.L., Chan K., Brook B.W. 2017. PaleoView: a tool for generating continuous climate projections spanning the last 21 000 years at regional and global scales. Ecography 40:1348–1358.

Fujita M.K., McGuire J.A., Donnellan S.C., Moritz, C.M. 2010. Diversification at the arid-monsoonal interface: Australia-wide biogeography of the Bynoe's gecko (*Heteronotia binoei*; Gekkonidae). Evolution 64:2293–2314.

Goolsby E.W., Bruggeman J., Ané C. 2017. Rphylopars: fast multivariate phylogenetic comparative methods for missing data and within-species variation. Methods Ecol. Evol. 8:22–27.

Herold N., Huber M., Greenwood D.R., Müller R.D., Seton M. 2011. Early to Middle Miocene monsoon climate in Australia. Geology 39:3–6.

Hijmans R.J., Cameron S.E., Parra J.L., Jones P.G., Jarvis A. 2005. Very high resolution interpolated climate surfaces for global land areas. Int. J. Climatol. 25:1965–1978.

Hill D.J. 2015. The non-analogue nature of Pliocene temperature gradients. Earth Planet. Sc. Lett. 425:232–241.

Hocknull S.A. 2005. Ecological succession during the late Cainozoic of central eastern Queensland: extinction of a diverse rainforest community. Mem. Queensland Mus. 51:39–122.

Hocknull S.A., Piper P.J., van den Bergh G.D., Due R.A., Morwood M.J., Kurniawan I. 2009. Dragon's paradise lost: palaeobiogeography, evolution and extinction of the largest-ever terrestrial lizards (Varanidae). PLoS ONE 4:e724.

Hocknull S.A., Zhao J-X., Feng Y-X., Webb G.E. 2007. Responses of Quaternary rainforest vertebrates to climate change in Australia. Earth Planet. Sc. Lett. 264:317–331.

Horn H.-G., Sweet S.S., Philipp K.M. 2007. On the distribution of the Papuan monitor (*Varanus salvadorii* Peters & Doria, 1878) in New Guinea. Advances in Monitor Research III, Mertensiella 3:25–43.

Jombart T., Kendall M., Almagro-Garcia J., Colijn C. 2017. Treespace: statistical exploration of landscapes of phylogenetic trees. Mol. Ecol. Resour. 17:1385–1392.

Jones A.R., Jessop T.S., Ariefiandy A., Brook B.W., Brown S.C., Ciofi C., Jackson Benu Y., Purwandana D., Sitorus T., Wigley T.M.L., Fordham D.A. 2020. Identifying island safe havens to prevent the extinction of the World's largest lizard from global warming. Ecol. Evol. (in press).

Kalyaanamoorthy S., Minh B.Q., Wong T.K.F., von Haeseler A., Jermiin L.S. 2017. ModelFinder: fast model selection for accurate phylogenetic estimates. Nat. Methods 14:587–589.

Karimi N., Grover C.E., Gallagher J.P., Wendel J.F., Ané C., Baum D.A. 2020. Reticulate evolution helps explain apparent homoplasy in floral biology and pollination in baobabs (*Adansonia*; Bombacoideae; Malvaceae). Syst. Biol. 69:462–478.

Lanfear R., Frandsen P.B., Wright A.M., Senfeld T., Calcott B. 2016. PartitionFinder 2: new methods for selecting partitioned models of evolution for molecular and morphological phylogenetic analyses. Mol. Biol. Evol. 34:772–773.

Lemey P., Rambaut A., Welch J.J., Suchard M.A. 2010. Phylogeography takes a relaxed random walk in continuous space and time. Syst. Biol. 27:1877–1885.

Lin L., Wiens J.J. 2017. Comparing macroecological patterns across continents: evolution of climatic niche breadth in varanid lizards. Ecography 40:960–970.

Liu C., Newell G., White M. 2016. On the selection of thresholds for predicting species occurrence with presence-only data. Ecol. Evol. 6:337–348.

Lundgren E.J., Ramp D., Rowan J., Middleton O., Schowanek S.D., Sanisidro O., Carroll S.P., Davis M., Sandom C.J., Svenning J.-C., Wallach A.D. 2020. Introduced herbivores restore Late Pleistocene ecological functions. P. Natl. Acad. Sci. USA 117:7871–7878.

Mackness B.S., Whitehead P.W., McNamara G.C. 2000. New Potassium-Argon basalt date in relation to the Pliocene Bluff Downs Local Fauna, northern Australia. Aust. J. Earth Sci. 47:807–811.

Margono B.A., Potapov P.V., Turubanova S., Stolle F., Hansen M.C. 2014. Primary forest cover loss in Indonesia over 2000–2012. Nat. Clim. Change 4:730–735.

Martin, H.A. 2006. Cenozoic climatic change and the development of the arid vegetation in Australia. J. Arid Environ. 66:533–563.

Martin C.H., Cutler J.S., Friel J.P., Dening Touokong C., Coop G., Wainwright P.C. 2015. Complex histories of repeated gene flow in Cameroon crater lake cichlids cast doubt on one of the clearest examples of sympatric speciation. Evolution 69:1406–1422.

Matzke N.J. 2013. Probabilistic historical biogeography: new models for founder-event speciation, imperfect detection, and fossils allow improved accuracy and model-testing. Front. Biogeogr. 5:242–248.

Molina-Venegas R., Moreno-Saiz J.C., Castro Parga I., Davies T.J., Peres-Neto P.R., Rodríguez M.Á. 2018. Assessing among-lineage variability in phylogenetic imputation of functional trait datasets. Ecography 41:1740–1749.

Molnar R.E. 2004. The long and honorable history of monitors and their kin. In: Pianka E., King D., editors. Varanoid lizards of the world. Bloomington: Indiana University Press. p. 10–67.

Morton S.R., Short J., Barker R.D. 1995. Refugia for biological diversity in arid and semi-arid Australia. Canberra: Department of the Environment, Sport and Territories.

Nakagawa S., de Villemereuil P. 2019. A general method for simultaneously accounting for phylogenetic and species sampling uncertainty via Rubin's rules in comparative analysis. Syst. Biol. 68:632–641.

Natusch D.J.D., Esquerré D., Lyons J.A., Hamidy A., Lemmon A.R., Lemmon E.M., Riyanto A., Keogh J.S., Donnellan S. 2020. Species delimitation and systematics of the green pythons (*Morelia viridis* complex) of melanesia and Australia. Mol. Phylogenet. Evol. 142:106640.

Nguyen L-T., Schmidt H.A., von Haeseler A., Minh B.Q. 2015. IQ-TREE: a fast and effective stochastic algorithm for estimating maximum-likelihood phylogenies. Mol. Biol. Evol. 32:268–274.

Oliver P.M., Smith K.L., Laver R.J., Doughty P., Adams M. 2014. Contrasting patterns of persistence and diversification in vicars of a widespread Australian lizard lineage (the *Oedura marmorata* complex). J. Biogeogr. 41:2068–2079.

Olson D.M., Dinerstein E., Wikramanayake E.D., Burgess N.D., Powell G.V.N., Underwood E.C., D'amico J.A., Itoua I., Strand H.E., Morrison J.C., Loucks C.J., Allnutt T.F., Ricketts T.H., Kura Y., Lamoreux J.F., Wettengel W.W., Hedao P., Kassem K.R. 2001. Terrestrial ecoregions of the world: a new map of life on earth: a new global map of terrestrial ecoregions provides an innovative tool for conserving biodiversity. BioScience 51:933–938.

Ouwens P.A. 1912. On a large *Varanus* species from the island of Komodo. B. Jard. Bot. Buitenzorg 6:1–3.

Paradis E., Schliep K. 2018. Ape 5.0: an environment for modern phylogenetics and evolutionary analyses in R. Bioinformatics 35:526–528.

Pepper M., Hamilton D.G., Merkling T., Svedin N., Cser B., Catullo R.A., Pryke S.R., Keogh J.S. 2017. Phylogeographic structure across one of the largest intact tropical savannahs: molecular and morphological analysis of Australia's iconic frilled lizard *Chlamydosaurus kingii*. Mol. Phylogenet. Evol. 106:217–227.

Pianka E., King D, editors. 2004. Varanoid lizards of the world. Bloomington: Indiana University Press.

Plummer M., Best N., Cowles K., Vines K. 2006. CODA: convergence diagnosis and output analysis for MCMC. R News 6:7–11.

Price G.J., Zhao J.X., Feng Y.X., Hocknull S.A. 2009. New records of Plio-Pleistocene koalas from Australia: palaeoecological and taxonomic implications. Rec. Aust. Mus. 61:39–48.

Price G.J., Louys J., Cramb J., Feng Y., Zhao J., Hocknull S.A., Webb G.E., Nguyen A.D., Joannes-Boyau R. 2015. Temporal overlap of humans and giant lizards (Varanidae; Squamata) in Pleistocene Australia. Quaternary Sci. Rev. 125:98–105.

Pyron R.A., Burbrink F.T., Wiens J.J. 2013. A phylogeny and revised classification of Squamata, including 4161 species of lizards and snakes. BMC Evol. Biol. 13:93.

Quintero I., Keil P., Jetz W., Crawford F.W. 2015. Historical biogeography using species geographical ranges. Syst. Biol. 64:1059–1073.

R Core Team. 2019. R: A language and environment for statistical computing, Vienna, Austria. Available from: https://www.R-project.org/.

Rannala B., Yang Z. 2003. Bayes estimation of species divergence times and ancestral population sizes using DNA sequences from multiple loci. Genetics 164:1645–1656.

Revell L.J. 2012. Phytools: an R package for phylogenetic comparative biology (and other things). Methods Ecol. Evol. 3:217–223.

Sabaj M.H. 2016. Standard symbolic codes for institutional resource collections in herpetology and ichthyology: an online reference. Version 6.5 (16 August 2016). Available from: http://www.asih.org/.

Sastrawan P., Ciofi C. 2002. Distribution and home range. In: Murphy J.B., Ciofi C., de La Panouse C., Walsh T., editors. Komodo dragons: biology and conservation. Washington, D.C.: Smithsonian Institution Press. p. 42–77.

Scanlon, J.D. 2014. Giant terrestrial reptilian carnivores of Cenozoic Australia. In: Glen A.S., Dickman C.R., editors. Carnivores of Australia: past, present and future. Collingwood: CSIRO Publishing. p. 27–52.

Schoener T.W. 1968. The Anolis lizards of Bimini: resource partitioning in a complex fauna. Ecology 49:704–726.

Shine R., Somaweera R. 2019. Last lizard standing: the enigmatic persistence of the Komodo dragon. Global Ecol. Conserv. 18:e00624.

Solís-Lemus C., Ané C. 2016. Inferring phylogenetic networks with maximum pseudolikelihood under incomplete lineage sorting. PLoS Genet. 12:e1005896.

Solís-Lemus C., Bastide P., Ané C. 2017. PhyloNetworks: a package for phylogenetic networks. Mol. Biol. Evol. 34:3292–3298.

Stekhoven D.J., Bühlmann P. 2012. MissForest—non-parametric missing value imputation for mixed-type data. Bioinformatics 28:112–118.

Storr G.M. 1980. The monitor lizards (genus *Varanus* Merrem, 1820) of Western Australia. Rec. West. Aust. Mus. 8:237–293.

Sutikna T., Tocheri M.W., Morwood M.J., Saptomo E.W., Jatmiko, Awe R.D., Wasisto S., Westaway K.E., Aubert M., Li B., Zhao J., Storey M., Alloway B.V., Morley M.W., Meijer H.J.M., van den Bergh G.D., Grün R., Dosseto A., Brumm A., Jungers W.L., Roberts R.G. 2016. Revised stratigraphy and chronology for *Homo floresiensis* at Liang Bua in Indonesia. Nature 532:366–369.

Swenson N.G. 2014. Phylogenetic imputation of plant functional trait databases. Ecography 37:105–110.

Tallowin O.J.S., Tamar K., Meiri S., Allison A., Kraus F., Richards S.J., Oliver P.M. 2014. Early insularity and subsequent mountain uplift were complementary drivers of diversification in a Melanesian lizard radiation (Gekkonidae: *Cyrtodactylus*). Mol. Phylogenet. Evol. 125:29–39.

Thompson G. 2004. *Varanus gouldii*. In: Pianka E., King D., editors. Varanoid lizards of the world. Bloomington: Indiana University Press. p. 380–400.

Toussaint E.F., Hall R., Monaghan M.T., Sagata K., Ibalim S., Shaverdo H.V., Vogler A.P., Pons J., Balke M. 2014. The towering orogeny of New Guinea as a trigger for arthropod megadiversity. Nat. Comm. 5:1–10.

van den Bergh G.D., Awe R.D., Morwood M.J., Sutikna T., Jatmiko, Saptomo E.W. 2008. The youngest *Stegodon* remains in Southeast Asia from the Late Pleistocene archaeological site Liang Bua, Flores, Indonesia. Quat. Int. 182:16–48.

van den Bergh G.D., de Vos J., Sondaar P.Y. 2001. The Late Quaternary palaeogeography of mammal evolution in the Indonesian Archipelago. Palaeogeogr. Palaeocl. Palaeoecol. 171:385–408.

van den Bergh G.D., Meijer H.J., Due R.A., Morwood M.J., Szabo K., van den Hoek Ostende L.W., Sutikna T., Saptomo E.W., Piper P.J., Dobney K.M. 2009. The Liang Bua faunal remains: a 95 k.yr. sequence from Flores, East Indonesia. J. Hum. Evol. 57:527–537.

Vidal N., Marin J., Sassi J., Battistuzzi F.U., Donnellan S., Fitch A.J., Fry B.G., Vonk F.J., Rodriguez de la Vega R.C., Couloux A., Hedges S.B. 2012. Molecular evidence for an Asian origin of monitor lizards followed by Tertiary dispersals to Africa and Australasia. Biol. Lett. 8:853–855.

Warren D.L., Glor R.E., Turelli M. 2008. Climate niche identity versus conservatism: quantitative approaches to niche evolution. Evolution 62:2868–2883.

Wilson P. 1992. On inferring hybridity from morphological intermediacy. Taxon 41:11–23.

Wroe S., Field H., Archer M., Grayson D.K., Price G.J., Louys J., Faith J.T., Webb G.E., Davidson I., Mooney S.D. 2013. Climate change frames debate over the extinction of megafauna in Sahul (Pleistocene Australia-New Guinea). P. Natl. Acad. Sci. USA 110:8777–8781.

Yang Z. 2007. PAML 4: phylogenetic analysis by maximum likelihood. Mol. Biol. Evol. 24:1586–1591.

Yang Z. 2015. The BPP program for species tree estimation and species delimitation. Curr. Zool. 61:854–865.

Yu Y., Nakhleh L. 2015. A maximum pseudo-likelihood approach for phylogenetic networks. BMC Genomics 16:S10.

Zhang C., Rabiee M., Sayyari E., Mirarab S. 2018. ASTRAL-III: polynomial time species tree reconstruction from partially resolved gene trees. BMC Bioinformatics 19:153.

CHAPTER IV

Supplementary Figures

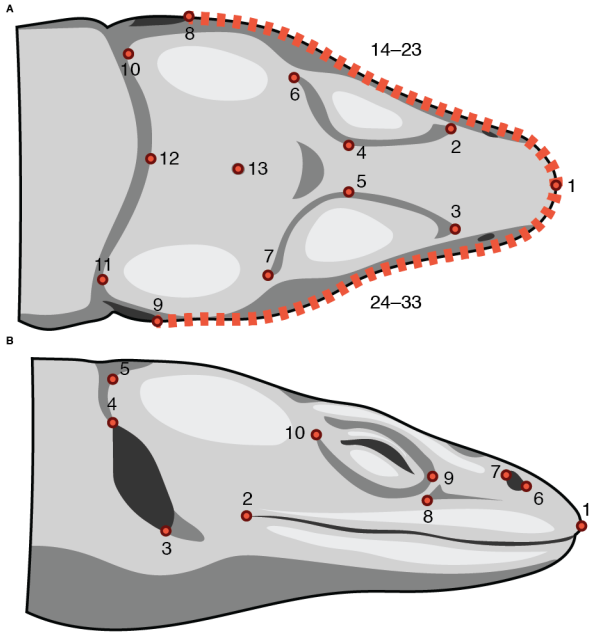

Figure S1. Landmark design used to characterize head shape in dorsal (top) and lateral (bottom) view. The dotted lines indicate sliding semi-landmarks.

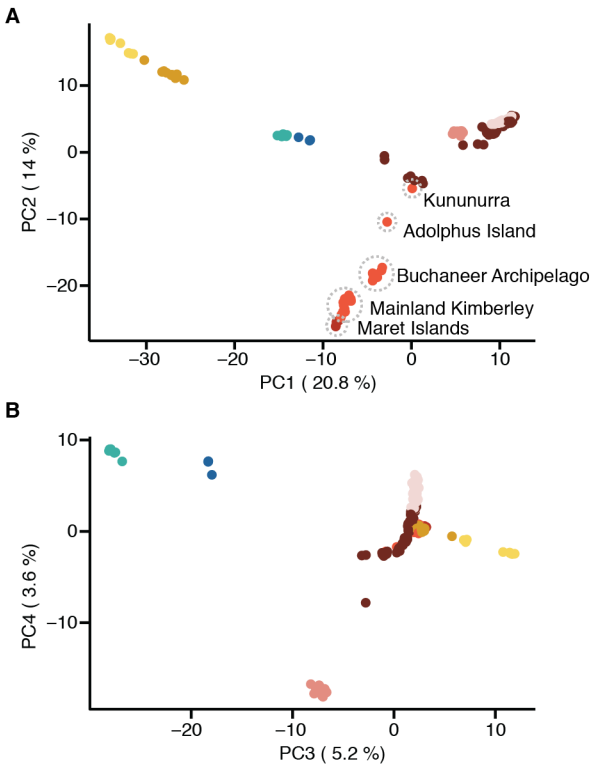

Figure S2. Principal component analysis of population SNP dataset. Colors follow Fig. 2. A) First and second principal components (PCs); clusters within the Kimberley and Maret Islands populations are indicated to highlight genetic structure in the islands of the Kimberley region. B) Third and fourth PCs.

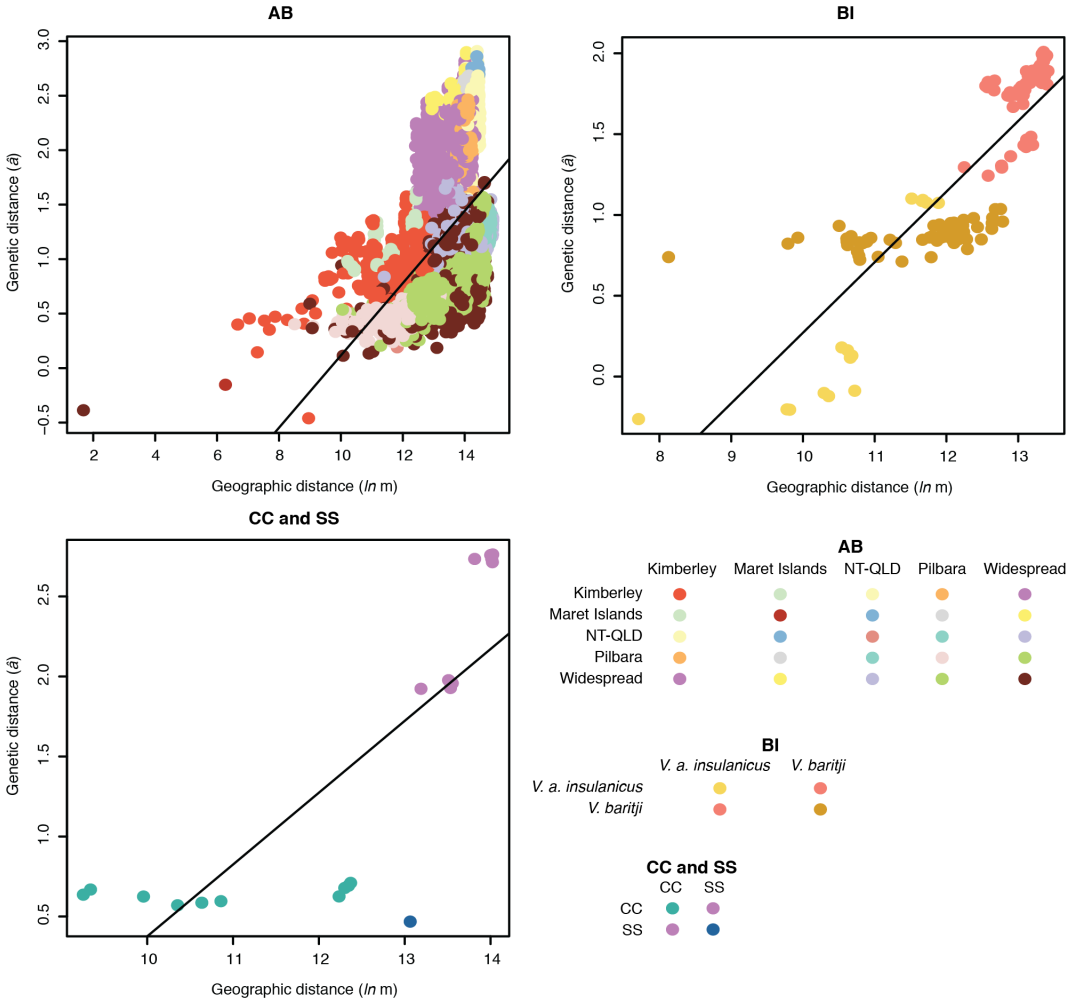

Figure S3. Isolation by distance within major population clusters. Colors are used to indicate the populations that are being compared according to the square matrices in the bottom right.

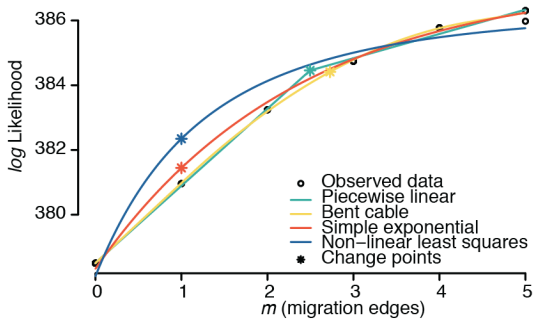

Figure S4. Likelihood of TreeMix runs with different values of *m* (migration edges) and regression under different models.

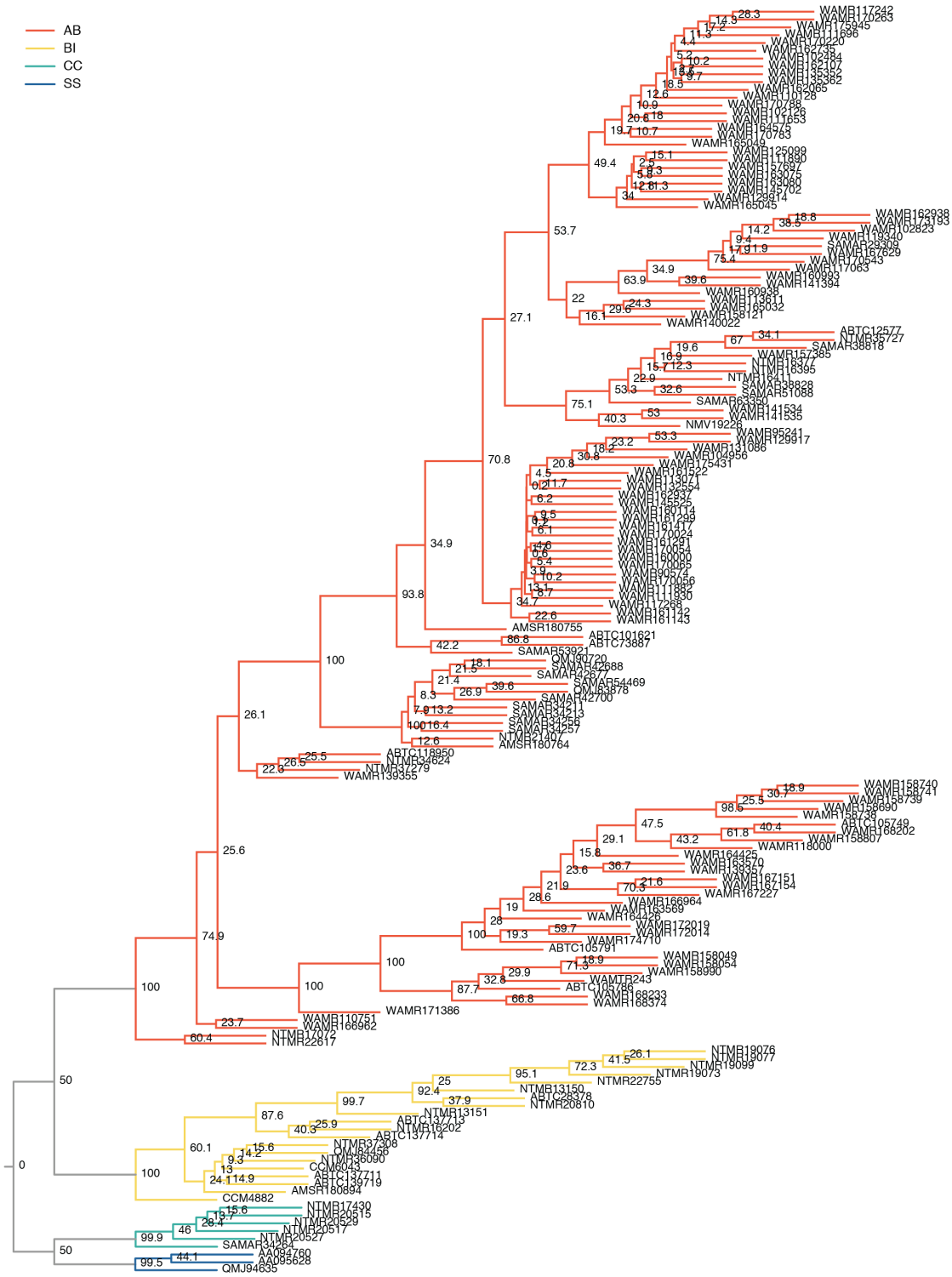

Figure S5. Individual-level nuclear tree obtained with SVDquartets. Numbers in nodes are bootstrap support values. ABTC stands for the Australian Biological Tissue Collection, and AA and CCM for field numbers. Other acronyms follow Sabaj (2019).

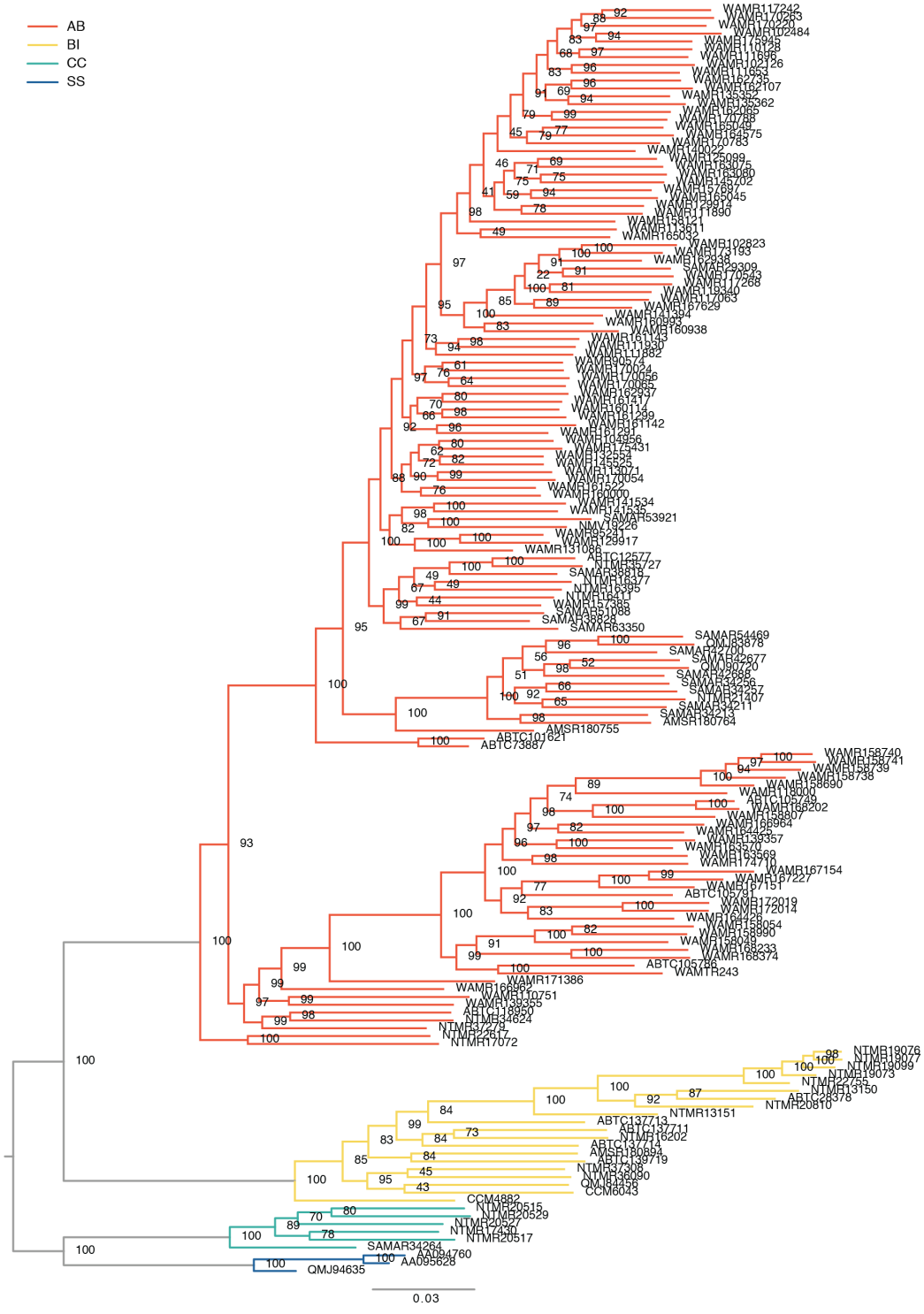

Figure S6. Individual-level nuclear tree obtained with IQ-TREE. Numbers in nodes are ultrafast bootstrap support values. Acronyms as in Fig. S5.

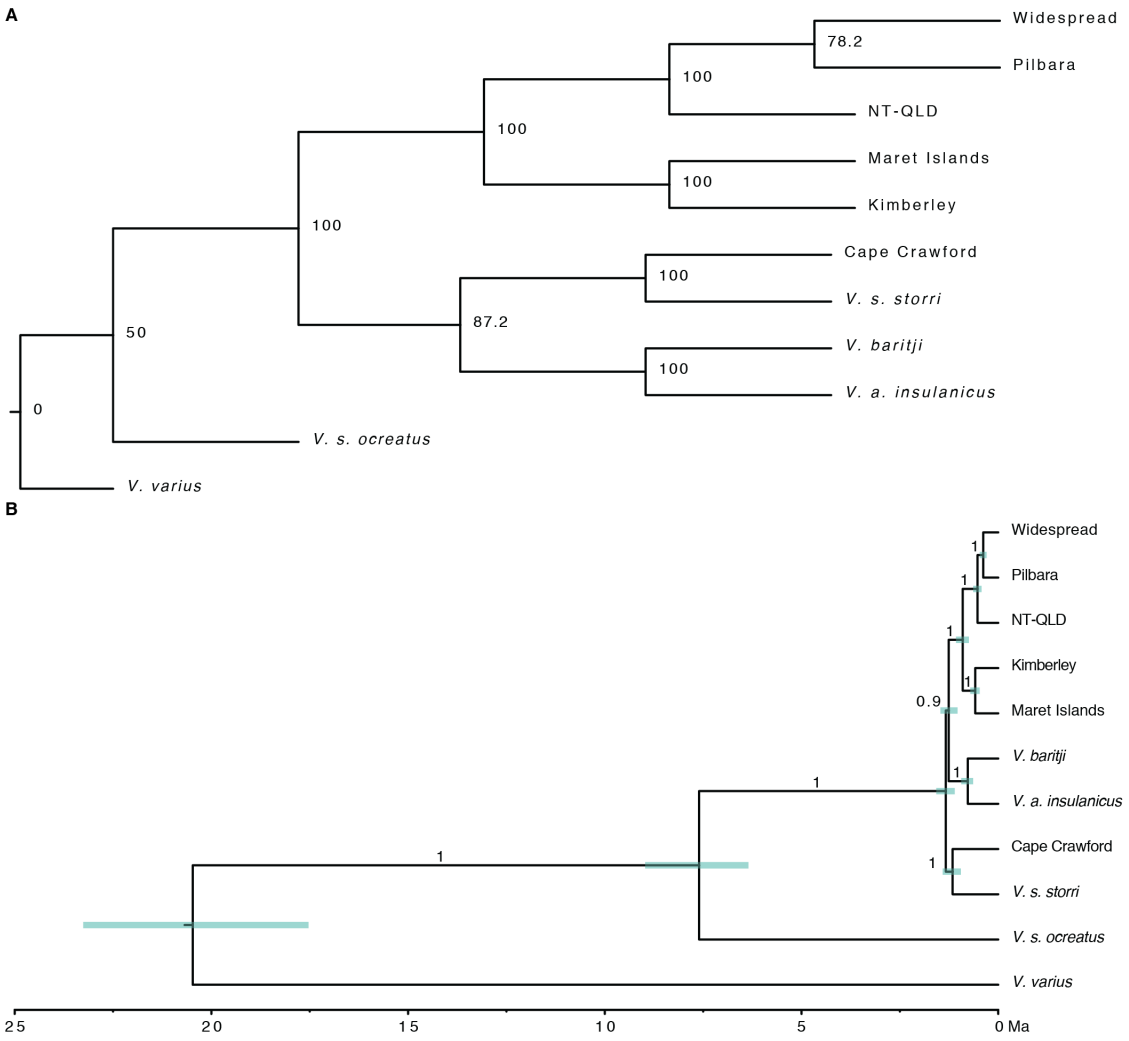

Figure S7. Relationships between the populations in the *V. acanthurus* complex obtained through species tree approach. A) SVDquartets tree; numbers in nodes are bootstrap support values. B) Time-calibrated SNAPP tree; numbers in node are posterior probabilities; bars indicate 95% highest posterior density of divergence times.

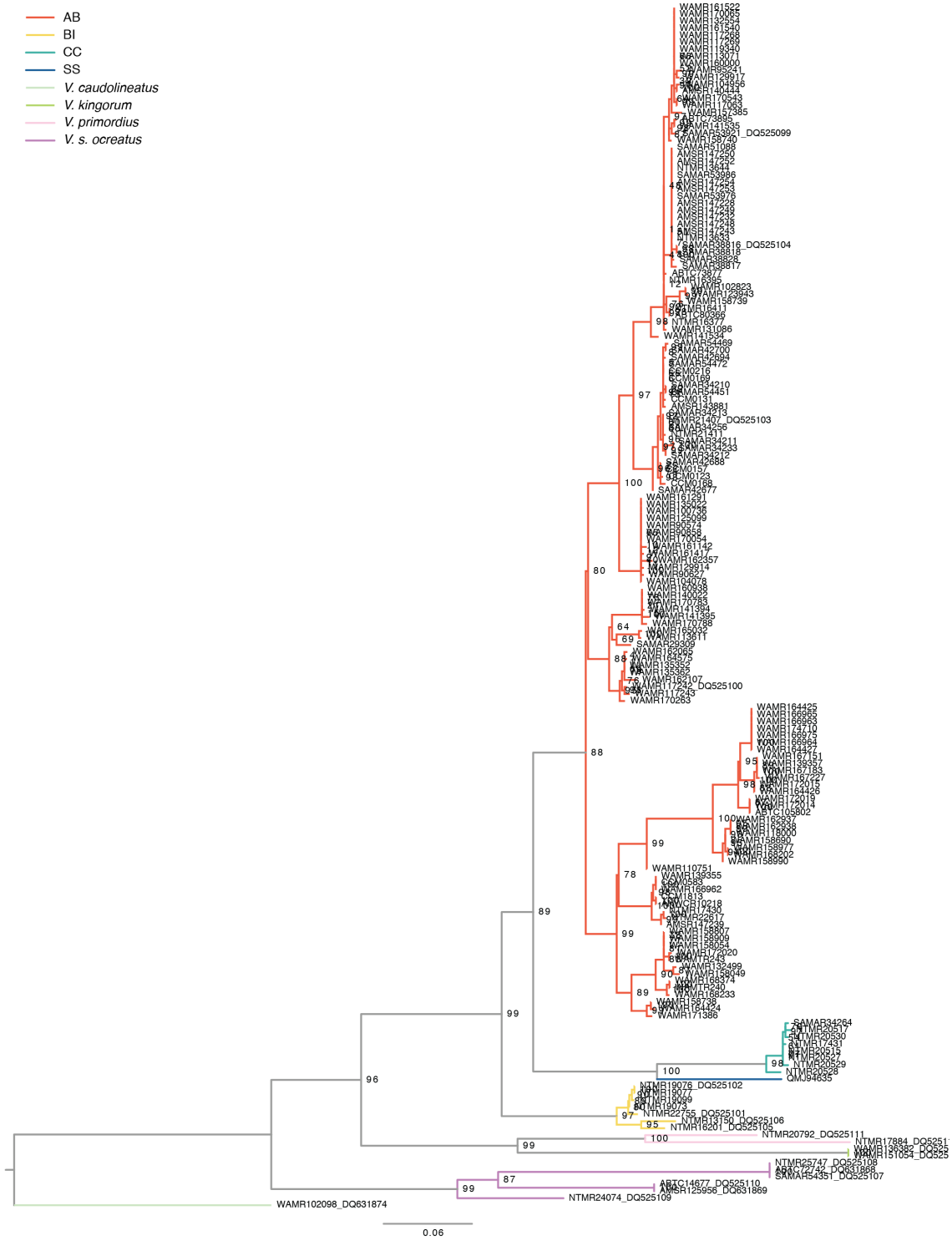

Figure S8. Mitochondrial tree obtained with IQ-TREE. Numbers in nodes are ultrafast bootstrap support values. The accession number of sequences from GenBank is shown after the voucher, separated by an underscore. Acronyms as in Fig. S5.

Supplementary References*

*Includes references in supplementary tables.

Pavón-Vázquez, C. J., Brennan, I. G., & Keogh, J. S. (2021). A comprehensive approach to detect hybridization sheds light on the evolution of Earth's largest lizards. Syst. Biol., syaa102.

Sabaj M. H. (2016). Standard symbolic codes for institutional resource collections in herpetology and ichthyology: an online reference. Version 6.5 (16 August 2016). Available at: http://www.asih.org/.